THE UNIVERSITY OF CHICAGO

DEVELOPMENT OF MODIFIED CELLULOSE NANOCRYSTALS AS ADDITIVES FOR SUSTAINABLE COMPOSITES

A DISSERTATION SUBMITTED TO
THE FACULTY OF THE PRITZKER SCHOOL OF MOLECULAR ENGINEERING
IN CANDIDACY FOR THE DEGREE OF
DOCTOR OF PHILOSOPHY

BY
NICHOLAS MACKE

CHICAGO, ILLINOIS
AUGUST 2024

Chapter 1 is adapted from: C. Calvino et al., "Development, processing and applications of bio-sourced cellulose nanocrystal composites", *Progress in Polymer Science* **2020**, *103*, 101221.

Chapter 2 is adapted from: N. Macke et al., "The effect of polymer grafting on the mechanical properties of PEG-grafted cellulose nanocrystals in poly(lactic acid)", *Journal of Polymer Science* **2022**, *60*, 3318–3330.

Chapter 3 is adapted from: Z. Oluz et al., "Melt-Functionalization of Cellulose Nanocrystals using Dynamic Hindered Ureas", *Journal of Polymer Science* **2024**.

For my grandparents.

"I can do all things through Christ who strengthens me."

Philippians 4:13

TABLE OF CONTENTS

LIST OF FIGURES

LIST OF TABLES

ACKNOWLEDGMENTS

There are a countless number of people who have helped me reach this milestone in life and, for all of them, I am extremely grateful.

Stuart, you were an incredible advisor over the past 6 years and I have learned so much from you scientifically and professionally. I came into graduate school naive and unaware of what I was getting into, and you helped me to understand what it means to analyze and solve complex problems at an elite level.

To Matt Tirrell and Paul Nealey, thank you for serving on my candidacy and dissertation committees, your willingness to help me learn from the very beginning of my time in graduate school has helped me to learn that you're never too far along to help someone begin their journey.

To the entire Rowan group and Tracy Walker, thank you all for making it so easy to come into work every day for the past 6 years. The level of intellectual curiosity and brilliance you all have, combined with your ability to chat on heretofore unseen levels, makes all of you so much fun to be around. Please never let the lab lose its high standards of excellence and whimsy. And Tracy, we all know that the entire building would be on fire without you in charge, so thank you for literally everything you do, seen and unseen.

To my undergraduate students - Sarah Candelaria, Christina Hemmingsen, Sarah Xi, Will Quintana, and Zach Leslie, you were all amazing. I enjoyed my time with each of you immensely and I hope I was able to teach you something along the way. I'm confident you will all go on to amazing things.

To Briana Konnick, thank you for giving me the confidence to step into the world of consulting for the next phase of my career. The advice and resources that you provided were invaluable in my job search and professional development.

To Laura Rico-Beck, where would any of us be without you? You taught me the importance and joy of connecting with anyone and everyone at their level and trying to teach them something new. I hope you realize how important your work is, and how much of an impact you had on my time here. You truly are the best of us.

To Charlie, you've been the heart and soul of the Rowan group for as long as I've been around and I can't imagine it any other way. The way you treat everyone around you with sincerity and care is incredible. I don't know what I'm going to do without our daily walks, brainstorming, and therapy sessions, but thank you for being the cornerstone of my time here. I'm excited to see what the future holds for you.

To Adarsh and Ellie, thank you for teaching me the magic of crossfire. Your friendship made the transition into graduate school so much easier and so much fun. Even 5 years later, every time we get together it's always a blast.

To my Purdudes - Alex, Beau, Elane, Emma, Grant, and Steven, you all have been an incredible core of friends that I can always count on. Visits with you all have been some of the highlights of my time in Chicago and I hope they continue. I'm so blessed to have all of you in my life and I'm looking forward to many more years of fun.

To Matt, there are no words to describe how important your friendship is to me. You've been involved in classes, research, friends, family, quarantine, relationships, hobbies, and quite literally everything else in my life for the past 5 years. As hard as this journey has been for both of us at times, you were always there to listen, advise, or distract when I needed you. No matter what life throws at us going forward, you'll always be my roomie.

To Madison, I knew a lot would change over my time in Chicago, but meeting you was definitely the biggest and best change I could have asked for. Through all of the ups and downs, you've been the best friend and partner imaginable. Your perseverance through hours and hours of board games during quarantine, your adventurous

spirit on road trips every other weekend during the summers, your kindness and helpfulness during holidays with our families, and your peace during quiet weekends at home cooking and watching TV are just a few of my favorite qualities of yours. As life continues to shift around us, I know you'll always be there to keep me grounded while continuing to push me to be my best self. I love you.

To my family, thank you for all of your love and support for the past 28+ years. Mom and dad, you taught me how to work hard and get things done from an early age and the passion you both have for helping others is inspiring. Matt, you've always been a great brother, showing me what it means to be strong and persevere through anything life throws at me. I love you all.

ABSTRACT

In chapter 1, a thorough review of the literature identifies key shortcomings in prior cellulose nanocrystal (CNC) composite research. In chapter 2, poly(ethylene glycol)-grafted CNCs are used as a model system for understanding the effects of polymer molecular weight and grafting density on the resulting mechanical properties of polymer-grafted CNC composites. In chapter 3, a method of functionalizing CNCs in the melt is developed that takes advantage of dynamic hindered urea chemistry to generate reactive isocyanate moieties *in-situ*, which can subsequently react with surface hydroxyl groups on the CNCs to attach a wide variety of polymer chains. Chapter 4 utilizes the fundamental lessons learned in chapters 2 and 3 to synthesize block copolymer-grafted CNCs in the melt and investigate their effect on composite mechanical properties, with a thorough analysis of grafting density with bulkier polymer chains. Finally, chapter 5 summarizes the work in more detail with personal perspectives and outlook for future research.

CHAPTER 1

INTRODUCTION TO CELLULOSE NANOCRYSTAL COMPOSITES

1.1 Summary

Plastic pollution concerns have catalyzed research into green materials with the specific goal of accessing new bio-derived and bio-degradable polymers with improved property profiles. One way to achieve these new materials is through the incorporation of nanofillers into bio-based polymer matrices. Cellulose nanocrystals (CNCs), which are extracted from biomass, have been investigated as one route to bio-based composites with enhanced performance. The combination of the excellent reinforcement capabilities of these bio-derived, nanosized particles along with relatively low production cost and biodegradability makes cellulose-based nanocomposites an attractive and promising approach to the next generation of green materials. Discussed herein is an overview of the use of CNCs to access reinforced bio-based nanocomposites, with particular focus on bio-available polyester and polysaccharide matrices. The characteristic changes provided by the incorporation of the nanofillers into the bio-based materials and their advantages and drawbacks are discussed. Specifically, the different parameters influencing mechanical reinforcement and barrier properties, such as the nature of processing, use of additives or CNC surface modifications are reviewed. Finally, the benefits of using CNC fillers in a number of potential future application areas, including polymer compatibilization, water purification, biomedical, and electronics are outlined.

1.2 Introduction

Ever since the existence of macromolecules was proposed 100 years ago by Hermann Staudinger, polymeric materials have played an ever-growing role in our daily life on account of their outstanding properties, which include robustness, light weight,

versatility, facile processing and low cost.[1] As a consequence, there has been a meteoric rise in production of commodity plastics since the Second World War, and worldwide plastic production surpassed 340 million metric tons in 2017 (Figure 1.1).[2–4] When these materials were developed, major efforts were focused on increasing their usable lifetime and preventing degradation; however, with mass consumption of plastics, the end-of-life of these materials has become a growing concern. It is currently estimated that less than 10 % of all plastics produced are recycled, around 10 % are incinerated, with the remaining 80 % accumulating in landfills or littered into terrestrial and aquatic environments.[5] The majority of plastics produced today are petroleum-based, such as polyethylene (PE), polypropylene (PP) and polystyrene (PS), and can take hundreds of years to degrade. Furthermore, approximately ten tons of these plastics are discarded into the ocean every minute.[6] As such, unless significant changes occur, the plastic accumulation in our marine environment will continue to grow over the coming years, to the point that it has been predicted that the amount of plastic in the ocean will outweigh fish by 2050.[7] The increase of non-biodegradable plastics in the environment is an ongoing global concern; for example, the 2019 Group of Twenty (G20) meeting on the global environment for sustainable growth proposed a framework for action to reduce marine plastic litter.[8]

Considering the continued rise in plastic consumption and impending depletion of fossil fuel reserves, next generation plastic technologies need to keep the environment in mind and take necessary actions to harmonize with it. Towards this goal, the development of "sustainable" polymeric materials has attracted much attention in recent years.[11–15] By definition, these materials should be produced from non-damaging, renewable feedstocks (a "green birth") and be able to be easily recycled (a "green rebirth") or quickly degraded into non-harmful components under mild environmental conditions (a "green death").[16,17] While such considerations are a good starting point

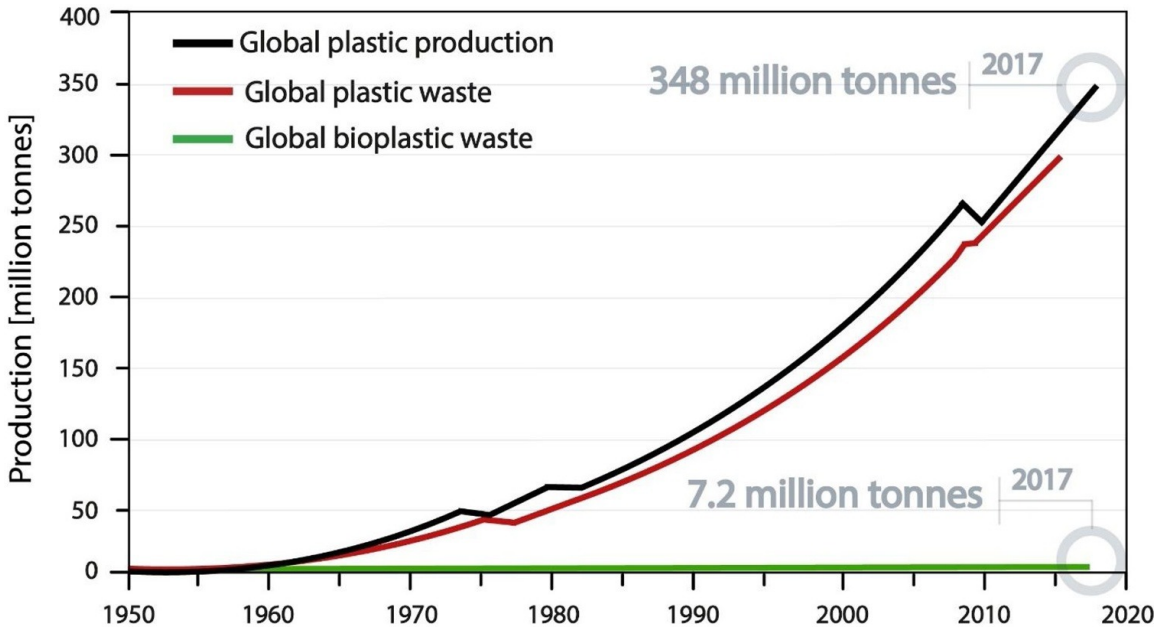

Figure 1.1: Graph showing the increase in global plastic production (black), global plastic waste (red), and bio-derived plastic production (green) from 1950 to 2017.[9,10]

for defining sustainability, it is important to recognize that one must also consider the wide range of factors that can play a part in the total emissions generated by a material over its entire life cycle, from initial planting to final degradation. For example, the use of pesticides during biomass growth and the energy needed to isolate the monomer/polymer from the feedstock are two factors that are not commonly considered and can push the total negative environmental impacts of bio-based materials beyond those of their fossil fuel counterparts.[18] As such, while not the focus of this review, it is important to note that any "sustainable" material system aiming for commercialization will need a full life cycle assessment to determine whether or not it is truly "more sustainable" than the existing solutions.

Additionally, while many bio-degradable polymers have been developed and commercialized as "environmentally friendly" plastics, most of these plastics are not currently sourced from renewable feedstocks. For example, polycaprolactone (PCL), poly(butylene adipate terephthalate) (PBAT) and poly(butylene succinate) (PBS)

are biodegradable, but predominately use fossil fuel-based chemicals to access their monomers on a commercial scale.[19] Some small-scale operations produce a minor portion of these monomers from biomass fermentation;[20] but, while this is a step in the right direction, it is not yet at a scale to make the polymers' life cycle sustainable. Increasing the percentage of these polyesters that are obtained from biomass-derived monomers is an active area of research.[21] If this can be achieved on a commercial scale, such polymers represent a significant advancement over their non-biodegradable alternatives. However, these polymers do not span the property profiles that are available from the wide range of commercially available petroleum-based plastics.

Today there are two major classes of fully bio-based polymers that are commercially-viable: alkyl polyesters – predominantly poly(lactic acid) (PLA)[22] but also polyhydroxyalkonates (PHA),[23] and carbohydrate-based plastics.[24] Unfortunately, these materials have relatively low thermal, physical, and/or mechanical performance relative to their petroleum-based counterparts, which limits their use in many applications.[25] Indeed, the production percentage of bio-degradable and/or bio-based polymers was less than 3 % of the total plastics market in 2017.[26] While growing public concerns about the environment will continue to push the development and commercialization of sustainable polymers, improved material properties at a competitive cost will be a controlling factor in driving the growth of these "eco-friendly" plastics.

Among the different strategies used to improve the mechanical properties of sustainable polymers, the addition of nanofillers, such as graphene, titanium dioxide, calcium carbonate, silica, etc., appears to be a promising approach.[27–30] By controlling geometric dimensions, polymer-nanofiller interactions, and particle dispersion, the incorporation of a small amount of nanofillers (usually less than 10 wt. %) has been shown to dramatically change bulk material properties, such as improving strength, thermal resistance, and gas permittivity.[19,31] However, the integration of non-bio-based

or non-bio-degradable fillers into sustainable polymers diametrically opposes the material's sustainability and complicates recycling or composting processes. Thus, a focus on the development of sustainable bio-based nanofillers with renewable and degradable characteristics is of importance to achieve nanocomposite materials with sustainable lifecycles.

Among the various bio-based nanofiller materials, cellulose holds a key position as an abundant raw organic material that can be obtained from virtually inexhaustible biomass feedstocks, capable of meeting the increasing demand for green and bio-based products.[32] The use of cellulose as a material has been known since the beginning of civilization, from clothes and paper to its use in construction materials, yet over the past few decades there has been renewed interest in cellulose as a nanomaterial.[33] A variety of nanoparticles can be extracted from cellulose owing to its hierarchical structure and semi-crystalline nature (Figure 1.2). Nanocelluloses are generally categorized by their size, aspect ratio, and crystallinity, most often being divided into cellulose nanofibers (CNFs), which have relatively low degrees of crystallinity (ca. 60–80 %) and dimensions of nanometers in width and microns in length, and cellulose nanocrystals (CNCs) which are more crystalline (ca. $>$ 85 %) but with aspect ratios generally less than 100. While CNFs have been employed as natural fillers for many polymer matrices including bio-based polymers, there have been a number of recent reviews that have summarized this work[34–37] and the interested reader is directed to these reviews for more information.

The focus of this thesis is on the other category of nanocellulose, namely cellulose nanocrystals and in particular on the use of CNCs to reinforce commercially-viable 100 % bio-based plastics. CNCs are isolated by extraction of the crystalline domains from the bio-sourced cellulosic material, usually by a combination of mechanical and chemical processes.[42] Commonly, to obtain CNCs from the biomass cellulose, acid hydrolysis is

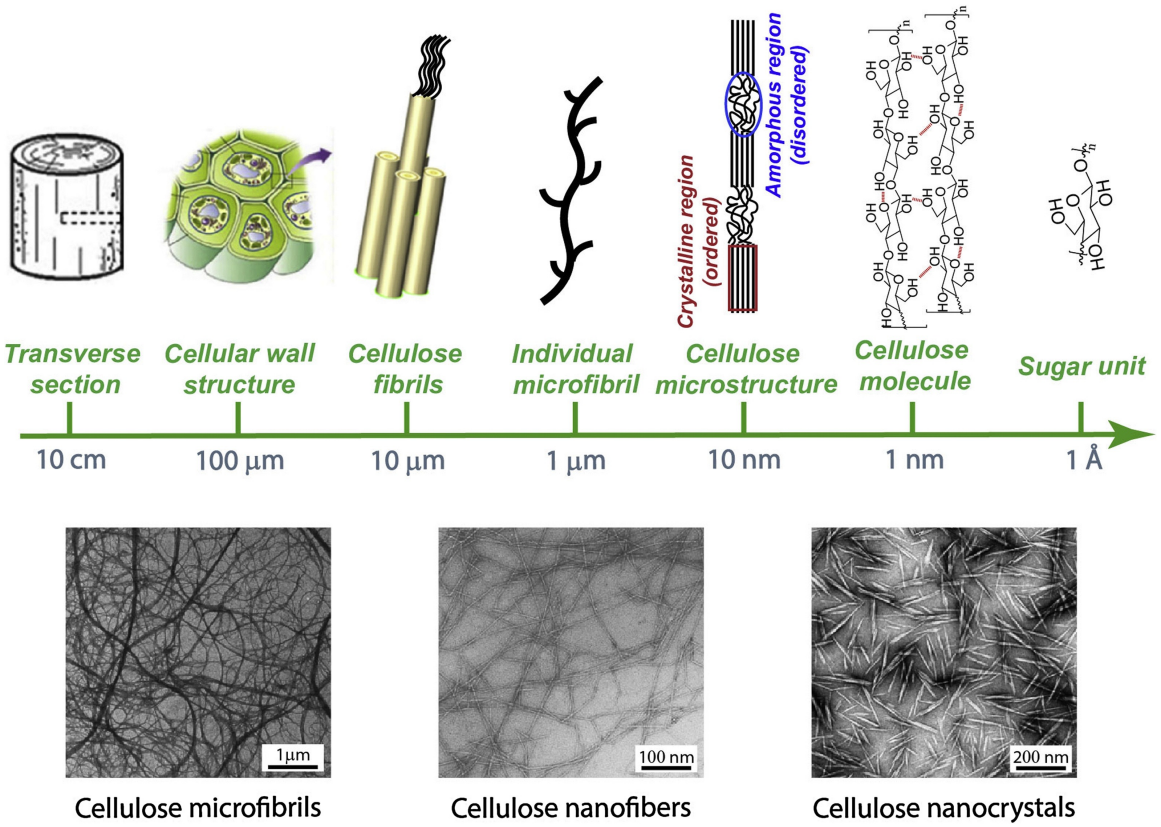

Figure 1.2: Hierarchical structure of cellulose and transmission electron micrographs of cellulose microfibrils, nanofibers and nanocrystals.[38–41]

carried out to degrade the amorphous connecting regions between crystals (Figure 1.2). Broadly, CNCs are needle or rod-like nanoparticles that can be produced from diverse starting bio-sources (Table 1.1), such as wood, plants (bamboo, straw and grass, e.g. Miscanthus x. giganteus[43,44]) and select living organisms (e.g. bacteria, algae and sea tunicates). For clarity, a consistent naming scheme will be used throughout this review when discussing CNCs and their composites (Table 1.1). CNCs will be described by "*bio-source*-CNC-*functionality*", so a tunicate CNC with sulfate half esters on its surface will be described as *t*-CNC-SO_3^-.

As shown in Table 1.1, the length, diameter, and aspect ratio of CNCs vary between 100-3000 nm, 3-50 nm, and 5-200 respectively, depending on the biological source and isolation protocol.[60] Removal of the non-crystalline cellulose results in CNCs having

Table 1.1: List of common sources used to access CNCs, CNC nomenclature used in this article along with their corresponding approximate length, width and aspect ratio.

Bio-source	Abbreviation	Length	Width	Aspect Ratio	Reference
Wood	*w*-CNC	100–200	3–5	20–60	[45,46]
Cotton (Filter Paper)	*c*-CNC	100–300	5–15	10–40	[47,48]
Ramie Fiber	*rf*-CNC	50–250	5–10	5–40	[40,49]
Tunicate	*t*-CNC	500–3000	10–30	10–200	[50,51]
Bamboo	*bamboo*-CNC	50–400	5–20	15–20	[52,53]
Bacteria	*b*-CNC	100–1000	5–50	5–200	[54,55]
Phormium tenax	*ph*-CNC	100–200	5–15	10–20	[56,57]
flax	*f*-CNC	100–500	10–30	10–50	[58,59]

a high degree of crystallinity, generally around 85 % or greater.[61] Depending on the bio-source and the isolation protocol, CNCs can have a single-crystal modulus as high as 140 GPa, a density of about 1.5 g/cm^3 and a specific modulus around 90 GPa g^{-1} cm^3.[62] This combination of size and strength gives the CNCs outstanding reinforcing potential and renders them competitive with other commercially available nanofillers, such as silica,[63] carbon nanofibers,[64] and nanoclays,[65] as a strong candidate for nanocomposite applications. In fact, wood-based CNCs have already begun production on a plant scale and are commercially available.[66]

The relatively high aspect ratio (AR) of CNCs when compared to spherical particles is an advantage for reinforcing polymers matrices as it defines the CNC loading required to form a percolating network throughout a material (higher AR means lower filling fractions are required for percolation).[67] A dramatic increase in mechanical stiffness is observed when percolation is achieved, making it an important consideration for the material's final properties. Despite these promising characteristics, there are still significant challenges to the use of CNCs in composite materials. In particular, the existence of hydroxyl groups on the surface of CNCs makes them hydrophilic in nature with a strong propensity for interparticle hydrogen bonding, causing agglomeration in polymer matrices, which significantly limits their reinforcement capability. However,

it is important to note that most CNCs that are commercially available and reported in the literature are negatively-charged, which enhances their dispersion in water and polar organic solvents. The surface negative charges are usually obtained during the CNC isolation procedure. As mentioned above CNCs are submitted to an acid treatment in order to remove the non-crystalline cellulose. If that acid treatment is sulfuric acid, then the surface of the CNCs will contain charged sulfate half-esters (CNC-SO_3^-). Another common negatively-charged CNC is carboxylate CNCs (CNC-COO^-), usually prepared via a TEMPO/bleach oxidation process from uncharged CNCs (obtained through the use of HCl during the isolation process). The dispersibility of these charged CNCs in aqueous and polar solvents renders solvent casting a powerful strategy to optimize their dispersion in polymer matrices, and for this reason solvent casting is currently the most employed approach to prepare CNC nanocomposites.[68] In fact, CNC-based nanocomposites can be traced back to the pioneering work of Cavaillé, Chanzy, and coworkers in the mid-1990s.[69–72] In these studies, they showed that sulfate functionalized CNCs obtained from either wheat straw or tunicin could be dispersed in an aqueous latex (of a styrene and butyl acrylate copolymer) solution and that a nanocomposite could be obtained by solution casting. The resulting film exhibited significant improvements in the mechanical strength of the material. Key to the success of this approach is both the latex and CNCs are dispersible in water, resulting in homogenous dispersions.

It is important to note that the surface hydroxyl groups of CNCs can be functionalized using various synthetic strategies to make the CNCs more dispersible in hydrophobic solvents and polymers, however, one must remember that functionalization will also impact the reinforcement capability of the CNCs by altering the interactions of the nanofillers with themselves and the matrix.[73]

CNCs, by their bio-derived nature, are already present in our ecosystems, albeit

usually embedded in a composite structure with other components, such as lignin, amorphous cellulose, and hemicelluloses. Nonetheless an important aspect that needs to be studied is their potential impact on human and environmental health. While, the complete story is not yet known and much more work remains to be done in this area to better understand their effects, this aspect of CNC research is starting to become more active. For example, Vartiainen and coworkers looked into *w*-CNF toxicity and found that no significant negative effects were observed in mouse and human cell viability tests.[74] An ecotoxicity test (V. fischeri) showed no effects of the *w*-CNFs below 300 mg/L and EC50 (effective concentration) values could not be obtained up to 2500 mg/L, meaning that the materials are safe unless concentrations are higher than those expected in worst-case environmental scenarios. More relevant to this review, the ecotoxicity of *w*-CNC-SO_3^- has been investigated by Kovacs and coworkers in nine different aquatic species, with most species not being significantly affected. A greater than 25 % reduction in the reproduction in one species (the fathead minnow) was observed only at high concentrations of the *w*-CNC-SO_3^- (> 290 mg/L).[75] Preliminary studies into human/mammalian health have shown little-to-no oral toxicity, no dermal toxicity and generally low cytotoxicity at low concentrations.[76] However, perhaps the biggest concern with any nanomaterial is its pulmonary toxicity.[77] Using a 3D in vitro triple cell coculture model of the human epithelial airway barrier, Rothen-Rutishauser and Weder observed that *c*-CNC-SO_3^-, when delivered as an aqueous suspension, do elicit dose-dependent cytotoxicity and (pro-)inflammatory response, but at a level that is significantly lower than multiwalled carbon nanotubes or crocidolite asbestos fibers.[78] However, other studies by Shvedova and coworkers on *w*-CNC-SO_3^- have shown that different and more adverse pulmonary outcomes can occur depending on whether the CNCs are in a suspension or are a freeze-dried powder.[79]

Part of the challenge here is that there is not enough data at the moment to fully

understand the effects of CNCs. Further complications arise as not all CNCs are created equal. For example, size and shape of the CNCs, as well as the nature of the functional groups on the CNCs will undoubtedly play a role in any ecological or biological effects. In addition, CNCs can be isolated using a range of protocols involving the use of different chemicals and different levels of purification, therefore leading to the fact that the different CNCs used in these studies may well have different levels of (toxic) contaminants. As such, there is certainly a need for more research in this area, the results of which will play an important role in the future of sustainable CNC composites.

1.3 CNC-reinforced bioderived polymers

1.3.1 Polysaccharide-based composites

Polysaccharides such as cellulose, starch, chitin, chitosan, alginates, and various naturally occurring gums have attracted great interest as a source of sustainable polymers on account of their abundant supply, low cost, renewability, biodegradability, and ease of chemical modification.[80] In addition, some polysaccharides and their derivatives also have good solubility in water, which readily disperses negatively-charged CNCs, thus allowing for relatively facile access to composite materials.

1.3.1.1 Chitosan and alginate-based composites with negatively-charged CNCs

Chitosan, derived from chitin – the second most abundant natural polysaccharide after cellulose, is a natural linear polysaccharide consisting of (1→4)-2-amino-2-deoxy-β-D-glucan and is soluble in acidic water (Figure 1.3). Chitosan has been investigated for use in a variety of different applications including biomedical, packaging, and as a thickening agent.[81–83]

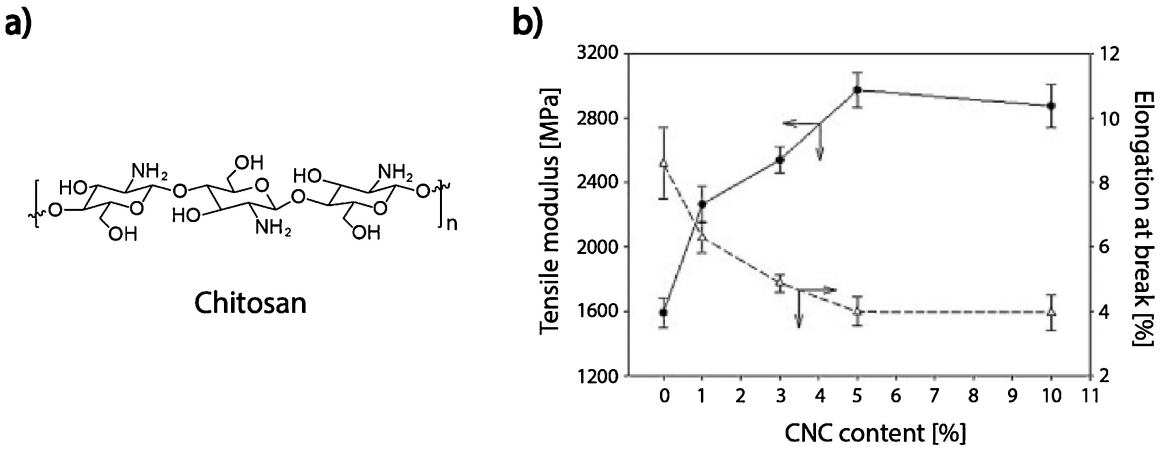

Figure 1.3: a) Molecular structure of chitosan. b) Graphic showing the tensile modulus and the elongation at break of chitosan composites loaded with different *w*-CNC-SO_3^- content.[84]

Chitosan/*w*-CNC-SO_3^- composite films have been prepared by simple aqueous mixing of a suspension of *w*-CNC-SO_3^- with a 1 % w/v chitosan acidic solution followed by solvent casting. The resulting composites show a roughly 80 % higher tensile modulus (ca. 3 vs. 1.6 GPa) and a 50 % reduction in elongation at break (4.0 vs. 8.6 %) with the inclusion of 5 wt. % *w*-CNC-SO_3^- when compared to the neat chitosan films.[84] The increase in the mechanical strength was ascribed to the formation of strong ionic bonding interactions between the negatively-charged *w*-CNC-SO_3^- and positively charged amine groups on chitosan. Additionally, the same filler content loading has been shown to lower the water vapor permeability by 25 % (2.4 vs. 3.3 g·mm/m^2/day/kPa), consistent with increased crystallinity induced by the incorporation of the CNCs. In fact, there are numerous reports that show mechanical property improvements in chitosan-based materials when CNCs are incorporated,[85,86] specifically for applications in drug delivery,[87] gas barrier,[88] and filtration materials.[89]

Alginate is another water-soluble polysaccharide (this time in basic solutions) from which CNC composites have been prepared and studied. For example, alginate/*w*-CNC-SO_3^- composite films prepared by solvent casting from an aqueous

mixture of sodium alginate and *w*-CNC-SO_3^- showed improved tensile strength relative to neat alginate. The tensile strength increased with *w*-CNC-SO_3^- content up to the addition of 5 wt. % (tensile strength of ca. 80 MPa vs ca. 55 MPa for neat alginate).[92] The presence of carboxylate moieties on the alginate means that alginate gels can be formed through the addition of Ca^{2+} ions on account of the formation of carboxylate-Ca^{2+}-carboxylate salt bridges (Figure 1.4a).[90] A number of reports in the literature investigate alginate/CNC hydrogels and aerogels crosslinked with Ca^{2+} ions.[93–95] As an example, alginate/CNC-based aerogels have been prepared by adding an aqueous Ca^{2+} solution to a lyophilized mixture of alginate and *c*-CNC-COOH (10 wt. % CNCs).[91] The resulting ionically-crosslinked gels were then lyophilized to yield the aerogel (Figure 1.4b). Mechanical properties of both the alginate/Ca^{2+} and alginate/*c*-CNC-COOH/Ca^{2+} aerogels showed that the addition of CNCs enhanced the

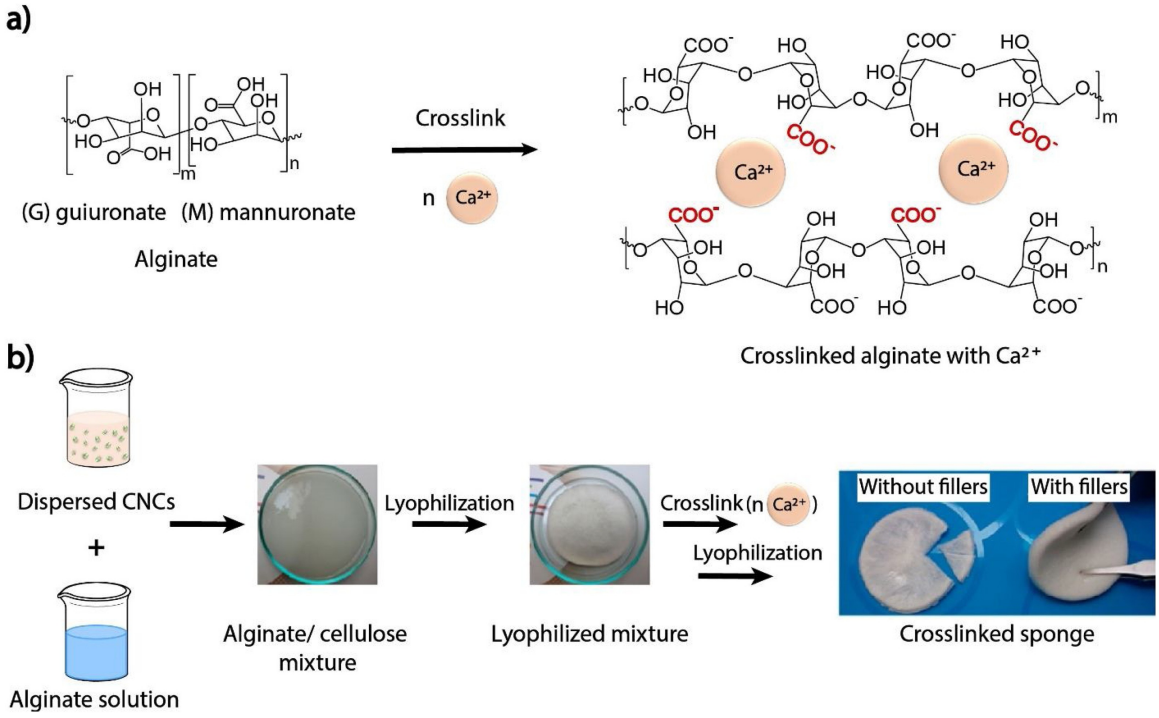

Figure 1.4: a) Molecular structure of alginate composed of guiuronate and mannuronate units and the proposed resulting crosslink structure upon addition of calcium cations. b) Scheme depicting the preparation of a crosslinked alginate sponge.[90,91]

compressive strength by ca. 190 % at 70 % compressive strain (compressive strength of ca. 130 kPa vs ca. 45 kPa for alginate/Ca^{2+} aerogel), and that carboxylic acid CNCs had a higher reinforcement effect relative to sulfated CNCs (ca. 100 kPa).

The incorporation of CNCs is not only a benefit for mechanical reinforcement; they can also be used to alter other properties of the material. For example, Tam et al. reported the use of CNC-containing alginate aerogel beads for the adsorption of the cationic dye methylene blue.[96]. Alginate/*w*-CNC-SO_3^-/Ca^{2+} (1 wt. % CNCs) hydrogel beads were prepared by dropping the aqueous mixture of alginate and *w*-CNC-SO_3^- into Ca^{2+} solution followed by freeze drying to obtain the aerogel material. The adsorption of methylene blue, conducted by stirring the aerogel beads in methylene blue aqueous solutions, showed that the dye removal increased from 20 % to 60 % by adding CNCs into the aerogel, presumably (at least in part) because of the increase in negative charges in the composite system.

1.3.1.2 Cellulose-based composites with negatively-charged CNCs

As mentioned before, cellulose is the most bio-available polysaccharide and historically, numerous cellulose derivatives have been produced and sold on a commercial scale. In particular, cellulose esters and cellulose ethers, produced by chemical modification of cellulose, have found use in a wide variety of applications.[97] For example, cellulose acetate butyrate (CAB) is one of the most commonly used cellulose esters in the coatings industry on account of its enhanced solubility relative to cellulose, its chemical resistance, and the fact that it is compatible with other polymers.[98] Furthermore, it is possible to tune the properties of these materials by altering the ratio of butyrate to acetate moieties on the cellulose backbone. Although the addition of CNC fillers may be expected to improve some of the properties of CAB, its general insolubility in water or polar solvents makes it difficult to prepare homogeneous CAB/CNC composite films.

As will been seen throughout this introduction, the insolubility of a polymer matrix in water or polar solvents is a recurring challenge in accessing many CNC composites. One way to tackle this difficulty is to use a solvent-exchange method. This approach involves the dispersion of the CNCs in water followed by the addition of an organic solvent that both dissolves the polymer and is miscible with water. The mixture is then centrifuged, the supernatant removed, more organic solvent is added to the remaining gel, and the system agitated. This process can be repeated to result in CNC-organic solvent dispersions that have limited temporal stability (Figure 1.5). To access the nanocomposites, a solution of the polymer dissolved in the organic solvent is added to the organic solvent-suspended CNCs and films are obtained by solution casting.

As an example, Oksman et al. reported CAB/*w*-CNC-SO_3^- composite films prepared via a solvent-exchange procedure (from water to acetone, a good solvent for CAB) followed by solution casting.[99] The CAB composite film with 10 wt. % *w*-CNC-SO_3^- showed 30 times higher storage modulus (ca. 85 MPa) than that of pure CAB (ca. 3 MPa) at 155 °C, above the glass transition temperature (136 °C).

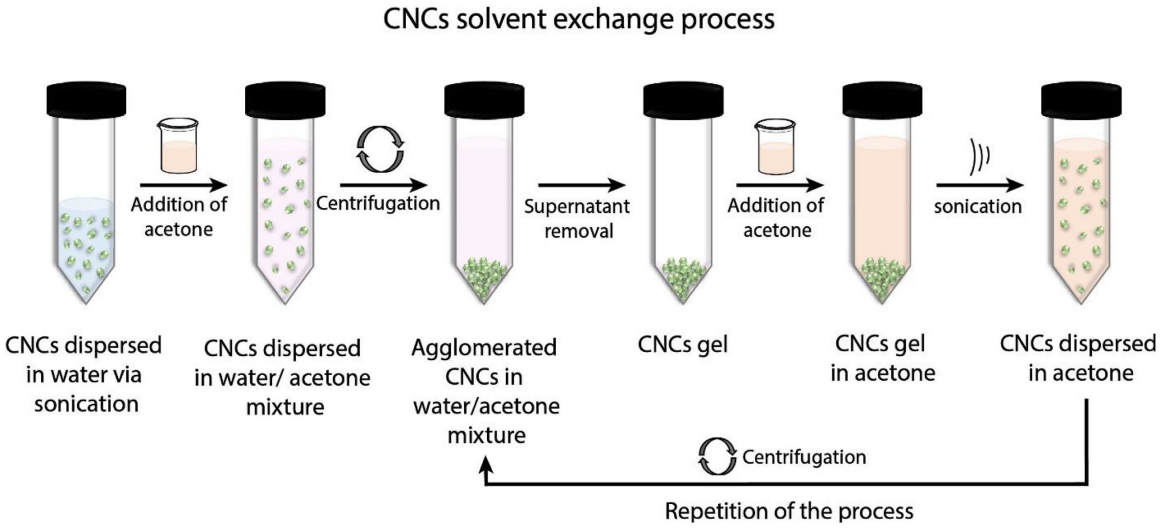

Figure 1.5: Scheme depicting a standard CNC solvent exchange process from aqueous solution to a water-miscible solvent such as acetone.

1.3.1.3 Starch-based composites with negatively-charged CNCs and plasticizer

Starch is another commercially available biopolymer that can be obtained from a number of renewable plant sources such as corn, potatoes, peas, rice, etc.[100,101] Starch is comprised of two polysaccharides, amylose (20-25 wt. %) and amylopectin (75-80 wt. %), which are the linear and branched polymers of α-glucose respectively (Figure 1.6a). In its natural form, the two components combine to form a semi-crystalline, hydrogen-bonded network, resulting in an insoluble material that is difficult to reprocess. Solution processing of the natural material is difficult as starch is insoluble in cold water and undergoes gelatinization in hot water, while melt processing is not possible as thermal decomposition starts to occur before T_m. Dried starch is brittle and mechanically weak, making it uninteresting as a replacement for any plastic.[102] While water is known to plasticize starch, the resulting material has poor properties that include high water vapor permeability and low tensile strength.[103] In addition, starch is hygroscopic, so its water content is often difficult to control. Nonetheless, starch is cheap and has generated considerable attention as a biodegradable granular filler in commodity plastics; however, such starch-based fillers generally have low reinforcing capability.[104]

Plasticizers other than water (such as polyols, urea, formamide, etc.) can be used to access more mechanically flexible and melt processable starch-based materials.[105] As such, these plasticized starches are able to be manufactured using traditional methods employed for synthetic plastics giving access to cheap and renewable bio-degradable materials that can be used in short-lived applications, such as packaging.[106] Unfortunately, the use of a plasticizer to improve processability comes at the cost of mechanical strength and usually does not improve water sensitivity issues. Thus, the use of a renewable filler such as CNCs as a reinforcing agent is one strategy to cope with the poor mechanical

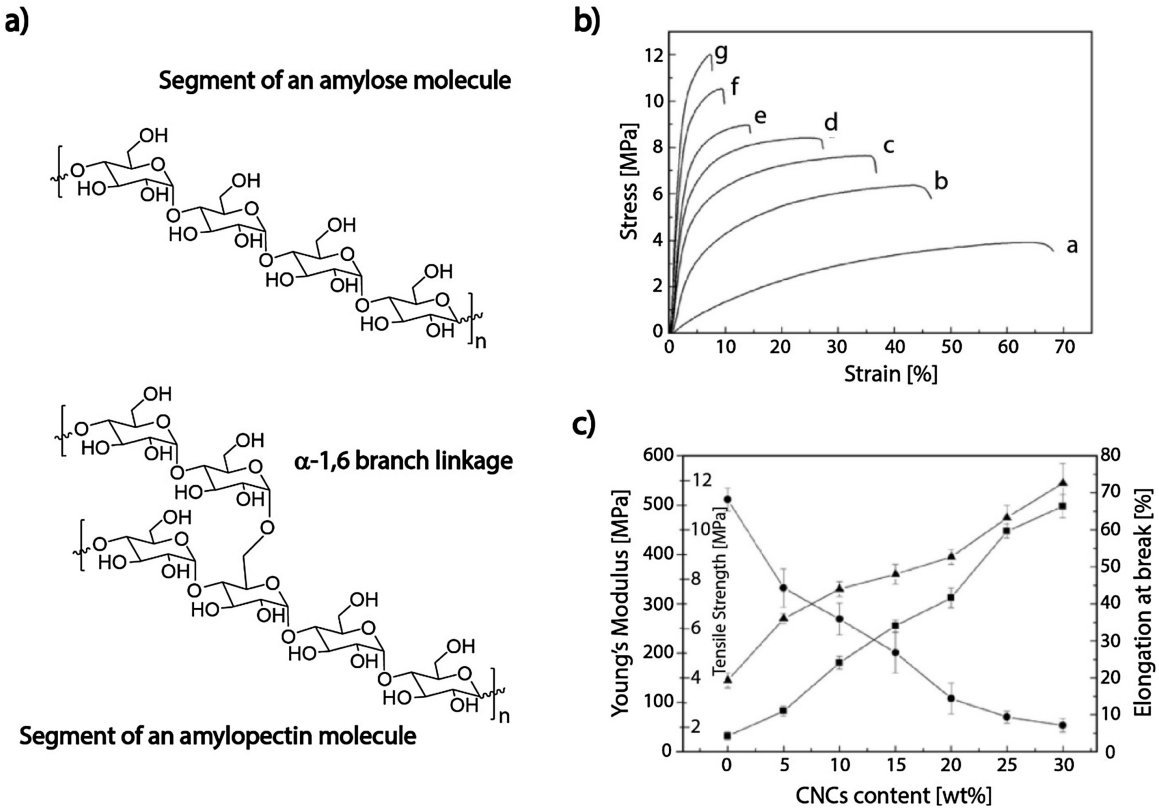

Figure 1.6: a) Molecular structure of the two polymers present in starch: the linear form – amylose, and the branched form – amylopectin. b) Strain-stress curves of starch/glycerol (ca. 35 wt. % of starch)/*f*-CNC-SO_3^- nanocomposite films with (a) 0 wt. %, (b) 5 wt. %, (c) 10 wt. %, (d) 15 wt. %, (e) 20 wt. %, (f) 25 wt. %, and (g) 30 wt. % of *f*-CNC-SO_3^-. c) The tensile strength (▲), Young's modulus (■), and elongation at break (●) of the same nanocomposite films. The composite films were kept at 43 % relative humidity.[109]

performance of plasticized starch while maintaining eco-friendly characteristics. Various reports have demonstrated a high compatibility between starch and CNC fillers, presumably as a consequence of the strong hydrogen bonding interactions between the two polysaccharide structures.[107,108]

Glycerol is a commonly used plasticizer to access thermoplastic starch,[110,111] although it has to be remembered that water also plays a role in such materials.[112] Interestingly, the addition of glycerol to starch yields a phase separated material (a glycerol-rich and amylopectin-rich phase) as highlighted by the presence of two glass transitions (ca. -50 and 40 °C).[112] Figures 1.6b and c show the effect that the

incorporation of f-CNC-SO_3^- has on the mechanical properties of starch/glycerol (ca. 35 wt. % of starch) composites.[109] Such CNC composites can be accessed by mixing starch granules, glycerol, and f-CNC-SO_3^- in water before gelatinizing via heat treatment. Drying of the gels results in composite films which exhibit properties commonly observed in CNC reinforced materials: increases in tensile strength (from 4 to 12 MPa) and Young's modulus (ca. 30 to 500 MPa) along with decreases in elongation at break (ca. 70 to 10 %) with varying CNC content from 0 to 30 wt. %, respectively. In comparison to multi-walled carbon nanotubes (MWCNT), a less sustainable filler that is also often used to reinforce polymers, the starch/CNC system performs just as well, if not better. While exact comparisons are difficult to make on account of variances in source materials and processing methods, the starch/glycerol/MWCNT materials showed around 40 % increase in Young's modulus, compared to nearly 250 % increase with f-CNC-SO_3^- at the same 5 % loading.[113] An advantage the CNCs have over MWCNTs from a mechanical reinforcement perspective is they are water dispersible and, as such, are generally easier to process from aqueous solutions to yield composites with more homogenous nanofiller dispersions.

The starch/f-CNC-SO_3^- composites also exhibited two glass transitions (T_gs) (similar to the unreinforced matrix) with both transitions shifting to slightly higher temperatures with higher CNC content. Wide-angle x-ray scattering (WAXS) measurements showed the appearance of a new amylopectin crystal peak in the starch/glycerol/f-CNC-SO_3^- composite materials, implying that the CNCs also act as a nucleating agent. The authors suggested that the glycerol (and water) rich phase would localize near the CNC surfaces[50,114] potentially leading to a two-fold effect: (1) the local plasticization of amylopectin chains near the CNCs, aiding in transcrystallization, and (2) antiplasticization of the amylopectin phase, reducing the overall material ductility.

The use of sorbitol in place of glycerol as a plasticizer for starch yields materials

that only exhibit one T_g, which has been ascribed to a decrease in mobility of the sorbitol. Starch/sorbitol (ca. 30 wt. % of starch) composite films containing *t*-CNC-SO_3^- have been prepared by solvent casting. Interestingly, these materials neither exhibit transcrystallization of amylopectin nor show a significant antiplasticizing effect, suggesting that sorbitol does not accumulate near the CNCs.[115] Compared to pure plasticized starch/sorbitol films, a starch/sorbitol/*t*-CNC-SO_3^- (ca. 25 wt. %) composite film showed an increase in tensile strength from ca. 5 MPa to 40 MPa and Young's modulus from ca. 50 MPa to 750 MPa (measured at 43 % relative humidity), while elongation at break of films with and without CNCs was low (below 10 %).[116] Overall the starch/sorbitol/*t*-CNC-SO_3^- materials showed better mechanical reinforcement than the starch/glycerol/*t*-CNC-SO_3^- composites. The authors suggested that the absence of sorbitol accumulation near the CNCs allows more effective stress transfer between CNCs and the starch matrix, leading to composites that exhibit a significant increase in the modulus and tensile strength relative to pure glycerol-plasticized materials.

1.3.2 Poly(lactic acid)-based composites

Poly(lactic acid) (PLA) (most commonly the L-lactide enantiomer, PLLA) is currently one of the most commercially relevant bio-based polymers on account of its easy, and relatively cheap, accessibility on a large scale as well as its overall eco-friendly properties, being bio-degradable, renewable, non-toxic, and compostable.[117–119] PLA can be prepared via ring opening polymerization of lactide monomers, which can be readily obtained via distillation from corn, sugar cane, and other fermentation crops.[120] Additionally, unlike other bio-sourced polymers, PLA can be melt-processed by extrusion, thermoforming, or injection molding into fibers, films, or other functional forms.[121]

While PLA has the potential to be a promising replacement for some commodity

petroleum-based plastics, it is limited in its mechanical and thermal properties, as with other bio-based polymers. For example, its heat distortion temperature (HDT, the temperature at which the polymer deforms under a specific load) is low (55 °C) which, along with its brittleness (strain at break ~2.5 %) and poor impact resistance (impact strength ~2.6 kJ/m^2), limits its utilization in a range of applications.[117] Nonetheless, PLA has already been used in some commercial applications, including packaging material (e.g. corn chip bags). However, the poor barrier properties of the neat material (oxygen transmission rate over 30 cm^3/m^2/day compared to most commercial materials with less than 15 cm^3/m^2/day) prevent application in air and water-tight systems.[122,123] Since plastic packaging was a $260 billion market in 2013, it is clear why improving these properties could make a major impact in the industry.[7]

A range of strategies have been developed to overcome these issues and improve PLA's overall properties, such as copolymerization, stereocomplexation, polymer blending, and addition of plasticizers and/or nanofillers.[124–127] While all of these approaches result in the enhancement of either thermomechanical or barrier properties of PLA, some of them require the addition of unsustainable components to the sustainable matrix, reducing the eco-friendly aspects of the material. The use of cellulose nanocrystals as a nanofiller, on the other hand has the potential to address the material drawbacks while maintaining the green nature of the material.

1.3.2.1 Poly(lactic acid)-based composites with negatively-charged CNCs

As discussed above, solution processing is the most common way to access CNC composites. Unfortunately, PLA is not soluble in water and as such, direct mixing with aqueous CNC suspensions is not possible. The most common solvent used for solution processing PLA in the literature is chloroform, however, good dispersion of CNCs in this

solvent is difficult. As discussed in Section 1.3.1.2, solvent exchange processes (Figure 1.5) can be used to access dispersions of CNCs in organic solvents. As chloroform is not miscible with water, the aqueous dispersion of CNCs needs to be first solvent exchanged into a water miscible organic solvent (e.g. acetone) and then exchanged to chloroform. Lagaron et al. investigated if such a solvent exchange process aids the dispersion of CNCs in a PLLA matrix.[128] To do this, chloroform dispersed *w*-CNC-SO_3^- were prepared either by the solvent exchange process or by adding in freeze-dried *w*-CNC-SO_3^- (from water) directly to chloroform followed by sonication. The two different chloroform CNCs suspensions were independently mixed with PLA in chloroform and cast to furnish nanocomposites loaded with 1, 2, 3, and 5 wt. % *w*-CNC-SO_3^-.

No matter how the CNCs were dispersed in chloroform, the modulus and tensile strength of the composites were reduced relative to neat PLLA suggesting inhomogeneous dispersion[128] and that solvent exchange into chloroform does not appear to be a viable route to homogenously dispersed CNCs in PLA. Nonetheless, the incorporation of CNCs by either route did result in an increase in the crystallinity of the PLLA (e.g. from ca. 9 % for neat PLLA to 15 % with 1 wt. % of freeze-dried *w*-CNC-SO_3^-) as well as to an increase in water and oxygen barrier properties (from 1.37×10^{-17} $m^3 \cdot m/s \cdot mm^2 \cdot Pa$ of O_2 for neat PLLA down to 0.23×10^{-17} $m^3 \cdot m/s \cdot mm^2 \cdot Pa$ with 1 wt. % of freeze-dried CNCs), suggesting that the CNCs act as a nucleating agent for PLLA.[129]

These latter observations have been made in a number of studies and as such, the ability of CNCs to enhance the barrier properties is one of the advantages of the PLA/CNC composites. It has been shown that the degree of barrier improvement for PLA-based CNC nanocomposites depends on the surface modification of the CNCs and the processing methods.[130,131] In addition, it was also reported that the type of CNC polymorph (cellulose I vs. cellulose II) employed can play a role in barrier properties. Dhar et al. showed that the incorporation of 3 wt. % *bamboo*-CNC-SO_3^- (either in the

cellulose I or cellulose II form) into PLLA by solvent exchange into chloroform (via acetone) and casting, resulted in films with different oxygen permeation properties; 14.0 $cm^3/m^2/day$ for cellulose I CNC composites and 7.8 $cm^3/m^2/day$ for cellulose II CNC composites.[122] A common hypothesis used to explain why CNCs improve barrier properties is that the addition of these non-permeable crystals results in a more tortuous pathway for transport of gas or water molecules through the film, whereas the matrix without crystals does not hinder this transport (Figure 1.7).[132] In addition, the increased PLLA crystallinity induced by the nucleating effect of the CNCs reduces free volume between chains and creates more internal impermeable barriers that further limit the diffusion of small molecules.[133] It is worth noting that improved barrier properties have been observed upon incorporating CNCs into other bio-based matrices such as alginate, polyhydroxybutyrate (PHB), and starch.[134–138]

Petersson et al. investigated a slightly different protocol to access PLA/CNC composites. In this case the *w*-CNC-SO_3^- were solvent transferred from water to *t*-butanol and the *t*-butanol CNC dispersion was then freeze-dried. Those freeze-dried CNCs were then dispersed in chloroform by ultrasonication.[139] *t*-Butanol has a melting point of 23–25 °C, which was expected to accelerate the freezing of the suspension and thereby limit the aggregation of the CNCs during the freezing process. The mechanical

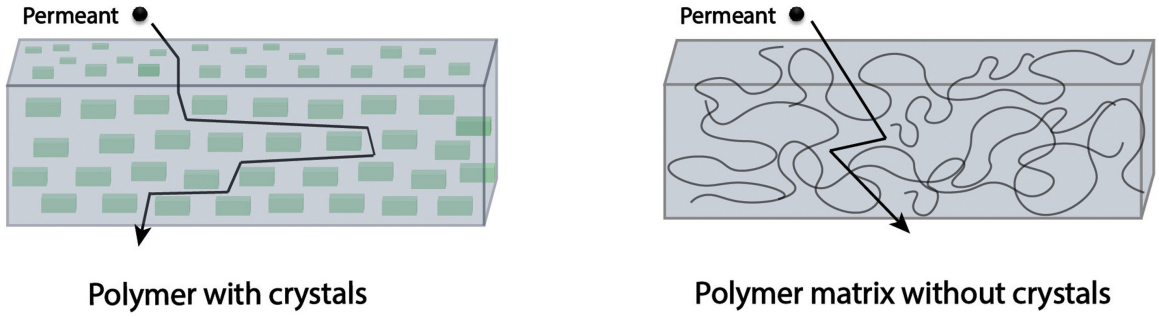

Figure 1.7: The presence of non-permeable crystals (e.g. CNCs) in the polymer matrix (left) increases the permeant tortuosity/path length, thus reducing permeability of water vapor and oxygen relative to an amorphous polymer matrix (right).[132]

properties of PLA/CNC composites prepared from chloroform suspensions of either *t*-butanol freeze-dried *w*-CNC-SO_3^- or water freeze-dried *w*-CNC-SO_3^- showed that there is indeed a better mechanical reinforcement when using the *t*-butanol freeze-dried *w*-CNC-SO_3^- (Figure 1.8a). At 60 °C there is 64 % increase in storage modulus (E′) for 5 wt. % *t*-butanol freeze-dried *w*-CNC-SO_3^- relative to a 23 % increase when using water freeze-dried *w*-CNC-SO_3^-. In addition, there is a shift to higher temperatures in the tan δ peak by 15 °C with the *t*-butanol freeze-dried *w*-CNC-SO_3^- films (compared to the films made with water freeze-dried *w*-CNC-SO_3^-), indicating a more pronounced effect on the segmental motion of PLA chains in these composites (Figure 1.8b) which is consistent with a better dispersion.

Petersson et al. also investigated the use of surfactants as an alternative to improve the dispersion of the CNCs in PLA. It was assumed that the surfactant would hinder the hydrogen bonding between the CNCs during the freeze-drying process and result in a better distribution within the matrix. The selected surfactant, Beycostat A B09 (BNA), a phosphoric ester of polyoxyethylene(9)nonylphenyl ether, had been employed earlier by Heux et al. as a coating for *c*-CNC-SO_3^- and *t*-CNC-SO_3^- to yield birefringent

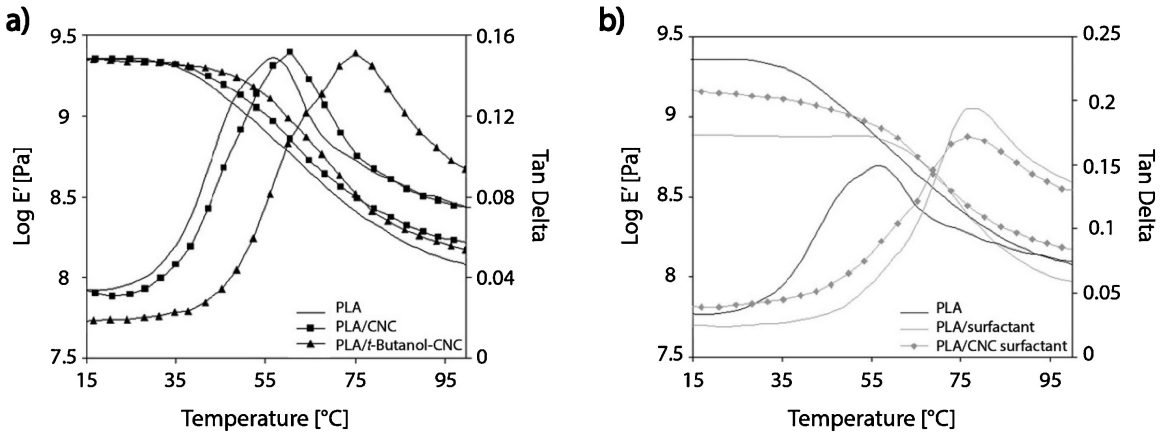

Figure 1.8: Storage modulus and tan delta curves determined by DMA measurements of a) a comparison of neat PLA, PLA/CNC, and PLA/*t*-butanol freeze-dried CNC composites and b) a comparison of neat PLA, PLA/BNA surfactant, and PLA/CNC/BNA surfactant composites.[139]

toluene suspensions.[48] The surfactant coated *w*-CNC-SO_3^- also showed birefringence when dispersed in chloroform (which was not observed with the t-butanol freeze-dried *w*-CNC-SO_3^- discussed above), highlighting the benefit of the surfactant to improve the dispersion of the nanofillers. The composites where made by simple solution casting, resulting in a transparent film upon melt pressing, consistent with good dispersion of the CNCs in the matrix. Comparison of dynamic mechanical analysis (DMA) curves of PLA/surfactant composites with the PLA/surfactant/*w*-CNC-SO_3^- composites showed that the CNC composite materials had an 83 % greater storage modulus at 20 °C. However, it is important to note that both materials show reduced modulus relative to neat PLA at this temperature. In fact, while there is a shift in tan δ of ca. + 20 °C for the surfactant containing materials relative to PLA, there is only a small increase in modulus for the PLA/*w*-CNC-SO_3^-/surfactant composites relative to PLA observed above 55 °C. Overall, while these CNCs may be well dispersed in the matrix, the mechanical studies are indicative of the surfactant coating on the CNCs preventing direct interactions between the PLA and the CNCs. As such, while it is important to obtain well dispersed CNCs in a matrix, this in and of itself is not enough to obtain good mechanical reinforcement. Ensuring good interfacial adhesion between the filler and matrix and/or good filler-filler interactions are also important considerations.

One application-focused benefit of surfactant addition is the blocking of hydrophilic groups on the CNC surfaces, which can reduce water uptake and transport. Reduced water vapor permeability (WVP) prevents bacterial growth in packaging materials, but the hydrophilic nature of negatively-charged CNCs can be antithetical to this goal.[140] In one study, Fortunati and coworkers showed that the reduction in WVP caused by increased tortuosity and crystallinity in a PLA matrix was offset entirely by the hydrophilicity of *w*-CNC-SO_3^- at 1 wt. % loading.[141] Adding surfactant (Beycostat A B09) blocked the hydrophilic surface groups from associating with water molecules and

decreased WVP by 34 % relative to the negatively-charged *w*-CNC-SO_3^- composites at the same 1 wt. % loading.

Water uptake of PLA-based materials can have significant effects on their material properties. The degradation rate of PLA has been shown to be influenced by the relative humidity of the surrounding environment, with more humid environments causing PLA to degrade more quickly.[142] More rapid degradation of PLA/cellulose fiber composites has been observed with both macrocellulose (wood pulp and wood fibers)[143] as well as nanocellulose[144] composites, where the rate changes are attributed to the increased water uptake caused by the hydrophilic cellulose. To further back up this hypothesis, the use of surfactant-coated CNCs at a 1:1 surfactant to CNC weight ratio resulted in a reduced PLA degradation rate under composting conditions with 5 wt. % *w*-CNC-SO_3^-/surfactant in a PLA matrix.[144] While not extensively investigated in many matrices, it may be possible to somewhat tune the degradation rate of CNC sustainable composites through the hydrophilic or hydrophobic modification of the nanocrystal surface, broadening the application window for bio-based CNC composite packaging materials.

The future of packaging materials is trending toward more active materials which, for example, have antimicrobial characteristics built into the packaging, reducing the likelihood of bacterial build up over the lifetime of the product. Unmodified negatively-charged CNCs have few to no antimicrobial properties, but the addition of other additives, such as silver nanoparticles, can impart these desired effects.[141] Unfortunately, the same hydrophobic surface modifications that have been used to reduce water uptake have also been shown to have negative effects on antibacterial nanoparticle migration and leeching. Fortunati and coworkers showed enhanced leeching in PLA films filled with *w*-CNC-SO_3^- coated with an ethoxylated nonylphenol surfactant and silver nanoparticles,[145] presumably on account of increased mobility

in the hydrophobic surfactant layer. In some cases, as much as a 10-fold increase in nanoparticle leeching was observed relative to the neat PLA films or PLA loaded with unmodified *w*-CNC-SO_3^-.

Surfactants are not the only additives that have been investigated to access improved PLA/CNC composites. Oksman et al. studied the use of N,N-dimethylacetamide (DMAc) with LiCl for the preparation of CNC-based PLA nanocomposites.[146] It is important to note that DMAc/LiCl mixtures with high LiCl content dissolve cellulose, generating individual cellulose macromolecules.[147,148] However, DMAc containing a lower amount of LiCl (0.5 wt. %) can be utilized to separate individual *w*-CNC-SO_3^- from microcrystalline cellulose (MCC) with ultrasonication and allow access to relatively concentrated *w*-CNC-SO_3^- suspensions (10–17 wt. %). Oksman et al. investigated melt mixing of PLA with the concentrated DMAc/LiCl/*w*-CNC-SO_3^- suspensions. The CNC suspensions (enough to obtain 5 wt. % CNCs in the final composite) were pumped directly into an extruder containing molten PLA at 170-200 °C. The extruder was equipped with several venting systems that allowed the removal of vapors upon heating (Figure 1.9a).[146] However, using this melt processing technique resulted in brown/degraded materials. To address this issue processing aids, such as polyethylene glycol (MW = 1,500 g/mol) (15 wt. %) or maleated PLA (PLA-MA, 2.2 % maleic anhydride) (10 wt. %), were incorporated into the molten PLA to decrease the viscosity or act as a coupling agent, respectively.

Figure 1.9b shows the stress-strain curves of three different compositions of the melt processed PLA using this technique. PLA_{DMAc} is the film formed by simply injecting a DMAc/LiCl solution (i.e. no CNCs) into molten PLA and shows stress at break and strain at break similar to neat PLA. Adding in the DMAc/LiCl/*w*-CNC-SO_3^- suspension to a molten mixture of PLA and PLA-MA results in a film that exhibits almost double the tensile strength relative the PLA_{DMAc} (ca. 78 and 40 MPa, respectively) and an

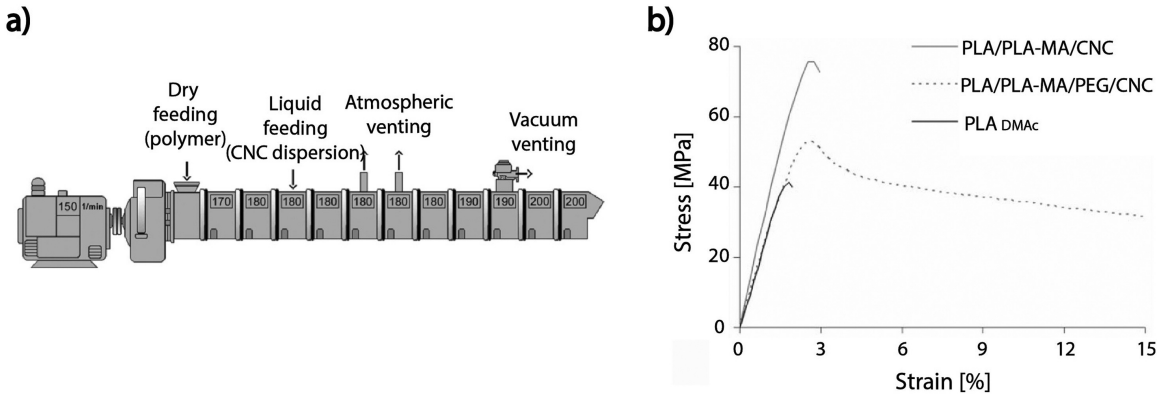

Figure 1.9: a) Scheme showing the different compartments (feeding zone, venting zone and vacuum zone) of an extruder used to process CNC composites, and b) the comparison of the measured tensile stress strain curves of PLA/PLA-MA/CNC, PLA/PLA-MA/PEG/CNC, and PLA_{DMAc}.[146]

increase in Young's Modulus (3.9 vs. 2.9 MPa). These values compare well with PLA composites containing maleic anhydride-modified multi-walled carbon nanotubes (MA-MWCNT).[149] The PLA/MA-MWCNT material showed a tensile strength of around 76 MPa at a similar 4 parts per hundred loading, showing that the CNC-based composites offer a competitive, renewable alternative to MWCNTs in this case.

Interestingly the addition of PEG (1500 g/mol) to the melt processed PLA/PLA-MA/PEG/*w*-CNC-SO_3^- films yields a more ductile material that exhibits an eight times increase in the strain at break (up to 18 %) while also showing a slight increase maximum tensile strength relative to PLA_{DMAc}. No explanation was provided on why the PEG improved the ductility of this PLA/PLA-MA/PEG/*w*-CNC-SO_3^- composite. However, similar effects have been observed previously in other PEG/CNC-containing composites and have been attributed to the interactions between the low molar mass PEG and CNCs, reducing CNC-CNC interactions and improving their dispersion in the matrix.[150] While the use of DMAc/LiCl/*w*-CNC-SO_3^- does allow access to melt processable PLA/CNC composites, the DMAc/LiCl appears to result in the degradation of the *w*-CNC-SO_3^- at high temperatures,[146] as was suggested by the brown-colored composites obtained. As such, optimization in the compounding process would require

the use of a feed medium which does not cause CNC (or PLA) degradation at the high temperatures required for processing. Additionally, this study highlights how the addition of a coupling/compatibilizing agent (in this case the PLA-MA) into the polymer melt can be used to prevent/inhibit the re-aggregation of the CNCs upon removal of the dispersing medium.[151,152]

The use of plasticizers has been investigated as a way to access more flexible PLA/CNC composites. For example, the natural compound limonene has been shown to plasticize PLA (20 wt. % blended into PLA drops the T_g from 58 to 42 °C), lower its crystallinity, and improve its barrier properties, which are important factors in packaging films. To access PLA/limonene/CNC composites, the PLA and limonene were melt blended (15–25 wt. % of the plasticizer at ca. 180 °C) prior to the direct addition of 1 or 3 wt. % of *ph*-CNC-SO_3^- (dried at 40 °C overnight) to the molten polymer.[57,153] The resulting films were transparent and exhibited a single T_g (DSC) at ca. 34 (1 wt. %) or 32 °C (3 wt. %). The DSC also revealed a decrease in the cold crystallization temperature (T_{cc}) of PLA in the composites consistent with the dispersed *ph*-CNC-SO_3^- promoting the crystallization of the matrix in the plasticized PLA.[154] The PLA/limonene/*ph*-CNC-SO_3^- composites revealed high values of elongation at break 288 % (1 wt. % CNC) and 272 % (3 wt. % CNC) primarily as a consequence of the plasticization effect of the limonene (PLA/limonene has an elongation of break ca. 250 %). As such, adding *ph*-CNC-SO_3^- (up to 3 wt. %) to the PLA/limonene system appears not to significant effect the mechanical properties.

The above discussion shows that it is possible to utilize different processing techniques and/or additives to enhance the dispersion of the CNCs in PLA. However, to date the amount of mechanical reinforcement in such composites has not been optimized. The use of plasticizers/surfactants may enhance the mobility of PLA chains in the matrix, benefiting elongation at break, but they can also block CNC-CNC interactions along with

filler-matrix interactions. As such, while the organization of such agents at the CNC surfaces may improve dispersion, it can also reduce the ability for stress transfer from the matrix to the filler, limiting mechanical reinforcement. Thus, a key challenge here is how one effectively quantifies the level of dispersion of the CNCs within the matrix. Does one method provide better dispersion than another? Given that the different processes discussed above add in a variety of different components, it is hard to isolate the simple effect of the added component from the effect of CNC dispersion on the material properties. Instead, one must rely on less objective evidence, like birefringence in solution and transparency of materials, but neither of these provide a quantifiable level of homogeneity. In the end, what is important is how well does a given processing technique improve the properties of the composite, but there is certainly an argument to be made for the development of more comprehensive methods for measuring the CNC filler dispersion.

1.3.2.2 Poly(lactic acid)-based composites with polymer-grafted CNCs

Given the challenges of dispersing CNCs in PLA, primarily on account of the differences in polarity of the filler and matrix, covalent functionalization of the CNCs is an alternative strategy to adding additives to aid their dispersion in PLA. Most of the work in this area has focused on grafting polymers to the CNCs and investigating the resulting PLA composites. It has been demonstrated that the grafting of polymer chains to the CNC surface can not only improve the dispersion of the CNCs within the matrix but can also enhance the interfacial adhesion between the filler and matrix.[155,156] Grafting of polymers to the CNCs prevents aggregation of the nanocrystals through steric hindrance and the nature of the interactions between the grafted polymer and matrix can be used to facilitate dispersion within the matrix.

Polymer grafting to the CNCs can be achieved by either a “grafting-to” approach,

where a pre-formed polymer chain is reacted with functional groups on the CNC surface, or "grafting-from" method, where an initiating site on the surface is used to polymerize the monomer directly from the CNCs. For PLA specifically, the "grafting-from" approach has generally been employed in the preparation of the modified fillers, predominantly through the use of the surface -OH groups as initiating sites for ring opening polymerization (ROP).[157–160] Not surprisingly, the most common polymer grafted from the CNCs in this context is PLA (Figure 1.10a). This is most commonly achieved using tin(II)-based catalysts and, through the variation of the monomer concentration, time, and/or the addition of "free" OH groups, the molecular weight of the grafts can be somewhat controlled.[161]

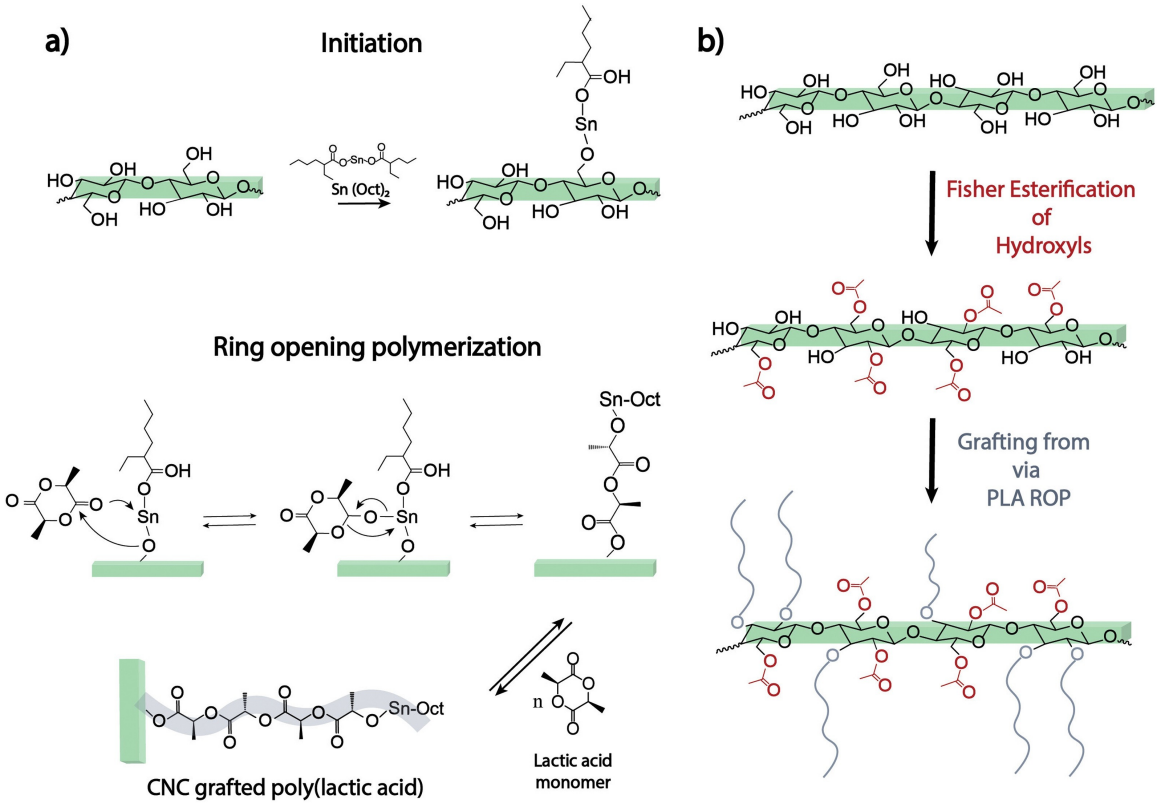

Figure 1.10: a) Synthetic path of a ring opening polymerization of poly(lactic acid) initiated on the surface of the CNC in the presence of catalyst, tin(II) 2-ethylhexanoate ($Sn(Oct)_2$). b) Scheme illustrating an acetylation procedure to partially functionalize the surface of the CNCs.[157]

Generally, it is expected that grafted chains with higher molecular weight will penetrate deeper into a polymer matrix, assuming a constant matrix molecular weight and neutral or favorable interactions between the polymer graft and the matrix.[162] This should enhance the interfacial adhesion between the matrix and filler and result in better stress transfer from the matrix to the nanomaterial when load is applied. While not on CNCs, Lönnberg et al. have shown that polycaprolactone (PCL) composites (matrix M_n ca. 80,000 g/mol) containing 10 wt. % PCL-grafted microfibrillated cellulose (MFC-*g*-PCL) exhibited better mechanical reinforcement with MFC-*g*-PCL that have longer grafts (Young's Modulus ca. 325 MPa for graft with M_n ca. 2200 g/mol and 290 MPa for graft with M_n ca. 700 g/mol). This compares to a Young's modulus of 190 MPa for the neat PCL and 260 MPa for the PCL reinforced with unmodified MFC.[163] However, this increase in stiffness does come at a cost of ductility, where the neat material had an elongation at break of roughly 900 % while all of the 10 wt. % composite materials fractured at less than 25 % strain. Chapter 2 of this thesis will investigate the effects of varying grafted polymer molecular weight and grafting density in-depth.

Goffin et al. prepared *rf*-CNC-*g*-PLLA by carrying out the ROP of L-lactide in toluene-dispersed *rf*-CNC-SO_3^-, obtained via a solvent exchange process. The polymer-grafted *rf*-CNC-*g*-PLLA were shown to result in more stable chloroform suspensions after 3 days than the unmodified *rf*-CNC-SO_3^- or a blend of PLLA with *rf*-CNC-SO_3^-, thus highlighting the benefits of the polymer modification for compatibility with non-polar media.[158] Composites were prepared by melt-blending *rf*-CNC-*g*-PLLA in PLLA with up to 8 wt. % filler, which resulted in nearly colorless materials with varying degrees of transparency depending on the CNC content (more CNCs resulted in hazier materials). Comparatively, materials prepared with *rf*-CNC-SO_3^- showed the expected thermal degradation upon melt processing at the same temperatures, 185–200 °C, suggesting that the polymer grafting aids the thermal stability of the CNCs. As seen

in Section 1.3.1.3 with negatively-charged CNCs, these functionalized CNCs are also capable of acting as nucleating agents in semi-crystalline matrices.[164] DSC analysis of the PLLA/*rf*-CNC-*g*-PLLA composites showed an increased in crystallinity and a decreased crystallization half-time (the time at which the extent of crystallization reaches 50 % completion) with the addition of *rf*-CNC-*g*-PLLA. At room temperature, no reinforcing effect is observed; however, reinforcement above T_g is seen and is primarily attributed to the increased PLLA crystallinity restricting the polymer chain mobility.[165] Interestingly, DMA showed a drop in the glass transition temperature at 8 wt. % loading, suggesting that the filler may also have a plasticizing effect on the matrix.

Braun et al. have investigated the use of CNCs with a lower polymer grafting density.[157,166] This was achieved by acetylation of freeze-dried CNCs (*w*-CNC-Ac) resulting in blocking/protecting many of the possible -OH initiation sites. This procedure gave access to *w*-CNC-Ac with up to 60–70 % of the OH groups functionalized according FTIR (Figure 1.10b). The group conducted grafting-from ROP reactions from freeze-dried *w*-CNC-Ac in either toluene solution or in the bulk monomer (L-lactide) to yield the polymer-grafted acetylated CNCs (*w*-CNC-Ac:-*g*-PLLA). The acetylation and PLLA grafting were confirmed by the appearance of characteristic ester carbonyl peaks at 1736 cm^{-1} for the acetate and 1760 cm^{-1} for the polymer (Figure 1.11a). PLA/*w*-CNC-Ac:-*g*-PLLA composites were prepared by mixing a PLA solution in chloroform with a chloroform suspension of *w*-CNC-Ac:-*g*-PLLA to create films with up to 25 wt. % *w*-CNC-Ac:-*g*-PLLA. After evaporation of the solvent, the resulting composites were compression molded and resulted in highly transparent materials, suggestive of a good dispersion of the modified fillers within the matrix (Figure 1.11b). Composites prepared with the solution-functionalized *w*-CNC-Ac:-*g*-PLLA had a substantially greater heat distortion temperature (150 °C at a filler loading of 15 wt. %) compared to composites made with the bulk-functionalized *w*-CNC-Ac:-*g*-PLLA

(115 °C at the same loading). This is compared to 70 °C for the neat PLA and 80 °C for the PLA/*w*-CNC-Ac composites (Figure 1.11c). The difference between the two *w*-CNC-Ac:-*g*-PLLA nanocomposites highlights the importance in considering the polymer grafting methodology, which will impact the amount and molecular weight of the grafted polymer, factors that can play a significant role in the final properties of the composites.

As before, the crystallization half-time of the PLA composites with 5 wt. % *w*-CNC-Ac:-*g*-PLLA quenched to 110 °C from the melt was 45 s compared to 90 s for neat PLA (Figure 1.11d). A further reduction of the crystallization half-time, down to 15 s, was observed upon increasing the CNC loading to 15 and 20 wt. % (Figure 1.11d). This is a useful result as one of the challenges of PLA from an industrial perspective is its slow crystallization time.[167]

An aspect of PLA that we have not yet touched upon is its ability to form stereocomplexes.[168] PLLA has a melting point of 170–190 °C and a T_g of 50–65 °C, while racemic PLA is amorphous with a T_g ca. 50–60 °C. PDLA/PLLA blends form semi-crystalline stereocomplexes that have a melting point at 220–240 °C and a T_g ca. 65–70 °C, showing thermal improvements over the individual components.[168] Thus, conceptually, one can envisage grafting one stereoisomer (i.e. D-lactide) from the CNC and incorporating it in a matrix of the other (i.e. L-lactide) to obtain a material with enhanced properties. Zhang and coworkers employed this approach and obtained transparent PLLA/*c*-CNC-*g*-PDLA composite films by solvent casting from chloroform, which suggested that the modified filler had good dispersion within the matrix.[169] The composites also exhibited significant improvements in heat distortion resistance (40 % strain for the 10 wt. % composite after 10 min at 80 °C with a load of 50 g vs. 220 % for neat PLLA under the same conditions), but T_g shifted to lower temperatures as *c*-CNC-*g*-PDLA content increased from 0 to 10 wt. %.

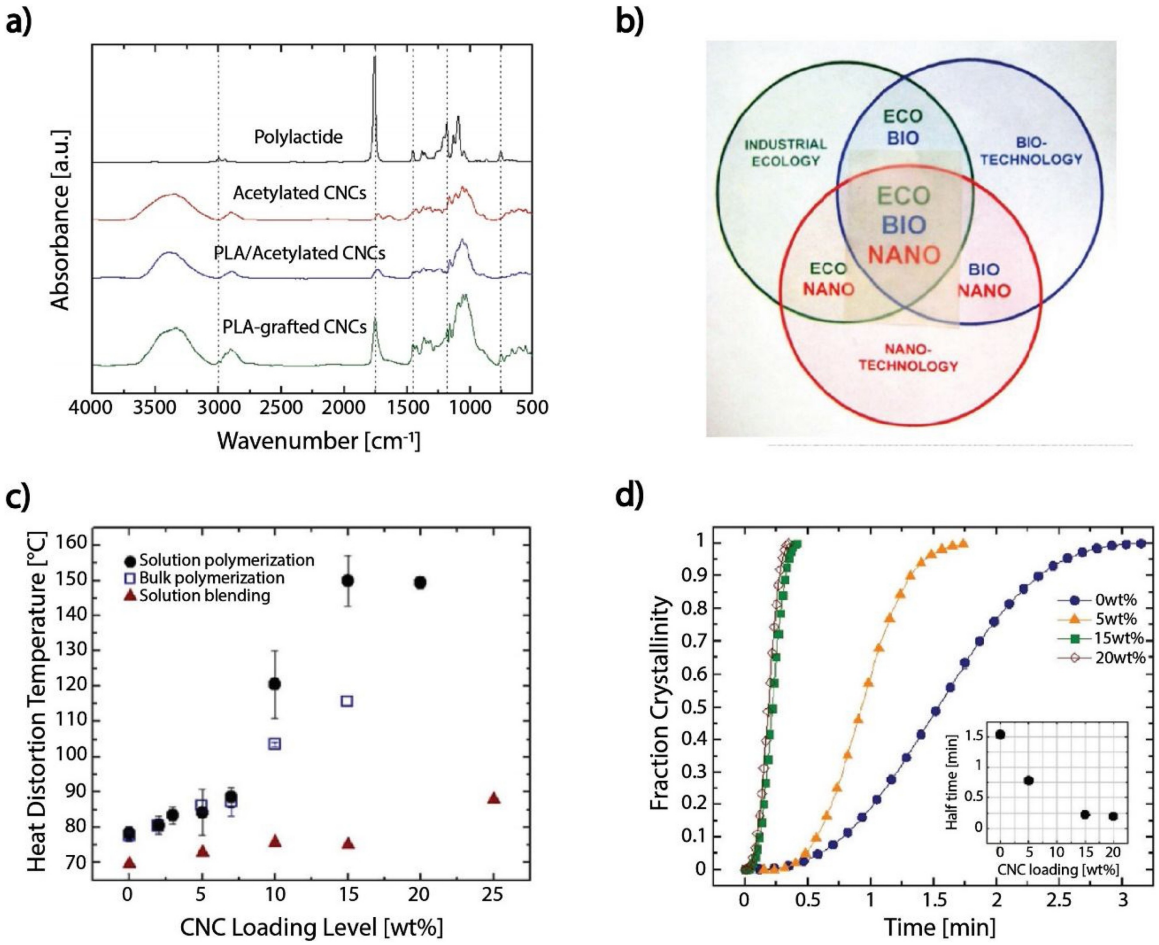

Figure 1.11: a) Comparison of FTIR spectra of PLA (black), *w*-CNC-Ac (red), PLA/*w*-CNC-Ac (blue) and *w*-CNC-Ac:-*g*-PLLA (green). Dotted lines indicate PLA signals that do not overlap with peaks originating from the CNCs. b) Melt-pressed films of PLA/*w*-CNC-Ac:-*g*-PLLA nanocomposite with 10 wt. % *w*-CNC-Ac:-*g*-PLLA loading. c) Comparison of the obtained heat distortion temperature for nanocomposites prepared by in situ polymerization in-solution and in-bulk compared with solution-blended nanocomposites, as a function of CNC weight loading. d) Comparison of the fraction of crystallinity over time for PLA composites with solution-polymerized *w*-CNC-Ac:-*g*-PLLA when the materials are quenched from the melt to 110 °C. The crystallization half-time as a function of the content of CNC is plotted in the inset.[157]

Another key challenge for PLA is to develop ways to improve its toughness. While toughness improvements can be achieved by blending soft, ductile polymers, such as natural rubber or poly(butylene succinate) (PBS), into the matrix,[170] an alternative approach has utilized PLA's stereocomplex characteristics.[168] Muiruri et al. grafted a

random copolymer block of ϵ-caprolactone (CL) and D-lactide (DLA) on *w*-CNCs in toluene followed by a homo-D-lactide block to act as a compatibilizing block between the filler and the matrix.[171] The inclusion of CL into the grafted polymer was intended to act as a rubbery phase to absorb deformation energy and improve toughness of the composite material. The nanocomposites were prepared by solution casting a mixture of PLLA and 2.5 wt. % *w*-CNC-*g*-P(CL-*r*-DLA-*b*-DLA) in chloroform and subsequently melt processing by injection molding. The stereocomplexation of the grafted D-lactide chains with the L-lactide matrix, enhanced filler–matrix interactions and inclusion of 2.5 % of the filler increased the toughness by 20 times, but decreased the tensile strength and modulus on account of plasticization. Scanning electron microscopy (SEM) and small-angle X-ray scattering (SAXS) measurements showed the major toughening mechanisms to be fibrillation and crazing during deformation of the nanocomposites.[171] Such a biodegradable and tough CNC-filled PLA nanocomposites could open up new application avenues for PLA-based materials and will be discussed further in Chapter 4 of this thesis.

1.3.3 Poly(3-hydroxybutyrate)-based composites with negatively-charged CNCs

Poly(3-hydroxybutyrate) (PHB) is a thermoplastic polyester belonging to the family of polyhydroxyalkanoates which can be produced by bacteria or from sources such as plants, sugar cane, etc.[172] As a result of its similar properties to petroleum-based polymers like PP (such as melting temperature ca. 180 °C and tensile strength ca. 30 MPa), combined with biodegradability and biocompatibility, PHB has been widely studied with a specific focus in biomedical[173,174] and food packaging applications.[175] However, material brittleness and a narrow processing window (low degradation temperature ca. 220 °C) still remain as challenges for broader implementation. One

approach to overcome these issues is the addition of plasticizers and fillers, such as CNCs, to tune the thermal and physical properties of PHB composites without altering the overall material biodegradability.[176–178]

PHB is insoluble in water, making the processing of well dispersed PHB/CNC materials a challenge, similar to most other CNC composite systems. As such, solvent casting is most often done from organic solvents that can dissolve PHB, like DMF or chloroform.[178] Simple composites of PHB with CNCs have been investigated, but the expected increase in brittleness without improving thermal stability was observed, which is why the use of other additives is also necessary.[178] For example, Orefice et al. were able to achieve a birefringent dispersion of *w*-CNC-SO_3^- in a PHB matrix by using low molar mass PEG (200 g/mol) as a dispersing agent and plasticizer.[179] At first, *w*-CNC-SO_3^- were dispersed in PEG by evaporating the water from a PEG/*w*-CNC-SO_3^- solution (Figure 1.12 inset), then the PEG/CNC blend was dissolved in a chloroform solution containing 5 w/v % PHB. Homogeneous PHB/PEG/*w*-CNC-SO_3^- (constant 15 wt. % PEG relative to PHB) composite films, as visualized under SEM, were obtained with varying CNC content by casting the mixture, evaporating off the solvent at room temperature, followed by drying at 40 °C. These PHB/PEG/*w*-CNC-SO_3^- nanocomposite films exhibited a significant increase of the elongation at break (50 times greater than neat PHB and 25 times greater than PHB/PEG blends). While there was no significant loss of tensile strength (ca. 15–20 MPa), these composite materials did exhibit a substantial decrease in modulus (from > 600 to < 100 MPa from 0 wt. % to 0.45 wt. %) (Figure 1.12). In addition to these mechanical changes, thermal stability was shown to be enhanced in the PHB/PEG/*w*-CNC-SO_3^- systems when compared to the PHB/PEG materials. The inclusion of CNCs was able to delay thermal degradation to be comparable to neat PHB, with degradation onset around 270 °C, which is around 40 °C better than the PHB/PEG system. All of these changes support the ability of CNCs to enhance the processing and

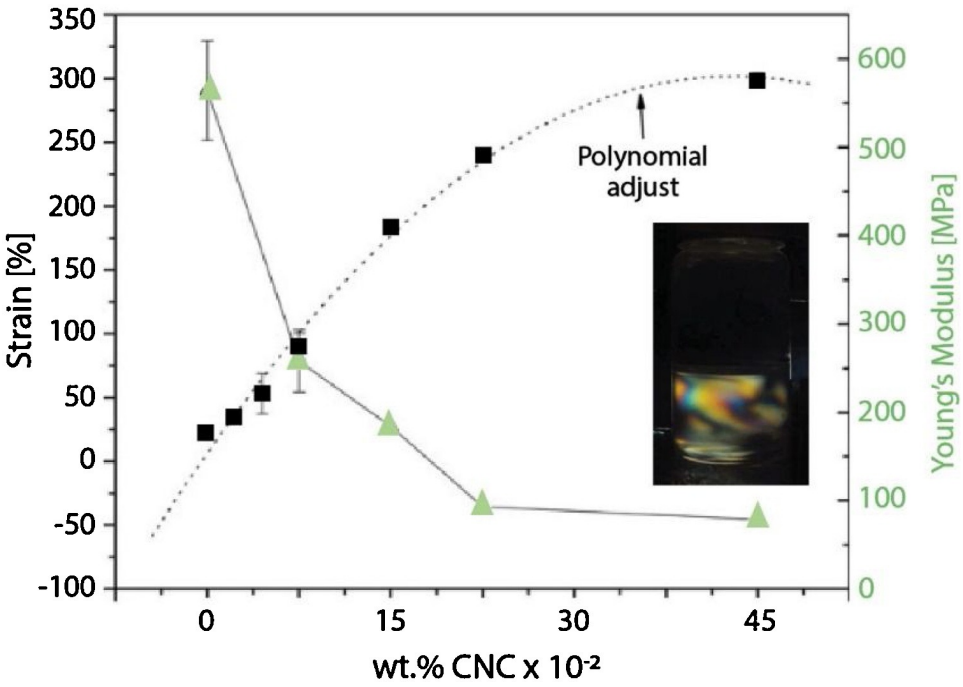

Figure 1.12: The strain at break and Young's modulus of PEG/PHB composite with low CNC content. (Inset: PEG/CNC dispersion at 1 wt. %, observed between cross-polarizers).[179]

application window of PHB.

PHB and PLA can be blended together to expand their property profile, resulting in improvements in both mechanical and barrier properties.[180] As such, CNC composites of these blended materials are also of interest.[141] Fortunati et al. melt-mixed 5 wt. % *w*-CNC-SO_3^- or freeze-dried surfactant-coated (STEPFAC 8170, nonylphenol phosphate ester) *w*-CNC-SO_3^- in 1:1 (w/w) with melt-blended PLLA/PHB (75:25 wt. %) plasticized with 15 wt. % of acetyl tri-n-butyl citrate (ATBC) (relative to the PLLA/PHB blend).[181] The ATBC was added to enhance the PLLA and PHB chain mobility and promote the dispersion of the CNCs within the matrix.[182] The transparency of the resulting materials suggested a good dispersion of the CNCs within the matrix for the composites made with either unmodified or surfactant-coated CNCs. However, transmission electron microscope images revealed some flakes within the PLLA/PHB/*w*-CNC-SO_3^- system, while the surfactant-modified CNCs did not show the formation of such

agglomerates. SEM micrographs of the fractured cross-sections revealed rough surfaces and the formation of voids in the PLLA/PHB/ATBC materials, while the incorporation of either unmodified *w*-CNC-SO_3^- or surfactant-coated *w*-CNC-SO_3^- eliminated these voids. The authors suggest that the ATBC plasticizer resulted in a reduction of viscosity in the system, which facilitated processing and ultimately promoted the dispersion of CNCs in the polymer blend. However, the ATBC plasticizer does have side effects, as noticed in the barrier properties of the films. The PLLA/PHB/*w*-CNC-SO_3^- transmitted 13 cm^3/m^2/day of oxygen while the plasticized PLLA/PHB/ATBC/*w*-CNC-SO_3^- showed a rate of 23 cm^3/m^2/day, both compared to neat PLA at ca. 30 cm^3/m^2/day. A T_g increase from 31 to ca. 45 °C with the incorporation of the CNCs into PLLA/PHB/ATBC suggests good filler matrix interactions (Figure 1.13). In addition, two melting peaks are observed for the plasticized blends, one for PLLA (149 °C) and one for PHB (172 °C). However, there is only one melting peak at 147 °C in the PLLA/PHB/ATBC/*w*-CNC-SO_3^- composites, suggesting a drop of the overall crystallinity in this material, possibility as a result of the *w*-CNC-SO_3^- increasing compatibility between the PLA and PHB. The incorporation of the *w*-CNC-SO_3^- to PLLA/PHB/ATBC resulted in almost no changes to the Young's modulus but did significantly reduce the elongation at break (27 vs. 90 %). However, the incorporation of surfactant modified *w*-CNC-SO_3^- into the polymeric blends resulted in an increase in the elongation at break (up to 147 %) allowing access to more ductile materials. These composite films showed a clear increase in degradation rate when CNCs and/or plasticizer were included in the blend, cutting degradation time in half for some samples. This is most likely attributable to the presence of more water within the matrix making hydrolysis more likely.

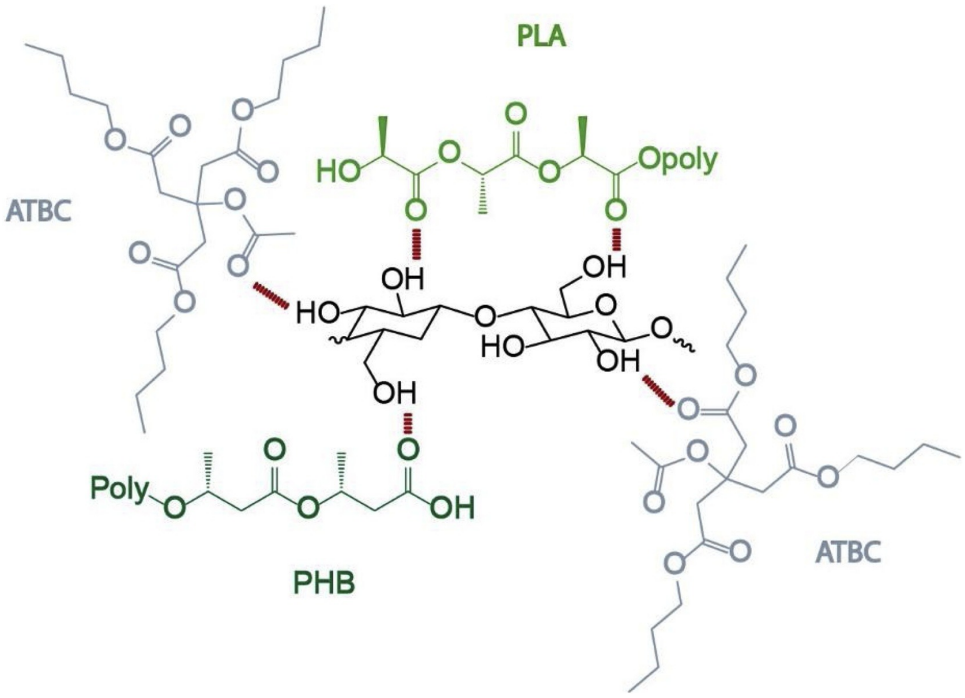

Figure 1.13: The suggested molecular interaction on the CNCs with PLA, PHB, and ATBC in the composite.[181]

1.4 Other potential applications of sustainable cellulose nanocomposites

As covered in the previous sections, the ability for cellulose nanocrystals to positively impact properties of bio-based polymers has received significant attention in the past decade. While understanding the structure-property-processing relationships in these sustainable composites is an important goal, a parallel question to be addressed is where are the potential applications for such materials? The following section aims to highlight selected application areas in which CNCs, and their bio-based composites, may show promise that go beyond the mechanical reinforcement and packaging applications that have been touched upon in the prior sections.

1.4.1 Compatibilization of immiscible polymers

Most polymers are immiscible and as such, when they are blended together, the result is a macrophase-separated material with poor physical properties. Compatibilization is the process of stabilizing the interface between the two immiscible polymers, thus creating a more homogenous material with improved properties. Compatibilizers include surfactant-like molecules and block copolymers that are able to organize at the interface and lower the surface energy between the two phases. From a recycling perspective, the use of compatibilizers is attractive as it potentially offers a more facile route to processing recycled polymers by reducing the need for costly separations.[183] Given that CNCs can be used to reinforce polymer matrices, if they can be used as a compatibilizer, as opposed to molecular or polymer-based surfactants, then the resulting recycled material may show even more enhanced mechanical properties. This would create a potential opportunity for upcycling plastic waste, which is when regenerated material has the same or more value than the virgin supply.[184]

Habibi and coworkers reported an early example of immiscible polymer blends being compatibilized by *rf*-CNC-SO_3^- in a PLLA/PCL system.[185] The ternary composites of the PLLA/PCL blend along with either *rf*-CNC-SO_3^- or *rf*-CNC-*g*-PLLA-b-PCL showed a 2 or 3 order of magnitude increase in the storage modulus (over 1000 MPa) when compared to the binary PLLA/PCL system (ca. 5 MPa). The composite microstructure appeared much more homogenous compared to the blend without CNCs (Figure 1.14). Similar compatibilization effects of CNCs have also been observed in less sustainable matrices, such as poly(vinyl alcohol)/PEO blends.[186] Such observations suggest that is may be possible to utilize CNC-based fillers to combine the previously mentioned mechanical, thermal, and barrier property improvements with compatibilization, expanding the capabilities of both virgin and recycled blends.

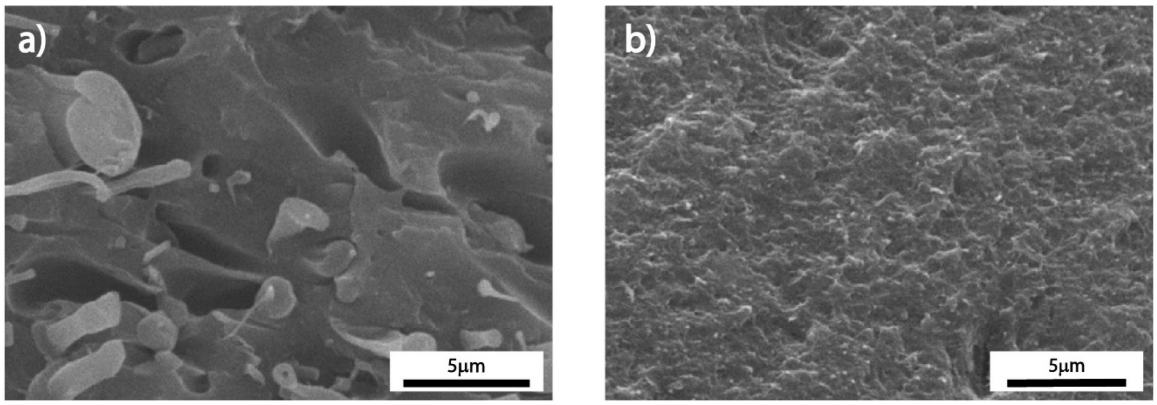

Figure 1.14: a) SEM image of PLLA/PCL (1:1) polymer blend showing clear phase inhomogeneity between the two polymeric materials and b) a PLLA/PCL (1:1) blend with 2 wt. % of *rf*-CNC-SO_3^- showing a much more homogenous morphology.[185]

1.4.2 Water filtration

As discussed earlier, hydrophilic CNCs enhance the diffusion of water into polymer matrices, begging the question of whether these systems would be viable as membranes and filters for water purification. If the CNCs are also functionalized with a binding motif, such systems could be tailored for selective filtration and toxin removal. Saito and Isogai were the first to show that TEMPO-oxidized *c*-CNC-COOH were capable of metal ion adsorption from aqueous solutions by association of the metal ions with the deprotonated carboxylate groups.[187] From that point, the field has expanded tremendously with work towards enhancing uptake of targeted ions, such as lead, through functionalization of the CNCs with specific binding motifs and towards stripping the sequestered material in order to recover and reuse the filtration material.[188–190] In one example, Mathew and coworkers made bio-based membranes by vacuum filtration of a 1:1 gelatin/*w*-CNC-PO_3^- solution on a cellulose microfiber support followed by melt pressing at 80 °C.[191] The resulting uniform membrane was capable of high flux (almost 3000 L/h/m^2 at 1 bar) and high capacity uptake of metal ions such as Cu^{2+} (358 mg/g of CNC in the filter) and Fe^{3+}/Fe^{2+} (512 mg/g). For comparison, carbon nanotubes have a

Cu^{2+} sorption capacity of 67.8 mg/g of filtration material.

1.4.3 Biomedical CNC-containing bio-based materials

CNCs have been investigated in a wide range of different biomedical materials. In this regard there are a few biomedical application areas for which fully bio-based composites have received some attention.[192,193]

One area where CNC-containing bio-based hydrogels have been investigated is as drug delivery vehicles. For example, Dufresne and coworkers blended *c*-CNC-SO_3^- into a crosslinked alginate core and subsequently adsorbed additional alginate onto the surface to create double-layer hydrogel particles (Figure 1.15).[194] The pure alginate outer layer showed relatively rapid degradation and drug release, while longer-term sustained release of the active pharmaceutical ingredient was observed from the inner alginate/*c*-CNC-SO_3^- sphere, which degraded at a slower rate. It was also suggested that the CNCs may cause slower diffusion of the drug within the matrix.

Bio-based nanocomposites have also attracted interest in tissue engineering applications. For instance, CNCs have been shown to delay implant degradation, increasing the amount of time cells that can grow into the scaffold before losing mechanical support. For example, it has been shown that while cell proliferation in alginate/*c*-CNC-SO_3^- gel composites was slowed relative to alginate gels, the improved mechanical strength and slower degradation rate made the material a promising candidate for bone stents for which rapid cellular growth is not required, but mechanical strength is needed.[195] In a related example, Yang et al. created hydroxyapatite/gelatin/*b*-CNC-COOH hydrogel composites where the amount of CNCs incorporated into the composite could be used to control the gel's degradation rate in simulated bodily fluid while maintaining tensile strength.[196]

CNC-based materials have also been investigated as anti-microbial agents. For

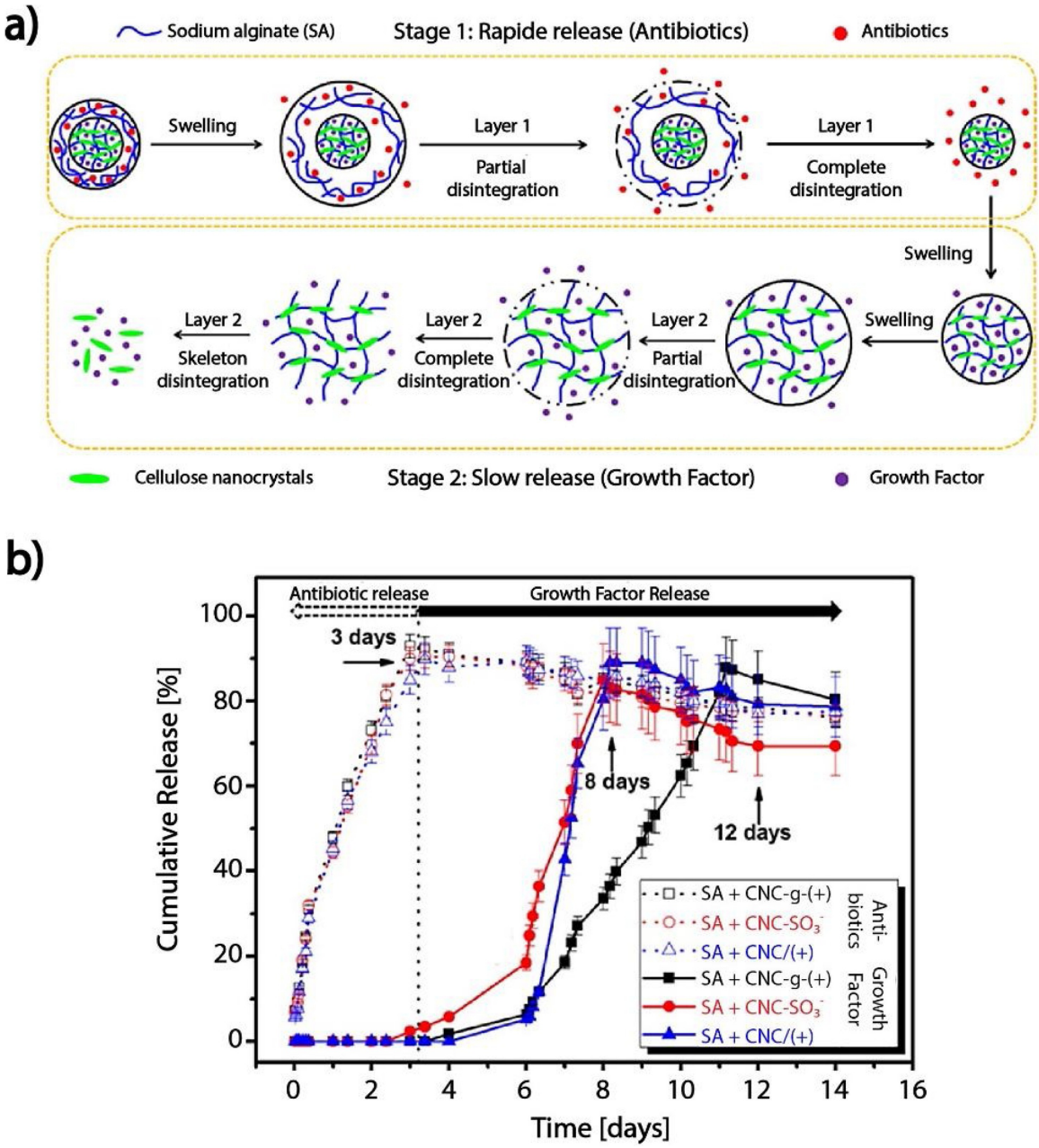

Figure 1.15: a) Drug release schematic for the release of the antibiotic ceftazidime hydrate loaded into the sodium alginate (SA) outer layer and human epidermal growth factor in the SA/CNC inner layer from double membrane alginate hydrogel particles. b) Graph of drug release times showing rapid release of the antibiotic from the outer layer, and a delayed onset release of growth factor . CNCs used were neat *w*-CNC-SO3-, CNCs modified by chemical grafting of a positively charged small molecule (CNC-*g*-(+)), and CNCs modified by physical adsorption of a positively charged polyelectrolyte polymer (CNC/(+)).[194]

example, CNCs have been grafted with a variety of molecules, such as rosin,[197] porphyrin,[198] and polyrhodanine[199] to create films and particles that have shown considerable success in reducing bacterial colony survival. While not composites, these functionalized CNC nanomaterials have been proposed to be incorporated into fabrics, papers, and coatings for the biomedical, food service, and packaging industries to access more sustainable and biocompatible alternatives to current solutions.

The future role of CNCs in the biomedical industry relies on the continued investigation of biological interactions with the many different forms of CNCs and in a wide range of environments. While some in vitro studies have been undertaken with CNC-based systems,[76,200] we have only scratched the surface and a much better understanding of in vivo interactions is necessary. Additionally, further degradation studies need to be undertaken so that the long-term impact of CNCs on the body can be better understood.

1.4.4 Electronics

CNCs have been investigated in a range of electronic applications, further highlighting their versatility as a nanomaterial. While not all of the materials used with the CNCs in this section are sustainable, the key goal is to replace actively toxic materials that are traditionally used in systems like batteries and solar cells, and as such, reducing the non-trivial contamination issues upon disposal.[201,202]

In battery applications, nanocellulose based materials are interesting on account of their mechanical strength and permeability.[203] Accordingly, studies have investigated the potential of CNC composites as separators, electrolytes,[204] and electrodes[205] in next-generation battery technologies. Dufresne and coworkers combined the needs of a separator and electrolyte by solvent casting *t*-CNC-SO_3^- into a PEO film to create a robust, conductive nanocomposite.[204] The material exhibited less than half an order of magnitude loss in ionic conductivity at 60 °C when compared to neat PEO, while also

achieving an order of magnitude increase in mechanical strength.

The complexity of electronic systems is one factor that makes fully sustainable devices difficult to design, but CNCs provide a foundation that can be built upon. Okahisa and coworkers used cellulose nanofiber mats dipped in various acrylic resins to create substrates with low coefficients of thermal expansion (CTE) for deposition of organic light-emitting diodes (OLEDs).[206] The low CTE, 12.1 ppm/K in the best case, showed a 94 % decrease over the neat resin and was essential to prevent delamination during thermal cycles encountered in regular use. This idea was advanced by Kippelen and coworkers, who used a glycerol/*w*-CNC-SO_3^- substrate to create a fully recyclable OLED.[207] Building on this work, the same group went on to employ the same optically clear composite of glycerol and *w*-CNC-SO_3^- as a substrate for recyclable solar cells (Figure 1.16), on top of which was deposited successive layers of silver, ethoxylated polyethyenimine, photoactive material, molybdenum oxide (MoO_3) and finally another layer of silver.[208] While the achieved power conversion efficiency of 2.7 % is nowhere near to the state-of-the-art solar cells(ca. 25 %) these cells were able to be completely recycled, showing that fully-recyclable solar cells are a legitimate possibility.

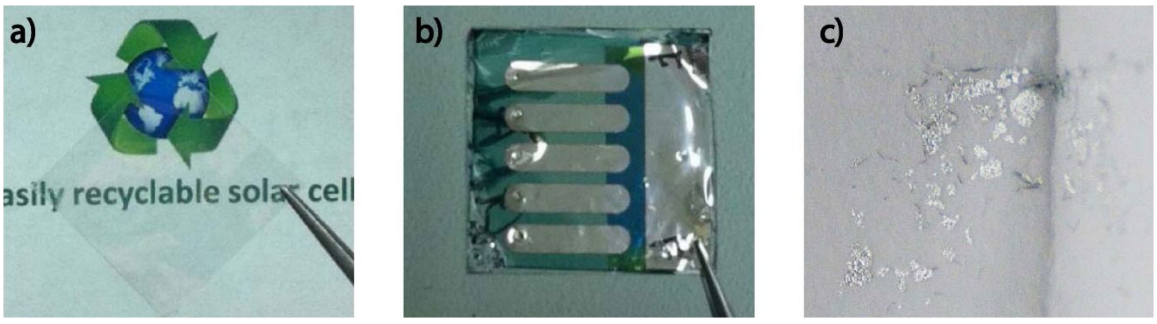

Figure 1.16: a) Transparent *w*-CNC-SO_3^- film used as the substrate for a recyclable solar cell, b) the fully assembled and recyclable solar cell on the CNC substrate and c) the solid remains (mainly consisting of Ag and MoO_3) after dissolving the solar cell into its constituent components through a series of washes in deionized water and chlorobenzene.[208]

1.5 Conclusion

The incorporation of bio-based cellulose nanocrystals into sustainable polymer matrices allows access to improvements in a number of important material properties, from mechanical strength and thermal resistance to barrier properties, without detracting from the material's sustainability. Although, it is important to note that while CNCs are components of many natural systems (in particular within trees and plants), more work is needed to better understand the environmental and biological impacts of isolated and functionalized CNCs. This critical aspect aside, the key to improved materials properties is the ability to access composites where the CNCs are well-dispersed within the host matrix. If the polymer matrix is soluble in water (or even polar organic solvents such as DMF), e.g. alginate and chitosan, then it is relatively easy to access CNC composites that show greatly enhanced properties by standard solution casting processes. The real challenge comes when the polymer matrix in question is not soluble in a solvent that disperses CNCs. Numerous methods have been tried to get around this problem, including transferring the CNCs into less polar solvents, to limited success. Additives (e.g. surfactants or dispersing agents) can be used to enhance CNC dispersion in the matrix. However, such molecules usually facilitate the dispersion by localizing at the CNC surfaces and as such, stress transfer between the CNCs themselves as well as between CNCs and the matrix is diminished, reducing the effectiveness of the reinforcement. To improve stress transfer, covalent grafting of the dispersing agent, usually a short-chain polymer, to the CNC surface has been conducted. The resulting materials exhibit some of the best properties of any CNC composites currently reported. Nonetheless, improvements in the large-scale synthesis and processing of such materials need to be made before commercial implementation will be achieved.

Solvent casting-based processes are currently the most frequently employed because

they offer the advantage of maximizing dispersion of the CNCs. However, such processing involves large amounts of solvent and, from a sustainability and commercialization point of view, any solution-based processing is not ideal. Unfortunately, melt processing of CNC composites is a major challenge, as it is with most nanocomposites, given their tendency to aggregate/phase separate and the fact that they can start to decompose at high temperatures. Most of the aforementioned strategies (functionalization of CNCs, addition of surfactants and plasticizers) are viable options, but as of yet, a scalable, cost effective process still needs to be developed.

The possibilities of commercialization are diverse, and work has been done in the areas of packaging, compatibilization, water purification, biomedical, and electronics, amongst others. The sustainability and ability to functionalize CNC surfaces with a wide variety of chemistries are part of what makes their appeal so broad. For example, grafting of binding sites allows sequestration of ions in contaminated water, attachment of antibacterial agents helps to prevent disease in biomedical applications, and grafting of conductive materials improves electronic or ionic conduction, opening the door to potentially accessing wholly sustainable systems that can impact fields ranging from energy storage to flexible bio-electronics. As such, while there are still unresolved challenges that need to be addressed, the potential of CNCs (and other nanocelluloses) to help expand the sustainable materials portfolio is clear.

1.6 References

[1] H. Staudinger, "Über Polymerisation", *Berichte der deutschen chemischen Gesellschaft (A and B Series)* **2007**, *53*, 1073–1085.

[2] Global plastic production statistics, **2019**.

[3] D. K. Schneiderman, M. A. Hillmyer, "50th Anniversary Perspective: There Is a Great Future in Sustainable Polymers", *Macromolecules* **2017**, *50*, 3733–3749.

[4] R. Geyer, J. R. Jambeck, K. L. Law, "Production, use, and fate of all plastics ever made", *Science advances* **2017**, *3*, e1700782.

[5] H. T. H. Nguyen, P. Qi, M. Rostagno, A. Feteha, S. A. Miller, "The quest for high glass transition temperature bioplastics", *Journal of Materials Chemistry A* **2018**, *6*, 9298–9331.

[6] J. R. Jambeck, R. Geyer, C. Wilcox, T. R. Siegler, M. Perryman, A. Andrady, R. Narayan, K. L. Law, "Plastic waste inputs from land into the ocean", *Science* **2015**, *347*, 768–771.

[7] E. MacArthur, D. Waughray, M. R. Stuchtey, The New Plastics Economy: Rethinking the Future of Plastics, tech. rep., Ellen MacArthur Foundation, **2016**, pp. 1–120.

[8] G20 Implementation Framework for Actions on Marine Plastic Litter, tech. rep., **2019**.

[9] Plastic pollution, **2018**.

[10] Global plastic waste totals 4.9 bilion tonnes, **2017**.

[11] S. A. Miller, Sustainable polymers: opportunities for the next decade, **2013**.

[12] M. Rose, R. Palkovits, "Cellulose-based sustainable polymers: State of the art and future trends", *Macromolecular Rapid Communications* **2011**, *32*, 1299–1311.

[13] M. Hong, E. Y. Chen, "Towards Truly Sustainable Polymers: A Metal-Free Recyclable Polyester from Biorenewable Non-Strained γ-Butyrolactone", *Angewandte Chemie - International Edition* **2016**, *55*, 4188–4193.

[14] D. J. Fortman, J. P. Brutman, G. X. De Hoe, R. L. Snyder, W. R. Dichtel, M. A. Hillmyer, "Approaches to sustainable and continually recyclable cross-linked polymers", *ACS Sustainable Chemistry & Engineering* **2018**, *6*, 11145–11159.

[15] Y. Zhu, C. Romain, C. K. Williams, "Sustainable polymers from renewable resources", *Nature* **2016**, *540*, 354.

[16] H. Nakajima, P. Dijkstra, K. Loos, "The recent developments in biobased polymers toward general and engineering applications: Polymers that are upgraded from biodegradable polymers, analogous to petroleum-derived polymers, and newly developed", *Polymers* **2017**, *9*, 1–26.

[17] B. Laycock, M. Nikolic, J. M. Colwell, E. Gauthier, P. Halley, S. Bottle, G. George, "Lifetime prediction of biodegradable polymers", *Progress in Polymer Science* **2017**.

[18] L. Chen, R. E. Pelton, T. M. Smith, "Comparative life cycle assessment of fossil and bio-based polyethylene terephthalate (PET) bottles", *Journal of Cleaner Production* **2016**, *137*, 667–676.

[19] A. K. Mohanty, S. Vivekanandhan, J.-M. Pin, M. Misra, "Composites from renewable and sustainable resources: Challenges and innovations", *Science* **2018**, *362*, 536–542.

[20] H. Storz, K.-D. Vorlop, "Bio-based plastics: status, challenges and trends", *Landbauforschung-Ger* **2013**, *63*, 321–332.

[21] S. Y. Lee, S. H. Hong, S. H. Lee, S. J. Park, "Fermentative production of chemicals that can be used for polymer synthesis", *Macromolecular Bioscience* **2004**, *4*, 157–164.

[22] D. Garlotta, "A Literature Review of Poly(Lactic Acid)", *Springer* **2002**, *9*.

[23] P. Suriyamongkol, R. Weselake, S. Narine, M. Moloney, S. Shah, "Biotechnological approaches for the production of polyhydroxyalkanoates in microorganisms and plants—a review", *Biotechnology advances* **2007**, *25*, 148–175.

[24] D. R. Lu, C. M. Xiao, S. J. Xu, "Starch-based completely biodegradable polymer materials", *Express Polymer Letters* **2009**, *3*, 366–375.

[25] N. Peelman, P. Ragaert, B. De Meulenaer, D. Adons, R. Peeters, L. Cardon, F. Van Impe, F. Devlieghere, "Application of bioplastics for food packaging", *Trends in Food Science & Technology* **2013**, *32*, 128–141.

[26] Bioplastics market development update 2023.

[27] T. Kuilla, S. Bhadra, D. Yao, N. H. Kim, S. Bose, J. H. Lee, "Recent advances in graphene based polymer composites", *Progress in Polymer Science* (*Oxford*) **2010**, *35*, 1350–1375.

[28] P. A. Sreekumar, M. A. Al-Harthi, S. K. De, "Reinforcement of starch/polyvinyl alcohol blend using nano¢ titanium dioxide", *Journal of Composite Materials* **2012**, *46*, 3181–3187.

[29] L. Jiang, J. Zhang, M. P. Wolcott, "Comparison of polylactide/nano-sized calcium carbonate and polylactide/montmorillonite composites: Reinforcing effects and toughening mechanisms", *Polymer* **2007**, *48*, 7632–7644.

[30] E. Reynaud, T. Jouen, C. Gauthier, G. Vigier, J. Varlet, "Nanofillers in polymeric matrix: A study on silica reinforced PA6", *Polymer* **2001**, *42*, 8759–8768.

[31] N. Saba, P. Tahir, M. Jawaid, "A review on potentiality of nano filler/natural fiber filled polymer hybrid composites", *Polymers* **2014**, *6*, 2247–2273.

[32] G. Siqueira, J. Bras, A. Dufresne, "Cellulosic bionanocomposites: A review of preparation, properties and applications", *Polymers.* **2010**, *2*, 728–765.

[33] R. J. Moon, A. Martini, J. Nairn, J. Simonsen, J. Youngblood, *Cellulose nanomaterials review: Structure, properties and nanocomposites*, *Vol. 40*, **2011**, pp. 3941–3994.

[34] H. P. S. A. Khalil, Y. Davoudpour, C. K. Saurabh, M. S. Hossain, A. S. Adnan, R. Dungani, M. T. Paridah, M. Z. I. Sarker, M. R. N. Fazita, M. I. Syakir, "A review on nanocellulosic fibres as new material for sustainable packaging: Process and applications", *Renewable and Sustainable Energy Reviews* **2016**, *64*, 823–836.

[35] H. P. S. A. Khalil, A. H. Bhat, A. F. I. Yusra, "Green composites from sustainable cellulose nanofibrils: A review", *Carbohydrate polymers* **2012**, *87*, 963–979.

[36] F. M. Al-Oqla, S. M. Sapuan, "Natural fiber reinforced polymer composites in industrial applications: feasibility of date palm fibers for sustainable automotive industry", *Journal of Cleaner Production* **2014**, *66*, 347–354.

[37] H. Kargarzadeh, J. Huang, N. Lin, I. Ahmad, M. Mariano, A. Dufresne, S. Thomas, A. Gałeski, "Recent developments in nanocellulose-based biodegradable polymers, thermoplastic polymers, and porous nanocomposites", *Progress in Polymer Science* **2018**, *87*, 197–227.

[38] A. Dufresne, J.-Y. Cavaillé, M. R. Vignon, "Mechanical behavior of sheets prepared from sugar beet cellulose microfibrils", *Journal of applied polymer science* **1997**, *64*, 1185–1194.

[39] T. Saito, S. Kimura, Y. Nishiyama, A. Isogai, "Cellulose nanofibers prepared by TEMPO-mediated oxidation of native cellulose", *Biomacromolecules* **2007**, *8*, 2485–2491.

[40] Y. Habibi, A.-L. Goffin, N. Schiltz, E. Duquesne, P. Dubois, A. Dufresne, "Bionanocomposites based on poly(ϵ-caprolactone)-grafted cellulose nanocrystals by ring-opening polymerization", *Journal of Materials Chemistry* **2008**, *18*, 5002–5010.

[41] N. Lin, A. Dufresne, "Nanocellulose in biomedicine: Current status and future prospect", *European Polymer Journal* **2014**, *59*, 302–325.

[42] D. Bondeson, A. P. Mathew, K. Oksman, "Optimization of the isolation of nanocrystals from microcrystalline cellulose by acid hydrolysis", **2006**, 171–180.

[43] E. Cudjoe, M. Hunsen, Z. Xue, A. E. Way, E. Barrios, R. A. Olson, M. J. Hore, S. J. Rowan, "Miscanthus Giganteus: A commercially viable sustainable source of cellulose nanocrystals", *Carbohydrate Polymers* **2017**, *155*, 230–241.

[44] H. Yang, Y. Zhang, R. Kato, S. J. Rowan, "Preparation of cellulose nanofibers from Miscanthus x. Giganteus by ammonium persulfate oxidation", *Carbohydrate Polymers* **2019**, *212*, 30–39.

[45] J. Araki, M. Wada, S. Kuga, T. Okano, "Flow properties of microcrystalline cellulose suspension prepared by acid treatment of native cellulose", *Colloids and Surfaces A: Physicochemical and Engineering Aspects* **1998**, *142*, 75–82.

[46] S. Beck-Candanedo, M. Roman, D. G. Gray, "Effect of reaction conditions on the properties and behavior of wood cellulose nanocrystal suspensions", *Biomacromolecules* **2005**, *6*, 1048–1054.

[47] X. M. Dong, T. Kimura, J.-F. Revol, D. G. Gray, "Effects of ionic strength on the isotropic-chiral nematic phase transition of suspensions of cellulose crystallites", *Langmuir* **1996**, *12*, 2076–2082.

[48] L. Heux, G. Chauve, C. Bonini, "Nonflocculating and chiral-nematic self-ordering of cellulose microcrystals suspensions in nonpolar solvents", *Langmuir* **2000**, *16*, 8210–8212.

[49] A. J. De Menezes, G. Siqueira, A. A. S. Curvelo, A. Dufresne, "Extrusion and characterization of functionalized cellulose whiskers reinforced polyethylene nanocomposites", *Polymer* **2009**, *50*, 4552–4563.

[50] M. N. Angles, A. Dufresne, "Plasticized starch/tunicin whiskers nanocomposites. 1. Structural analysis", *Macromolecules* **2000**, *33*, 8344–8353.

[51] S. Elazzouzi-Hafraoui, Y. Nishiyama, J.-L. Putaux, L. Heux, F. Dubreuil, C. Rochas, "The Shape and Size Distribution of Crystalline Nanoparticles Prepared by Acid Hydrolysis of Native Cellulose", *Biomacromolecules* **2008**, 57–65.

[52] B. S. L. Brito, F. V. Pereira, J.-L. Putaux, B. Jean, "Preparation, morphology and structure of cellulose nanocrystals from bamboo fibers", *Cellulose* **2012**, *19*, 1527–1536.

[53] R. Singla, S. Soni, P. M. Kulurkar, A. Kumari, S. Mahesh, V. Patial, Y. S. Padwad, S. K. Yadav, "In situ functionalized nanobiocomposites dressings of bamboo cellulose nanocrystals and silver nanoparticles for accelerated wound healing", *Carbohydrate polymers* **2017**, *155*, 152–162.

[54] M. Grunert, W. T. Winter, "Nanocomposites of cellulose acetate butyrate reinforced with cellulose nanocrystals", *Journal of Polymers and the Environment* **2002**, *10*, 27–30.

[55] J. Araki, M. Wada, S. Kuga, Steric stabilization of a cellulose microcrystal suspension by poly(ethylene glycol) grafting, **2001**.

[56] E. Fortunati, D. Puglia, M. Monti, L. Peponi, C. Santulli, J. M. Kenny, L. Torre, "Extraction of cellulose nanocrystals from Phormium tenax fibres", *Journal of Polymers and the Environment* **2013**, *21*, 319–328.

[57] E. Fortunati, F. Luzi, D. Puglia, F. Dominici, C. Santulli, J. M. Kenny, L. Torre, "Investigation of thermo-mechanical, chemical and degradative properties of PLA-limonene films reinforced with cellulose nanocrystals extracted from Phormium tenax leaves", *European Polymer Journal* **2014**, *56*, 77–91.

[58] X. Cao, H. Dong, C. M. Li, "New nanocomposite materials reinforced with flax cellulose nanocrystals in waterborne polyurethane", *Biomacromolecules* **2007**, *8*, 899–904.

[59] Y. Chen, X. Cao, P. R. Chang, M. A. Huneault, "Comparative study on the films of poly(vinyl alcohol)/pea starch nanocrystals and poly(vinyl alcohol)/native pea starch", *Carbohydrate Polymers* **2008**, *73*, 8–17.

[60] Y. Habibi, L. A. Lucia, O. J. Rojas, "Cellulose Nanocrystals : Chemistry , Self-Assembly , and Applications", *Chemical Reviews* **2010**, *d*, 3479–3500.

[61] D. Trache, M. H. Hussin, M. K. M. Haafiz, V. K. Thakur, "Recent progress in cellulose nanocrystals: sources and production", *Nanoscale* **2017**, *9*, 1763–1786.

[62] S. J. Eichhorn, A. Dufresne, M. Aranguren, N. E. Marcovich, J. R. Capadona, S. J. Rowan, C. Weder, W. Thielemans, M. Roman, S. Renneckar, W. Gindl, S. Veigel, J. Keckes, H. Yano, K. Abe, M. Nogi, A. N. Nakagaito, A. Mangalam, J. Simonsen, A. S. Benight, A. Bismarck, L. A. Berglund, T. Peijs, *Review: Current international research into cellulose nanofibres and nanocomposites*, *Vol. 45*, **2010**, pp. 1–33.

[63] I. A. Rahman, V. Padavettan, "Synthesis of Silica Nanoparticles by Sol-Gel : Size-Dependent Properties , Surface Modification , and Applications in Silica-Polymer Nanocomposites — A Review", **2012**, *2012*.

[64] M. H. Al-saleh, U. Sundararaj, "Review of the mechanical properties of carbon nanofiber / polymer composites", *Composites Part A* **2011**, *42*, 2126–2142.

[65] M. T. Albdiry, B. F. Yousif, H. Ku, K. T. Lau, "A critical review on the manufacturing processes in relation to the properties of nanoclay / polymer composites", **2012**.

[66] R. J. Moon, G. T. Schueneman, J. Simonsen, "Overview of cellulose nanomaterials, their capabilities and applications", *Jom* **2016**, *68*, 2383–2394.

[67] V. Favier, J. Y. Cavaille, G. R. Canova, S. C. Shrivastava, "Mechanical percolation in cellulose whisker nanocomposites", *Polymer Engineering & Science* **1997**, *37*, 1732–1739.

[68] K. Oksman, Y. Aitomäki, A. P. Mathew, G. Siqueira, Q. Zhou, S. Butylina, S. Tanpichai, X. Zhou, S. Hooshmand, "Review of the recent developments in cellulose nanocomposite processing", *Composites Part A: Applied Science and Manufacturing* **2016**, *83*, 2–18.

[69] V. Favier, G. R. Canova, J. Y. Cavaillé, H. Chanzy, A. Dufresne, C. Gauthier, "Nanocomposite materials from latex and cellulose whiskers", *Polymers for Advanced Technologies* **1995**, *6*, 351–355.

[70] A. Dufresne, J.-Y. Cavaille, W. Helbert, "New nanocomposite materials: microcrystalline starch reinforced thermoplastic", *Macromolecules* **1996**, *29*, 7624–7626.

[71] V. Favier, H. Chanzy, J. Y. Cavaillé, "Polymer Nanocomposites Reinforced by Cellulose Whiskers", *Macromolecules* **1995**, *28*, 6365–6367.

[72] A. Dufresne, J.-Y. Cavaillé, W. Helbert, "Thermoplastic nanocomposites filled with wheat straw cellulose whiskers. Part II: effect of processing and modeling", *Polymer composites* **1997**, *18*, 198–210.

[73] J. Tang, J. Sisler, N. Grishkewich, K. C. Tam, "Functionalization of cellulose nanocrystals for advanced applications", *Journal of Colloid and Interface Science* **2017**, *494*, 397–409.

[74] P. Lahtinen, H. Alenius, A. Kapanen, P. Eronen, L. Pylkkänen, P. Hiekkataipale, K. Putkisto, J. Ruokolainen, J. Vartiainen, U. Tapper, J. Hokkinen, T. Pöhler, K. Sirola, A. Laukkanen, "Health and environmental safety aspects of friction grinding and spray drying of microfibrillated cellulose", *Cellulose* **2011**, *18*, 775–786.

[75] T. Kovacs, V. Naish, B. O'Connor, C. Blaise, F. Gagne, L. Hall, V. Trudeau, P. Martel, "An ecotoxicological characterization of nanocrystalline cellulose (NCC)", *Nanotoxicology* **2010**, *4*, 255–270.

[76] A. M. Weiss, N. Macke, Y. Zhang, C. Calvino, A. P. Esser-Kahn, S. J. Rowan, "In Vitro and in Vivo Analyses of the Effects of Source, Length, and Charge on the Cytotoxicity and Immunocompatibility of Cellulose Nanocrystals", *ACS Biomaterials Science and Engineering* **2021**, *7*, 1450–1461.

[77] M. Roman, "Toxicity of Cellulose Nanocrystals: A Review", *Industrial Biotechnology* **2015**, *11*, 25–33.

[78] M. J. D. Clift, E. J. Foster, D. Vanhecke, D. Studer, P. Wick, P. Gehr, B. Rothen-Rutishauser, C. Weder, "Investigating the Interaction of Cellulose Nanofibers Derived from Cotton with a Sophisticated 3D Human Lung Cell Coculture", *Biomacromolecules* **2011**, *12*, 3666–3673.

[79] N. Yanamala, M. T. Farcas, M. K. Hat, E. R. Kisin, V. E. Kagan, C. L. Geraci, A. A. Shvedova, "In Vivo Evaluation of the Pulmonary Toxicity of Cellulose Nanocrystals: A Renewable and Sustainable Nanomaterial of the Future", **2014**.

[80] A. K. Mohanty, M. Misra, G. Hinrichsen, "Biofibres, biodegradable polymers and biocomposites: An overview", *Macromolecular Materials and Engineering* **2000**, *276-277*, 1–24.

[81] R. Jayakumar, D. Menon, K. Manzoor, S. V. Nair, H. Tamura, "Biomedical applications of chitin and chitosan based nanomaterials — A short review", *Carbohydrate Polymers* **2010**, *82*, 227–232.

[82] P. J. Smith, "Utilizing Renewable Resources To Create Functional Polymers : Chitosan-Based Associative Thickener", **2002**, *36*, 3446–3454.

[83] H. No, S. Meyers, W. Prinyawiwatkul, Z. Xu, "Applications of Chitosan for Improvement of Quality and Shelf Life of Foods: A Review", *Journal of Food Science* **2007**, *72*.

[84] A. Khan, R. A. Khan, S. Salmieri, C. Le, B. Riedl, J. Bouchard, V. Tan, M. R. Kamal, M. Lacroix, "Mechanical and barrier properties of nanocrystalline cellulose reinforced chitosan based nanocomposite films", *Carbohydrate Polymers* **2012**, *90*, 1601–1608.

[85] H. Mao, C. Wei, Y. Gong, S. Wang, W. Ding, "Mechanical and water-resistant properties of eco-friendly chitosan membrane reinforced with cellulose nanocrystals", *Polymers* **2019**, *11*.

[86] M. Mujtaba, A. M. Salaberria, M. A. Andres, M. Kaya, A. Gunyakti, J. Labidi, "Utilization of flax (Linum usitatissimum) cellulose nanocrystals as reinforcing material for chitosan films", *International Journal of Biological Macromolecules* **2017**, *104*, 944–952.

[87] W. S. Abo-Elseoud, M. L. Hassan, M. W. Sabaa, M. Basha, E. A. Hassan, S. M. Fadel, "Chitosan nanoparticles/cellulose nanocrystals nanocomposites as a carrier system for the controlled release of repaglinide", *International Journal of Biological Macromolecules* **2018**, *111*, 604–613.

[88] F. Li, P. Biagioni, M. Finazzi, S. Tavazzi, L. Piergiovanni, "Tunable green oxygen barrier through layer-by-layer self-assembly of chitosan and cellulose nanocrystals", *Carbohydrate Polymers* **2013**, *92*, 2128–2134.

[89] Z. Karim, A. P. Mathew, M. Grahn, J. Mouzon, K. Oksman, "Nanoporous membranes with cellulose nanocrystals as functional entity in chitosan: Removal of dyes from water", *Carbohydrate Polymers* **2014**, *112*, 668–676.

[90] M. Szekalska, K. Sosnowska, A. Czajkowska-Kósnik, K. Winnicka, "Calcium chloride modified alginate microparticles formulated by the spray drying process: A strategy to prolong the release of freely soluble drugs", *Materials.* **2018**, *11*, 1–14.

[91] N. Lin, C. Bruzzese, A. Dufresne, "TEMPO-oxidized nanocellulose participating as crosslinking aid for alginate-based sponges", *ACS applied materials & interfaces* **2012**, *4*, 4948–4959.

[92] T. Huq, S. Salmieri, A. Khan, R. A. Khan, C. Le Tien, B. Riedl, C. Fraschini, J. Bouchard, J. Uribe-Calderon, M. R. Kamal, "Nanocrystalline cellulose (NCC) reinforced alginate based biodegradable nanocomposite film", *Carbohydrate polymers* **2012**, *90*, 1757–1763.

[93] K. J. De France, T. Hoare, E. D. Cranston, "Review of hydrogels and aerogels containing nanocellulose", *Chemistry of Materials* **2017**, *29*, 4609–4631.

[94] M. Smyth, M. S. M'Bengue, M. Terrien, C. Picart, J. Bras, E. J. Foster, "The effect of hydration on the material and mechanical properties of cellulose nanocrystal-alginate composites", *Carbohydrate Polymers* **2018**, *179*, 186–195.

[95] X. Ma, R. Li, X. Zhao, Q. Ji, Y. Xing, J. Sunarso, Y. Xia, "Biopolymer composite fibres composed of calcium alginate reinforced with nanocrystalline cellulose", *Composites Part A: Applied Science and Manufacturing* **2017**, *96*, 155–163.

[96] N. Mohammed, N. Grishkewich, R. M. Berry, K. C. Tam, "Cellulose nanocrystal–alginate hydrogel beads as novel adsorbents for organic dyes in aqueous solutions", *Cellulose* **2015**, *22*, 3725–3738.

[97] H. Shaghaleh, X. Xu, S. Wang, "Current progress in production of biopolymeric materials based on cellulose, cellulose nanofibers, and cellulose derivatives", *RSC Advances* **2018**, *8*, 825–842.

[98] K. J. Edgar, C. M. Buchanan, J. S. Debenham, P. A. Rundquist, B. D. Seiler, M. C. Shelton, D. Tindall, "Advances in cellulose ester performance and application", **2001**, *26*.

[99] J. E. Ayuk, A. P. Mathew, K. Oksman, "The effect of plasticizer and cellulose nanowhisker content on the dispersion and properties of cellulose acetate butyrate nanocomposites", *Journal of Applied Polymer Science* **2009**, *114*, 2723–2730.

[100] B. Khan, M. Bilal Khan Niazi, G. Samin, Z. Jahan, "Thermoplastic Starch: A Possible Biodegradable Food Packaging Material—A Review", *Journal of Food Process Engineering* **2017**, *40*, 1–17.

[101] E. Ogunsona, E. Ojogbo, T. Mekonnen, "Advanced material applications of starch and its derivatives", *European Polymer Journal* **2018**, *108*, 570–581.

[102] M. L. Sanyang, S. M. Sapuan, M. Jawaid, M. R. Ishak, J. Sahari, "Effect of plasticizer type and concentration on tensile, thermal and barrier properties of biodegradable films based on sugar palm (Arenga pinnata) starch", *Polymers* **2015**, *7*, 1106–1124.

[103] X. Ge, L. Yu, Z. Liu, H. Liu, Y. Chen, L. Chen, "Developing acrylated epoxidized soybean oil coating for improving moisture sensitivity and permeability of starch-based film", *International Journal of Biological Macromolecules* **2019**, *125*, 370–375.

[104] D. Le Corre, J. Bras, A. Dufresne, "Starch nanoparticles: A review", *Biomacromolecules* **2010**, *11*, 1139–1153.

[105] H. Liu, F. Xie, L. Yu, L. Chen, L. Li, "Thermal processing of starch-based polymers", *Progress in Polymer Science (Oxford)* **2009**, *34*, 1348–1368.

[106] Z. W. Abdullah, Y. Dong, "Recent advances and perspectives on starch nanocomposites for packaging applications", *Journal of Materials Science* **2018**, *53*, 15319–15339.

[107] Y. Lu, L. Weng, X. Cao, "Biocomposites of plasticized starch reinforced with cellulose crystallites from cottonseed linter", *Macromolecular Bioscience* **2005**, *5*, 1101–1107.

[108] A. M. Slavutsky, M. A. Bertuzzi, "Water barrier properties of starch films reinforced with cellulose nanocrystals obtained from sugarcane bagasse", *Carbohydrate Polymers* **2014**, *110*, 53–61.

[109] X. Cao, Y. Chen, P. R. Chang, A. D. Muir, G. Falk, "Starch-based nanocomposites reinforced with flax cellulose nanocrystals", *Express Polym Lett* **2008**, *2*, 502–510.

[110] P. M. Forssell, J. M. Mikkilä, G. K. Moates, R. Parker, "Phase and glass transition behaviour of concentrated barley starch-glycerol-water mixtures, a model for thermoplastic starch", *Carbohydrate Polymers* **1998**, *34*, 275–282.

[111] M. L. Fishman, D. R. Coffin, R. P. Konstance, C. I. Onwulata, "Extrusion of pectin/starch blends plasticized with glycerol", *Carbohydrate Polymers* **2000**, *41*, 317–325.

[112] P. Forssell, J. Mikkilä, T. Suortti, J. Seppälä, K. Poutanen, "Plasticization of barley starch with glycerol and water", *Journal of Macromolecular Science - Pure and Applied Chemistry* **1996**, *33*, 703–715.

[113] X. Ma, J. Yu, N. Wang, "Glycerol plasticized-starch/multiwall carbon nanotube composites for electroactive polymers", *Composites Science and Technology* **2008**, *68*, 268–273.

[114] M. N. Angles, A. Dufresne, "Plasticized starch/tunicin whiskers nanocomposite materials. 2. Mechanical behavior", *Macromolecules* **2001**, *34*, 2921–2931.

[115] A. P. Mathew, A. Dufresne, "Morphological investigation of nanocomposites from sorbitol plasticized starch and tunicin whiskers", *Biomacromolecules* **2002**, *3*, 609–617.

[116] A. P. Mathew, W. Thielemans, A. Dufresne, "Mechanical properties of nanocomposites from sorbitol plasticized starch and tunicin whiskers", *Journal of Applied Polymer Science* **2008**, *109*, 4065–4074.

[117] E. Castro-Aguirre, F. Iñiguez-Franco, H. Samsudin, X. Fang, R. Auras, "Poly (lactic acid)—Mass production, processing, industrial applications, and end of life", *Advanced Drug Delivery Reviews* **2016**, *107*, 333–366.

[118] Y. Chen, L. M. Geever, J. A. Killion, J. G. Lyons, C. L. Higginbotham, D. M. Devine, "Review of multifarious applications of poly (lactic acid)", *Polymer-Plastics Technology and Engineering* **2016**, *55*, 1057–1075.

[119] M. L. Di Lorenzo, R. Androsch, *Industrial Applications of Poly (lactic acid), Vol. 282*, Springer, **2018**.

[120] S. Jacobsen, H. G. Fritz, P. Degée, P. Dubois, R. Jérôme, "Polylactide (PLA)—a new way of production", *Polymer Engineering & Science* **1999**, *39*, 1311–1319.

[121] E. T. H. Vink, K. R. Rábago, D. A. Glassner, P. R. Gruber, "Applications of life cycle assessment to NatureWorks™ polylactide (PLA) production", *Polymer Degradation and Stability* **2003**, *80*, 403–419.

[122] P. Dhar, D. Tarafder, A. Kumar, V. Katiyar, "Effect of cellulose nanocrystal polymorphs on mechanical, barrier and thermal properties of poly(lactic acid) based bionanocomposites", *RSC Advances* **2015**, *5*, 60426–60440.

[123] B. J. Lange, Y. Wyser, "Recent innovations in barrier technologies for plastic packaging - a review", *Packaging Technology and Science* **2003**, *16*, 149–158.

[124] K. S. Anderson, K. M. Schreck, M. A. Hillmyer, "Toughening polylactide", *Polymer Reviews* **2008**, *48*, 85–108.

[125] Z. Li, B. H. Tan, T. Lin, C. He, "Recent advances in stereocomplexation of enantiomeric PLA-based copolymers and applications", *Progress in Polymer Science* **2016**, *62*, 22–72.

[126] B. H. Tan, J. K. Muiruri, Z. Li, C. He, "Recent progress in using stereocomplexation for enhancement of thermal and mechanical property of polylactide", *ACS Sustainable Chemistry & Engineering* **2016**, *4*, 5370–5391.

[127] Q. K. Meng, M. Hetzer, D. De Kee, "PLA/clay/wood nanocomposites: nanoclay effects on mechanical and thermal properties", *Journal of Composite Materials* **2011**, *45*, 1145–1158.

[128] M. D. Sanchez-Garcia, J. M. Lagaron, "On the use of plant cellulose nanowhiskers to enhance the barrier properties of polylactic acid", *Cellulose* **2010**, *17*, 987–1004.

[129] A. Dufresne, M. B. Kellerhals, B. Witholt, "Transcrystallization in Mcl-PHAs/cellulose whiskers composites", *Macromolecules* **1999**, *32*, 7396–7401.

[130] M. Martínez-Sanz, A. Lopez-Rubio, J. M. Lagaron, "Optimization of the dispersion of unmodified bacterial cellulose nanowhiskers into polylactide via melt compounding to significantly enhance barrier and mechanical properties", *Biomacromolecules* **2012**, *13*, 3887–3899.

[131] E. Fortunati, M. Peltzer, I. Armentano, L. Torre, A. Jiménez, J. M. Kenny, "Effects of modified cellulose nanocrystals on the barrier and migration properties of PLA nano-biocomposites", *Carbohydrate Polymers* **2012**, *90*, 948–956.

[132] J. M. Lagaron, R. Catalá, R. Gavara, "Structural characteristics defining high barrier properties in polymeric materials", *Materials Science and Technology* **2004**, *20*, 1–7.

[133] E. Fortunati, I. Armentano, Q. Zhou, D. Puglia, A. Terenzi, L. A. Berglund, J. M. Kenny, "Microstructure and nonisothermal cold crystallization of PLA composites based on silver nanoparticles and nanocrystalline cellulose", *Polymer Degradation and Stability* **2012**, *97*, 2027–2036.

[134] H. M. Azeredo, L. H. Capparelli Mattoso, T. Habig, "Nanocomposites in Food Packaging – A Review", *Advances in Diverse Industrial Applications of Nanocomposites* **2012**.

[135] H. M. Azeredo, L. H. C. Mattoso, D. Wood, T. G. Williams, R. J. Avena-Bustillos, T. H. McHugh, "Nanocomposite Edible Films from Mango Puree Reinforced with Cellulose Nanofibers", *Journal of Food Science* **2009**, *74*, N31–N35.

[136] H. Yu, C. Yan, J. Yao, "Fully biodegradable food packaging materials based on functionalized cellulose nanocrystals/poly(3-hydroxybutyrate-co-3-hydroxyvalerate) nanocomposites", *RSC Advances* **2014**, *4*, 59792–59802.

[137] A. Dufresne, M. R. Vignon, "Improvement of starch film performances using cellulose microfibrils", *Macromolecules* **1998**, *31*, 2693–2696.

[138] M. Abdollahi, M. Alboofetileh, R. Behrooz, M. Rezaei, R. Miraki, "Reducing water sensitivity of alginate bio-nanocomposite film using cellulose nanoparticles", *International Journal of Biological Macromolecules* **2013**, *54*, 166–173.

[139] L. Petersson, I. Kvien, K. Oksman, "Structure and thermal properties of poly (lactic acid)/cellulose whiskers nanocomposite materials", *Composites Science and Technology* **2007**, *67*, 2535–2544.

[140] T. P. Labuza, "Effect of water activity on reaction kinetics of food deterioration", *Food Technology* **1980**, *34*, 36–41.

[141] E. Fortunati, I. Armentano, Q. Zhou, A. Iannoni, E. Saino, L. Visai, L. A. Berglund, J. M. Kenny, "Multifunctional bionanocomposite films of poly(lactic acid), cellulose nanocrystals and silver nanoparticles", *Carbohydrate Polymers* **2012**, *87*, 1596–1605.

[142] K.-l. G. Ho, A. L. Pometto, P. N. Hinz, "Effects of temperature and relative rumidity on polylactic acid plastic degradation", *Journal of Environmental Polymer Degradation* **1999**, *7*, 83–92.

[143] A. P. Mathew, K. Oksman, M. Sain, "Mechanical properties of biodegradable composites from poly lactic acid (PLA) and microcrystalline cellulose (MCC)", *Journal of Applied Polymer Science* **2005**, *97*, 2014–2025.

[144] M. P. Arrieta, E. Fortunati, F. Dominici, E. Rayón, J. López, J. M. Kenny, "PLA-PHB/cellulose based films: Mechanical, barrier and disintegration properties", *Polymer Degradation and Stability* **2014**, *107*, 139–149.

[145] E. Fortunati, M. A. Peltzer, I. Armentano, A. Jiménez, J. M. Kenny, "Combined effects of cellulose nanocrystals and silver nanoparticles on the barrier and migration properties of PLA nano-biocomposites", *Journal of Food Engineering* **2013**, *118*, 117–124.

[146] K. Oksman, A. P. Mathew, D. Bondeson, I. Kvien, "Manufacturing process of cellulose whiskers/polylactic acid nanocomposites", *Composites Science and Technology* **2006**, *66*, 2776–2784.

[147] D. Bondeson, I. Kvien, K. Oksman in *Cellulose Nanocomposites*, American Chemical Society (ACS), **2006**, pp. 10–25.

[148] A. Potthast, T. Rosenau, J. Sartori, H. Sixta, P. Kosma, "Hydrolytic processes and condensation reactions in the cellulose solvent system N, N-dimethylacetamide/lithium chloride. Part 2: degradation of cellulose", *Polymer* **2003**, *44*, 7–17.

[149] C. F. Kuan, H. C. Kuan, C. C. M. Ma, C. H. Chen, "Mechanical and electrical properties of multi-wall carbon nanotube/poly(lactic acid) composites", *Journal of Physics and Chemistry of Solids* **2008**, *69*, 1395–1398.

[150] M. Pereda, N. E. Kissi, A. Dufresne, "Extrusion of polysaccharide nanocrystal reinforced polymer nanocomposites through compatibilization with poly(ethylene oxide)", *ACS Applied Materials and Interfaces* **2014**, *6*, 9365–9375.

[151] W. Helbert, J.-Y. Cavaillé, A. Dufresne, "Thermoplastic nanocomposites filled with wheat straw cellulose whiskers. Part I: processing and mechanical behavior", *Polymer composites* **1996**, *17*, 604–611.

[152] S. S. Ray, M. Okamoto, "Biodegradable polylactide and its nanocomposites: opening a new dimension for plastics and composites", *Macromolecular Rapid Communications* **2003**, *24*, 815–840.

[153] M. P. Arrieta, J. López, S. Ferrándiz, M. A. Peltzer, "Characterization of PLA-limonene blends for food packaging applications", *Polymer Testing* **2013**, *32*, 760–768.

[154] K. Halász, L. Csóka, "Plasticized biodegradable poly (lactic acid) based composites containing cellulose in micro-and nanosize", *Journal of Engineering* **2013**, *2013*.

[155] S. Wohlhauser, G. Delepierre, M. Labet, G. Morandi, W. Thielemans, C. Weder, J. O. Zoppe, "Grafting Polymers from Cellulose Nanocrystals: Synthesis, Properties, and Applications", *Macromolecules* **2018**, *51*, 6157–6189.

[156] N. Macke, C. M. Hemmingsen, S. J. Rowan, "The effect of polymer grafting on the mechanical properties of PEG-grafted cellulose nanocrystals in poly(lactic acid)", *Journal of Polymer Science* **2022**, *60*, 3318–3330.

[157] B. Braun, J. R. Dorgan, L. O. Hollingsworth, "Supra-molecular ecobionanocomposites based on polylactide and cellulosic nanowhiskers: synthesis and properties", *Biomacromolecules* **2012**, *13*, 2013–2019.

[158] A.-L. Goffin, J.-M. Raquez, E. Duquesne, G. Siqueira, Y. Habibi, A. Dufresne, P. Dubois, "From interfacial ring-opening polymerization to melt processing of cellulose nanowhisker-filled polylactide-based nanocomposites", *Biomacromolecules* **2011**, *12*, 2456–2465.

[159] N. Bitinis, R. Verdejo, J. Bras, E. Fortunati, J. M. Kenny, L. Torre, M. A. López-Manchado, "Poly (lactic acid)/natural rubber/cellulose nanocrystal bionanocomposites Part I. Processing and morphology", *Carbohydrate Polymers* **2013**, *96*, 611–620.

[160] E. Lizundia, E. Fortunati, F. Dominici, J. L. Vilas, L. M. León, I. Armentano, L. Torre, J. M. Kenny, "PLLA-grafted cellulose nanocrystals: role of the CNC content and grafting on the PLA bionanocomposite film properties", *Carbohydrate polymers* **2016**, *142*, 105–113.

[161] A. Carlmark, E. Larsson, E. Malmström, "Grafting of cellulose by ring-opening polymerisation - A review", *European Polymer Journal* **2012**, *48*, 1646–1659.

[162] C. J. Clarke, R. A. Jones, J. L. Edwards, K. R. Shull, J. Penfold, "The Structure of Grafted Polystyrene Layers in a Range of Matrix Polymers", *Macromolecules* **1995**, *28*, 2042–2049.

[163] H. Lönnberg, K. Larsson, T. Lindström, A. Hult, E. Malmström, "Synthesis of polycaprolactone-grafted microfibrillated cellulose for use in novel bionanocomposites-influence of the graft length on the mechanical properties", *ACS Applied Materials and Interfaces* **2011**, *3*, 1426–1433.

[164] A. Pei, Q. Zhou, L. A. Berglund, "Functionalized cellulose nanocrystals as biobased nucleation agents in poly (l-lactide)(PLLA)–Crystallization and mechanical property effects", *Composites Science and Technology* **2010**, *70*, 815–821.

[165] G. Siqueira, J. Bras, A. Dufresne, "Cellulose whiskers versus microfibrils: influence of the nature of the nanoparticle and its surface functionalization on the thermal and mechanical properties of nanocomposites", *Biomacromolecules* **2008**, *10*, 425–432.

[166] B. Braun, J. R. Dorgan, "Single-step method for the isolation and surface functionalization of cellulosic nanowhiskers", *Biomacromolecules* **2008**, *10*, 334–341.

[167] M. J. Sobkowicz, J. R. Dorgan, K. W. Gneshin, A. M. Herring, J. T. McKinnon, "Renewable cellulose derived carbon nanospheres as nucleating agents for polylactide and polypropylene", *Journal of Polymers and the Environment* **2008**, *16*, 131–140.

[168] K. Fukushima, Y. Kimura, "Stereocomplexed polylactides (Neo-PLA) as high-performance bio-based polymers: their formation, properties, and application", *Polymer International* **2006**, *55*, 626–642.

[169] H. Wu, S. Nagarajan, L. Zhou, Y. Duan, J. Zhang, "Synthesis and characterization of cellulose nanocrystal-graft-poly(D-lactide) and its nanocomposite with poly(L-lactide)", *Polymer* **2016**, *103*, 365–375.

[170] R. Jaratrotkamjorn, C. Khaokong, V. Tanrattanakul, "Toughness Enhancement of Poly(lactic acid) by Melt Blending with Natural Rubber", *Journal of Applied Polymer Science* **2010**, *124*, 5027–5036.

[171] J. K. Muiruri, S. Liu, W. S. Teo, J. Kong, C. He, "Highly biodegradable and tough polylactic acid–cellulose nanocrystal composite", *ACS Sustainable Chemistry & Engineering* **2017**, *5*, 3929–3937.

[172] G. Q. Chen, G. Zhang, S. J. Park, S. Y. Lee, "Industrial scale production of poly(3-hydroxybutyrate-co-3-hydroxyhexanoate)", *Applied Microbiology and Biotechnology* **2001**, *57*, 50–55.

[173] M. Zinn, B. Witholt, T. Egli, "Occurrence, synthesis and medical application of bacterial polyhydroxyalkanoate", *Advanced Drug Delivery Reviews* **2001**, *53*, 5–21.

[174] D. Kai, X. J. Loh, "Polyhydroxyalkanoates: Chemical modifications toward biomedical applications", *ACS Sustainable Chemistry and Engineering* **2014**, *2*, 106–119.

[175] D. Z. Bucci, L. B. Tavares, I. Sell, "PHB packaging for the storage of food products", *Polymer Testing* **2005**, *24*, 564–571.

[176] J. C. C. Yeo, J. K. Muiruri, W. Thitsartarn, Z. Li, C. He, "Recent advances in the development of biodegradable PHB-based toughening materials: Approaches, advantages and applications", *Materials Science and Engineering C* **2018**, *92*, 1092–1116.

[177] I. T. Seoane, L. B. Manfredi, V. P. Cyras, L. Torre, E. Fortunati, D. Puglia, "Effect of cellulose nanocrystals and bacterial cellulose on disintegrability in composting conditions of plasticized PHB nanocomposites", *Polymers* **2017**, *9*.

[178] I. T. Seoane, P. Cerrutti, A. Vazquez, L. B. Manfredi, V. P. Cyras, "Polyhydroxybutyrate-based nanocomposites with cellulose nanocrystals and bacterial cellulose", *Journal of Polymers and the Environment* **2017**, *25*, 586–598.

[179] P. Patrício, F. V. Pereira, M. C. dos Santos, P. P. de Souza, J. P. B. Roa, R. L. Orefice, "Increasing the Elongation at Break of Polyhydroxybutyrate Biopolymer : Effect of Cellulose Nanowhiskers on Mechanical and Thermal Properties", *Journal of Applied Polymer Science* **2013**, *127*, 3613–3621.

[180] M. P. Arrieta, M. D. Samper, M. Aldas, J. López, "On the use of PLA-PHB blends for sustainable food packaging applications", *Materials* **2017**, *10*, 1–26.

[181] M. P. Arrieta, E. Fortunati, F. Dominici, J. López, J. M. Kenny, "Bionanocomposite films based on plasticized PLA–PHB/cellulose nanocrystal blends", *Carbohydrate Polymers* **2015**, *121*, 265–275.

[182] M. P. Arrieta, E. Fortunati, F. Dominici, E. Rayón, J. López, J. M. Kenny, "Multifunctional PLA-PHB/cellulose nanocrystal films: Processing, structural and thermal properties", *Carbohydrate Polymers* **2014**, *107*, 16–24.

[183] J. M. Eagan, J. Xu, R. Di Girolamo, C. M. Thurber, C. W. Macosko, A. M. La Pointe, F. S. Bates, G. W. Coates, "Combining polyethylene and polypropylene: Enhanced performance with PE/iPP multiblock polymers", *Science* **2017**, *355*, 814–816.

[184] C. Zhuo, Y. A. Levendis, "Upcycling Waste Plastics into Carbon Nanomaterials : A Review", **2014**, *39931*, 1–14.

[185] A.-L. Goffin, Y. Habibi, J.-M. Raquez, P. Dubois, "Polyester-grafted cellulose nanowhiskers: A new approach for tuning the microstructure of immiscible polyester blends", *ACS Applied Materials and Interfaces* **2012**, *4*, 3364–3371.

[186] C. Yong, C. Mei, M. Guan, Q. Wu, X. Sun, B. Xu, K. Wang, "Interfacial modification mechanism of nanocellulose as a compatibilizer for immiscible binary poly(vinyl alcohol)/poly(ethylene oxide) blends", *Journal of Applied Polymer Science* **2018**, *135*, 1–11.

[187] T. Saito, A. Isogai, "Ion-exchange behavior of carboxylate groups in fibrous cellulose oxidized by the TEMPO-mediated system", *Carbohydrate Polymers* **2005**, *61*, 183–190.

[188] D. Wang, "A critical review of cellulose-based nanomaterials for water purification in industrial processes", *Cellulose* **2018**, *26*, 687–701.

[189] J. Lu, R.-N. Jin, C. Liu, Y.-F. Wang, X.-k. Ouyang, "Magnetic carboxylated cellulose nanocrystals as adsorbent for the removal of Pb(II) from aqueous solution", *International Journal of Biological Macromolecules* **2016**, *93*, 547–556.

[190] S. Hokkanen, E. Repo, M. Sillanpää, "Removal of heavy metals from aqueous solutions by succinic anhydride modified mercerized nanocellulose", *Chemical Engineering Journal* **2013**, *223*, 40–47.

[191] Z. Karim, A. P. Mathew, V. Kokol, J. Wei, M. Grahn, "High-flux affinity membranes based on cellulose nanocomposites for removal of heavy metal ions from industrial effluents", *RSC Advances* **2016**, *6*, 20644–20653.

[192] E. Lam, K. B. Male, J. H. Chong, A. C. Leung, J. H. Luong, "Applications of functionalized and nanoparticle-modified nanocrystalline cellulose", *Trends in Biotechnology* **2012**, *30*, 283–290.

[193] M. Jorfi, E. J. Foster, "Recent advances in nanocellulose for biomedical applications", *Journal of Applied Polymer Science* **2015**, *132*, 1–19.

[194] N. Lin, A. Gèze, D. Wouessidjewe, J. Huang, A. Dufresne, "Biocompatible Double-Membrane Hydrogels from Cationic Cellulose Nanocrystals and Anionic Alginate as Complexing Drugs Codelivery", *ACS Applied Materials and Interfaces* **2016**, *8*, 6880–6889.

[195] K. Wang, K. C. Nune, R. Misra, "The functional response of alginate-gelatin-nanocrystalline cellulose injectable hydrogels toward delivery of cells and bioactive molecules", *Acta Biomaterialia* **2016**, *36*, 143–151.

[196] M. Yang, W. Zhen, H. Chen, Z. Shan, "Biomimetic Design of Oxidized Bacterial Cellulose-gelatin-hydroxyapatite Nanocomposites", *Journal of Bionic Engineering* **2016**, *13*, 631–640.

[197] D. O. de Castro, J. Bras, A. Gandini, N. Belgacem, "Surface grafting of cellulose nanocrystals with natural antimicrobial rosin mixture using a green process", *Carbohydrate Polymers* **2016**, *137*, 1–8.

[198] E. Feese, H. Sadeghifar, H. S. Gracz, D. S. Argyropoulos, R. A. Ghiladi, "Photobactericidal porphyrin-cellulose nanocrystals: Synthesis, characterization, and antimicrobial properties", *Biomacromolecules* **2011**, *12*, 3528–3539.

[199] J. Tang, Y. Song, S. Tanvir, W. A. Anderson, R. M. Berry, K. C. Tam, "Polyrhodanine Coated Cellulose Nanocrystals: A Sustainable Antimicrobial Agent", *ACS Sustainable Chemistry and Engineering* **2015**, *3*, 1801–1809.

[200] Q. Shi, C. Zhou, Y. Yue, W. Guo, Y. Wu, Q. Wu, "Mechanical properties and in vitro degradation of electrospun bio-nanocomposite mats from PLA and cellulose nanocrystals", *Carbohydrate Polymers* **2012**, *90*, 301–308.

[201] A. Binek, M. L. Petrus, N. Huber, H. Bristow, Y. Hu, T. Bein, P. Docampo, "Recycling Perovskite Solar Cells to Avoid Lead Waste", *ACS Applied Materials and Interfaces* **2016**, *8*, 12881–12886.

[202] C. J. Rydh, "Environmental assessment of vanadium redox and lead-acid batteries for stationary energy storage", *Journal of Power Sources* **1999**, *80*, 21–29.

[203] L. Jabbour, R. Bongiovanni, D. Chaussy, C. Gerbaldi, D. Beneventi, "Cellulose-based Li-ion batteries: A review", *Cellulose* **2013**, *20*, 1523–1545.

[204] M. A. S. A. Samir, F. Alloin, W. Gorecki, J. Y. Sanchez, A. Dufresne, "Nanocomposite polymer electrolytes based on poly(oxyethylene) and cellulose nanocrystals", *Journal of Physical Chemistry B* **2004**, *108*, 10845–10852.

[205] X. Wu, V. L. Chabot, B. K. Kim, A. Yu, R. M. Berry, K. C. Tam, "Cost-effective and Scalable Chemical Synthesis of Conductive Cellulose Nanocrystals for High-performance Supercapacitors", *Electrochimica Acta* **2014**, *138*, 139–147.

[206] Y. Okahisa, A. Yoshida, S. Miyaguchi, H. Yano, "Optically transparent wood-cellulose nanocomposite as a base substrate for flexible organic light-emitting diode displays", *Composites Science and Technology* **2009**, *69*, 1958–1961.

[207] E. Najafabadi, Y. H. Zhou, K. A. Knauer, C. Fuentes-Hernandez, B. Kippelen, "Efficient organic light-emitting diodes fabricated on cellulose nanocrystal substrates", *Applied Physics Letters* **2014**, *105*.

[208] Y. Zhou, C. Fuentes-Hernandez, T. M. Khan, J. C. Liu, J. Hsu, J. W. Shim, A. Dindar, J. P. Youngblood, R. J. Moon, B. Kippelen, "Recyclable organic solar cells on cellulose nanocrystal substrates", *Scientific Reports* **2013**, *3*, 24–26.

CHAPTER 2

THE EFFECT OF POLYMER GRAFTING ON THE MECHANICAL PROPERTIES OF PEG-GRAFTED CELLULOSE NANOCRYSTALS IN POLY(LACTIC ACID)

2.1 Summary

Poly(lactic acid) (PLA) is a commercially available bio-based polymer that is a potential alternative to many petrochemical-based commodity polymers. However, PLA's thermomechanical properties limit its use in many applications. Incorporating polymer-grafted cellulose nanocrystals (CNCs) is one potential route to improving these mechanical properties. One key challenge in using these polymer-grafted nanoparticles is to understand which variables associated with polymer grafting are most important for improving composite properties. In this work, poly(ethylene glycol)-grafted CNCs are used to study the effects of polymer grafting density and molecular weight on the properties of PLA composites. All CNC nanofillers are found to reinforce PLA above the glass transition temperature, but non-grafted CNCs and CNCs grafted with short PEG chains (< 2 kg/mol) are found to cause significant embrittlement, generally resulting in less than 3 % elongation-at-break. By grafting higher molecular weight PEG (10 kg/mol) onto the CNCs at a grafting density where the polymer chains are predicted to be in the semi-dilute polymer brush conformation ($\sim$0.1 chains/nm^2), embrittlement can be avoided.

2.2 Introduction

Poly(lactic acid) (PLA) is one of the most commercially successful bio-based polymers to emerge over the past few decades. PLA's popularity comes as a result of its high

strength and the fact that it can be produced on an industrial scale,[1] making it a potential alternative to many commodity polymers that are traditionally sourced from petrochemicals. Unfortunately, the poor toughness (elongation-at-break of less than 10 %) and thermal stability (glass transition temperature [T_g] around 60 °C) of PLA limit its use in many applications.[2] There have been a number of approaches explored to improve the toughness of PLA using polymer blends,[3] plasticizers,[4] and filler particles,[5] each achieving varying degrees of success; however, many of these methods employ non-bio-based or less sustainable components.

One potentially more sustainable approach for reinforcing polymer matrices that has attracted significant attention in the recent years is the incorporation of cellulose nanocrystals (CNCs) into composites.[6] CNCs are a strong,[7] sustainable,[6] and biocompatible[8] nanofiller that can be isolated from a wide range of bio-sources including trees, grasses, cotton, and even some animals like sea tunicates.[9] After a series of base washes, bleaching, and acid hydrolysis to remove the non-cellulosic components and amorphous regions of the source material, it is possible to isolate rod- or ribbon-like nanoparticles with dimensions dependent upon the specific isolation procedure and bio-source from which the CNCs were isolated.[9]

On account of their strength and sustainable sourcing, CNCs have been used as a reinforcing filler[10] in a variety of host matrices including poly(vinyl acetate),[11] poly(vinyl alcohol),[12] starch,[13] chitosan,[14] and many more.[6] Dispersing CNCs in these hydrophilic matrices is relatively easy; however, obtaining homogenous dispersions of the hydrophilic CNCs in a more hydrophobic matrix like PLA is more challenging.[15] A number of approaches have been employed over the years to improve dispersion in hydrophobic media such as solvent transfer processes,[16] emulsion techniques,[17,18] and surface modification of the CNCs. Surface modification is used to reduce CNC-CNC interactions and enhance the interactions between the CNCs

and the targeted hydrophobic matrix. This can be achieved by adsorption of small molecules[19] or macromolecules,[20] addition of surfactants,[21] or the grafting of small molecules[18] or polymers;[22] however, the observed increases in the mechanical strength of these composite materials usually come at the cost of elongation-at-break. In some applications, such embrittlement is inconsequential, but for many real-world consumer products, such as packaging, it can immediately disqualify the material from use. If CNC-based composites are to compete with commodity plastics more broadly, then it is important to find ways to reinforce the matrix polymer without sacrificing other properties, such as elongation-at-break.

The embrittlement caused by the incorporation of CNCs is a result of several different factors. One of these factors is the ability of these high aspect ratio nanoparticles[23] to form a rigid, hydrogen-bonded, percolating network throughout the host matrix when the nanoparticles are well dispersed. This percolating network results in a substantial increase in the elastic modulus, but reduces the flexibility of the material.[23] Another cause of embrittlement is poor matrix-filler interactions.[24] When hydrophilic CNCs are added to a hydrophobic matrix, the polymer chains surrounding the nanofiller do not have beneficial interactions with the CNCs. This results in defect points that can lead to premature failure. One way to prevent both these problems is by grafting polymer chains to the surface of the CNCs. The grafted polymers reduce CNC–CNC interactions by shielding the CNC surfaces, limiting the hydrogen bonding required to form a rigid network. In addition, grafting a polymer that is compatible with the host matrix makes the matrix–filler interactions more favorable, allowing stress to be transferred more effectively between the matrix and filler.[25] While some degree of strengthening may be lost by removing the hydrogen-bonded percolating CNC network, the rigid nanoparticles will still act as reinforcing filler, as predicted by the Halpin-Kardos model for nanoparticle composites.[26]

Polymer-grafted CNC composites have, of course, been studied in the past for applications ranging from compatibilizers for immiscible polymer blends[27] to scaffolds for bone cell growth[28] as well as many more.[22] A few studies have explored the effect of polymer-grafted CNCs incorporated into a PLA host matrix.[6,22,29] The most common of such composite materials uses PLA-grafted CNCs as the filler.[30,31] Generally, these reports show improved tensile strength and Young's modulus with the addition of the PLA-grafted CNCs,[32] with a few studies exploring the impact on the crystallization[33,34] and barrier properties[35,36] of the resulting composites. One particularly interesting report by Muiruri et al. investigated PLLA (poly[L-lactic acid]) composites that contained CNCs grafted with diblock polymers where the inner block was a low T_g random copolymer of ϵ-caprolactone (CL) and lactide, while the outer block was PDLA (poly[D-lactic acid]).[37] These materials showed a significant increase in toughness, which was assigned to the inclusion of the rubbery PCL-r-PLA block. Other polymer-grafted CNC composites in PLA have explored the use of poly(butylene succinate) (PBS)[38] or poly(glutamic acid)-grafted CNCs.[39]

The addition of poly(ethylene glycol) (PEG)-grafted cellulose nanoparticles to a PLA matrix[40] has attracted particular attention on account of the ease of grafting PEG to CNCs,[22] and the fact that PEG and PLA have been shown to be compatible.[41] Yin et al. used amine-epoxy chemistry to attach PEG chains to CNC surfaces and observed improved crystallization behavior along with minor changes in the thermal and mechanical properties of the resulting PLA composites.[42] Li et al. attached PEG to the surface of CNCs by first polymerizing dopamine to coat the CNCs, then attaching the PEG to the polydopamine.[43] Composites of these nanoparticles with PLA were studied as packaging materials, showing improved crystallization and barrier properties relative to neat PLA. Yu et al. studied PEG-grafted cellulose nanospheres in PLA and explored their properties in the context of packaging materials.[44] However, it is difficult

to compare these results to the CNC composite literature on account of their use of nanospheres rather than nanorods.

Introducing PEG-grafted CNCs in these systems clearly provides a benefit to the properties of PLA, however it is still unclear what aspects of such grafted nanoparticles are required for optimal material improvement. Polymer-grafted nanoparticle literature outside of CNCs shows that the molecular weight of the grafted polymer needs to be considered in conjunction with its grafting density. Together, these factors determine the grafted polymer chain conformation which, in turn, affects how these polymers are able to interact with the host matrix.[45] In the context of polymer-grafted CNCs these ideas were supported by the recent study by Lettow et al. that showed, in one-component nanocomposites of polystyrene-grafted CNCs, the fracture toughness can be related to the polymer conformation on the nanoparticle surface.[46]

As mentioned previously, a key reason for polymer grafting is to enhance interactions between the nanoparticle and filler to allow for better stress transfer between the two components. When polymer chains are attached to a surface, there are three main conformations that they can adopt – mushroom, semi-dilute polymer brush (SDPB), and concentrated polymer brush (CPB) – depending on the molecular weight and grafting density of the polymer chains.[45,47] If the chains are relatively short or widely spread out on the surface such that adjacent chains do not interact with each other, the polymers adopt a mushroom conformation. In this regime, the bare particle surface is still very much exposed to the host matrix, minimizing any positive stress transfer effects of the polymer graft through unfavorable matrix–filler interactions.[48] If the density of the grafted chains is increased to a point where they overlap, then the polymers adopt a SDPB conformation. In this state, there are sufficient chains on the surface to cover the nanoparticle,[49] but it is still possible for the host matrix polymers to interpenetrate and entangle with the grafted polymer chains. Such entanglements provide an effective stress

transfer mechanism between the matrix and filler, making this the ideal conformation for mechanical reinforcement.[50] As the chains continue to pack even more tightly, they will elongate and form a CPB.[51] In this conformation, the polymer chains are packed so densely that the host matrix polymers are unable to effectively penetrate and entangle with the brush and stress transfer is once again diminished, resulting in lesser mechanical reinforcement.[46]

On nanoparticles with a radius on the same order of magnitude as the radius of gyration (R_g) of the grafted polymer, polymer chains may adopt a CPB/SDPB conformation at high molecular weights. This means that, some distance away from the rounded nanoparticle surface, there is a transition from a CPB to a SDPB conformation as the volume increases.[52] Recently, Keten et al. computationally studied this transition for polymer-grafted CNCs.[53] Their work allowed the development of a polymer conformation "phase space" that is dependent on the molecular weight and grafting density of the attached polymer.[46] Thus, with the goal of developing a better understanding of how polymer-grafted CNCs can impact the mechanical properties of PLA, reported herein are studies on PLA/PEG-grafted CNC composites in which the grafted polymer molecular weights and grafting densities on the CNCs are varied.

2.3 Results and Discussion

2.3.1 Poly(ethylene glycol)-grafted CNCs

Cellulose nanocrystals were isolated from Miscanthus x. Giganteus (MxG) using literature procedures.[11,54] The isolated *MxG*-CNC-OH were subjected to TEMPO oxidation to introduce carboxylate groups to the CNC surface, resulting in a fluffy white powder of *MxG*-CNC-COOH. Conductometric titrations of the oxidized material revealed that there were 1100 $\pm$ 100 mmol –COOH per kg (Figure S2.1, Table S2.1),

which translates to about 1.2 $\pm$ 0.1 groups per nm^2 across the CNC surface. Wide angle X-ray scattering (WAXS) was used to determine that the *MxG*-CNC-COOH had a crystallinity index of 0.84 (Figure S2.2) and atomic force microscopy (AFM) revealed a nanoparticle dimension of 250 $\pm$ 170 nm in length, 13 $\pm$ 2 nm in width, and 2.4 $\pm$ 0.6 nm in height (Figure 2.1a).

To target PEG-grafted CNCs within each conformation regime, amine-terminated methoxy poly(ethylene glycol) (PEG-NH_2) of various molecular weights was grafted to *MxG*-CNC-COOH (Figure 2.1b). Initial work focused on using 1-ethyl-3-(3-dimethylaminopropyl)carbodiimide (EDC) and N-hydroxysuccinimide (NHS) as the peptide coupling reagents and the reaction was carried out in DI water. One key challenge with using such a "grafting-to" approach is the removal of any remaining free polymer that has not been attached to the CNC surface. It is important in this system that as much as

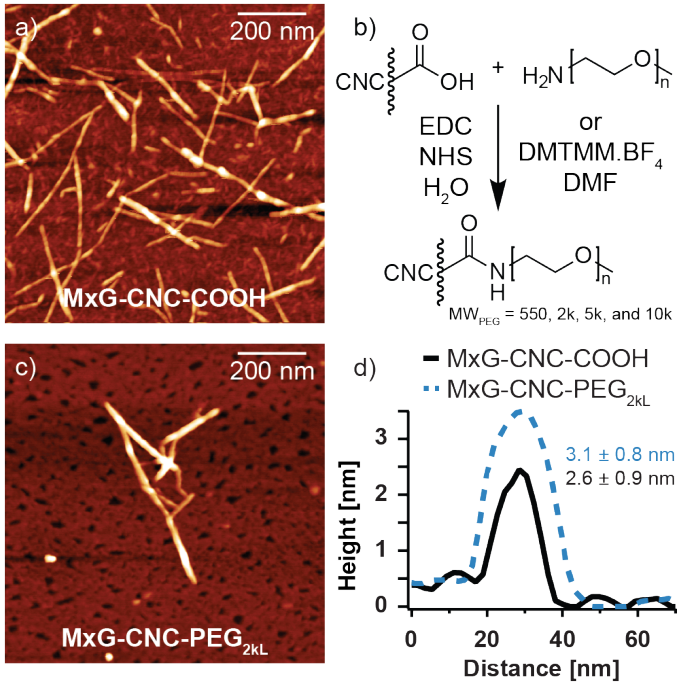

Figure 2.1: a) AFM height image of *MxG*-CNC-COOH, b) grafting scheme for attaching PEG-NH_2 to *MxG*-CNC-COOH, c) AFM height image of *MxG*-CNC-*g*-PEG$_{2kL}$, and d) AFM height profile comparison between *MxG*-CNC-COOH and *MxG*-CNC-*g*-PEG$_{2kL}$ (PEG$_{2kL}$ refers to 2000 g/mol PEG grafted using EDC/NHS)

possible of the non-grafted PEG is removed as any remaining free PEG will plasticize the PLA host matrix,[55] impacting the mechanical properties of the final composite. To this end, a series of washes were carried out to purify the synthesized nanoparticles by suspending the *MxG*-CNC-*g*-PEG particles in water, centrifuging, and then removing the supernatant. The supernatant was then filtered to collect any CNC-*g*-PEG that did not sediment and the filtrate was added to the sedimented sample to minimize the amount of material lost during cleaning. Kaiser tests for primary amines were carried out on each supernatant to track the amount of amine-terminated free polymer removed by each wash.[56] The final *MxG*-CNC-*g*-PEG materials were also resuspended and subjected to Kaiser tests to measure the remaining free polymer in the products, showing that there was less than 5 wt. % of non-grafted polymer remaining in each sample (Figures S2.3 and S2.4). Figure 2.1c shows an AFM image of the resulting *MxG*-CNC-*g*-PEG (grafted with 2000 g/mol PEG). Height profiles of the CNCs before and after grafting (Figure 2.1d) show an increase in nanoparticle height after grafting, which is consistent with polymer being attached to the nanoparticle surface.

The total amount of polymer remaining on the CNC was measured using high-resolution thermogravimetric analysis (Hi-Res TGA).[57] There are two distinct degradation events that are observed in the Hi-Res TGA of the *MxG*-CNC-*g*-PEGs (Figures 2.2, S2.5, and S2.6). The low-temperature degradation event is associated with cellulose degradation, while the higher temperature degradation is associated with PEG. By integrating the area under the PEG peak of the dTG curve, PEG weight fractions ranging from 15 wt. % for CNCs grafted with PEG_{2k} to 27 wt. % for PEG_{10k}-grafted CNCs can be estimated. Using this weight fraction, minus the free polymer measured from the Kaiser test, a polymer grafting density can be calculated for each sample (Table 2.1, Figure 2.3, and the method for calculating polymer grafting density can be found in the Supporting Information). The data show that the EDC/NHS/water procedure for

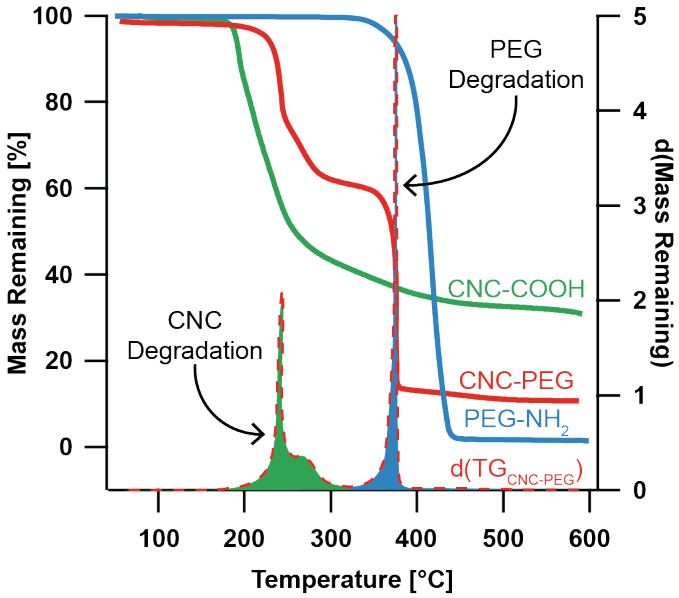

Figure 2.2: Hi-res TGA curves of *MxG*-CNC-COOH (green), PEG-NH_2 (blue), and *MxG*-CNC-*g*-PEG_{5kH} (solid red). The derivative of the *MxG*-CNC-*g*-PEG_{5kH} (dotted red) is presented to show the two distinct degradation peaks, first for cellulose degradation, then for PEG degradation (PEG_{5kH} refers to 5000 g/mol PEG grafted using DMTMM·BF_4)

Table 2.1: Polymer content and grafting density for low grafting density (*MxG*-CNC-*g*-PEG_L) and high grafting density (*MxG*-CNC-*g*-PEG_H) samples with various molecular weights of grafted PEG.

Sample	Total polymer (wt. %)[a]	Non-grafted polymer (wt. %)[b]	Grafted polymer (wt. %)[c]	Grafting density (chains/nm^2)[d]
MxG-CNC-*g*-PEG_{550L}	17	2	15	0.35
MxG-CNC-*g*-PEG_{2kL}	15	2	13	0.09
MxG-CNC-*g*-PEG_{5kL}	27	5	22	0.06
MxG-CNC-*g*-PEG_{10kL}	25	4	21	0.03
MxG-CNC-*g*-PEG_{550H}	21	<1	21	0.52
MxG-CNC-*g*-PEG_{2kH}	39	1	38	0.33
MxG-CNC-*g*-PEG_{5kH}	49	<1	49	0.20
MxG-CNC-*g*-PEG_{10kH}	40	<1	40	0.07

[a] Measured via TGA

[b] Measured via UV-Vis from Kaiser Test

[c] Grafted Polymer = Total Polymer - Non-grafted Polymer

[d] Calculations shown in the Supporting Information

grafting resulted in relatively low grafting densities – ranging from 0.35 chains/nm^2 for the lower molecular weight PEG (550 g/mol) to 0.03 chains/nm^2 for the higher molecular weight PEG (10,000 g/mol) – with all the samples being either within or on the border of the mushroom regime. This boundary between mushroom and brush (the red line in Figure 2.3) was approximated by taking the inverse of the area of a circle defined by the R_g of the grafted polymer.[47] The concentrated brush to semi-dilute brush transition (the blue line in Figure 2.3) was calculated based on work by Hansoge et al. and is based on polybutadiene, which has similar backbone flexibility to PEG.[53]

To access CNC-*g*-PEGs with higher grafting densities, an alternate method of attaching PEG to the CNC surface was sought. Recently, it has been reported[46] that higher grafting densities of amine-terminated polystyrene on *MxG*-CNC-COOH can be obtained using 4-(4,6-dimethoxy-1,3,5-triazin-2-yl)-4-methylmorpholinium

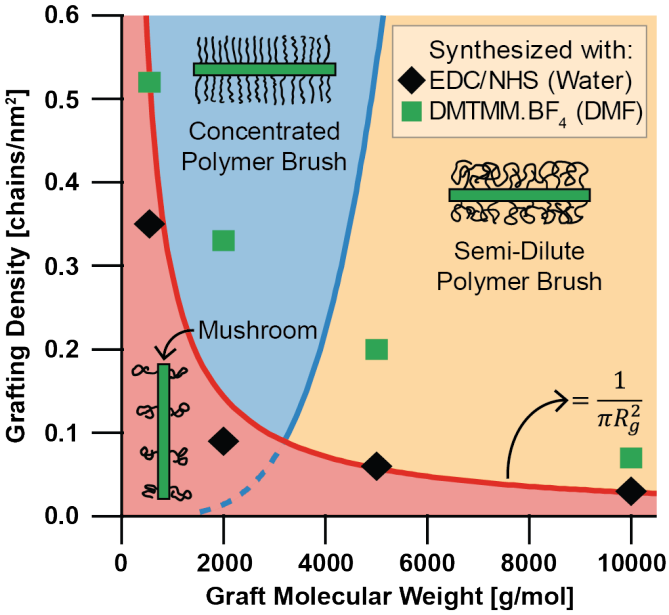

Figure 2.3: Polymer conformation phase space with synthesized *MxG*-CNC-*g*-PEG samples plotted: Grafting PEG with EDC/NHS in water (black diamonds) and grafting PEG with DMTMM·BF_4 in DMF (green squares). The concentrated to semi-dilute brush transition (blue line) is modeled based off polybutadiene.[53] The red mushroom to brush transition (red line) is estimated based on when circles defined by the R_g of the polymer would begin to overlap.

tetrafluoroborate (DMTMM·BF_4) as the coupling agent in dimethylformamide (DMF). Using this coupling protocol and following the same purification and characterization procedure discussed previously, it was found that a significantly higher density of PEG-chains on the CNC surface was obtained (Table 2.1). The resulting PEG chain densities, which ranged from 0.52 chains/nm^2 for the 550 g/mol PEG to 0.07 chains/nm^2 for the 10,000 g/mol PEG, allowed access to more of the conformational phase space with samples now located within the concentrated and semi-dilute polymer brush regimes (Figure 2.3).

To help differentiate samples prepared using different coupling agents, the lower grafting density samples made with EDC/NHS/water are designated as *MxG*-CNC-*g*-PEG_{XXXL} while the higher density samples made with DMTMM·BF_4/DMF are labeled as *MxG*-CNC-*g*-PEG_{XXXH}, where *XXX* represents the molecular weight of the grafted PEG chain.

2.3.2 PLA/CNC-g-PEG composites

To make composites with PLA (120 kg/mol, 12 % D-lactide content,[58]) a solvent casting method was employed to obtain films which were then melt pressed to improve uniformity. It is important to note that this amorphous form of PLA was chosen to minimize convoluting the effects of the nanofiller with the effects of increased PLA crystallinity caused by nucleation from CNCs.[59,60] Dogbone samples were cut from these PLA/*MxG*-CNC-*g*-PEG films according to the ASTM standard D1708 and were subsequently dried in a vacuum oven at 80 °C overnight before melting at 150 °C for 3 min to remove any crystallinity that may have developed during thermal processing (Figure S2.7). A characteristic set of dogbone samples can be seen in Figure 2.4. It is worth noting that all films appear homogenous, although the transparency of all samples decreases as more filler is added. In addition to the PLA/*MxG*-CNC-*g*-PEG

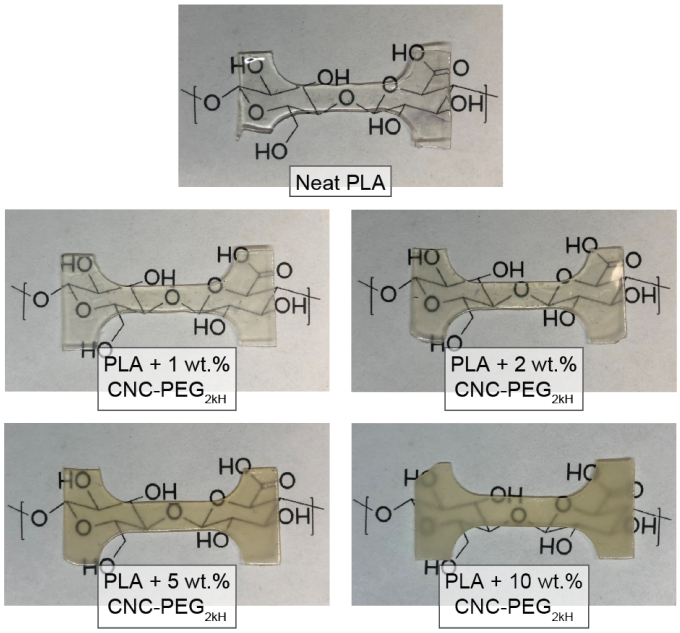

Figure 2.4: Optical images of characteristic dogbones of neat PLA and composites (PLA/*MxG*-CNC-*g*-PEG_{2kH}).

composites, two sets of control samples were prepared: one with *MxG*-CNC-COOH in PLA (PLA/*MxG*-CNC-COOH), and one with *MxG*-CNC-COOH and non-grafted PEG-OH (10 kg/mol) blended into PLA (PLA/*MxG*-CNC-COOH/PEG_{10k}). This blended control was made at the same ratio as *MxG*-CNC-*g*-PEG_{10kH} (40 wt. % PEG) to allow for direct comparisons.

Dynamic mechanical analysis (DMA) was conducted on the dogbone samples (Figures 2.5a, S2.8, S2.9, S2.10, S2.11, and S2.12) to obtain the thermomechanical properties of the different composites. Table 2.2 summarizes the glass transition temperature (T_g) and the storage modulus at both room (25 °C) temperature and above T_g (T_g + 20 °C, roughly 80 °C) of the composite films. As expected, the room temperature moduli in all composites are relatively unaffected by the filler because of the glassy nature of PLA at room temperature (Table 2.2). All composites samples show a broadening of the T_g which is commonly observed with CNC composites and attributed to an increase in free volume around the nanoparticles.[25,42] It is worthwhile noting

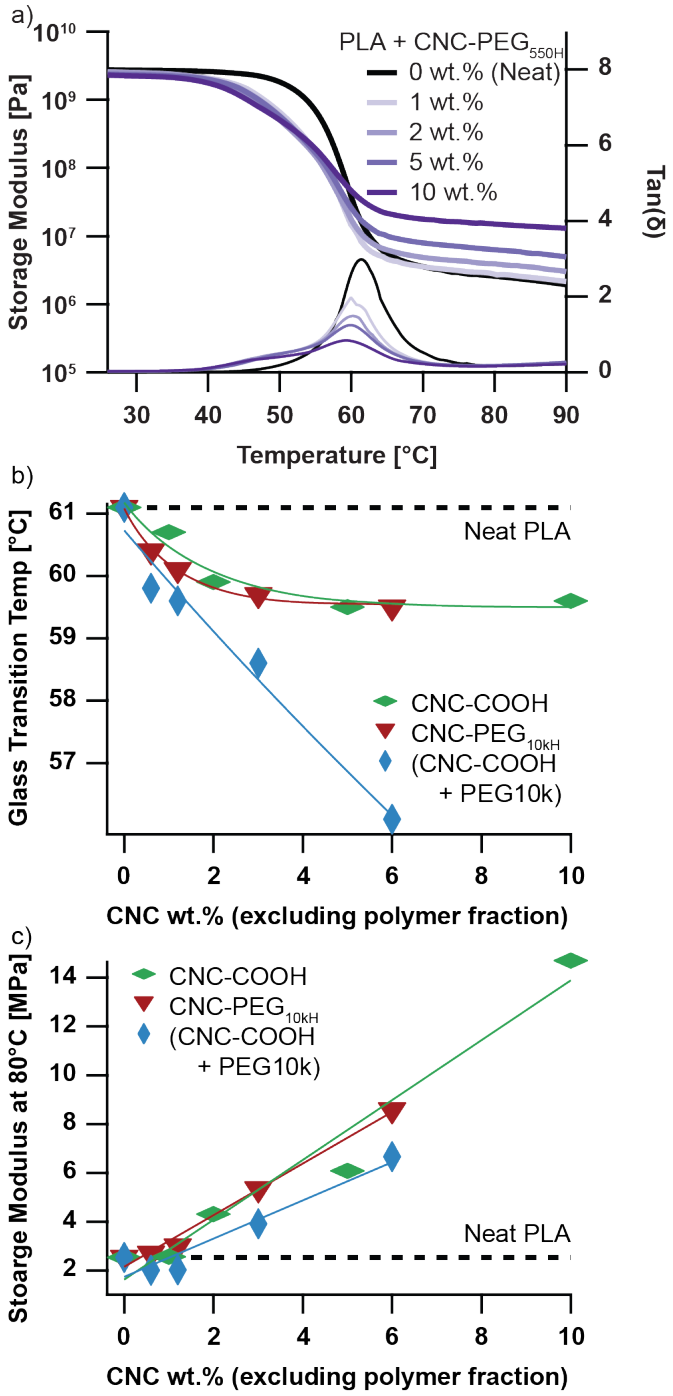

Figure 2.5: a) Characteristic DMA (1 Hz, 3 °C/min) data of PLA/*MxG*-CNC-*g*-PEG_{550H} at various loadings, b) glass transition temperature, and c) high-temperature moduli of PLA/*MxG*-CNC-COOH (green horizontal diamonds), PLA/*MxG*-CNC-COOH/PEG_{10k} (red triangles), and PLA + *MxG*-CNC-*g*-PEG_{10kH} (blue vertical diamonds) plotted against CNC content. Trend lines are provided to guide the eye.

that all PLA/*MxG*-CNC-*g*-PEG composites show a similar T_g (around 59–60 °C), which is only slight less than neat PLA (T_g = 61 °C). The PLA/*MxG*-CNC-COOH/PEG_{10k} composites on the other hand, show a significant decrease in the T_g as the filler loading increases on account of the PLA being plasticized by the unattached PEG (Figure 2.5b).[55] These results provide further evidence that the majority of unattached PEG is removed during the purification process and highlights the fact that covalently grafting the PEG to the CNC surface removes its ability to plasticize the bulk of the matrix.

While the room temperature modulus is dominated by the glassy nature of PLA, the storage modulus above T_g is where the CNC reinforcement can be easily observed. All samples have a dramatic increase in the storage modulus above T_g as the amount of filler is increased (Figure 2.5c). At 5 wt. % filler, all samples have a storage modulus of at least 5 MPa at 80 °C, which is a 100 % increase relative to 2.5 MPa exhibited by neat PLA (Table 2.2). At greater loadings, even more reinforcement is observed: for example, by adding 10 wt. % *MxG*-CNC-*g*-PEG_{5kH} to PLA, the modulus is increased to 13 MPa, a 500 % increase over neat PLA. This reinforcement is independent of grafting density and grafted polymer molecular weight and is controlled predominantly by the CNC fraction of the filler, not the grafted polymer. This is a reasonable expectation as the PEG alone will not provide any strength to the matrix, only the rigid nanorod that the polymer is attached to will reinforce the surrounding PLA. For this reason, all data are plotted against CNC content (calculated by subtracting the polymer weight fraction from the total filler content) rather than filler content.

To measure the strength and elongation-at-break of the composite materials, dogbones were tensile tested to failure following ASTM D1708 (Figures 2.6a, S2.13, S2.14, S2.15, S2.16, and S2.17). Consistent with the CNC composite literature,[6] composites with 1 wt. % *MxG*-CNC-COOH exhibit a tensile strength that is similar to that of neat PLA, around 40 MPa, but a 64 % reduction in elongation-at-break (6.6 to 2.4 %).

Table 2.2: DMA and tensile testing statistics for all samples tested

Sample	**Filler loading (wt. %)**	**Low T modulus (GPa)[a]**	**Glass transition temp (°C)**	**High T modulus (MPa)[b]**	**Tensile strength (MPa)**	**Elongation-at-break (%)**
Neat PLA	NA	2.80	61.1	2.54	43.9 ± 0.2	6.6 ± 1.4
PLA + MxG-CNC-COOH	1	2.51	60.7	2.56	38.4 ± 0.6	2.4 ± 0.3
	2	2.79	59.9	4.31	40.3 ± 0.6	1.8 ± 0.2
	5	2.67	59.5	6.09	35.9 ± 0.7	1.5 ± 0.1
	10	2.96	59.6	14.7	34.4 ± 1.0	1.1 ± 0.2
	50	4.09	61.7	131	30.1	0.7
PLA + MxG-CNC-COOH + PEG_{10k}	1	1.88	59.8	2.01	26.2 ± 1.0	2.5 ± 0.5
	2	1.73	59.6	2.03	27.6 ± 1.1	3.1 ± 0.7
	5	2.3	58.6	3.92	27.7 ± 0.8	3.3 ± 0.2
	10	2.34	56.1	6.67	24.6 ± 0.8	3.2 ± 0.7
PLA + MxG-CNC-g-PEG_{550L}	1	2.51	61.2	2.69	35.7 ± 0.7	3.4 ± 0.6
	2	2.41	59.8	3.05	35.1 ± 0.9	2.1 ± 0.3
	5	2.53	59.5	6.94	32.7 ± 0.3	2.0 ± 0.2
	10	2.59	59.3	9.14	31.7 ± 0.3	1.6 ± 0.1
PLA + MxG-CNC-g-PEG_{2kL}	1	2.44	60.2	2.37	33.4 ± 1.5	4.3 ± 0.9
	2	2.56	59.6	4.17	34.8 ± 1.3	3.3 ± 0.2
	5	2.36	59.2	7.1	32.1 ± 0.6	5.0 ± 1.1
	10	2.46	59.6	12.6	28.0 ± 1.0	6.7 ± 0.6
PLA + MxG-CNC-g-PEG_{5kL}	1	2.43	59.4	2.32	35.1 ± 1.3	3.6 ± 1.1
	2	2.36	60.4	2.8	36.7 ± 0.6	5.2 ± 0.3
	5	2.64	59.8	6.18	33.2 ± 0.5	2.0 ± 0.3
	10	2.68	59.9	15.3	29.9 ± 0.7	2.2 ± 0.3
PLA + MxG-CNC-g-PEG_{10kL}	1	2.22	60.5	1.77	35.4 ± 0.6	4.4 ± 1.1
	2	2.41	60.4	3.39	34.7 ± 0.4	3.2 ± 0.5
	5	2.53	60.5	6.57	32.9 ± 0.1	4.5 ± 0.3
	10	2.52	60.1	12.7	29.4 ± 1.1	3.6 ± 1.0
PLA + MxG-CNC-g-PEG_{550H}	1	2.6	59.9	2.71	37.0 ± 0.9	3.6 ± 0.5
	2	2.61	60.3	3.86	36.9 ± 0.1	3.4 ± 0.2
	5	2.4	59.5	6.38	37.3 ± 0.7	2.7 ± 0.6
	10	2.32	59.3	15.2	33.2 ± 0.4	2.7 ± 0.1
PLA + MxG-CNC-g-PEG_{2kH}	1	2.49	60.7	3.5	34.9 ± 0.3	4.0 ± 0.2
	2	2.39	60.2	2.96	32.9 ± 0.4	5.1 ± 0.8
	5	2.37	59.8	4.97	32.4 ± 0.2	4.5 ± 0.3
	10	2.32	59	11.2	28.3 ± 0.3	3.9 ± 0.4
PLA + MxG-CNC-g-PEG_{5kH}	1	2.21	60	2.34	36.6 ± 0.3	4.1 ± 0.8
	2	2.25	60	2.66	36.8 ± 1.7	3.4 ± 0.2
	5	2.46	59.2	5.47	29.2 ± 0.8	4.1 ± 0.1
	10	2.41	58.8	13	30.6 ± 1.7	3.4 ± 0.1
PLA + MxG-CNC-g-PEG_{10kH}	1	2.41	60.4	2.71	35.8 ± 0.3	5.7 ± 0.2
	2	2.45	60.1	3	34.6 ± 0.5	6.0 ± 0.8
	5	2.29	59.7	5.34	31.2 ± 0.4	5.5 ± 0.9
	10	1.98	59.5	8.58	30.2 ± 0.3	7.4 ± 0.5
	50	2.46	59.4	245	26.9	2.4

[a] Measured at 25 °C, [b] Measured at T_g + 20 °C

Note: For tensile strength and elongation-at-break, standard errors are presented (n = 3). If no error is present, only one sample was tested.

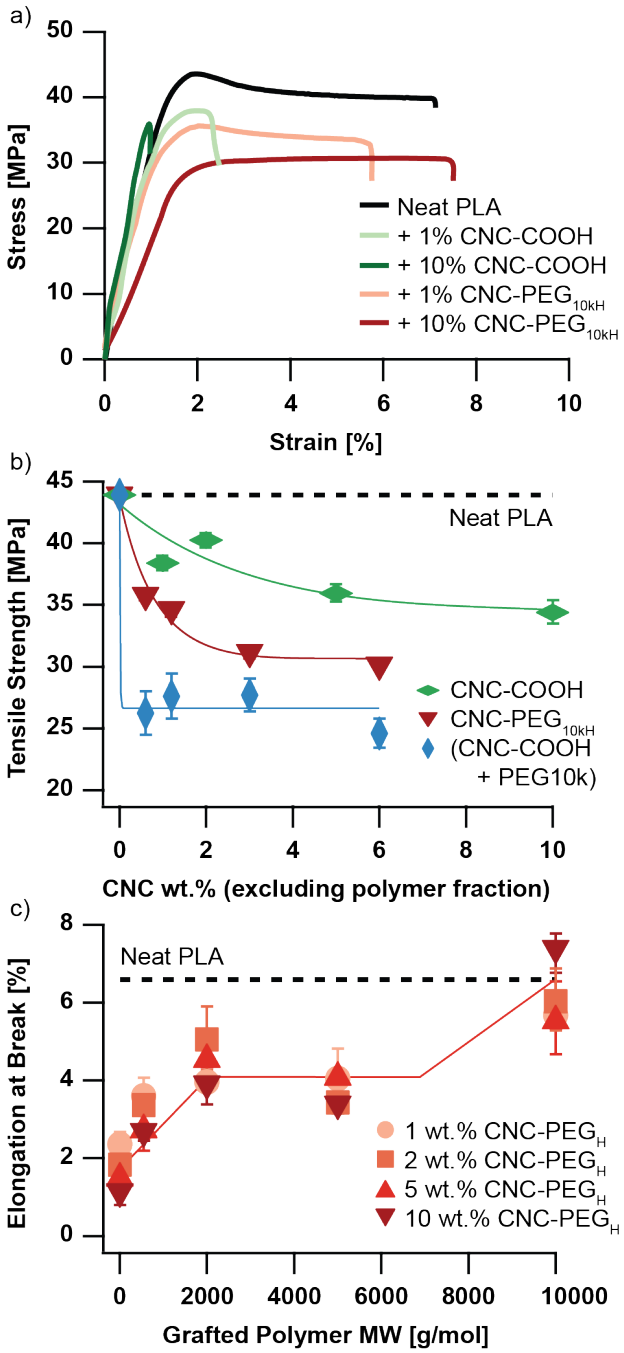

Figure 2.6: (A) Tensile testing (1 mm/min) curves of neat PLA, PLA/*MxG*-CNC-COOH, and PLA/*MxG*-CNC-*g*-PEG_{10kH}, (B) tensile strength plotted against CNC content for PLA/*MxG*-CNC-COOH (green horizontal diamonds), PLA/*MxG*-CNC-COOH/PEG_{10k} (red triangles), and PLA/*MxG*-CNC-*g*-PEG_{10kH} (blue vertical diamonds), and (C) elongation-at-break plotted against grafted polymer molecular weight for high grafting density samples at 1, 2, 5, and 10 wt. % filler. Trend lines are provided to guide the eye.

When *MxG*-CNC-*g*-PEG_{10kH} is added, there is not only a notable reduction in this embrittlement, but also a slight drop in the tensile strength, or maximum stress (Figure 2.6b). This reduction in tensile strength is consistent across all samples as more filler is added to the composite materials. It is certainly possible that the drop in tensile strength with increasing filler content is related to poor dispersion of the nanofiller. However, an alternative explanation for the drop in tensile strength is a softening of the matrix at the nanoparticle interface on account of localized plasticization by the grafted PEG, allowing the surrounding matrix to deform under less stress. As more filler is added and the total surface area of filler is increased in the composite, it could be expected that this interfacial plasticization would allow deformation to occur more readily, resulting in the observed drop in tensile strength as loading increases. Additionally, it is observed that the PLA/*MxG*-CNC-*g*-PEG_{2kH} samples loaded at 5 wt. % have a drop in tensile strength of about 26 %, whereas PLA/*MxG*-CNC-COOH/PEG_{10k} samples at the same 5 wt. % of filler exhibit an even larger drop (almost 37 %) as the entire matrix is softened by the non-attached PEG chains, as evidenced by the drop in the composite T_g (Table 2.2). These phenomena have been observed in the literature with PEG-grafted CNCs, but are often overshadowed by an increase in crystallinity caused by the nucleating effect of the CNCs.[43]

Thus far, all trends discussed have been consistent between the low and high grafting density samples, with both groups showing an increase in modulus above T_g, broadening of T_g, and slight reduction in tensile strength. However, this consistency is not present when looking at the elongation-at-break of the samples, as no trends are observed in the low grafting density samples (Figures S2.16 and S2.17). This is likely a result of inconsistencies in CNC surface coverage. Based on their placement in Figure 2.3, all low-density samples are either in the mushroom regime or very close to the estimated mushroom-to-brush transition, meaning that the grafted polymer likely

does not completely cover the hydrophilic CNC surface. If some of the CNC surface is exposed, then there will be unfavorable interactions between the nanofiller and the hydrophobic PLA matrix, which could act as defect points that cause premature failure. When the grafting density is increased, consistency improves dramatically, and trends can be identified (Figure 2.6c). With no polymer grafting or grafting with PEG_{550} the resulting composites are brittle and generally exhibit less than 3 % elongation-at-break. The *MxG*-CNC-*g*-PEG_{550H} filler is still in the mushroom regime, which means that there is likely some exposed CNC surface that would have unfavorable interactions with the PLA matrix, causing embrittlement.

Increasing the molecular weight of the grafted polymer to 2000 g/mol results in the grafted polymer adopting a CPB conformation and the elongation-at-break of the PLA/*MxG*-CNC-*g*-PEG_{2kH} composites increases slightly, to around 4 %, regardless of the amount of filler in the sample. This suggests that although the hydrophilic surface is completely covered, there may not be enough stress transfer between the filler and the matrix to improve the mechanical properties of these composites. While Figure 2.3 shows that the *MxG*-CNC-*g*-PEG_{5kH} samples are in the CPB/SDPB region, these composites behave similarly to the *MxG*-CNC-*g*-PEG_{2kH} materials with a 4 % elongation-at-break (Figure 2.6c). For the *MxG*-CNC-*g*-PEG_{5kH} filler, only about 1000 g/mol of the polymer graft exists in the SDPB conformation (Figure S18), but the entanglement molecular weight of PEG is almost 2000 g/mol.[61] This means that there may not be enough penetrable brush on the *MxG*-CNC-*g*-PEG_{5kH} sample to promote efficient stress transfer between the filler and matrix. As such, while there are no unfavorable interactions with exposed CNC surface, there are also limited opportunities for entanglements between the polymer matrix and grafted polymers that would enhance the composite properties.

The analysis is supported by the properties of the PLA/*MxG*-CNC-*g*-PEG_{10kH} composites. In this case, the higher overall molecular weight of the graft (and the

grafting density) means that the length of the polymer in the SDPB regime is larger. For this filler, Figure 3 suggests that there is roughly 3000 g/mol in a CPB conformation and around 7000 g/mol in the SDPB conformation (Figure S2.18), which should allow for significant interpenetration, entanglement, and stress transfer with the surrounding matrix. The tensile properties confirm this observation with an elongation-at-break of around 7 %, which is equivalent to that of neat PLA. One interesting observation in the *MxG*-CNC-*g*-PEG_{10kH} samples is that the elongation is maintained regardless of the filler loading (Figure 6c). This is unusual because elongation-at-break usually decreases as filler loading increases, akin to what is observed in the *MxG*-CNC-COOH samples that were tested in this study.

To explore this observation a bit more, two PLA composite samples were prepared that contained 50 wt. % filler using either *MxG*-CNC-COOH or *MxG*-CNC-*g*-PEG_{10kH}. The 50 wt. % PLA/*MxG*-CNC-COOH material behaved as expected, with less than 1 % elongation-at-break and over 5000 % increase in the high-temperature modulus relative to neat PLA (Table 2.2, Figures S2.8 and S2.13). The 50 wt. % PLA/*MxG*-CNC-*g*-PEG_{10kH} sample showed significant embrittlement as well, but a yield point was observed even at this high filler loading and the storage modulus was 9500 % times greater than neat PLA above T_g (Table 2.2, Figures S2.10 and S2.15). This improved reinforcement compared to PLA/*MxG*-CNC-COOH as well as the observed yielding in these high loading composites emphasize the observation that these PLA/*MxG*-CNC-*g*-PEG_{10kH}, where the grafted polymer reside in the SDPB or CPB/SDPB regimes, have better interactions with the host matrix.

2.4 Conclusions

In summary, for the *MxG*-CNC-*g*-PEG nanoparticles investigated here, the grafted polymer density and molecular weight play key roles in the resulting mechanical

properties of PLA composites. By grafting PEG to the nanoparticle surface, the plasticizing ability of the PEG in PLA was minimized while still imparting significant reinforcement above T_g. Through analysis of the polymer conformation on the CNC surface, it was found that samples in the mushroom regime exhibited inconsistent behavior and significant embrittlement at low molecular weights, likely because of exposed hydrophilic CNC surfaces having unfavorable interactions with the more hydrophobic PLA matrix. In the concentrated polymer brush regime, the complete CNC surface coverage resulted in less composite embrittlement, but the tightly packed polymer chains were unable to interface effectively with the surrounding matrix, resulting in little-to-no improvement of mechanical properties. With long enough polymer chains in the semi-dilute polymer brush regime, the grafted polymers had a greater ability to interact and entangle with the surrounding PLA, resulting in embrittlement being avoided entirely.

Overall, this work points to a few key variables that should be considered when targeting mechanical reinforcement in polymer-grafted CNC composites in a PLA matrix. Ideally, it is important to ensure that (1) the surface grafting density is high enough to completely cover the CNC surface and (2) the grafted polymer molecular weight is high enough to interface effectively with the surrounding matrix.

2.5 Materials, Methods, and Instrumentation

2.5.1 Materials

Miscanthus x. Giganteus (MxG) stalks were kindly provided by Prof. Geoff Coates, who grew the grass in his backyard in New York. Amorphous poly(lactic acid) (PLA) 4060D was kindly provided by Natureworks via the Ellison group at the University of Minnesota. Sodium hydroxide (NaOH), sodium hypochlorite (NaOCl), acetic acid,

chloroform ($CHCl_3$), dimethylformamide (DMF), potassium cyanide (KCN), ninhydrin, butanol, and phenol were purchased from Thermo Fisher Scientific. Sodium chlorite ($NaClO_2$), hydrochloric acid (HCl), 2,2,6,6-tetramethylpiperidine 1-oxyl (TEMPO), sodium bromide (NaBr), N-hydroxysuccinimide (NHS), N-methylmorpholine, sodium tetrafluoroborate ($NaBF_4$), and pyridine were purchased from Millipore Sigma. 1-Ethyl-3-(3-dimethylamino-propyl)carbodiimide (EDC) was purchased from Combi-Blocks. 2-Chloro-4,6,-dimethoxy-1,3,5-triazine was purchased from Chem-Impex International. Amine-terminated methoxy poly(ethylene glycol) (PEG-NH_2) of various molecular weights (550, 2,000, 5,000, and 10,000 g/mol) were purchased from CreativePEGWorks. All water used was deionized in-house and all chemicals were used as-received without further purification.

2.5.2 Methods

2.5.2.1 Isolating *MxG*-CNC-OH from MxG stalks

MxG-CNC-OH were isolated using a previously published procedure.[11]

2.5.2.2 TEMPO oxidation of *MxG*-CNC-OH to obtain *MxG*-CNC-COOH

TEMPO oxidation was conducted immediately after isolating the *MxG*-CNC-OH, without drying, following the previously published procedure with slight modifications.[11] In brief, the CNCs resulting from dried MxG stalks (250 g) were suspended with 3 wt. % TEMPO (7.5 g) and 30 wt. % NaBr (75 g) relative to the original stalk mass. 50 wt. % of NaOCl (110 ml) was added, then the pH was adjusted to 10.5 with 10 M NaOH. The pH was maintained between 10 and 11 for 3 h, then the resulting *MxG*-CNC-COOH were centrifuged at 10,000 rpm and resuspended $\sim$5 times in DI water to clean the nanoparticles. The resulting material was suspended in DI water and freeze dried to

obtain a fluffy white powder of *MxG*-CNC-COOH.

2.5.2.3 Quantifying carboxylate groups on *MxG*-CNC-COOH

Conductivity titration was used to determine the amount of carboxylate groups on the surface of the *MxG*-CNC-COOH nanoparticles. *MxG*-CNC-COOH (100 mg) were dispersed in DI water (100 ml) using probe sonication. The pH was then adjusted to 2–3 using concentrated HCl. Using a syringe pump, 0.01 M NaOH (60 ml) was then added dropwise over the course of roughly 4 h. The pH and conductivity of the solution were recorded every 15 s to construct conductivity vs. volume added plot. When graphed, the length of the weak acid plateau is used to calculate the number of carboxylate groups per unit mass. This number can then be converted to a number of groups per unit area using the dimensions of the CNCs. All these calculations can be found in the supporting information.

2.5.2.4 Grafting PEG-NH_2 to *MxG*-CNC-COOH in water

MxG-CNC-COOH were suspended in DI water at 10 mg/mL using a sonic bath to promote dispersion. Relative to the carboxylate content determined by conductivity titration, PEG-NH_2 (1 eq.) of the desired molecular weight was added to the CNC suspension and allowed to dissolve. EDC (3 eq.) was added and stirred for 5 min before adding NHS (3 eq.). The reaction proceeded overnight before centrifuging and resuspending in DI water 5 times to remove any remaining EDC, NHS, and free polymer. The supernatant from each wash was also filtered with Sterlitech 0.2 μm PVDF filter membranes and the collected material was re-added to the product to ensure that any *MxG*-CNC-*g*-PEG that did not sediment during centrifugation was not lost. After purification, the resulting *MxG*-CNC-*g*-PEGs were suspended in water and freeze dried to obtain a fluffy white powder.

2.5.2.5 Preparation of DMTMM·BF_4

First, 2-chloro-4,6,-dimethoxy-1,3,5-triazine was dissolved in DI water at 100 mg/mL and N-methylmorpholine (1 eq.) was added dropwise while stirring. After 30 min, 0.01 M $NaBF_4$ (1.3 eq.) solution was added and allowed to react for 2 hours. The product of 4-(4,6-Dimethoxy-1,3,5-triazin-2-yl)-4-methylmorpholinium tetrafluoroborate (DMTMM·BF_4) precipitated from the solution and was collected via filtration. The product was washed twice with DI water, then dried using high vacuum to yield the final product. 1H NMR (400 MHz, CD_3CN, 25 °C): $\delta = 4.45$ (m, 2H, OCH_2), 4.13 (s, 6H, OCH_3), 4.01 (m, 2H, OCH_2), 3.74 (m, 4H, NCH_2), 3.40 (s, 3H, NCH_3).

2.5.2.6 Grafting PEG-NH_2 to *MxG*-CNC-COOH in DMF

MxG-CNC-COOH were suspended in DMF at 10 mg/mL using a sonic bath to promote dispersion. Relative to the carboxylate content determined by conductivity titration, PEG-NH_2 (1 eq.) of the desired MW was added to the CNC suspension. After the PEG dissolved, DMTMM·BF_4 (1.1 eq.) was added and the reaction proceeded overnight. The resulting *MxG*-CNC-*g*-PEG was centrifuged and resuspended three times in DMF and twice in DI water, filtering the supernatant with Sterlitech 0.2 μm PVDF filter membranes after each wash to collect any CNCs that did not sediment. The washes were done to remove any leftover DMTMM·BF_4 and PEG that did not graft to the surface. After purification, the resulting *MxG*-CNC-*g*-PEGs were suspended in water and freeze dried to obtain a fluffy white powder.

2.5.2.7 Measuring free polymer remaining in *MxG*-CNC-*g*-PEG

The amount of non-grafted polymer remaining in the nanomaterial was measured using a Kaiser test for primary amines. Three separate solutions were prepared for the testing

process: (A) KCN (0.65 mg) was dissolved in DI water (1 ml) then added to pyridine (49 ml), (B) ninhydrin (1 g) was dissolved in butanol (20 ml), and (C) phenol (40 g) was dissolved in butanol (20 ml). To conduct a test, sample solution (1 ml) was placed in a vial on a hot plate at 100 °C. Two drops of each solution were added and allowed to react, shaking occasionally. After 10 min, DI water (3 ml) was added to each solution to improve transparency for UV–Vis testing. The solutions were then tested with UV–Vis to quantify the concentration of amine groups present in the solution via the intensity of the 569 nm absorbance peak. Using this method, the supernatant solution from each wash was measured to track the reduction in primary amines over subsequent washes and the *MxG*-CNC-*g*-PEG was resuspended at 5 mg/mL in DI water and tested as well to measure the amount of free PEG in the final material. This concentration could then be used to estimate the mass of free PEG relative to the mass of *MxG*-CNC-*g*-PEG in the solution.

2.5.2.8 Measuring total polymer in *MxG*-CNC-*g*-PEG

The total amount of PEG in the *MxG*-CNC-*g*-PEG materials was measured using high resolution thermogravimetric analysis (Hi-Res TGA). Using Hi-Res TGA, which slows the heating rate when a mass loss event is detected, two distinct degradation events can be seen for cellulose degradation and PEG degradation. Taking the derivative of the mass loss curve, the area under the peak associated with PEG degradation can be measured to determine the weight fraction of PEG relative to CNC. By subtracting the amount of free polymer measured via UV–Vis from the amount of total polymer measured, a polymer grafting density can be obtained. The calculations for these conversions can be found in the Supporting Information.

2.5.2.9 Preparation of PLA + MxG-CNC composites

To prepare composites of PLA with *MxG*-CNC-*g*-PEG and *MxG*-CNC-COOH, a 10 wt. % PLA stock solution was first prepared by dissolving PLA (30 g) in $CHCl_3$ (270 g). As an example, amounts will be presented for a 5 wt. % CNC film, but films of 1, 2, 5, and 10 wt. % were produced for each type of filler. Using a sonic bath and vigorous shaking, the desired CNCs (150 mg) were suspended directly in $CHCl_3$ (20 ml). To that suspension, the 10 wt. % PLA stock solution (28.5 g) was added and shaken thoroughly to mix. The solution was allowed to mix in a sonic bath for a couple hours, then cast into a Teflon petri dish to dry overnight while covered with holey foil to moderate the evaporation rate. Once the films could be removed from the petri dish, they were placed in a vacuum oven at 60 °C to dry overnight. The films were then cut into pieces and melt pressed to obtain films of uniform thickness. From these films were cut dogbones according to the ASTM standard D1708. These dogbones were then dried again in a vacuum oven, ramping from room temperature up to 80 °C over the course of 2 days to ensure the samples were as dry as possible before melting. The dogbones were then placed on a hot plate at 150 °C for 3 min to melt any crystals that may have formed during the melt pressing and drying steps. The dogbones were then quenched on the 20 °C bench top to prevent any further crystallization.

2.5.2.10 Tensile testing of composites

Tensile testing of composite materials was conducted according to the standard ASTM D1708. Using the video extensometer to track elongation prior to yielding and the crosshead distance to track elongation after yielding gave a more accurate measurement of extension in the elastic regime while also accounting for irregular plastic deformation after yielding. All samples were tested in triplicate unless otherwise noted and an

average tensile strength and elongation-at-break were extracted for each sample.

2.5.2.11 DMA testing of composites

DMA temperature ramps were done on each sample from 25 to 100 °C at a rate of 1 Hz. The room temperature storage modulus (25 °C), glass transition temperature ($\tan[\delta]$ peak), and high-temperature storage modulus (T_g + 20 °C) were extracted for each sample.

2.5.3 Instrumentation

Atomic force microscopy (*AFM*) measurements were conducted with a Cypher ES Environmental AFM using FS-1500 probes (Asylum Research). Samples were prepared by freshly cleaving a mica surface, drop casting 100 μl of poly(L-lysine), gently rinsing with DI water after 3 min, drop casting 100 μl of the desired sample suspended in DI water, gently rinsing with DI water after 3 min, then drying overnight at room temperature. Images were recorded in ultra-high-frequency tapping mode and analyzed with Gwyddion software (Czech Metrology Institute).

Conductivity and pH measurements were conducted with an Accumet XL benchtop pH-conductivity meter on aqueous solutions.

Dynamic mechanical analysis (*DMA*) was conducted with a TA Instruments RSA-G2 DMA on films of each sample ($\sim$ 3 mm × 1 mm × 20 mm). Temperature ramps were run from 25 to 100 °C at 3 °C/min at a frequency of 1 Hz.

Dynamic scanning calorimetry (*DSC*) was conducted with a TA Instruments Discovery 2500 DSC. Samples were heated from 25 °C to 200 °C at 10 °C/min, then cooled to -90 °C at 5 °C/min, then heated back up to 200 °C at 10 °C/min. Crystallinity data were taken from the first heating cycle.

Melt pressing was conducted with a Carver AccuStamp Model 3693 melt press. Sam-

ples were pressed between two sheets of Teflon into 0.5 mm thick Teflon molds at 95 °C for 2 h at 2 tons of pressure.

Nuclear magnetic resonance (*NMR*) was conducted with a Bruker Avance III HD 400 MHz spectrometer for 1H nuclei. Samples were prepared in $CDCl_3$ with the residual solvent peak (7.26 ppm) used as the reference. MestrReNova software was used to process the data.

Tensile testing was conducted with a Zwick-Roell zwickiLine Z0.5 instrument. Dogbones were tested in accordance with ASTM D1708 (crosshead speed = 1 mm/min) and tracked with a VideoXtens extensometer up to yielding, followed by crosshead distance tracking.

Thermogravimetry (*TGA*) was conducted with a TA Instruments Discovery TGA using the high resolution procedure (Hi-Res TGA) with default settings (sensitivity = 1, amplitude 5 °C, period 200 s, ramp = 5 °C/min to 600 °C, resolution = 6) in platinum pans.[57]

UV–Visible light spectroscopy (*UV–Vis*) was conducted with a Shimadzu UV-3600 Plus UV–Vis–NIR spectrophotometer from 350 to 800 nm wavelengths. Samples were run at 1 nm resolution in quartz cuvettes.

Wide-angle X-ray scattering (*WAXS*) was conducted with a SAXSLAB GANESHA 300XL using a Cu Kα source (λ = 0.154 nm) at a voltage and power of 40 kV and 40 mA, respectively. Samples were packed between two pieces of Kapton tape and data were collected for 1 hour at 2θ = 1–32°. Crystallinity was measured by modeling the crystal planes and amorphous residual as Gaussian peaks and comparing their area, as described previously.[62]

2.6 Supporting Information

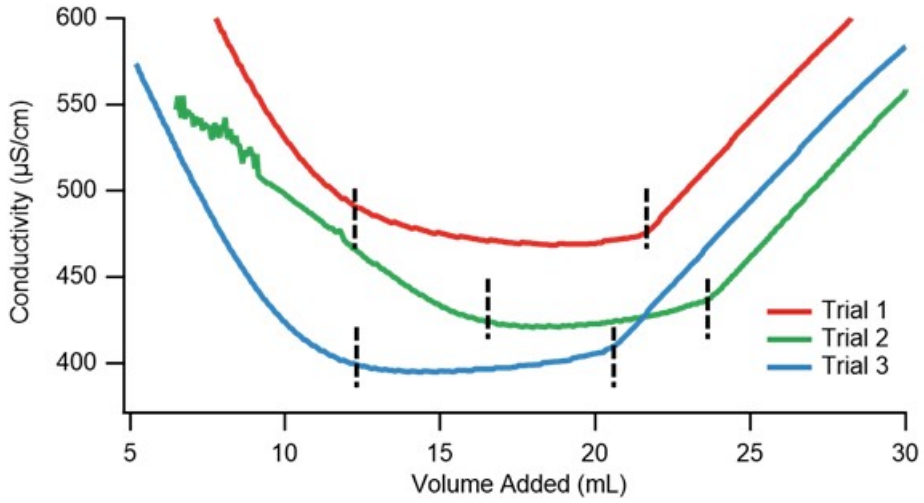

Figure S2.1: Plot of conductivity vs. volume of 0.01 M NaOH added in order to measure the amount of -COOH present on *MxG*-CNC-COOH. The dotted black lines denote the plateau associated with -COOH neutralization.

Table S2.1: Results of conductivity titration tests to measure the -COOH content on the surface of *MxG*-CNC-COOH.

Trial	CNC Mass (mg)	Plateau Volume (mL)	-COOH Concentration (mmol/kg)	-COOH Density (groups/nm^2)
1	68	7.8	1147	1.20
2	48	5.9	1229	1.28
3	65	6.9	1062	1.11
Average			1100 $\pm$ 100	1.2 $\pm$ 0.1

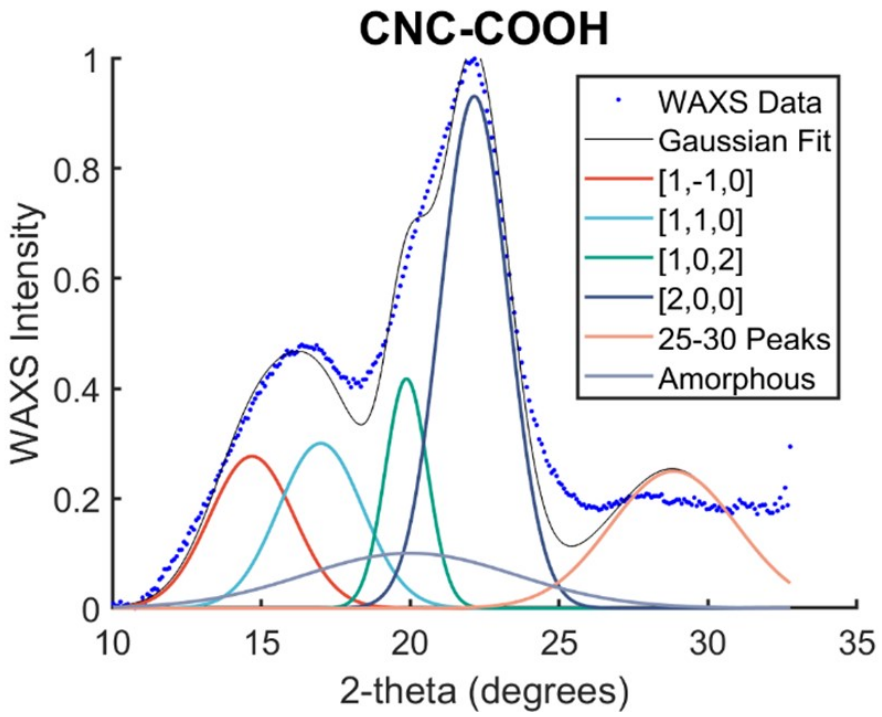

Figure S2.2: Wide angle X-ray scattering data for *MxG*-CNC-COOH (blue dots) plotted with deconvolution peaks associated with each crystal plane.

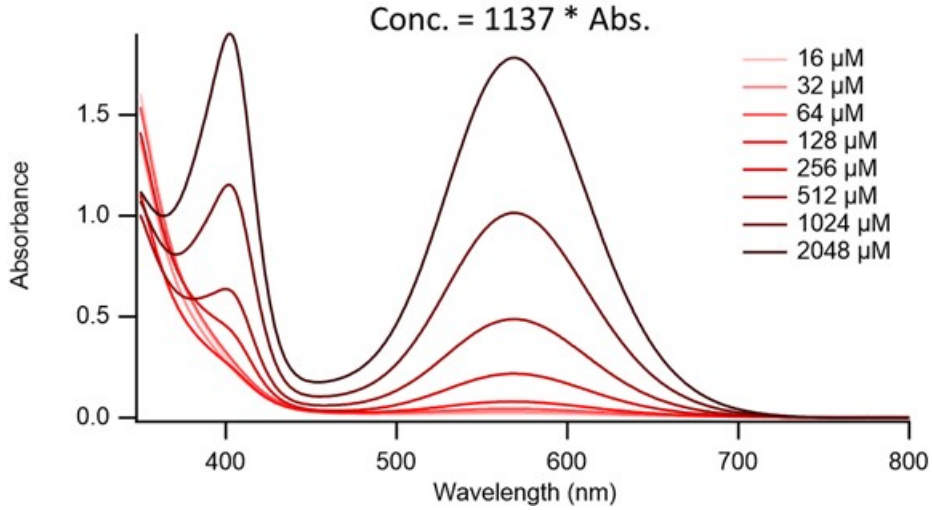

Figure S2.3: UV-Vis spectra of the calibration curve developed for Kaiser testing. Calibration samples were made with *n*-butyl amine. After linear fitting of the 569 nm peak absorbance vs. concentration, the fitting equation was measured as Concentration (μM) = 1137 * Absorbance, which translates to an extinction coefficient of 880 M^{-1} cm^{-1}.

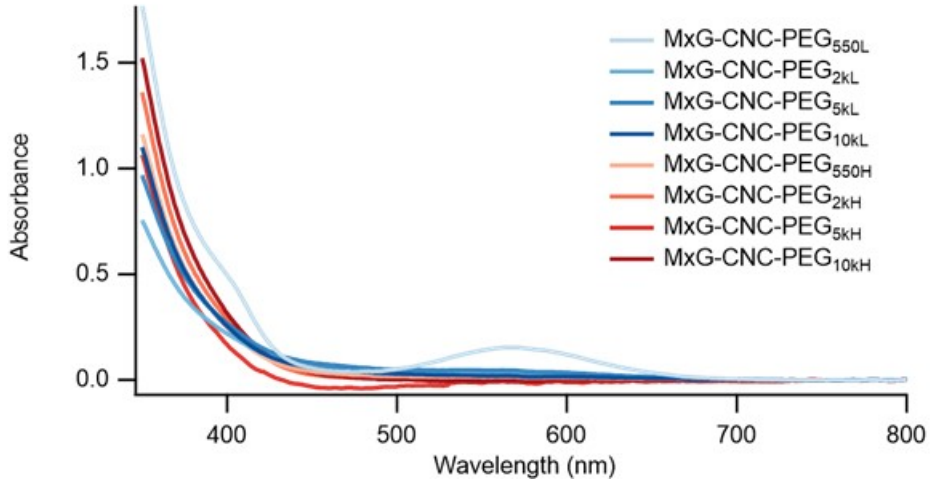

Figure S2.4: UV-Vis data of the Kaiser testing of *MxG*-CNC-*g*-PEG samples suspended in DI water at 5 mg/mL after purification procedures to remove any non-grafted polymer. The 569 nm peak absorbance was used to calculate non-grafted PEG-NH_2 content.

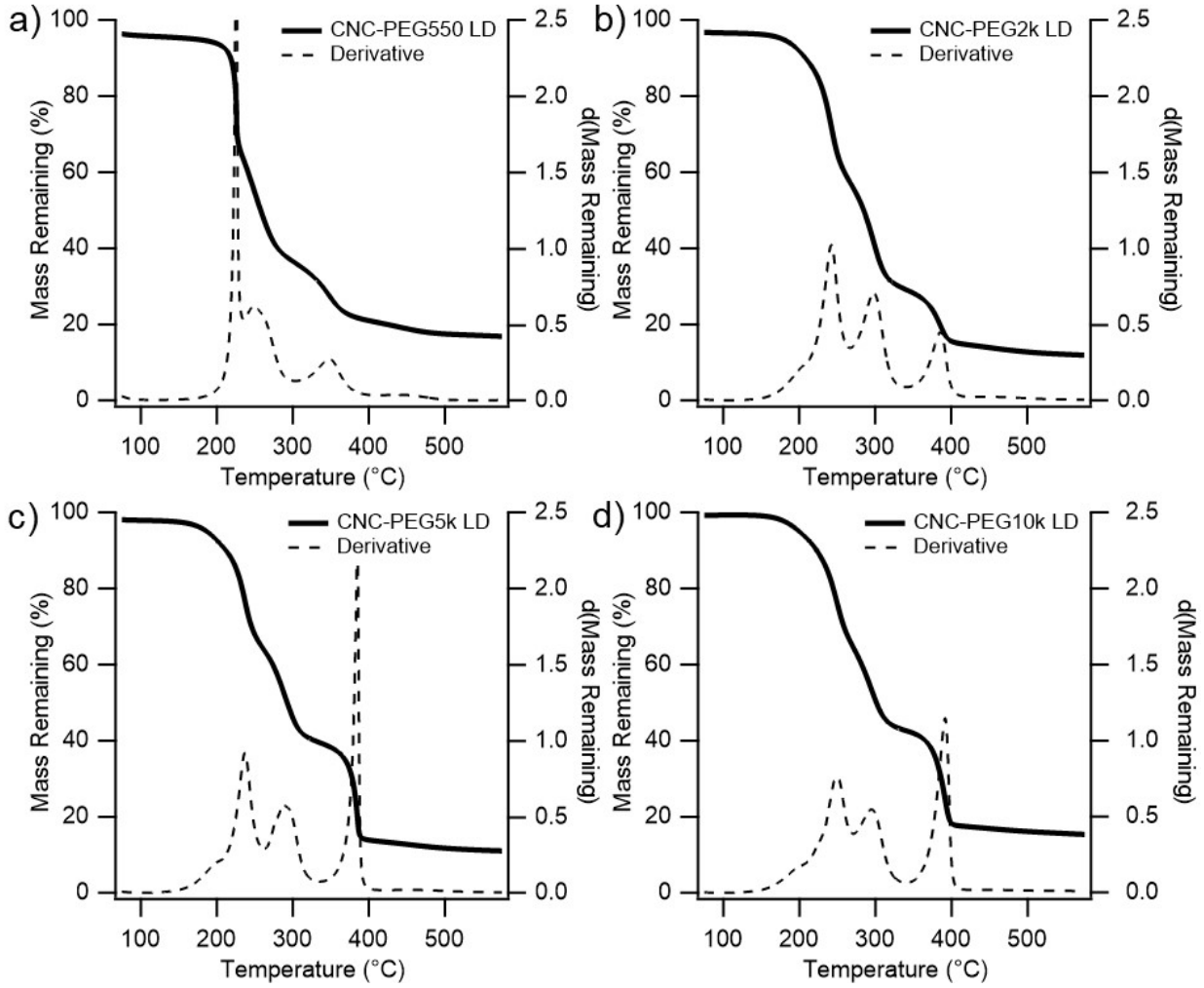

Figure S2.5: Hi-Res TGA (see the experimental section of the manuscript for details) decomposition curves for low grafting density *MxG*-CNC-*g*-PEG_L samples (solid line) with a) 550, b) 2k, c) 5k, and d) 10k g/mol and the associated derivatives (dashed line), showing two peaks for cellulose degradation and a third peak for PEG degradation.

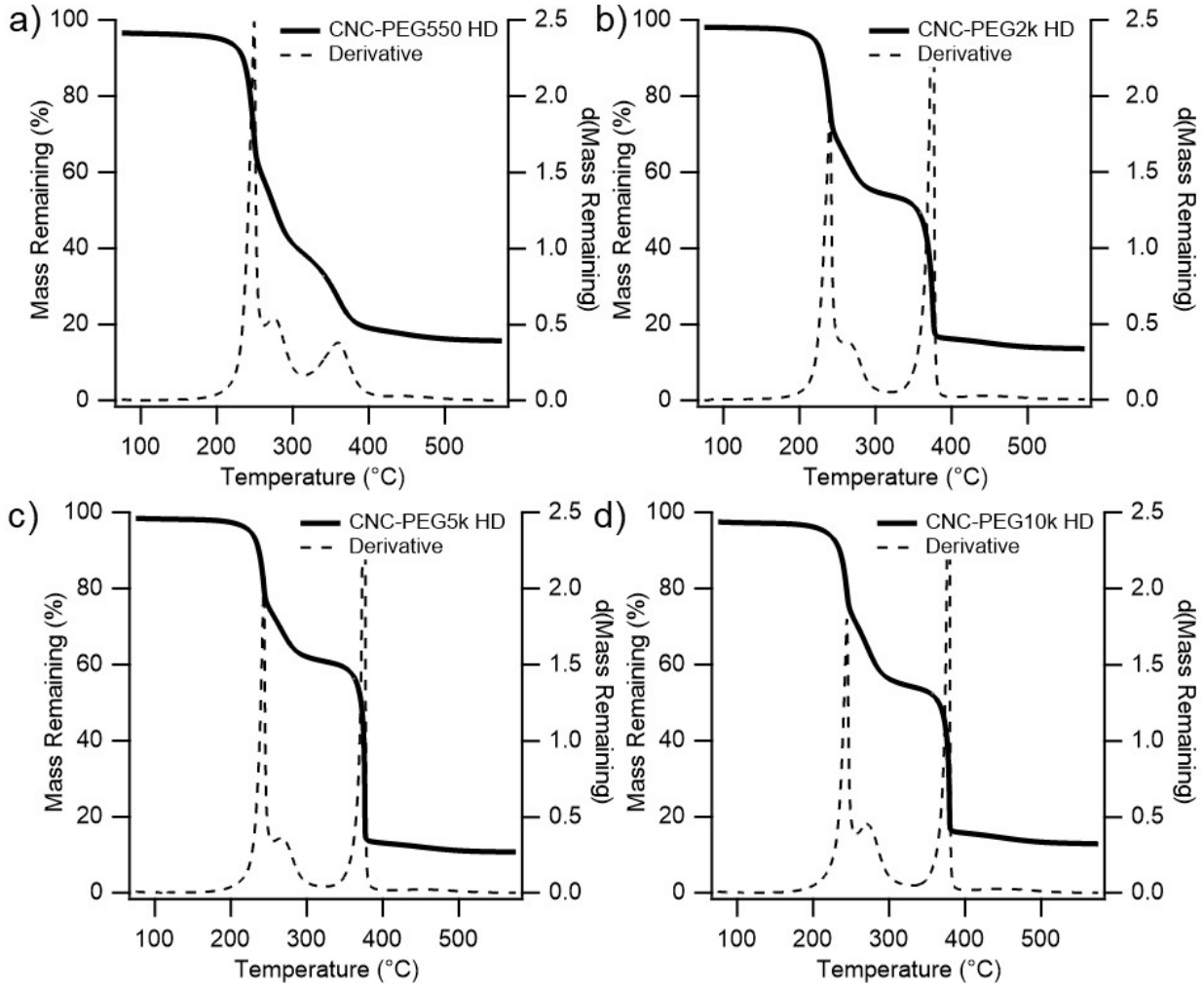

Figure S2.6: Hi-Res TGA (see the experimental section of the manuscript for details) decomposition curves for high grafting density *MxG*-CNC-*g*-PEG_H samples (solid line) with a) 550, b) 2k, c) 5k, and d) 10k g/mol and the associated derivatives (dashed line), showing two peaks for cellulose degradation and a third peak for PEG degradation.

Grafting Density Calculations

Assuming that the CNCs are 100 % crystalline with a crystal unit cell size of 1.038 x 0.820 x 0.778 nm[63] and nanoparticle dimensions of 250 x 8 x 3 nm (based on AFM of *MxG*-CNC-COOH), we can tile 6519 unit cells across the surface of the CNC (assuming that the largest unit cell face is being tiled).

$$\frac{2 * (250 * 8 + 250 * 3 + 8 * 3) \frac{nm^2}{crystal}}{1.038 * 0.820 \frac{nm^2}{unit\ cell}} = 6519 \frac{unit\ cells}{crystal}$$

Knowing that each unit cell has one exposed primary -OH group and the other primary -OH is group buried within the crystal structure, we can calculate that there are 1.18 primary -OH groups per nm^2 across the CNC surface.

$$\frac{6519 \frac{unit\ cells}{crystal}}{2 * (250 * 8 + 250 * 3 + 8 * 3) \frac{nm^2}{crystal}} * 1 \frac{-OH\ group}{unit\ cell} = 1.18 \frac{-OH\ group}{nm^2}$$

Based on the density of cellulose being 1.6 g/cm^3,[64] we can calculate the mass of a single crystal to be 9.6 * 10^{-21} kg, meaning that there are 1.04 * 10^{20} crystals per kg.

$$1600 \frac{kg}{m^3} * (250 * 8 * 3) * (10^{-9})^3 \frac{m^3}{crystal} = 9.6 * 10^{-21} \frac{kg}{crystal} = 1.04 * 10^{20} \frac{crystals}{kg}$$

With this information and the number of primary -OH groups per nm^2 calculated earlier, we can calculate the number of primary -OH groups per kg of CNCs to be 6.8 * 10^{23}, which converts to 1,130 mmol of primary -OH groups kg of material.

$$6519 \frac{unit\ cells}{crystal} * 1.04 * 10^{20} \frac{crystals}{kg} = 6.8 * 10^{23} \frac{groups}{kg} = 1130 \frac{mmol}{kg}$$

To convert between surface density (groups/nm^2) and concentration (mmol/kg), the following conversion can be used (note that this conversion only works for the specific crys-

tal dimensions used in the calculations above):

$$1130\frac{mmol}{kg} = 1.18\frac{-OH\ group}{nm^2}$$

These numbers represent the theoretical maximum for grafting density when attaching polymer chains to primary -OH groups on the CNC surface. If polymer chains are grafted to secondary -OH groups as well, the number of theoretically available sites is multiplied by 3.

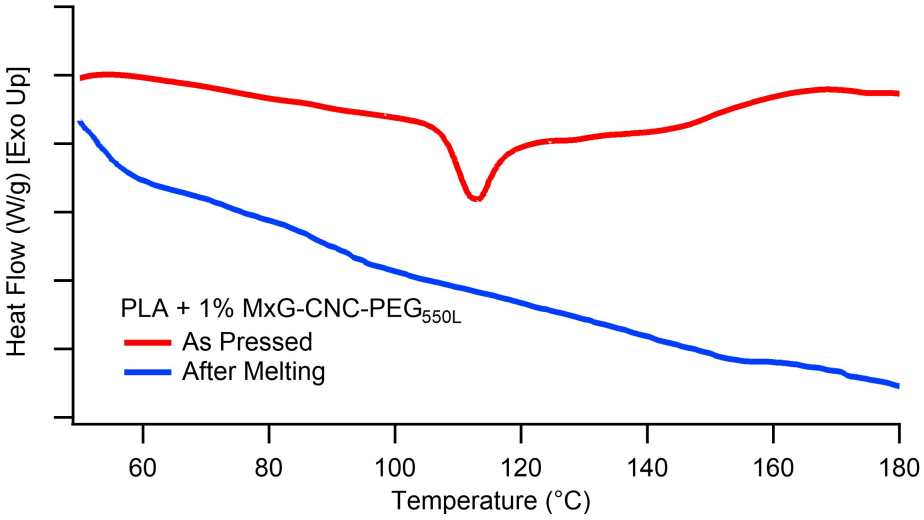

Figure S2.7: DSC traces of the first heating cycle (10 °C/min) of a representative PLA composite (PLA/*MxG*-CNC-*g*-PEG_{550L}) that shows PLA crystallization after drying and melt pressing (red), and the resulting amorphous sample (blue) after melting at 150 °C for three minutes.

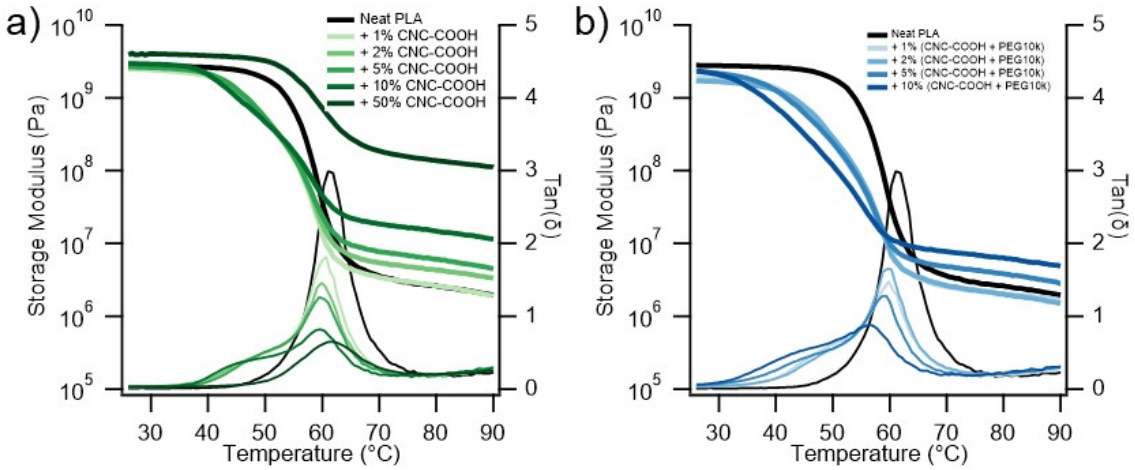

Figure S2.8: Dynamic mechanical analysis (DMA) curves (1 Hz, 3 °C/min) for the composite controls: a) PLA/*MxG*-CNC-COOH and b) PLA/*MxG*-CNC-COOH/PEG_{10k}. Each plot contains a single filler at various loading levels (1, 2, 5, 10, 50 wt. %).

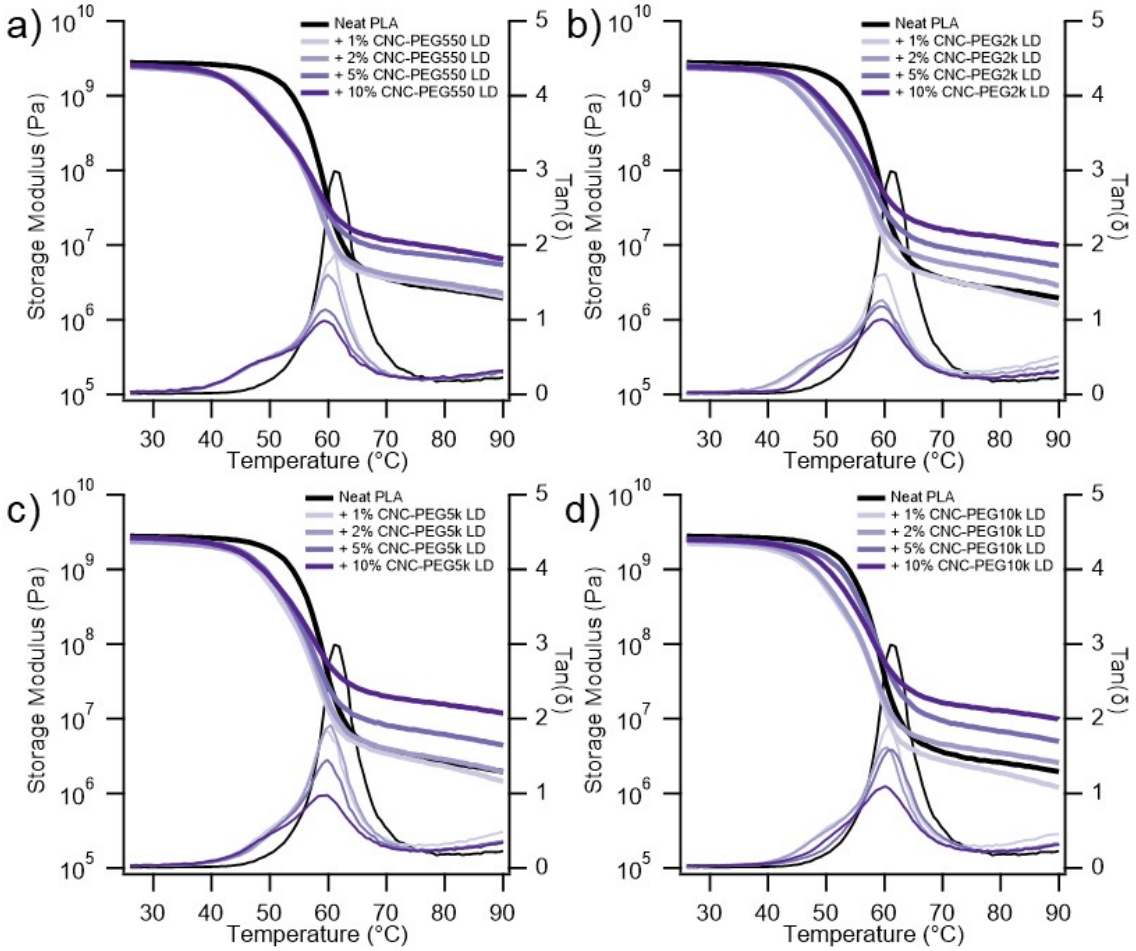

Figure S2.9: Dynamic mechanical analysis (DMA) curves (1 Hz, 3 °C/min) for the composites filled with low grafting density filler with a) 550, b) 2k, c) 5k, and d) 10k g/mol PEG (PLA/*MxG*-CNC-*g*-PEG_L). Each plot contains a single filler at various loading levels (1, 2, 5, 10 wt. %).

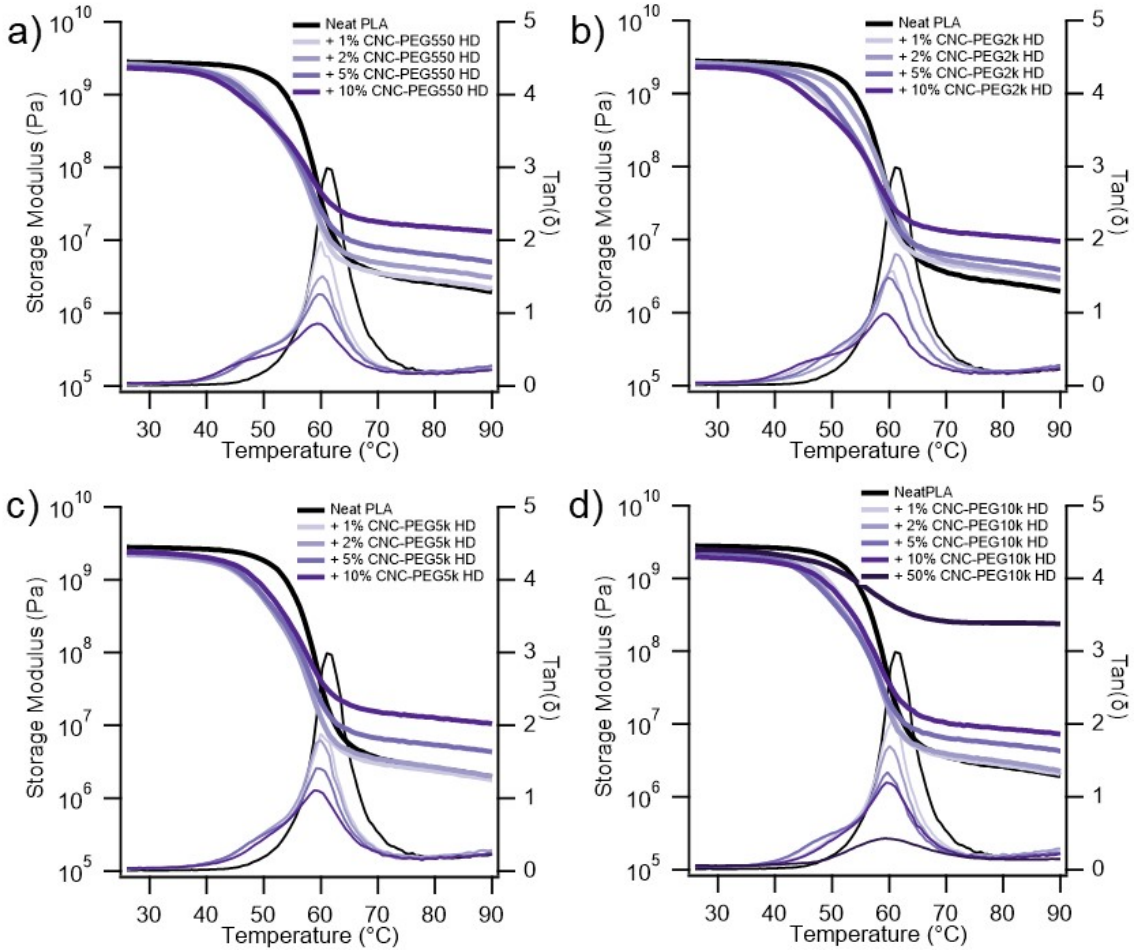

Figure S2.10: Dynamic mechanical analysis (DMA) curves (1 Hz, 3 °C/min) for the composites filled with high grafting density filler with a) 550, b) 2k, c) 5k, and d) 10k g/mol PEG (PLA/*MxG*-CNC-*g*-PEG_H). Each plot contains a single filler at various loading levels (1, 2, 5, 10, 50 wt. %).

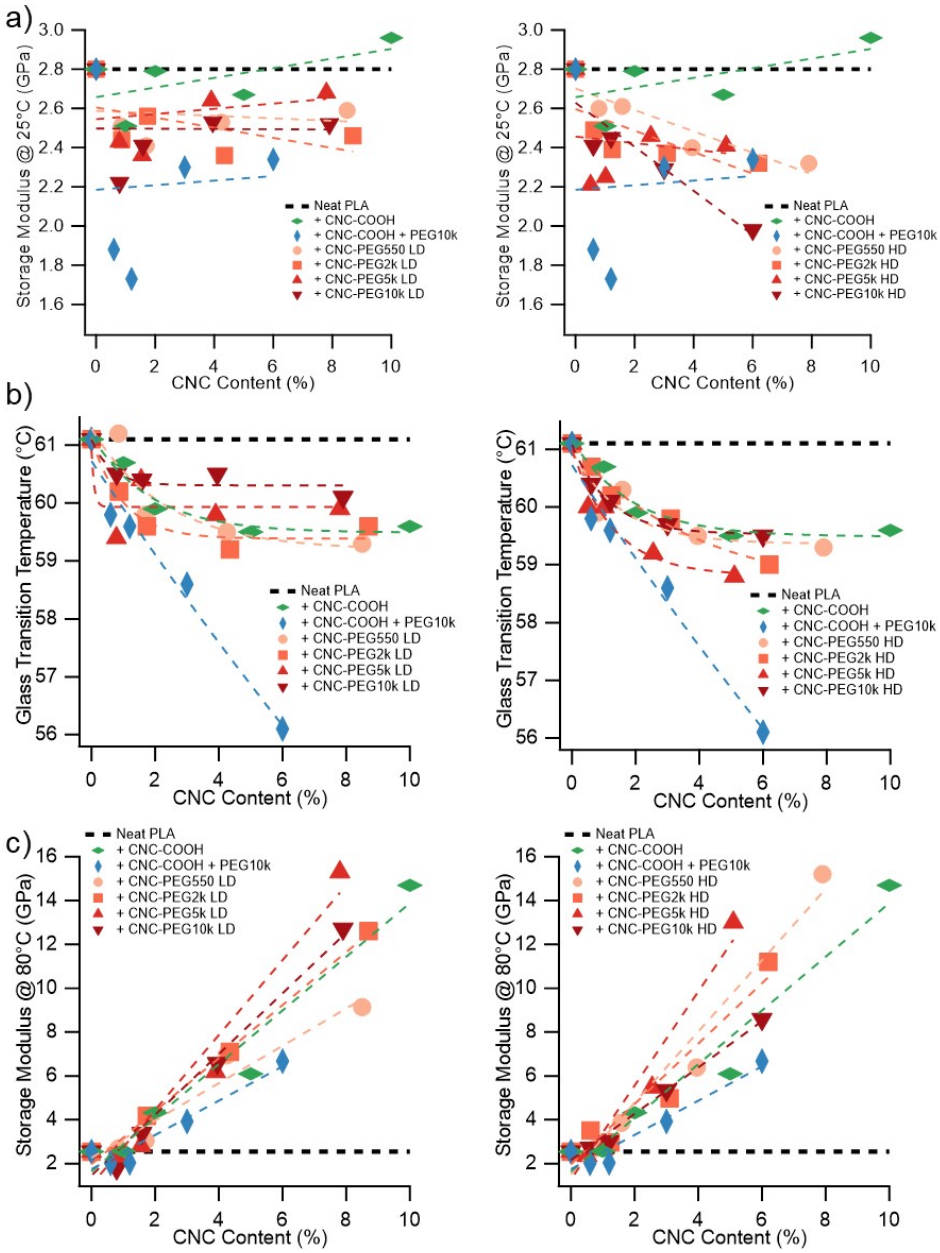

Figure S2.11: Plots of a) low temperature modulus (25 °C), b) glass transition temperature (tan[δ] peak), and c) high temperature modulus (T_g + 20 °C, ~80 °C) vs. CNC content for all composites, extracted from the DMA curves. The left side plots show data for composites made with the low grafting density nanofillers (*MxG*-CNC-*g*-PEG_L) and the right side show the same data for the high grafting density filler (*MxG*-CNC-*g*-PEG_H).

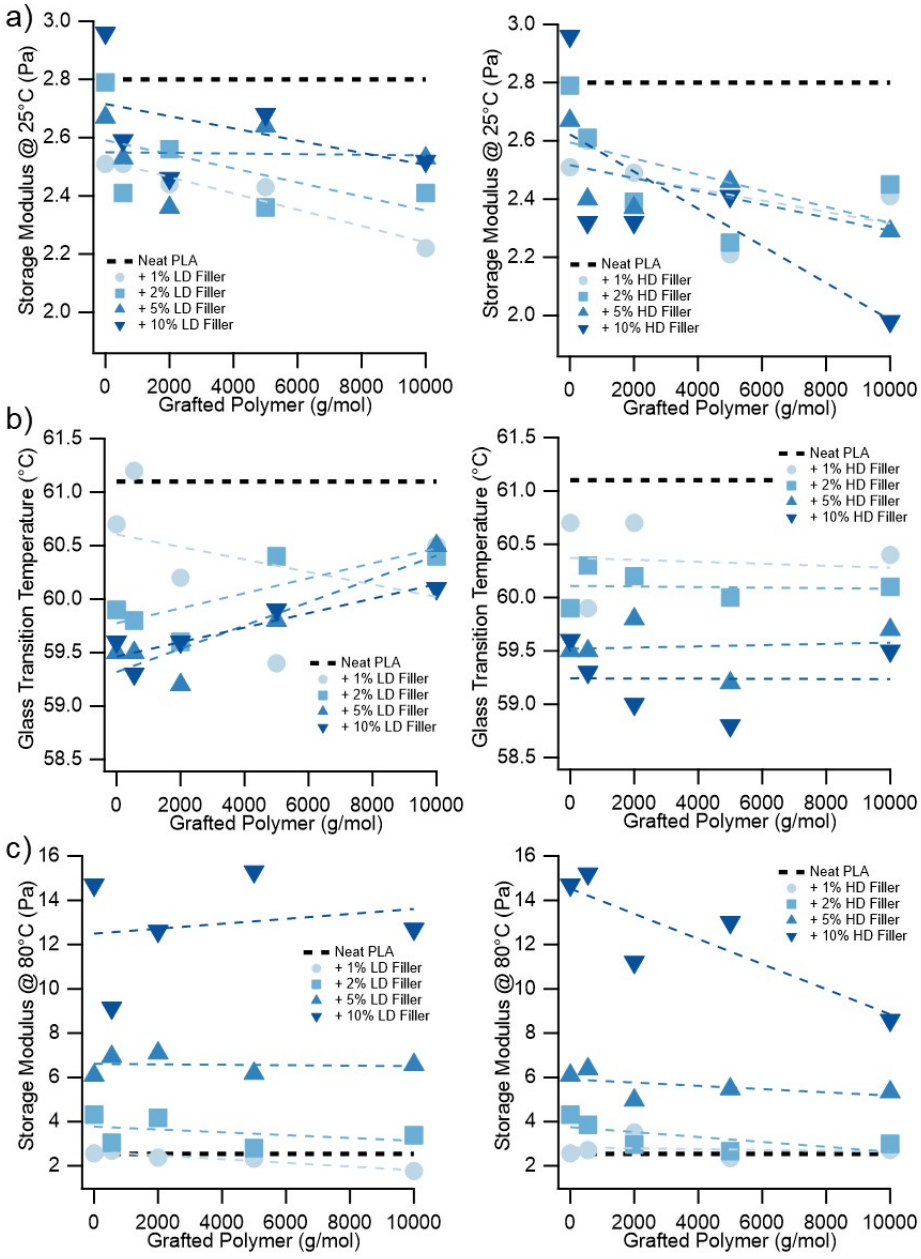

Figure S2.12: Plots of a) low temperature modulus (25 °C), b) glass transition temperature (tan[δ] peak), and c) high temperature modulus (T_g + 20 °C, ~80 °C) vs. grafted polymer molecular weight for all composites, extracted from the DMA curves. The left side plots show data for composites made with the low grafting density nanofillers (*MxG*-CNC-*g*-PEG_L) and the right side show the same data for the high grafting density filler (*MxG*-CNC-*g*-PEG_H).

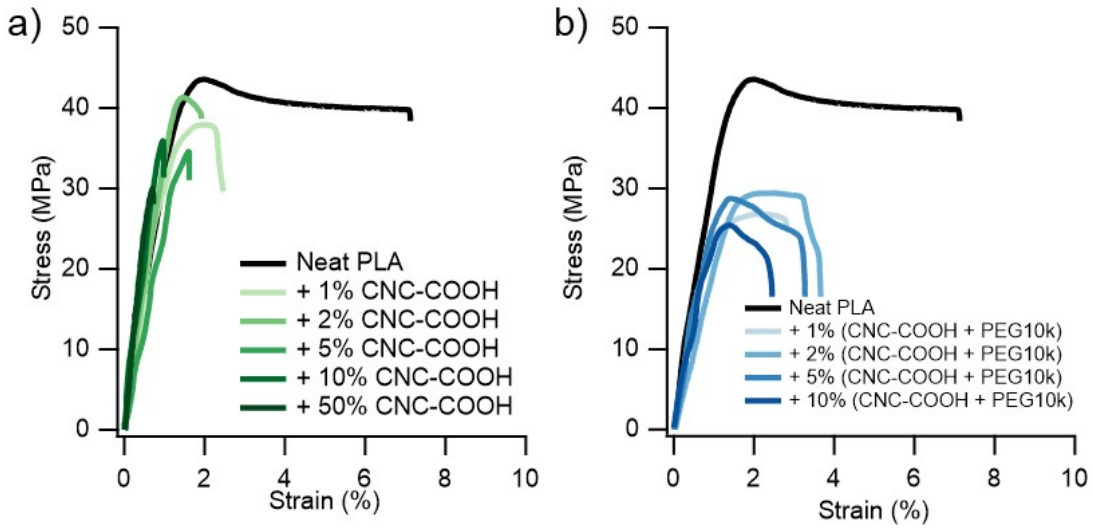

Figure S2.13: Tensile testing curves (1 mm/min) for the composite controls: a) PLA/*MxG*-CNC-COOH and b) PLA/*MxG*-CNC-COOH/PEG_{10k}. Each plot contains a single filler at various loading levels (1, 2, 5, 10, 50 wt.%).

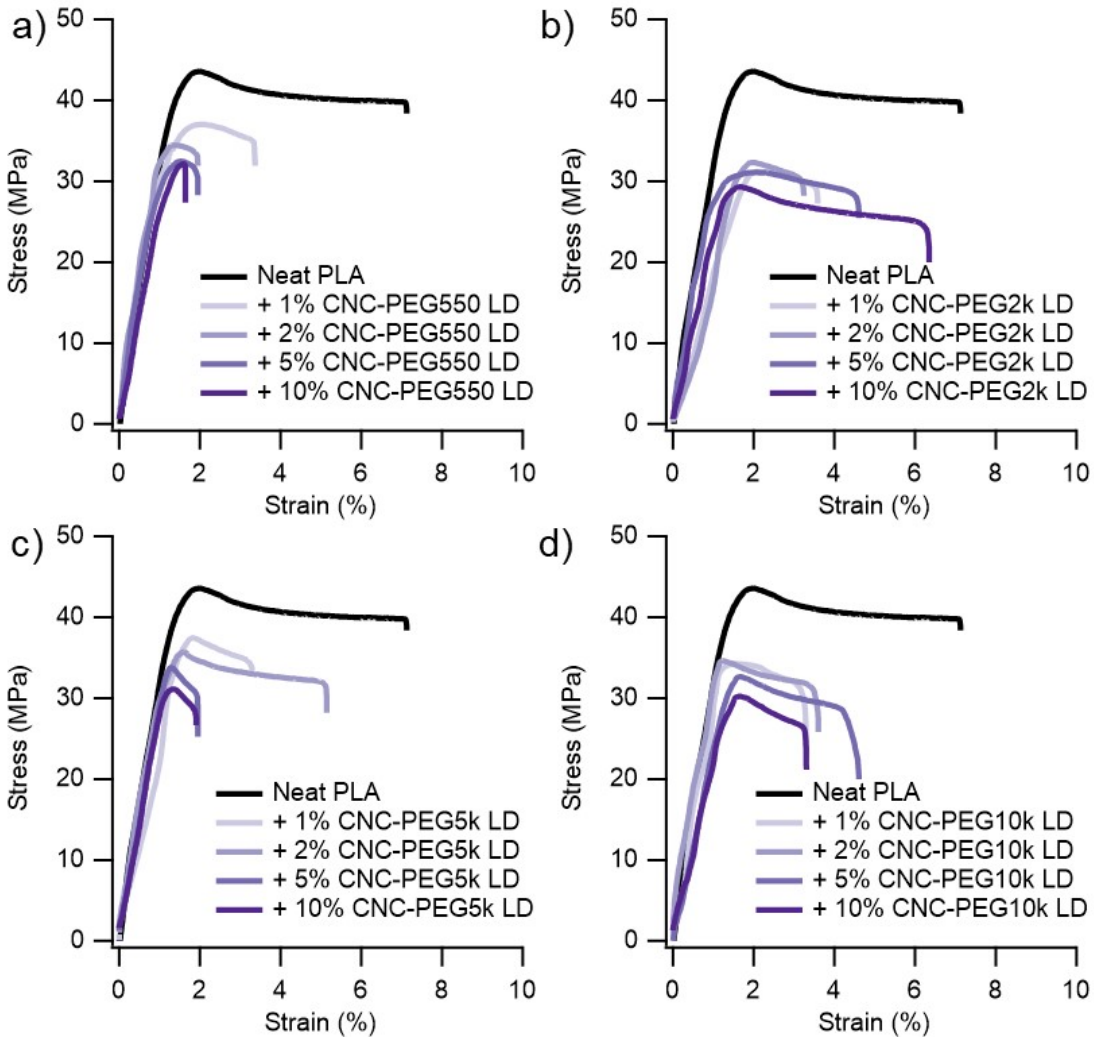

Figure S2.14: Tensile testing curves (1 mm/min) for the composites filled with low grafting density filler with a) 550, b) 2k, c) 5k, and d) 10k g/mol PEG (PLA/*MxG*-CNC-*g*-PEG_L). Each plot contains a single filler at various loading levels (1, 2, 5, 10 wt. %).

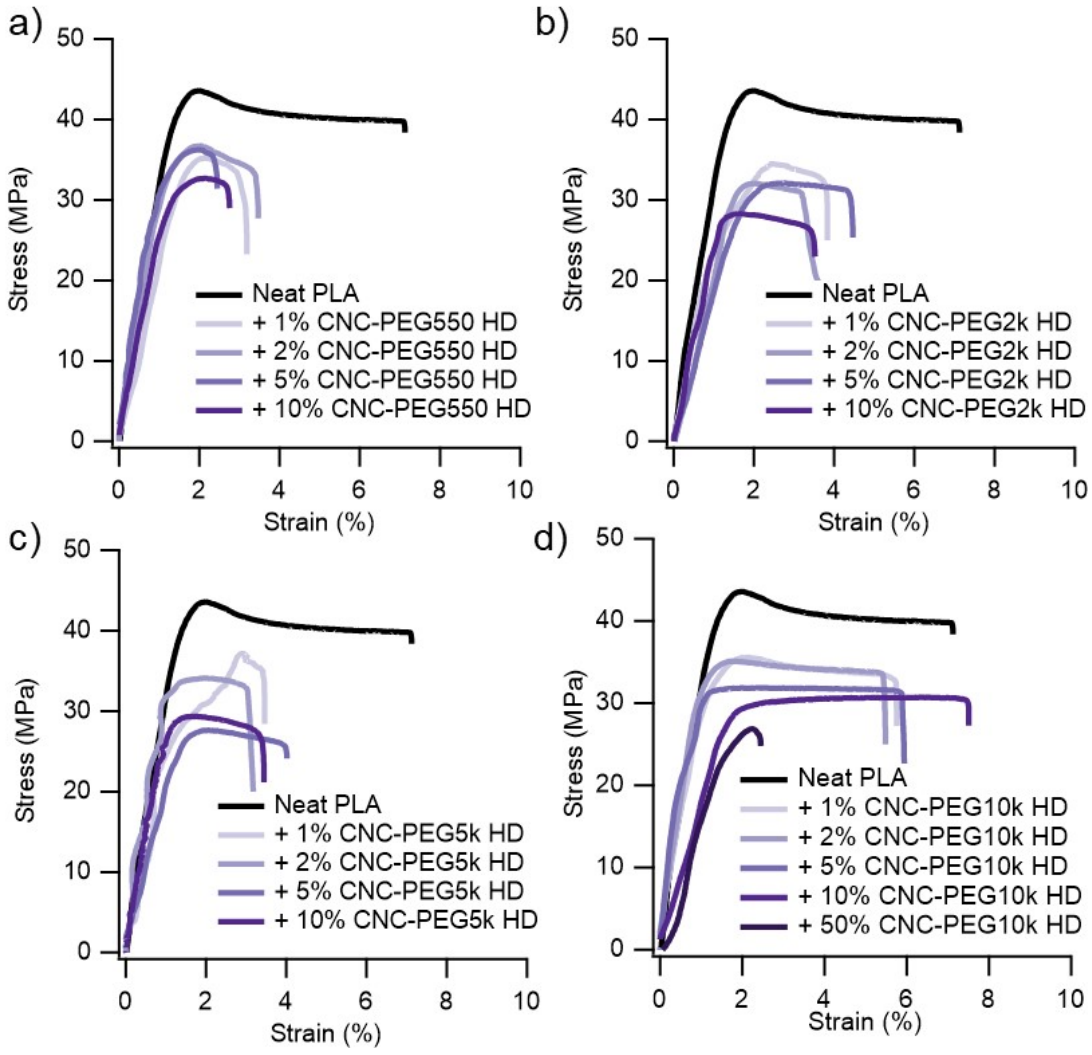

Figure S2.15: Tensile testing curves (1 mm/min) for the composites filled with high grafting density filler with a) 550, b) 2k, c) 5k, and d) 10k g/mol PEG (PLA/*MxG*-CNC-*g*-PEG_H). Each plot contains a single filler at various loading levels (1, 2, 5, 10, 50 wt. %).

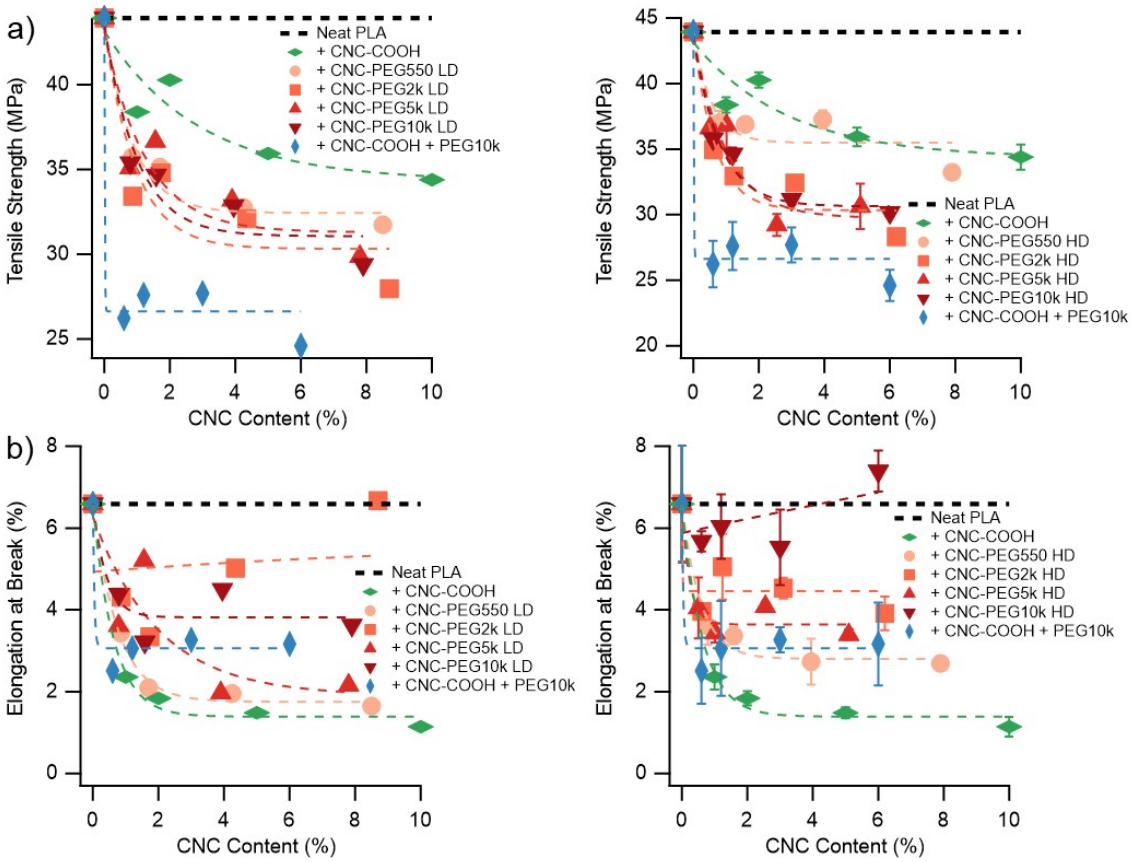

Figure S2.16: Plots of a) tensile strength and (b) elongation at break vs. CNC content for all composites, extracted from tensile testing data. The left side plots show data for composites made with the low grafting density nanofillers (*MxG*-CNC-*g*-PEG_L) and the right side show the same data for the high grafting density filler (*MxG*-CNC-*g*-PEG_H).

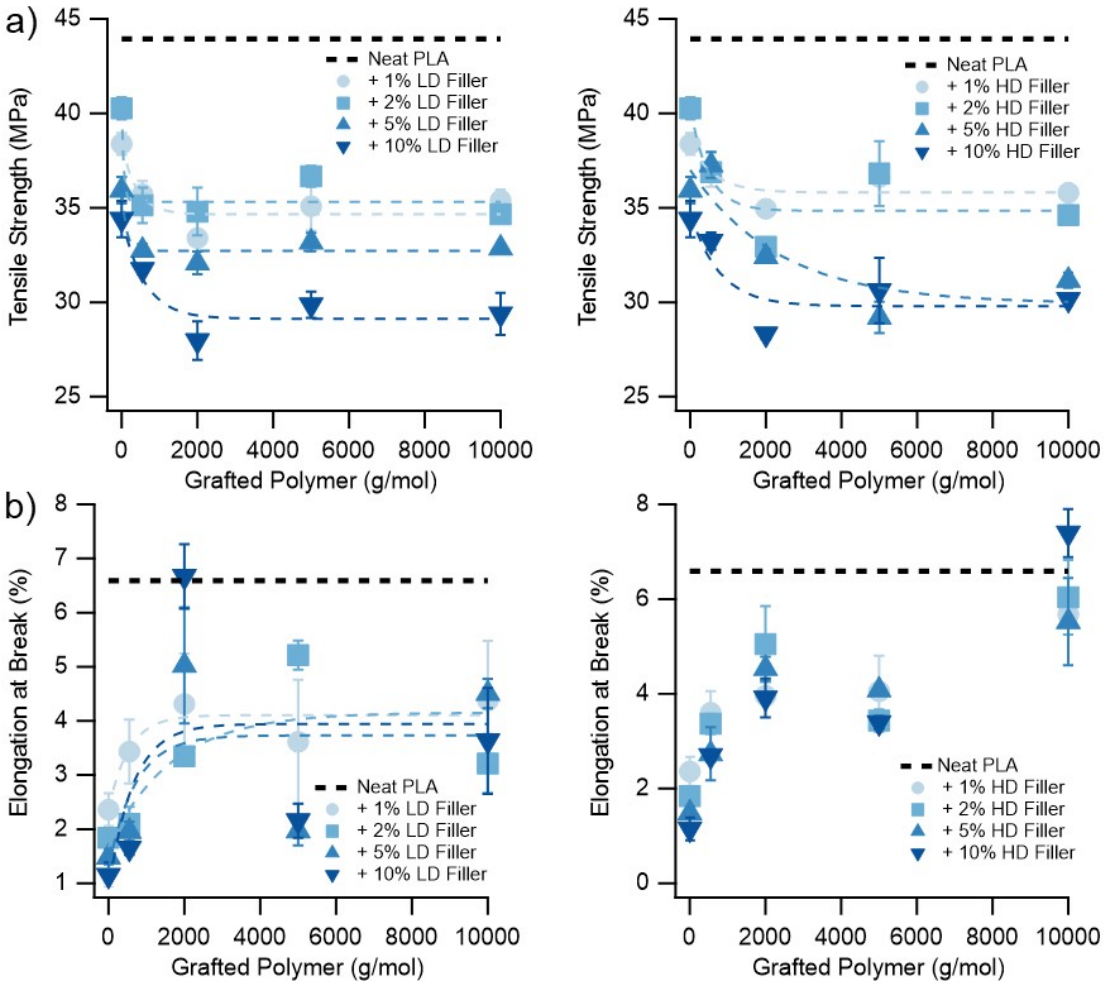

Figure S2.17: Plots of a) tensile strength and b) elongation at break vs. grafted polymer molecular weight for all composites, extracted from tensile testing data. The left side plots show data for composites made with the low grafting density nanofillers (*MxG*-CNC-*g*-PEG_L) and the right side show the same data for the high grafting density filler (*MxG*-CNC-*g*-PEG_H).

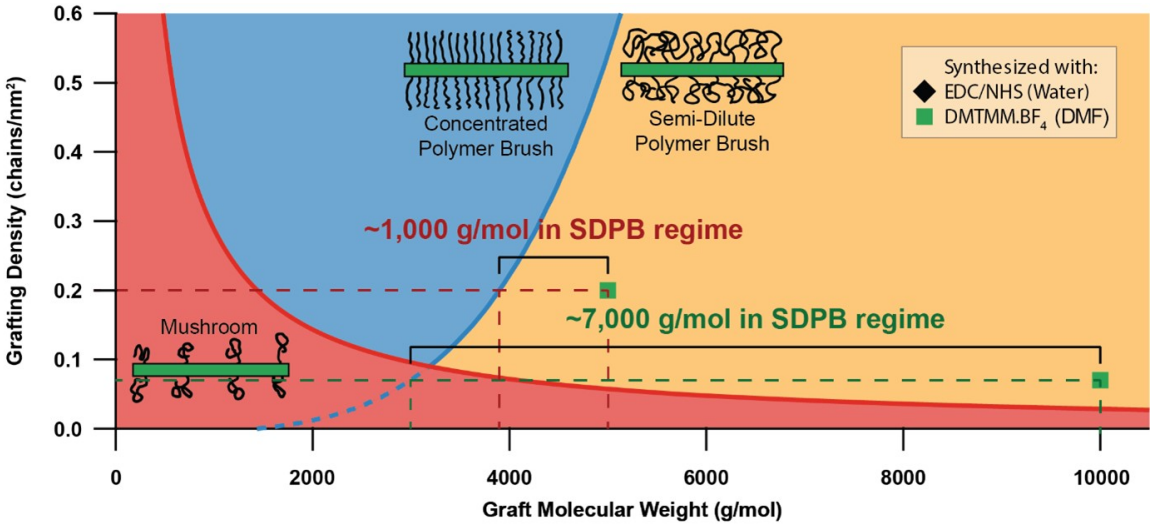

Figure S2.18: Polymer conformation phase space with *MxG*-CNC-*g*-PEG_{5kH} and *MxG*-CNC-*g*-PEG_{10kH} samples plotted. The concentrated to semi-dilute brush transition (blue line) is modeled based off polybutadiene,[53] which has similar backbone flexibility to PEG. The red mushroom to brush transition (red line) is estimated based on when circles defined by the radius of gyration of the polymer would begin to overlap. The annotation shows the amount of grafted polymer that is in the semi-dilute polymer brush regime with the remaining length in the concentrated polymer brush regime.

2.7 References

[1] E. Castro-Aguirre, F. Iñiguez-Franco, H. Samsudin, X. Fang, R. Auras, "Poly (lactic acid)—Mass production, processing, industrial applications, and end of life", *Advanced Drug Delivery Reviews* **2016**, *107*, 333–366.

[2] S. Farah, D. G. Anderson, R. Langer, "Physical and mechanical properties of PLA, and their functions in widespread applications — A comprehensive review", *Advanced Drug Delivery Reviews* **2016**, *107*, 367–392.

[3] X. Zhao, H. Hu, X. Wang, X. Yu, W. Zhou, S. Peng, "Super tough poly(lactic acid) blends: A comprehensive review", *RSC Advances* **2020**, *10*, 13316–13368.

[4] H. Liu, J. Zhang, "Research progress in toughening modification of poly(lactic acid)", *Journal of Polymer Science Part B: Polymer Physics* **2011**, *49*, 1051–1083.

[5] J. M. Raquez, Y. Habibi, M. Murariu, P. Dubois, "Polylactide (PLA)-based nanocomposites", *Progress in Polymer Science* **2013**, *38*, 1504–1542.

[6] C. Calvino, N. D. Macke, R. Kato, S. J. Rowan, "Development, processing and applications of bio-sourced cellulose nanocrystal composites", *Progress in Polymer Science* **2020**, *103*, 101221.

[7] V. Favier, H. Chanzy, J. Y. Cavaillé, "Polymer Nanocomposites Reinforced by Cellulose Whiskers", *Macromolecules* **1995**, *28*, 6365–6367.

[8] A. M. Weiss, N. Macke, Y. Zhang, C. Calvino, A. P. Esser-Kahn, S. J. Rowan, "In Vitro and in Vivo Analyses of the Effects of Source, Length, and Charge on the Cytotoxicity and Immunocompatibility of Cellulose Nanocrystals", *ACS Biomaterials Science and Engineering* **2021**, *7*, 1450–1461.

[9] D. Trache, M. H. Hussin, M. K. M. Haafiz, V. K. Thakur, "Recent progress in cellulose nanocrystals: sources and production", *Nanoscale* **2017**, *9*, 1763–1786.

[10] A. Šturcová, G. R. Davies, S. J. Eichhorn, "Elastic modulus and stress-transfer properties of tunicate cellulose whiskers", *Biomacromolecules* **2005**, *6*, 1055–1061.

[11] E. Cudjoe, M. Hunsen, Z. Xue, A. E. Way, E. Barrios, R. A. Olson, M. J. Hore, S. J. Rowan, "Miscanthus Giganteus: A commercially viable sustainable source of cellulose nanocrystals", *Carbohydrate Polymers* **2017**, *155*, 230–241.

[12] M. Roohani, Y. Habibi, N. M. Belgacem, G. Ebrahim, A. N. Karimi, A. Dufresne, "Cellulose whiskers reinforced polyvinyl alcohol copolymers nanocomposites", *European polymer journal* **2008**, *44*, 2489–2498.

[13] Y. Chen, C. Liu, P. R. Chang, X. Cao, D. P. Anderson, "Bionanocomposites based on pea starch and cellulose nanowhiskers hydrolyzed from pea hull fibre: effect of hydrolysis time", *Carbohydrate Polymers* **2009**, *76*, 607–615.

[14] H. Mao, C. Wei, Y. Gong, S. Wang, W. Ding, "Mechanical and water-resistant properties of eco-friendly chitosan membrane reinforced with cellulose nanocrystals", *Polymers* **2019**, *11*.

[15] M. Mariano, N. El Kissi, A. Dufresne, "Cellulose nanocrystals and related nanocomposites: Review of some properties and challenges", *Journal of Polymer Science Part B: Polymer Physics* **2014**, *52*, 791–806.

[16] K. L. Dagnon, K. Shanmuganathan, C. Weder, S. J. Rowan, "Water-triggered modulus changes of cellulose nanofiber nanocomposites with hydrophobic polymer matrices", *Macromolecules* **2012**, *45*, 4707–4715.

[17] H. Yao, J. Zhou, H. Li, J. Zhao, "Nanocrystalline cellulose/fluorinated polyacrylate latex via RAFT-mediated surfactant-free emulsion polymerization and its application as waterborne textile finishing agent", *Journal of Polymer Science Part A: Polymer Chemistry* **2019**, *57*, 1305–1314.

[18] Y. Zhang, V. Karimkhani, B. T. Makowski, G. Samaranayake, S. J. Rowan, "Nanoemulsions and Nanolatexes Stabilized by Hydrophobically Functionalized Cellulose Nanocrystals", *Macromolecules* **2017**, *50*, 6032–6042.

[19] T. Abitbol, H. Marway, E. D. Cranston, "Surface modification of cellulose nanocrystals with cetyltrimethylammonium bromide", *Nordic Pulp & Paper Research Journal* **2014**, *29*, 46–57.

[20] M. Mariano, F. Pilate, F. B. De Oliveira, F. Khelifa, P. Dubois, J. M. Raquez, A. Dufresne, "Preparation of Cellulose Nanocrystal-Reinforced Poly(lactic acid) Nanocomposites through Noncovalent Modification with PLLA-Based Surfactants", *ACS Omega* **2017**, *2*, 2678–2688.

[21] Z. Hu, S. Ballinger, R. Pelton, E. D. Cranston, "Surfactant-enhanced cellulose nanocrystal Pickering emulsions", *Journal of Colloid and Interface Science* **2015**, *439*, 139–148.

[22] S. A. Kedzior, J. O. Zoppe, R. M. Berry, E. D. Cranston, "Recent advances and an industrial perspective of cellulose nanocrystal functionalization through polymer grafting", *Current Opinion in Solid State & Materials Science* **2019**, *23*, 74–91.

[23] V. Favier, J. Y. Cavaille, G. R. Canova, S. C. Shrivastava, "Mechanical percolation in cellulose whisker nanocomposites", *Polymer Engineering & Science* **1997**, *37*, 1732–1739.

[24] E. DiLoreto, E. Haque, A. Berman, R. J. Moon, K. Kalaitzidou, "Freeze dried cellulose nanocrystal reinforced unsaturated polyester composites: challenges and potential", *Cellulose* **2019**, *26*, 4391–4403.

[25] N. Lin, G. Chen, J. Huang, A. Dufresne, P. R. Chang, "Effects of polymer-grafted natural nanocrystals on the structure and mechanical properties of poly(lactic acid): A case of cellulose whisker-graft-polycaprolactone", *Journal of Applied Polymer Science* **2009**, *113*, 3417–3425.

[26] J. C. Halpin, J. L. Kardos, "Moduli of crystalline polymers employing composite theory", *Journal of Applied Physics* **1972**, *43*, 2235–2241.

[27] A.-L. Goffin, Y. Habibi, J.-M. Raquez, P. Dubois, "Polyester-grafted cellulose nanowhiskers: A new approach for tuning the microstructure of immiscible polyester blends", *ACS Applied Materials and Interfaces* **2012**, *4*, 3364–3371.

[28] C. Zhang, M. R. Salick, T. M. Cordie, T. Ellingham, Y. Dan, L. S. Turng, "Incorporation of poly(ethylene glycol) grafted cellulose nanocrystals in poly(lactic acid) electrospun nanocomposite fibers as potential scaffolds for bone tissue engineering", *Materials Science and Engineering C* **2015**, *49*, 463–471.

[29] L. Zhou, K. Ke, M. B. Yang, W. Yang, "Recent progress on chemical modification of cellulose for high mechanical-performance Poly(lactic acid)/Cellulose composite: A review", *Composites Communications* **2020**.

[30] H. Lönnberg, Q. Zhou, H. Brumer, T. T. Teeri, E. Malmström, A. Hult, "Grafting of cellulose fibers with poly(ϵ-caprolactone) and poly(L-lactic acid) via ring-opening polymerization", *Biomacromolecules* **2006**, *7*, 2178–2185.

[31] B. Braun, J. R. Dorgan, D. M. Knauss, "Reactively compatibilized cellulosic polylactide microcomposites", *Journal of Polymers and the Environment* **2006**, *14*, 49–58.

[32] A. Mujica-Garcia, S. Hooshmand, M. Skrifvars, J. M. Kenny, K. Oksman, L. Peponi, "Poly(lactic acid) melt-spun fibers reinforced with functionalized cellulose nanocrystals", *RSC Advances* **2016**, *6*, 9221–9231.

[33] B. Braun, J. R. Dorgan, L. O. Hollingsworth, "Supra-molecular ecobionanocomposites based on polylactide and cellulosic nanowhiskers: synthesis and properties", *Biomacromolecules* **2012**, *13*, 2013–2019.

[34] J. Dong, M. Li, L. Zhou, S. Lee, C. Mei, X. Xu, Q. Wu, "The influence of grafted cellulose nanofibers and postextrusion annealing treatment on selected properties of poly(lactic acid) filaments for 3D printing", *Journal of Polymer Science Part B: Polymer Physics* **2017**, *55*, 847–855.

[35] C. Miao, W. Y. Hamad, "In-situ polymerized cellulose nanocrystals (CNC)—poly(L-lactide) (PLLA) nanomaterials and applications in nanocomposite processing", *Carbohydrate Polymers* **2016**, *153*, 549–558.

[36] A. Gupta, V. Katiyar, "Cellulose Functionalized High Molecular Weight Stereocomplex Polylactic Acid Biocomposite Films with Improved Gas Barrier, Thermomechanical Properties", *ACS Sustainable Chemistry and Engineering* **2017**, *5*, 6835–6844.

[37] J. K. Muiruri, S. Liu, W. S. Teo, J. Kong, C. He, "Highly biodegradable and tough polylactic acid–cellulose nanocrystal composite", *ACS Sustainable Chemistry & Engineering* **2017**, *5*, 3929–3937.

[38] X. Zhang, Y. Zhang, "Reinforcement effect of poly(butylene succinate) (PBS)-grafted cellulose nanocrystal on toughened PBS/polylactic acid blends", *Carbohydrate Polymers* **2016**, *140*, 374–382.

[39] I. V. Averianov, M. A. Stepanova, I. V. Gofman, A. L. Nikolaeva, V. A. Korzhikov-Vlakh, M. Karttunen, E. G. Korzhikova-Vlakh, "Chemical modification of nanocrystalline cellulose for improved interfacial compatibility with poly(lactic acid)", *Mendeleev Communications* **2019**, *29*, 220–222.

[40] Y. Chen, L. M. Geever, J. A. Killion, J. G. Lyons, C. L. Higginbotham, D. M. Devine, "Review of multifarious applications of poly (lactic acid)", *Polymer-Plastics Technology and Engineering* **2016**, *55*, 1057–1075.

[41] T. Li, J. Zhang, D. K. Schneiderman, L. F. Francis, F. S. Bates, "Toughening Glassy Poly(lactide) with Block Copolymer Micelles", *ACS Macro Letters* **2016**, *5*, 359–364.

[42] Y. Yin, J. Ma, X. Tian, X. Jiang, H. Wang, "Cellulose nanocrystals functionalized with amino-silane and epoxy-poly(ethylene glycol) for reinforcement and flexibilization of poly(lactic acid): material preparation and compatibility mechanism", *Cellulose* **2018**, *25*, 6447–6463.

[43] L. Li, R. Y. Bao, T. Gao, Z. Y. Liu, B. H. Xie, M. B. Yang, W. Yang, "Dopamine-induced functionalization of cellulose nanocrystals with polyethylene glycol towards poly(L-lactic acid) bionanocomposites for green packaging", *Carbohydrate Polymers* **2019**, *203*, 275–284.

[44] H.-y. Yu, H. Zhang, S. Yassin, H. Abdalkarim, L. Yang, J. Zhu, J. Gu, J. Yao, "Interfacial compatible poly(ethylene glycol) chains modified cellulose nanosphere as bifunctional reinforcements in green polylatic acid for food packagings", *Journal of the Taiwan Institute of Chemical Engineers* **2019**, *95*, 583–593.

[45] Y. Jiao, A. Tibbits, A. Gillman, M. S. Hsiao, P. Buskohl, L. F. Drummy, R. A. Vaia, "Deformation Behavior of Polystyrene-Grafted Nanoparticle Assemblies with Low Grafting Density", *Macromolecules* **2018**, *51*, 7257–7265.

[46] J. H. Lettow, H. Yang, P. F. Nealey, S. J. Rowan, "Effect of Graft Molecular Weight and Density on the Mechanical Properties of Polystyrene-Grafted Cellulose Nanocrystal Films", *Macromolecules* **2021**, *54*, 10594–10604.

[47] W. R. Lenart, M. J. Hore, "Structure–property relationships of polymer-grafted nanospheres for designing advanced nanocomposites", *Nano-Structures and Nano-Objects* **2018**, *16*, 428–440.

[48] P. Akcora, H. Liu, S. K. Kumar, J. Moll, Y. Li, B. C. Benicewicz, L. S. Schadler, D. Acehan, A. Z. Panagiotopoulos, V. Pryamitsyn, V. Ganesan, J. Ilavsky, P. Thiyagarajan, R. H. Colby, J. F. Douglas, "Anisotropic self-assembly of spherical polymer-grafted nanoparticles", *Nature Materials* **2009**, *8*, 354–359.

[49] S. Fischer, A. Salcher, A. Kornowski, H. Weller, S. Förster, "Completely miscible nanocomposites", *Angewandte Chemie - International Edition* **2011**, *50*, 7811–7814.

[50] A. C. Genix, V. Bocharova, A. Kisliuk, B. Carroll, S. Zhao, J. Oberdisse, A. P. Sokolov, "Enhancing the Mechanical Properties of Glassy Nanocomposites by Tuning Polymer Molecular Weight", *ACS Applied Materials and Interfaces* **2018**, *10*, 33601–33610.

[51] K. Ohno, T. Morinaga, S. Takeno, Y. Tsujii, T. Fukuda, "Suspensions of silica particles grafted with concentrated polymer brush: A new family of colloidal crystals", *Macromolecules* **2006**, *39*, 1245–1249.

[52] J. Kalb, D. Dukes, S. K. Kumar, R. S. Hoy, G. S. Grest, "End grafted polymer nanoparticles in a polymeric matrix: Effect of coverage and curvature", *Soft Matter* **2011**, *7*, 1418–1425.

[53] N. K. Hansoge, S. Keten, "Effect of Polymer Chemistry on Chain Conformations in Hairy Nanoparticle Assemblies", *ACS Macro Letters* **2019**, *8*, 1209–1215.

[54] E. M. Hodgson, D. J. Nowakowski, I. Shield, A. Riche, A. V. Bridgwater, J. C. Clifton-Brown, I. S. Donnison, "Variation in Miscanthus chemical composition and implications for conversion by pyrolysis and thermo-chemical bio-refining for fuels and chemicals", *Bioresource Technology* **2011**, *102*, 3411–3418.

[55] S. Jacobsen, H. G. Fritz, "Plasticizing polylactide - the effect of different plasticizers on the mechanical properties", *Polymer Engineering and Science* **1999**, *39*, 1303–1310.

[56] E. Kaiser, R. L. Colescott, C. D. Bossinger, P. I. Cook, "Color test for detection of free terminal amino groups in the solid-phase synthesis of peptides", *Analytical Biochemistry* **1970**, *34*, 595–598.

[57] K. Mohomed, Thermogravimetric Analysis (TGA) Theory and Applications, **2016**.

[58] Á. Kmetty, K. Litauszki, "Development of poly (lactide acid) foams with thermally expandable microspheres", *Polymers* **2020**, *12*.

[59] A. Pei, Q. Zhou, L. A. Berglund, "Functionalized cellulose nanocrystals as biobased nucleation agents in poly (l-lactide)(PLLA)–Crystallization and mechanical property effects", *Composites Science and Technology* **2010**, *70*, 815–821.

[60] C. Xu, Q. Lv, D. Wu, Z. Wang, "Polylactide/cellulose nanocrystal composites: a comparative study on cold and melt crystallization", *Cellulose* **2017**, *24*, 2163–2175.

[61] R. Hidema, K.-y. Fujito, H. Suzuki, "Drag force of polyethyleneglycol in flows of polymer solutions measured using a scanning probe microscope", *Soft Matter* **2022**, *18*, 455–464.

[62] S. Park, J. O. Baker, M. E. Himmel, P. A. Parilla, D. K. Johnson, "Cellulose crystallinity index: measurement techniques and their impact on interpreting cellulase performance", *Biotechnology for Biofuels* **2010**, *3*, 1–10.

[63] S. Elazzouzi-Hafraoui, Y. Nishiyama, J.-L. Putaux, L. Heux, F. Dubreuil, C. Rochas, "The Shape and Size Distribution of Crystalline Nanoparticles Prepared by Acid Hydrolysis of Native Cellulose", *Biomacromolecules* **2008**, 57–65.

[64] R. J. Moon, A. Martini, J. Nairn, J. Simonsen, J. Youngblood, *Cellulose nanomaterials review: Structure, properties and nanocomposites*, *Vol. 40*, **2011**, pp. 3941–3994.

CHAPTER 3

MELT-FUNCTIONALIZATION OF CELLULOSE NANOCRYSTALS USING DYNAMIC HINDERED UREA CHEMISTRY

3.1 Summary

Cellulose nanocrystal (CNC)-reinforced composites are gaining commercial attention on account of their high strength and sustainable sourcing. Grafting polymers to the CNCs in these composites has the potential to improve their properties, but current solution-based synthesis methods limit their production at scale. Utilizing dynamic hindered urea chemistry, a new method for the melt-functionalization of cellulose nanocrystals has been developed. This method does not require toxic solvents during the grafting step and can achieve grafting densities competitive with state-of-the-art solution-based grafting methods. Using cotton-sourced, TEMPO-oxidized CNCs, multiple molecular weights of poly(ethylene glycol) (PEG) as well as dodecane, polycaprolactone, and poly(butyl acrylate) were grafted to the CNC surface. With PEG-grafted nanoparticles, grafting densities of 0.61 chains/nm^2 and 0.13 chains/nm^2 were achieved with 2,000 and 10,000 g/mol polymer chains respectively, both of which represent significant improvements over previous reports for solution-based PEG grafting onto CNCs.

3.2 Introduction

Cellulose nanocrystals (CNCs) have become an attractive, sustainable additive to provide mechanical reinforcement in polymeric materials. These bio-derived nanorods, which have dimensions of roughly 10 nm in width and 100-500 nm in length, are directly extracted from cellulosic biomass and have shown outstanding reinforcement capabilities

when used as fillers in composites.[1] A key challenge in accessing such nanocomposites is the ability to achieve a uniform dispersion of CNCs within a given matrix and this has limited the use of CNCs to a relatively narrow range of applications.[2] The poor dispersion of CNCs in many solvents or solid polymer matrices arises from the numerous hydroxyl functional groups present on the surface of the particles that make them very hydrophilic and capable of forming inter-particle hydrogen bonds. Since many potential host polymers are hydrophobic, the inter-particle interactions between CNCs cause the formation of agglomerates, significantly impeding their ability to reinforce the host matrix.[3]

Surface modification of CNCs has been widely explored to overcome these dispersion issues and promote more homogenous mechanical reinforcement of the material.[4] Some surface modification routes utilize these interactions to physisorb or electrostatically adsorb surfactants or polymers onto CNCs.[5–7] Additionally, surface modification can be achieved through covalent attachment of small molecules via different chemical reactions such as esterification, etherification, silylation, amidation, and urethanization.[8–10] A third, widely-employed method of CNC surface modification involves the covalent grafting of polymer chains.[11,12] In addition to improving dispersion, such polymer-grafted nanoparticles can also show enhanced interfacial adhesion between the filler and the polymer matrix through entanglements or other matrix-filler interactions.[12] Depending on the grafted polymer conformation, which is a function of the polymer molecular weight and grafting density, these interactions can greatly aid both the processing and properties of the resulting nanocomposite materials.[13,14]

Different pathways have been developed to graft polymers on the surface of CNCs, including “grafting-to”, “grafting-from”, and “grafting-through” approaches, among others.[15–17] The “grafting-from” approach relies on covalent attachment of an initiator

on the CNC surface and allows for initiation of the polymerization directly from the nanoparticle surface.[16] The advantages of "grafting-from" include synthetic simplicity and the ability to achieve relatively high surface grafting densities of 0.1 to 0.4 chains/nm^2, even for high molecular weight polymers (greater than 10,000 g/mol).[18] The main drawbacks of "grafting-from" methods are the challenges to characterizing the molecular weight, composition, and surface density of the grafted polymers. Additionally, these are solution-based reactions, which can limit scalability.

Comparatively, "grafting-to" methods typically involve the direct attachment of end-functionalized polymer chains to the surface of the nanocrystals.[19] The benefit of these methods is the ability to attach well-characterized polymer chains to CNCs, allowing for more thorough characterization of grafting density, polymer molecular weight, and brush structure. Surface brush conformation is known to play a significant role in resulting material properties, such as improved ionic conductivity[20] and water transport[21] at higher grafting densities and improved reinforcement potential with semi-dilute brush conformations.[14,22] Unfortunately, "grafting-to" functionalization relies on sequential attachment of polymer chains on the CNC surface. As the surface is populated, unreacted chains in solution can be sterically hindered from reacting with the surface, which can limit grafting density.

Additionally, the most common "grafting-to" methods, which include carbodiimide coupling,[23] epoxy ring opening,[24] and isocyanate-mediated grafting,[25] are all typically performed in solution (most commonly in water and DMF), once again limiting the use of these methods to lab-scale.[12,26] This use of potentially toxic solvents during the grafting reaction for both "grafting-to" and "grafting-from" techniques is antithetical to the core purpose of using sustainable nanoparticles. Thus, it is paramount to find more industrially relevant routes toward functionalization of CNCs that can achieve high grafting density with a range of polymers and molecular weights while preserving the

renewable character of the nanoparticles.

One promising "grafting-to" method that has industrial relevance is the use of isocyanate moieties that can react with the hydroxyl groups on CNCs to form urethane linkages. This reaction is ubiquitous in the polyurethane industry[27] and has also been used to functionalize CNCs.[8] One limitation of this method when used with CNCs is the hygroscopic nature of the nanoparticles. Isocyanates can react with any water present, releasing CO_2 and degrading into an amine, which can further react with other isocyanates, consuming the reactant before it is able to attach to a CNC surface. One approach to overcome this loss is using a significant excess of isocyanate to counter the water carried by CNCs.[28] An alternative approach that is commonly used in industry, particularly for waterborne polyurethanes, is the use of blocked isocyanates.[29] Such blocked isocyanates can dissociate at elevated temperatures to release the blocking group, regenerating the isocyanate to react with an appropriate hydroxyl or other nucleophilic moiety. For example, Chowdhury et al. utilized blocked isocyanate chemistry to incorporate CNCs into waterborne polyurethane coatings.[30] One class of blocked isocyanate is the hindered urea (HU), where the isocyanate is reacted with a bulky amine compound. Hindered urea moieties are dynamic bonds and have a range of dissociation temperatures depending on the bulkiness of the amine blocking group.[31,32]

In this work, a solvent-free "grafting-to" method is reported. By taking advantage of dynamic covalent HU chemistry, an isocyanate-terminated polymer is generated *in-situ* (Figure 3.1a), which can subsequently react with surface hydroxyl groups to form a urethane bond, thus functionalizing the CNCs (Figure 3.1b). This study first demonstrates the viability of the concept with model reactions, then translates the developed functionalization process toward the modification of CNCs with a range of polymers.

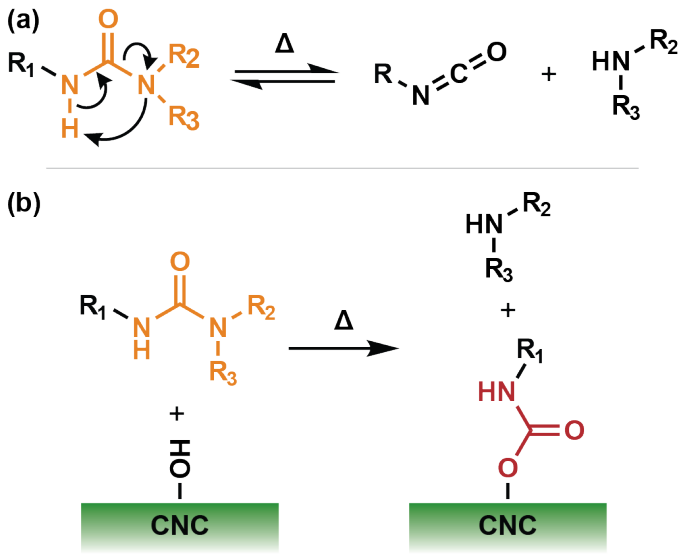

Figure 3.1: (a) Schematic of a dynamic hindered urea motif and its dissociation into an isocyanate and secondary amine, and (b) a schematic of the reaction between a dynamic hindered urea and hydroxyl groups on the surface of cellulose nanocrystals, forming a urethane on the CNC surface and releasing the secondary amine.

3.3 Results and Discussion

When designing a hindered urea system for grafting onto CNCs, the dissociation temperature of the blocked isocyanate is a key consideration. Depending on surface functionality, CNCs can begin to degrade around 165 °C,[33] so the isocyanate must be regenerated below that limit. Depending on the amine group used to block the isocyanate, hindered urea groups can activate between 30 - 200+ °C.[32,34] For this reason, *N-tert*-butylmethylamine was chosen as the blocking group because of its K_{eq} of roughly 90 M^{-1} at 130 °C, which corresponds to about 8 mol.% hindered urea activation.[34] This activation temperature is above room temperature and the boiling point of water to limit premature reactions, but well below the CNC degradation threshold.

3.3.1 *Isolation and Characterization of c-CNC-OSO_3 and c-CNC-COOH*

Following a previously reported procedure,[35] cellulose nanocrystals were isolated from cotton-based cellulose filter paper using sulfuric acid (*c*-CNC-OSO_3) and hydrochloric acid (*c*-CNC-OH). Following isolation, the *c*-CNC-OH nanoparticles were treated with (2,2,6,6-tetramethylpiperidin-1-yl)oxyl (TEMPO) to oxidize primary alcohol groups on the CNC surface into carboxylate groups, transforming *c*-CNC-OH into *c*-CNC-COOH. The resulting nanoparticles were freeze-dried for easier handling before full characterization. In brief, atomic force microscopy (AFM) was used to measure the dimensions of the *c*-CNC-COOH to be 170 $\pm$ 80 nm in length, 23 $\pm$ 5 nm in width, and 10 $\pm$ 3 nm in height (Figure S3.1a and S3.1b). The dimensions of *c*-CNC-OSO_3 were 148 $\pm$ 93 nm, 60 $\pm$ 10 nm, and 8 $\pm$ 3 nm in length, width, and height, respectively (Figure S3.2a). Conductivity titration determined the surface carboxylate density to be 410 $\pm$ 60 mmol/kg (Figure S3.1c) and surface sulfate density to be 285 $\pm$ 24 mmol/kg (Figure S3.2b). Wide angle X-ray scattering (WAXS) measured the crystallinity index to be 0.67 (Figure S3.1d) for *c*-CNC-COOH and 0.85 for *c*-CNC-OSO_3 (Figure S3.2c). Finally, thermogravimetric analysis (TGA) showed a degradation onset ($T_{d,95}$) of 226 °C for *c*-CNC-COOH (Figure S3.1e) and 175 °C for *c*-CNC-OSO_3 (Figure S3.2d).

3.3.2 *Reactions of Alkyl Hindered Ureas with Protected Sugars and CNCs*

To study the dissociation temperature of the selected hindered urea component, a series of model experiments were conducted with a hindered urea-terminated alkyl chain. Specifically, dodecyl isocyanate was reacted with *N-tert*-butylmethylamine in toluene to make dodecyl-HU. The dissociation of dodecyl-HU was monitored in the melt over a range of temperatures using *in-situ* Fourier Transform Infrared (FTIR) spectroscopy (Figure S3.3a). Dodecyl-HU was heated from 30 °C to 130 °C in increments of 10 °C,

waiting 10 minutes between each increment. During this test, a characteristic isocyanate N=C=O stretching peak at 2270 cm^{-1} began appearing around 100 °C, indicating the dissociation of hindered urea group and the evaporation of the *N-tert*-butylmethylamine (b.p. 69 °C) (Figure S3.3b). The intensity of the isocyanate band continued to increase with temperature up to 130 °C. Concomitantly, the hindered urea C=O stretching band at 1630 cm^{-1} disappeared as a new band appeared at 1654 cm^{-1}, corresponding to C=O stretching of the isocyanate (Figure S3.3b).

Prior to examining the ability of the dodecyl-HU to react with CNCs, a model experiment was carried out by reacting dodecyl-HU with 1,2:3,4-di-O-isopropylidene-α-D-galactopyranose (referred to as PG) (Figure 3.2a). PG is a protected galactose derivative with only the primary 5-hydroxyl group available for reaction, which allows for easier characterization of urethane bond formation.[36] Dodecyl-HU and PG were mixed in a 1:1 molar ratio using a minimal amount of acetone. The solvent was removed under high vacuum and the reaction proceeded in the melt at 120 °C for 5 hours. The disappearance of the hindered urea and formation of the urethane compound were monitored by *in-situ* FTIR (Figure 3.2b), highlighting the disappearance of the urea C=O stretching peak at 1645 cm^{-1} and the concomitant appearance of the urethane C=O stretching peak at 1722 cm^{-1}. It is worthwhile to note that no other significant peaks appear in the carbonyl region, suggesting that this reaction is relatively clean and avoids the formation of side products.

The covalent attachment of dodecyl-HU to CNC was then explored by combining a 2:1 molar ratio of HU to surface alcohol groups on the *c*-CNC-OSO_3 (calculated based on prior literature[14]) in minimal acetone to blend the components (Figure 3.3a). In this initial test, sulfate-functionalized CNCs were selected due to the presence of reactive primary hydroxyl groups as well as charged sulfate surface groups to promote dispersion and mixing.[37] After removing the acetone with vacuum, the bulk mixture

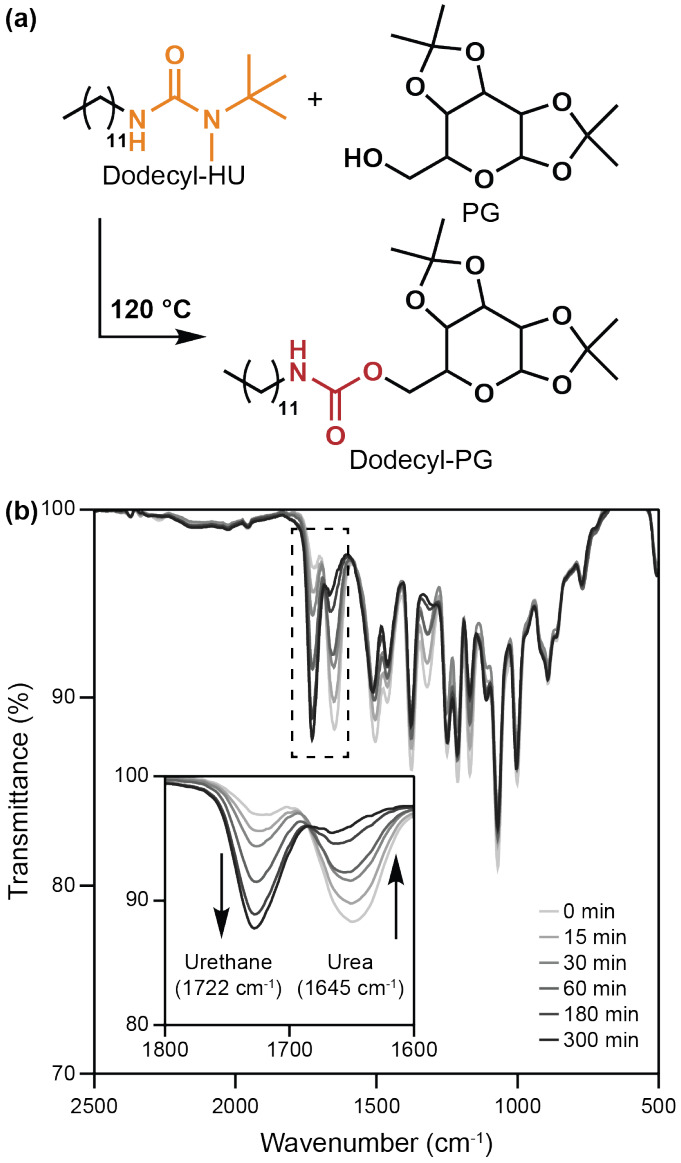

Figure 3.2: (a) Schematic of the reaction between PG and dodecyl-HU to form a urethane bond and (b) the FTIR spectra of the reaction over time, showing the disappearance of the urea peak at 1645 cm^{-1} and the appearance of the urethane peak at 1722 cm^{-1}.

was heated to 120 °C for 2 hours to avoid CNC degradation at prolonged times. To characterize the grafting, it was necessary to remove the unreacted dodecyl-HU from the functionalized CNCs, which was achieved by washing the reaction mixture five times with acetone (see supporting information (SI) for full procedure). The resulting *c*-CNC-*g*-dodecane was characterized using FTIR, which showed the appearance of

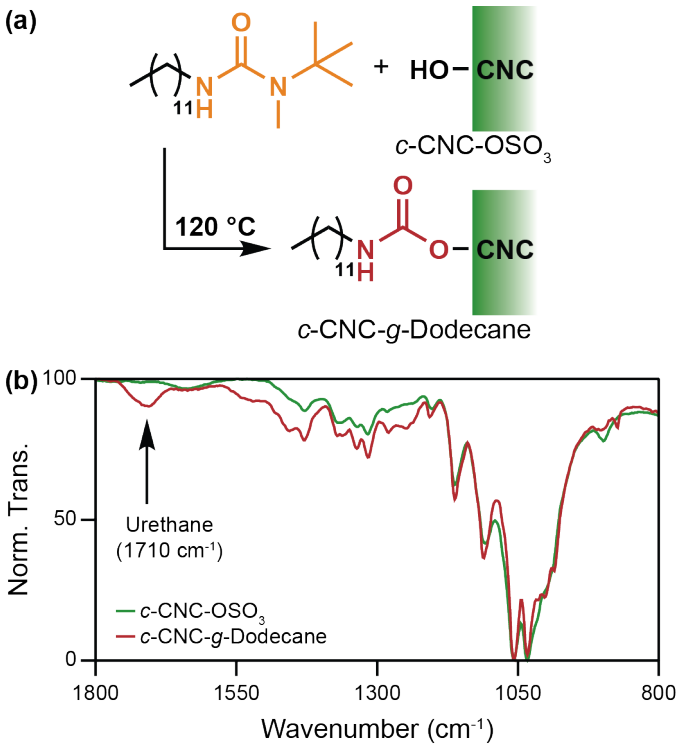

Figure 3.3: (a) A schematic of the reaction between dodecyl-HU and surface alcohol groups on CNCs and (b) FTIR spectra of the resulting *c*-CNC-*g*-dodecane, highlighting the appearance of the urethane peak at 1710 cm^{-1}.

the urethane C=O peak at 1710 cm^{-1} (Figure 3.3b). It is noteworthy that although the broadness of the urethane peak could indicate the formation of side products, such as allophanates,[38] the increased thermal stability of *c*-CNC-*g*-dodecane seen in the TGA curve still supports surface modification (Figure S3.4).While these measurements did not allow for quantification of the dodecyl group surface density, these results confirm a successful reaction between the CNCs and the small molecule hindered urea.

Having confirmed that it is possible to functionalize the CNC surface with a small molecule using dynamic hindered urea chemistry in the bulk, the next step was to explore the grafting of polymers onto CNC surfaces using this approach.

3.3.3 Synthesis and Characterization of Hindered Urea-Terminated Polymers

To demonstrate the versatility of this functionalization method, four polymers were chosen for functionalization onto CNC surfaces: poly(ethylene glycol) at 2,000 and 10,000 g/mol (PEG_{2k} and PEG_{10k}) as well as polycaprolactone (PCL_{10k}) and poly(butyl acrylate) (PBA_{10k}), both at 10,000 g/mol. PEG was chosen to allow comparison with previously reported solution-based "grafting-to" chemistries that have been used to synthesize PEG-grafted CNCs,[14] bio-based PCL was chosen to highlight the ability to make fully sustainable nanoparticles, and PBA was chosen to highlight the ability to functionalize and graft polymers synthesized via controlled, living polymerization techniques.

3.3.3.1 Synthesis and Characterization of PEG-HU and PCL-HU

After purchasing and synthesizing[39] PEG-OH and PCL-OH respectively (see SI for synthetic details), the next step was to create hindered urea-terminated polymers. For simplicity, discussion about synthesis and characterization will focus on PEG_{2k}, but reaction conditions and observations were similar between all PEG and PCL materials. Isocyanate-terminated PEG_{2k} (PEG_{2k}-NCO) was synthesized at 40 °C in dry toluene using an excess of hexamethylene diisocyanate and dibutyltin dilaurate (DBTDL) as catalyst (Figure 3.4a). During the work-up of this intermediate, it was vital to maintain an inert atmosphere and keep the material cold. Even brief exposure to atmospheric conditions resulted in impurities in the final product. Once the PEG_{2k}-NCO had been reacted with *N-tert*-butylmethylamine (Figure 3.4a), the resulting hindered urea-terminated PEG_{2k} (PEG_{2k}-HU) was much more stable and could be stored at ambient conditions for an extended period. The same phenomena were also observed when synthesizing PEG_{10k}-NCO and PEG_{10k}-HU as well as PCL_{10k}-NCO and PCL_{10k}-HU.

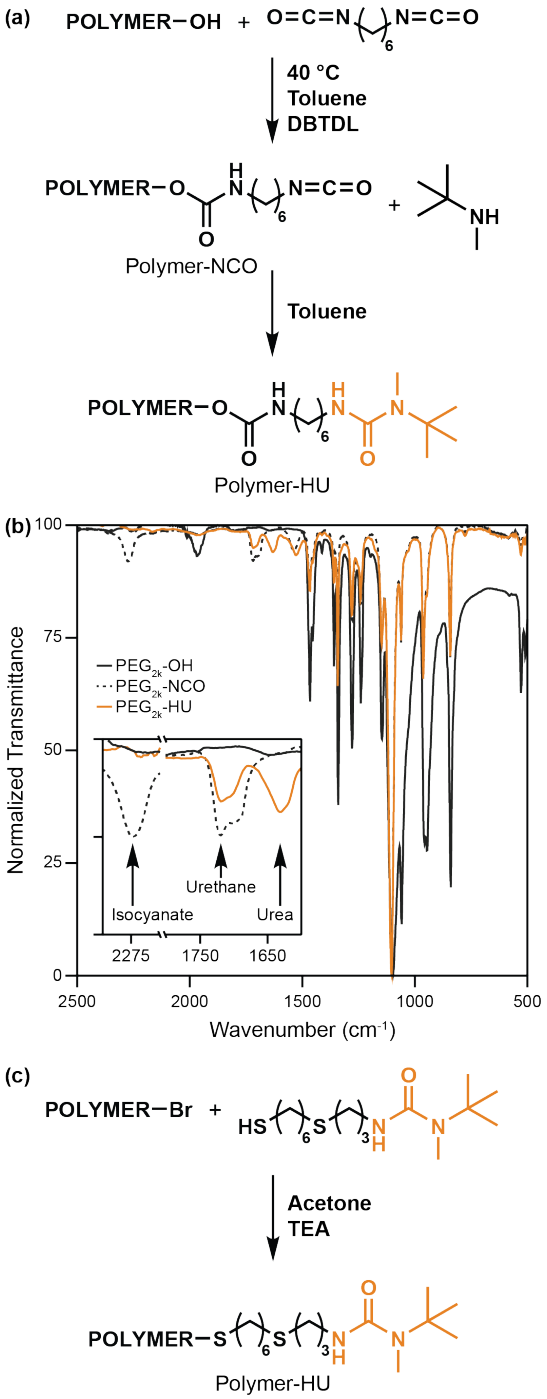

Figure 3.4: (a) Schematic for the conversion of polymers with alcohol end groups into hindered urea-terminated polymers, (b) FTIR spectra of PEG_{2k}-OH, PEG_{2k}-NCO, and PEG_{2k}-HU showing the appearance of the isocyanate peak at 2272 cm^{-1} in PEG_{2k}-NCO and the urea peak at 1631 cm^{-1} in PEG_{2k}-HU, and (c) a schematic for the conversion of polymers with bromine end groups into hindered urea-terminated polymers.

PEG_{2k}-NCO was characterized with FTIR (Figure 3.4b), size exclusion chromatography (SEC) (Figure S3.5a), and ^{1}H NMR (Figure S3.5b) to verify its structure prior to protecting the isocyanate with the secondary amine. Once protected with *N-tert*-butylmethylamine, ^{1}H NMR was repeated to confirm the appearance of peaks at 2.81 ppm and 1.39 ppm, corresponding to the methyl and *tert*-butyl groups of the HU, respectively (Figure S3.5b). Additionally, the appearance of the urea peak at 1631 cm^{-1} in FTIR confirmed successful synthesis (Figure 3.4b). Shoulders around the urethane peak imply that isocyanate side reactions could be occurring, such as the formation of allophanates and biurets. This is further suggested by the presence of a small peak in the SEC that is roughly double the initial polymer mass (Figure S3.5a). While the presence of these components would impact the stoichiometry of grafting reactions, their relatively small mass fraction (15 wt.% based on the PEG_{2k}-HU SEC peak) means that these are minor side reactions. Similar characterization was conducted on PEG_{10k}-NCO and -HU as well as PCL_{10k}-NCO and -HU (Figures S3.6 and S3.7).

3.3.3.2 Synthesis and Characterization of PBA-HU

Synthesis of bromine-terminated PBA-Br was achieved using Cu(0)-mediated living radical polymerization with ethyl α-bromoisobutyrate as the initiator (Figure S3.8).[40] To substitute a hindered urea group onto the bromine chain end, a thiol-functionalized hindered urea was synthesized by blocking allyl isocyanate with *N-tert*-butylmethylamine (Figure S3.9). Then, thiol-ene click chemistry was used with an excess of 1,6-hexanedithiol to generate the desired thio-HU small molecule (Figure S3.10). Finally, nucleophilic substitution was conducted between the thio-HU and bromine end group to connect the hindered urea to the polymer chain (Figure 3.4c). After purification of PBA-HU, SEC showed a small shift to shorter retention times, consistent with the substitution of the bromine by the thio-HU moiety (Figure S3.8a).

Additionally, ^{1}H NMR showed the appearance of the methyl and *tert*-butyl group peaks at 2.81 ppm and 1.39 ppm respectively (Figure S3.8b).

3.3.4 *Preparation, Characterization, and Optimization of PEG_{2k}-grafted c-CNCs*

In prior work, it has been shown that it is possible to quantify the amount of PEG grafted to CNC-COOH using dynamic thermogravimetric analysis.[14] During initial HU-terminated polymer grafting tests using sulfate-functionalized *c*-CNC-OSO_3, it was found that the broader degradation range of the *c*-CNC-OSO_3 (Figure S3.2d) made quantification of the polymer content on the grafted nanoparticles difficult via TGA. For this reason, grafting to *c*-CNC-COOH with a narrower degradation window (Figure S3.1e) was adopted, resulting in better separation of cellulose and PEG degradation via thermogravimetry. The key difference between these types of CNC is the presence of the more reactive primary hydroxyl groups on the *c*-CNC-OSO_3, whereas most of the primary alcohols have been converted to carboxylate groups on the *c*-CNC-COOH. However, isocyanates can also react with the secondary alcohols on a sugar unit, albeit at a lower rate.[41]

To prepare for grafting, freeze-dried *c*-CNC-COOH were dispersed in water at a concentration of 5 mg/mL and solvent exchanged into acetone. Using PEG_{2k} as a preliminary sample, 400 mg (approx. 2.7 mol eq. relative to surface -OH groups) of PEG_{2k}-HU were dissolved in the CNC dispersion per 100 mg of *c*-CNC-COOH. The acetone was then removed under high vacuum at ambient temperature. The resulting powder was melted at 120 °C and stirred for 2 hours under vacuum (120 mbar) to remove the volatile amine and yield *c*-CNC-*g*-PEG_{2k} (Figure 3.5a).

To explore the effects of the amine blocking group on CNC grafting, grafting was also conducted with PEG_{2k}-NCO (Figure 3.5b). Experimentally, the procedure was identical

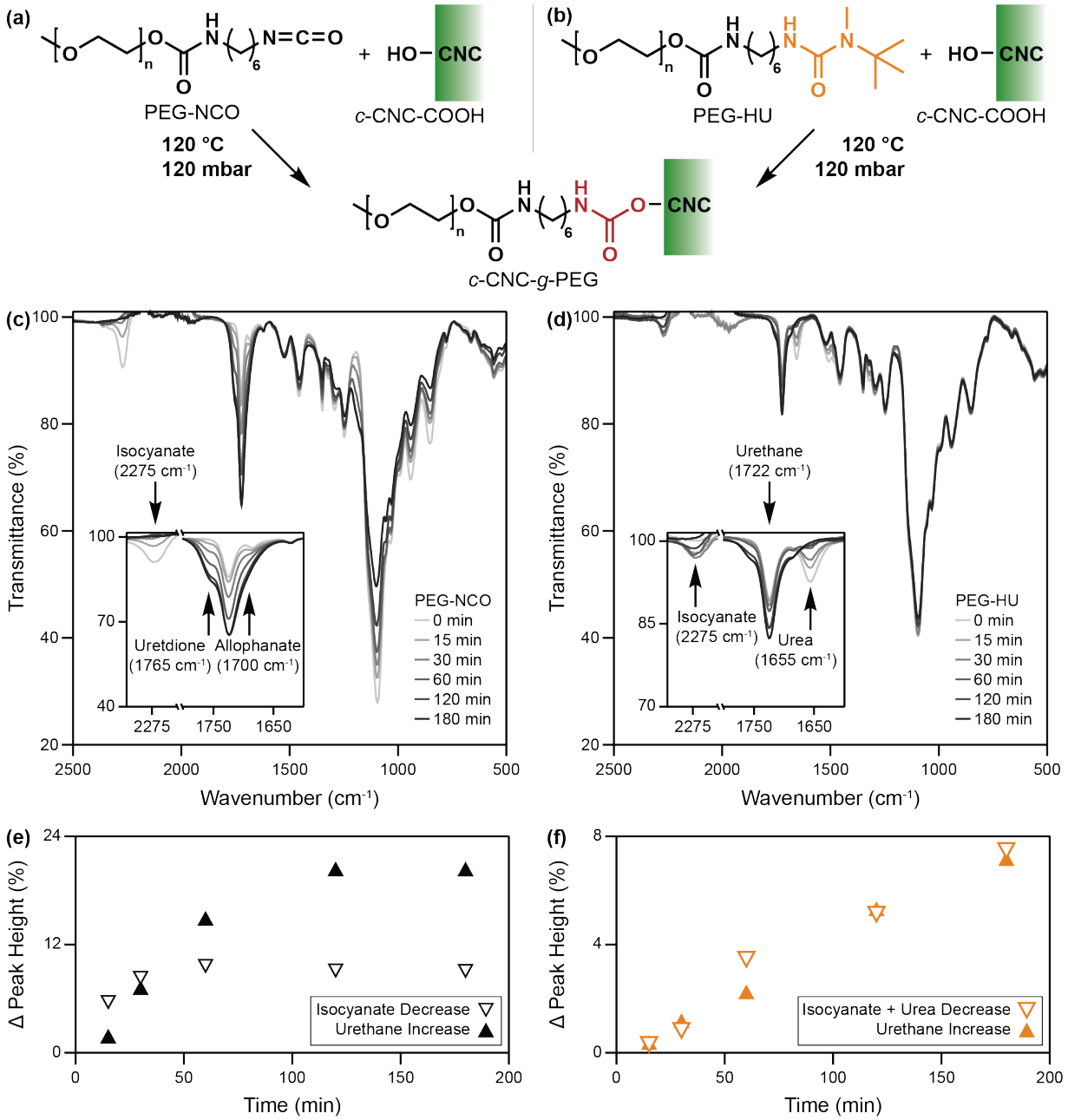

Figure 3.5: (a) Schematic of grafting PEG-NCO onto the hydroxyl groups of CNCs, (b) schematic of grafting PEG-HU onto the hydroxyl groups of CNCs, (c) time-resolved FTIR of PEG_{2k}-NCO grafting to *c*-CNC-COOH highlighting the shoulders appearing around the urethane peak, (d) time-resolved FTIR of PEG_{2k}-HU grafting to *c*-CNC-COOH with no such shoulders, (e) change in reactant (isocyanate) and product (urethane) peak heights plotted against time for PEG_{2k}-NCO grafting, and (f) change in reactant (isocyanate + urea) and product (urethane) peak heights plotted against time for PEG_{2k}-HU grafting.

to PEG_{2k}-HU grafting, but was done immediately after PEG_{2k}-NCO preparation to avoid any loss of the isocyanate that could occur from hydrolysis or other side reactions during storage. Grafting was conducted under vacuum on an FTIR thermal stage so that spectra could be gathered *in-situ*. The resulting spectra for PEG_{2k}-NCO (Figure 3.5c) highlight the proclivity of the isocyanate to undergo side reactions with large shoulders appearing around 1765 and 1700 cm^{-1} in the grafted sample (Figure 3.5c inset). These peaks likely correspond to uretdione[42] and allophanate[38] production, respectively. The PEG_{2k}-HU-grafted sample shows notably smaller shoulders (Figure 3.5d). To quantify these differences, the decrease of the isocyanate (2275 cm^{-1}) and urea (1655 cm^{-1}) reactant peaks is plotted against time along with the increase of the product urethane peak (1722 cm^{-1}). In an ideal system, the consumption of reactants should translate directly into product growth, indicating inhibition of any side reactions taking place. For grafting with PEG-NCO (Figure 3.5e), these two curves diverge within the first 30 minutes of the reaction, emphasizing the fact that the isocyanate moiety is undergoing side reactions. In contrast, the PEG-HU grafting curves (Figure 3.5f) show strong alignment throughout the reaction, consistent with increased control with the hindered urea relative to the unblocked isocyanate. Based on this analysis, the blocked isocyanate shows superior performance compared to the unblocked system, allowing for more controlled grafting reactions.

To confirm that the polymer chains were indeed grafted to the CNCs, it is important to remove any unreacted polymer and carry out detailed characterization of the degree of functionalization on the polymer-grafted CNCs. To ensure thorough removal of excess unreacted polymer after surface functionalization, a diagnostic test was done by adding dye-tagged PEG to the reaction after completion and tracking the amount of dye remaining in the product after each wash (Figure S3.11). It was found that the most effective washing method for PEG removal was a 1:1 mixture of acetone:water.

After 12 centrifugation and resuspension cycles, no residual dye could be detected in the supernatant, implying that most, if not all, of the non-attached polymer chains had been removed. This strategy was then employed for the removal of untagged free polymer chains in all other samples.

After thorough cleaning, the amount of grafted polymer was measured using high resolution, dynamic TGA. Dynamic TGA is a procedure that slows the heating rate of the experiment whenever a mass loss event is detected, which helps to isolate individual degradation events. This method allowed for enhanced separation of CNC and polymer degradation, allowing for more accurate quantification of polymer content via thermogravimetry (Figure 3.6a).[43] By integrating the area under the PEG degradation peak between 330-400 °C (Figures 3.6b and S3.12), the PEG mass fraction could be determined and used to calculate the surface grafting density based on the crystal structure of cellulose and the CNC dimensions measured via AFM.[14,44]

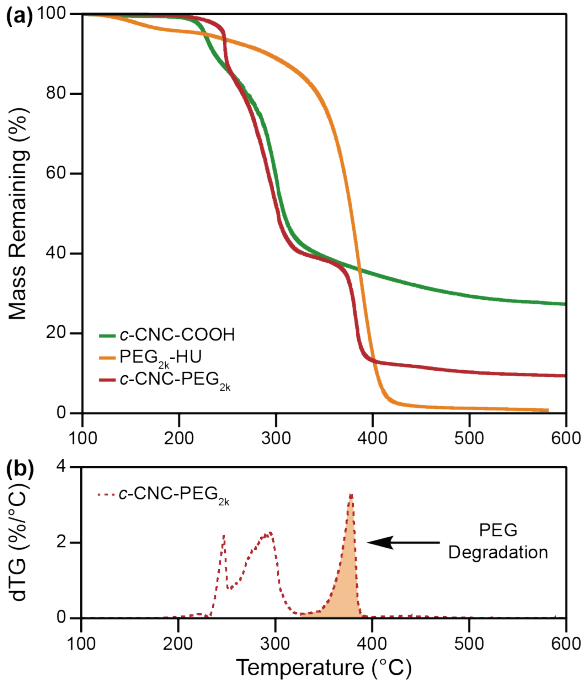

Figure 3.6: (a) TGA degradation curves of *c*-CNC-COOH, PEG_{2k}-HU, and a characteristic sample of *c*-CNC-*g*-PEG_{2k} and (b) the derivative of the *c*-CNC-*g*-PEG_{2k} degradation curve, highlighting the separation of CNC degradation and PEG degradation (shaded).

With characterization established, a series of experiments were done to optimize the reaction conditions for grafting PEG_{2k}-HU to *c*-CNC-COOH by varying the reaction time, reaction temperature, and ratio of polymer to surface hydroxyl groups (Table 3.1). The model reactions discussed earlier helped to define upper and lower limits for these tests, with 2 hours, 120 °C, and 400 mg PEG for every 100 mg *c*-CNC-COOH being considered the baseline conditions. From these studies, two hours was found to be the optimal reaction time, with shorter reactions not allowing for full HU conversion and longer reactions allowing more time for side reactions to reduce grafting density. The optimal reaction temperature was found to be 130 °C, with lower temperatures not activating the hindered urea groups efficiently enough and higher temperatures promoting side reactions.

While it was expected that grafting efficiency would decrease as the ratio of polymer to *c*-CNC-COOH mass increased, it was found that the grafting density plateaued above

Table 3.1: An array of *c*-CNC-*g*-PEG_{2k} grafting reaction conditions and the resulting reaction efficiencies and grafting densities.

***c*-CNC-COOH [mg]**	**PEG_{2k}-HU [mg (mol eq.)[a]]**	**Time [hr]**	**Temperature [°C]**	**Reaction Efficiency [% of chains grafted]**	**Grafting Density [chains/nm^2]**
100	400 (2.7)	1.5	120	6.3	0.41
[b]100	400 (2.7)	2	120	7.9	0.51
100	400 (2.7)	3	120	7	0.45
100	400 (2.7)	4	120	5.7	0.37
100	400 (2.7)	2	110	6.3	0.4
[b]100	400 (2.7)	2	120	7.9	0.51
100	400 (2.7)	2	130	9.5	0.61
100	400 (2.7)	2	140	6.5	0.42
100	100 (0.7)	2	120	21.7	0.35
100	200 (1.4)	2	120	16.9	0.54
[b]100	400 (2.7)	2	120	7.9	0.51
100	800 (5.4)	2	120	4.1	0.53
100	1600 (10.9)	2	120	1.9	0.48

[a] molar equivalent relative to surface alcohol groups on the *c*-CNC-COOH

[b] denotes the same baseline data, repeated for clarity

200 mg of PEG_{2k}-HU. It is possible that the higher ratio of polymer chains results in an increased concentration of isocyanate groups that can react with each other rather than the CNC surface. Additionally, steric bulk at the CNC surface may provide a physical limit as more polymer chains attach to the nanoparticles. By reducing the polymer:CNC ratio further to 1:1 by mass, too few polymer chains are present in the system, causing grafting density to be reduced from 0.54 to 0.35 chains/nm^2. In fact, varying the polymer:CNC mass ratio allows access to *c*-CNC-*g*-PEG_{2k} with grafting densities that range from 0.35 to 0.54 chains/nm^2. It is worth noting that the reaction efficiency (polymer grafted vs. polymer added to the reaction) is better at lower polymer:CNC mass ratios. The optimized reaction conditions for PEG_{2k} grafting (1.4 eq. of polymer relative to surface hydroxyl groups, 2 hour reaction time, and 130 °C) were used to graft all other polymers to the CNC surface to allow for comparison.

3.3.5 Results and Analysis of Grafting with a Variety of Polymers

To explore the versatility of this technique, grafting was also carried out with HU-terminated PEG_{10k}, PCL_{10k}, and PBA_{10k} in addition to PEG_{2k} with the established optimized conditions. For PCL and PBA-grafted CNCs, the cleaning washes were done with THF, which is a good solvent for both polymers.

It was not possible to determine the amount of PCL in the *c*-CNC-*g*-PCL_{10k} samples using dynamic TGA as PCL degradation could not be deconvoluted from CNC degradation. Thus, an FTIR calibration curve was created by mixing varying ratios of PCL and CNCs and measuring the relative intensity of the 1724 cm^{-1} peak in the normalized spectra, corresponding to the carbonyl group in the PCL repeat unit (Figure 3.7). When plotted against PCL content, the peak heights generated a linear relation that could be used to estimate grafted PCL content (Figure 3.7 inset). For PBA, both dynamic TGA and FTIR calibration curves were used to quantify the grafted polymer content, and both

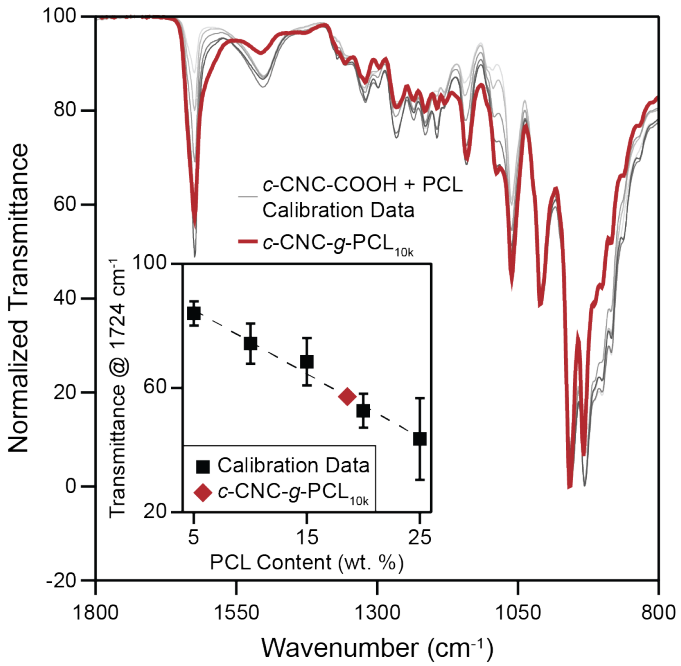

Figure 3.7: FTIR data for *c*-CNC-COOH mixed with PCL_{10k}-OH at various ratios along with the resulting calibration curve (inset) with the polymer-grafted *c*-CNC-*g*-PCL_{10k} overlayed on both.

methods corroborated each other (Figures S3.13 and S3.14).

The results for grafting all polymers with the optimized conditions can be seen in Table 3.2. Putting these results in the context of other grafting methods, prior work from Rowan and coworkers used peptide coupling in DMF to access PEG-grafted CNCs.[14] With PEG_{2k}, the best reaction conditions resulted in a grafting density of

Table 3.2: Grafting results for a variety of polymers onto *c*-CNC-COOH using optimized grafting conditions.

Sample	**Polymer Mass Fraction [wt.%]**	**Grafting Density [chains/nm^2]**
c-CNC-*g*-PEG_{2k}	26.5[a]	0.58
c-CNC-*g*-PEG_{10k}	28.0[a]	0.13
c-CNC-*g*-PCL_{10k}	18.6[b]	0.07
c-CNC-*g*-PBA_{10k}	8.7[b]	0.03

[a] measured via dynamic TGA

[b] measured via FTIR calibration curve

0.33 chains/nm^2. This work observed a grafting density of 0.58 chains/nm^2 using the optimized conditions, which is significantly higher than the grafting density achieved in solution. It is, of course, important to note that the isocyanates can react with the 2- and 3-hydroxyl groups on the cellulose unit, whereas only the primary 6-hydroxyl can react with the amine during peptide coupling. It is possible to use the hindered urea grafting approach to replicate the solution grafting density reported in this prior literature using half as much polymer reactant by mass.

For PEG_{10k} grafting, the resulting grafting density was 0.13 chains/nm^2, which is lower than the PEG_{2k}-grafted sample presumably on account of the steric bulk of the larger polymer chains. Compared to the highest solution grafting density results of 0.07 chains/nm^2 for PEG_{10k}, the hindered urea grafting method developed herein is able to achieve greater grafting densities than solution-based grafting methods.[14]

Based on the FTIR calibration curve for *c*-CNC-*g*-PCL_{10k}, the calculated grafting density of 0.07 chains/nm^2 is slightly lower than the PEG_{10k} grafting density. While the different polymer structures make these results difficult to compare, it is hypothesized that the reduced flexibility of the polycaprolactone chain (Kuhn length b = 7.0 Å for PCL[45] vs. b = 6.0 Å for PEG[46]) likely increases the steric hinderance at the nanoparticle surface, resulting in fewer polymer chains finding a reactive site on the CNC. Nearly all PCL-grafted CNCs in literature are synthesized via ring opening polymerization from the CNC surface, which is a technique that makes it difficult to characterize the grafted chain length or density. As an elementary comparison, a few reports have used FTIR to characterize their PCL-grafted CNCs and the relative intensity of the 1724 cm^{-1} peak corresponding to the carbonyl in the PCL backbone is roughly similar to the relative intensity observed here (Figure 3.7), suggesting that the PCL content of the resulting nanoparticles is competitive with grafting-from techniques.[10,47,48]

Finally, PBA_{10k} grafting resulted in 0.03 chains/nm^2, which is notably lower than the PEG_{10k} and PCL_{10k} counterparts. This reduction in grafting density has been attributed to a further increase in the steric bulk from the butyl pendant group. Additionally, the more hydrophobic nature of this polymer may hinder mixing during the melt grafting process, further limiting surface functionalization. Regardless, the FTIR and TGA traces (Figures S3.13 and S3.14) show clear evidence of grafting, and the synthesis method is potentially applicable to a wide range of bromine-terminated polymers.

3.4 Conclusions

Taking inspiration from the polyurethane industry, a method has been developed for the melt-functionalization of cellulose nanocrystals. By installing dynamic hindered urea moieties on the end of polymer chains, isocyanate groups were formed *in-situ* in the bulk. The isocyanate groups generated were able to react with surface hydroxyl groups on the CNCs, linking the polymer to the nanoparticle via a urethane linkage. The efficacy of the reaction was verified with a model small molecule system before being optimized with hindered urea-terminated PEG_{2k} chains on cotton-based, TEMPO-oxidized CNCs. Compared to the unblocked isocyanate, the hindered urea-functionalized polymer chains showed fewer side reactions, emphasizing the increased synthetic control afforded by the blocked system. The resulting polymer-grafted nanoparticles exhibited grafting densities that were superior to solution-based functionalization methods without the need for harmful solvents during the grafting reaction. Finally, the versatility of this method was highlighted by grafting CNC surfaces with hindered urea-terminated dodecane, PEG_{10k}, PCL_{10k}, and PBA_{10k}. Each of the resulting polymer-grafted nanoparticles showed polymer contents that were competitive with literature. Sustainable and efficient processing are crucial characteristics for polymer-grafted CNC to achieve commercial success going forward, and this method advances both of those metrics while achieving

strong grafting densities with a range of polymers.

3.5 Materials, Methods, and Instrumentation

3.5.1 Materials

If not specified otherwise, all compounds and solvents were used as received, without further purification. Hydrochloric acid (HCl), sodium bromide (NaBr), sodium hypochlorite (NaOCl), D-(+)-galactose, sulfuric acid, dodecyl isocyanate, *N-tert*-butylmethylamine, methoxy-poly(ethylene glycol) (2,000 g/mol and 10,000 g/mol, PEG_{2k}-OH and PEG_{10k}-OH), hexamethylene diisocyanate, dibutyltin dilaurate (DBTDL), disperse orange 3 (DO3), benzyl alcohol, 1,5,7-Triazabicyclo[4.4.0]dec-5-ene, ϵ-caprolactone, ethyl α-bromoisobutyrate (EBiB), butyl acrylate, tris[2-(dimethylamino)ethyl]amine (Me_6TREN), copper (II) bromide ($CuBr_2$), allyl isocyanate, 2,2-dimethoxy-2-phenylacetophenone (DMPA), triethylamine (TEA) and chloroform-d ($CDCl_3$) were all purchased from Sigma-Aldrich. Whatman filter paper, sodium hydroxide (NaOH), sodium carbonate, copper(0) wire, basic alumina, neutral alumina, and all solvents, acetone, toluene, hexanes, dimethyl sulfoxide (DMSO), diethyl ether, chloroform, tetrahydrofuran (THF), dichloromethane (DCM), ethyl acetate, and N,N-dimethylformamide (DMF), were purchased from Fisher Scientific. (2,2,6,6-tetramethylpiperidin-1-yl)oxyl (TEMPO) was purchased from Ambeed, poly-(L)-lysine was purchased from Ted Pella, and 1,6,-hexanedithiol was purchased from Oakwood Chemical.

3.5.2 Methods

3.5.2.1 Preparation of *c*-CNC-OSO_3

10 g of Whatman Number 1 Grade Filter Paper were cut into small pieces, poured into 500 mL deionized water, and blended until formation of a pulp. The CNC-pulp solution

was then placed into an ice bath and 280 mL of concentrated sulfuric acid (98 %) was slowly added under stirring. During the addition, the temperature of the reaction was maintained below 35°C. After complete addition, the mixture was heated to 45 °C and stirred for 5 h. The mixture was then cooled to room temperature and filtered through a fine-fritted glass filter. The CNCs were centrifuged at 8000 rpm and resuspended in water ~5 times until the supernatant reached a neutral pH. Finally, the thoroughly washed material was suspended in DI and freeze-dried to yield *c*-CNC-OSO_3 in fluffy powder form (7.6 g).

3.5.2.2 Preparation of *c*-CNC-OH

10 g of Whatman Number 1 Grade Filter Paper were cut into small pieces, mixed with 500 mL deionized water, and blended into a uniform pulp. In a 2 L round bottom flask, 75 mL of concentrated HCl was combined with 225 mL of DI water and heated to 100 °C. Once at temperature, the CNC-pulp solution was added to the HCl solution and stirred for 90 minutes. The mixture was then filtered through fine-fritted glass filter before resuspending the *c*-CNC-OH in DI water. The CNCs were centrifuged at 8000 rpm and resuspended in water ~5 times until the supernatant reached neutral pH. Finally, the thoroughly washed material was suspended in DI water and freeze-dried to yield *c*-CNC-OH in fluffy powder form (7 g).

3.5.2.3 Preparation of *c*-CNC-COOH via TEMPO Oxidation

TEMPO oxidation of *c*-CNC-OH was conducted based on a prior literature report.[49] In brief, 7 g of *c*-CNC-OH were dispersed in 700 mL of DI water and dispersed with probe sonication. To the dispersed CNCs, pre-dissolved TEMPO (0.109 g, 0.7 mmol), NaBr (0.306 g, 3.5 mmol), and NaOCl (14.08 mL, 210 mmol) were added. The pH was adjusted to 10-10.5 and maintained in that range using 1 M NaOH for 2 hours, or until

the pH stopped decreasing. Once the reaction was complete, the solution was filtered through fine-fritted glass filter before resuspending the *c*-CNC-COOH in DI water. The CNCs were centrifuged at 8000 rpm and resuspended in water ~5 times. Finally, the thoroughly washed material was suspended in DI water and freeze-dried to yield *c*-CNC-COOH as a fluffy white powder (6 g).

3.5.2.4 Determination of Surface Carboxylate Concentration

To determine the carboxylate content of the isolated and oxidized *c*-CNC-COOH, conductivity titration was performed with a pH probe by recording conductivity and pH following dropwise addition of 0.01 M NaOH. The resulting conductivity data was plotted against the volume of added NaOH and the weak acid plateau was used to determine the concentration of carboxylates on the surface of the CNCs. The functional group density was determined using the following equation:

$$Carboxylate\ Density(\frac{mol}{kg}) = \frac{Concentration * Volume_{plateau}}{Mass(kg)}$$

To convert from surface concentration (mol/kg) to surface density (groups/nm^2), the calculated value is multiplied by 3.21, which was calculated based on the crystal structure of cellulose Iβ as well as the CNC dimensions measured via AFM.[14] For example, a measured surface concentration of 0.37 mol/kg equates to 1.2 groups/nm^2.

3.5.2.5 Synthesis of the Isopropylidene-Protected D-galactose (PG)

The isopropylidene protection of D-(+)-galactose was prepared following a previously reported procedure.[36] D-(+)-galactose (5 g, 27.7 mmol, 1 eq.) was dissolved in acetone (185 mL) and the solution was put in an ice bath. Concentrated sulfuric acid (98%) was added dropwise into the mixture (5.5 mL, 1.1 mL/g). The reaction mixture was then

stirred at room temperature for 5 h and neutralized with a solution of sodium carbonate until reaching a pH of 7. The resulting white precipitate was filtered and washed with acetone. The filtrate was collected and dried under high vacuum to remove residual solvent and yield the protected galactose (PG) as a light-yellow oil. ^{1}H NMR (400 MHz, $CDCl_3$) δ 5.56 (d, J = 5.0 Hz, 1H), 4.61 (dd, J = 8.0, 2.5 Hz, 1H), 4.33 (dd, J = 4.92, 2.63 Hz, 1H), 4.27 (dd, J = 8.1, 1.7 Hz, 1H), 3.90 – 3.80 (m, 2H), 3.72 (dd, J = 10.8, 3.5 Hz, 1H), 1.52 (s, 3H), 1.45 (s, 3H), 1.33 (s, 6H).

3.5.2.6 Synthesis of alkyl end-functionalized hindered urea (Dodecyl-HU)

Dodecyl isocyanate (1.14 mL, 5.3 mmol, 1 eq.) and *N-tert*-butylmethylamine (0.65 mL, 5.5 mmol, 1.02 eq.) were solubilized in dry toluene (100 mL). The mixture was stirred at room temperature for 6 h. The resulting precipitate was filtered, thoroughly washed with hexanes, and dried under high vacuum to yield dodecyl-HU as a white powder. ^{1}H NMR (400 MHz, $CDCl_3$) δ 4.22 (br, 1H), 3.17 (dt, J = 7.5, 5.6 Hz, 2H), 2.81 (s, 3H), 1.48 (t, J = 7.3 Hz, 3H), 1.39 (s, 9H), 1.34 – 1.20 (m, 18H), 0.87 (t, J = 6.8 Hz, 3H).

3.5.2.7 Procedure for PG and Docedyl-HU model reaction in melt

In a desired ratio, PG and dodecyl-HU compounds were dissolved in a small vial using a minimal amount of acetone (ca. 1-2 mL). A final weight of 200 mg of compound was targeted, to ensure enough material for analysis. The solvent was removed under high pressure vacuum overnight to yield a dried solid powder. The powder was then heated to 120 °C and stirred in ambient atmosphere for 8 h. The experiment was track with *in-situ* FTIR, focusing on the urea and urethane peaks at 1645 and 1722 cm^{-1}, respectively.

3.5.2.8 Synthesis of Isocyanate-terminated PEG (PEG-NCO)

Poly (ethylene glycol) methyl ether (2 g, 1 mmol), previously azeotropically dried from toluene under high vacuum, was dissolved in dry toluene (20 mL) under inert atmosphere. Hexamethylene diisocyanate (1.6 ml, 10 mmol) and a trace amount of DBTDL were added into the solution. The mixture was heated at 40 °C under stirring and nitrogen atmosphere for 2 h. The polymer was precipitated in cold hexanes (200 mL) twice from a concentrated toluene solution, taking extreme care to keep the polymer under inert atmosphere as much as possible. The resulting PEG-NCO was dried under high vacuum to yield a solid white material for characterization. ^{1}H NMR (400 MHz, $CDCl_3$) δ 4.83 (br, 1H), 4.21 (t, J = 4.8 Hz, 2H), 3.83 – 3.42 (backbone), 3.37 (s, 3H), 3.30 (t, J = 6.6 Hz, 2H), 3.16 (q, J = 6.7 Hz, 2H), 1.67 – 1.20 (m, 8H). SEC (THF) Mn, 2k = 4,730 g/mol, Đ2k = 1.10; Mn, 10k = 10,600 g/mol, Đ10k = 1.008.

3.5.2.9 Synthesis of Hindered-urea Terminated PEG (PEG-HU)

Dried PEG-NCO (1.75 g, 0.8 mmol) and N-tert-butylmethylamine (0.945 mL, 8 mmol) were dissolved in dry toluene (35 mL) under inert atmosphere. The mixture was stirred at room temperature for 2 h. The product was then precipitated 4 times in cold hexane (350 mL) from a concentrated toluene solution and dried to yield PEG-HU as a solid white material. ^{1}H NMR (400 MHz, $CDCl_3$) δ 4.86 (br, 1H), 4.28 (br, 1H), 4.20 (t, J = 4.7 Hz, 2H), 3.83 – 3.42 (backbone), 3.37 (s, 3H), 3.16 (m, 4H), 2.81 (s, 3H), 1.48 (m, 4H), 1.38 (s, 9H), 1.33 (m, 4H). SEC (THF) Mn, 2k = 3,130 g/mol, Đ2k = 1.10, Mn, 10k = 13,000 g/mol, Đ10k = 1.07.

3.5.2.10 Synthesis of Disperse Orange 3-terminated PEG (PEG-DO3)

PEG-HU (1 g, 0.5 mmol) was dissolved in dry DMSO along with DO3 (1.21 g, 5 mmol). The solution was heated to 120°C under vacuum (200 mbar) for 2 hours to remove the urea blocking group without evaporating the solvent. The DMSO was removed via liquid-liquid extraction with water and chloroform, where the DMSO went into the aqueous layer and the product remained in the organic layer. After concentrating, the organic layer was precipitated in diethyl ether 3 times before drying and characterizing the resulting PEG-DO3. ^{1}H NMR (400 MHz, $CDCl_3$) δ 8.41 – 7.55 (ar, 8H), 5.70 (br, 1H), 5.10 (br, 1H), 4.20 (t, J = 4.7 Hz, 2H), 3.83 – 3.42 (backbone), 3.37 (s, 3H), 3.22 (m, 4H), 1.48 (m, 4H), 1.33 (m, 4H).

3.5.2.11 Synthesis of Polycaprolactone (PCL)

Benzyl alcohol (0.24 mL, 23.1 mmol), 1,5,7-triazabicyclo[4.4.0]dec-5-ene (6.4 mg, 0.05 mmol, 0.1 mol.%), and ϵ-caprolactone (5 mL, 462.4 mmol) were mixed under inert atmosphere. The mixture was heated at 60 °C for 4 hours, then quenched with benzyl alcohol (2.5 mL). The polymer was precipitated 5 times in cold diethyl ether (200 mL) from concentrated solution of THF and dried to yield PCL as a white solid material. ^{1}H NMR (400 MHz, $CDCl_3$) δ 7.35 (ar, 5H), 4.05 (m, 2H), 2.30 (m, 2H), 1.64 (m, 4H), 1.38 (m, 2H). SEC (THF) M_n = 9,070 g/mol, Đ = 1.23.

3.5.2.12 Synthesis of PCL end-functionalize isocyanate (PCL-NCO)

PCL (2.051 g, 1.26 mmol), previously azeotropically dried from toluene under high vacuum, was dissolved in dry THF (100 mL) under inert conditions. Hexamethylene diisocyanate (3 mL, 25 mmol) and a tiny amount of DBTDL were added into the solution. The mixture was heated at 40 °C under stirring and nitrogen atmosphere for 2 h. The

polymer was precipitated 4 times in cold diethyl ether (100 mL) from a concentrated THF solution and dried to yield PCL-NCO as a white solid material. ^{1}H NMR (400 MHz, $CDCl_3$) δ 7.35 (ar, 5H), 4.68 (br, 1H), 4.06 (m, backbone), 3.30 (m, 2H), 3.16 (m, 2H), 2.30 (m, backbone), 1.64 (m, backbone), 1.51 (m, 4H), 1.38 (m, backbone), 1.28 (m, 4H). SEC (THF) M_n = 14,300 g/mol, Đ = 1.43.

3.5.2.13 Synthesis of PCL end-functionalize hindered urea (PCL-HU)

Dried PCL-NCO (1.72 g) and *N-tert*-butylmethylamine (2 mL, 16.68 mmol) were dissolved in dry THF (60 mL) under inert atmosphere. The mixture was stirred at room temperature for 2 h. The product was then precipitated 4 times in cold ether (100 mL) from a concentrated THF solution and dried to yield PCL-HU as a solid white material. ^{1}H NMR (400 MHz, $CDCl_3$) δ 7.35 (ar, 5H), 4.74 (br, 1H), 4.29 (br, 1H), 4.06 (m, backbone), 3.16 (m, 4H), 2.81 (s, 3H), 2.30 (m, backbone), 1.64 (m, backbone), 1.50 (m, 4H), 1.38 (m, backbone + 9H), 1.25 (m, 4H). SEC (THF) M_n = 11,100 g/mol, Đ = 1.34.

3.5.2.14 Synthesis of Poly(Butyl Acrylate) (PBA-Br)

PBA-Br was synthesized via Cu(0)-mediated living radical polymerization, following a published procedure.[40] In brief, butyl acrylate was filtered through basic alumina to remove any inhibitor, then the initiator (EBiB) (1 eq.), monomer (targeting 10,000 g/mol at 50% conversion), $CuBr_2$ (0.05 eq.), and DMF (targeting 75 vol.% relative to all other reactants) were all added to a round-bottom flask. The flask was sparged with inert gas for 15 minutes before adding the Me_6TREN ligand (0.12 eq.). A stir bar was wrapped in 10 cm of copper wire and cleaned with concentrated HCl, then rinsed with acetone and DMF before dropping it into the flask to begin the reaction. NMR aliquots were taken every 30 minutes to track conversion and the reaction was quenched by opening it to air and removing the stir bar once it reached 50% conversion. The polymer was purified by

rotary evaporation of any remaining monomer, redissolving in DCM, running it through a neutral alumina plug to remove the copper and ligand, then drying on high vacuum overnight before characterizing. The pure polymer was characterized with ^{1}H NMR and SEC to confirm the product. ^{1}H NMR (400 MHz, $CDCl_3$) δ 4.03 (m, 2H), 2.28 (m, 1H), 1.90 (m, 1H), 1.60 (m, 3H), 1.37 (m, 2H), 0.93 (m, 3H). SEC (THF) M_n = 13,000 g/mol, Đ = 1.21.

3.5.2.15 Preparation of Thio-HU for End Group Functionalization

Thio-HU was synthesized in a two-step process before being added to the polymer chain end. First, an allyl-hindered urea was synthesized by mixing allyl isocyanate (1 eq.) with *N-tert*-butylmethylamine (1.1 eq.) at 1 M concentration in DCM. The resulting allyl-HU was purified with high vacuum to remove all solvent and remaining reactants, resulting in a white solid, before characterizing with ^{1}H NMR, ^{13}C NMR, and high-resolution mass spectrometry. ^{1}H NMR (400 MHz, $CDCl_3$) δ 5.87 (ddt, J = 17.2, 10.2, 5.6 Hz, 1H), 5.14 (dq, J = 17.2, 1.7 Hz, 1H), 5.06 (dq, J = 10.2, 1.5 Hz, 1H), 4.33 (br, 1H), 3.80 (tt, J = 5.6, 1.6 Hz, 2H), 2.82 (s, 3H), 1.37 (s, 9H). ^{13}C NMR (101 MHz, $CDCl_3$) δ 159.09 (C = O), 136.13 (C = C – C), 115.40 (C = C), 55.71 (C), 43.31 (C = C – C), 31.84 (CH3), 29.05 (3CH3). HRMS (ESI) m/z: $[M + H]^+$ calcd for $C_9H_{18}N_2O$, 171.1453; found, 171.1497.

A thiol group was added to the allyl-HU by dissolving 1 eq. of allyl-HU in 15 eq. of 1,6-hexanedithiol along with 0.5 eq. DMPA photoinitiator. Once dissolved, the solution was placed on a low-power UV source (bug zapper) for 30 minutes. The resulting thio-HU molecule was purified by loading the crude mixture onto a silica column with 9:1 hexanes:ethyl acetate. This 9:1 mixture pushed the excess dithiol and initiator fragments through, while retaining the product in the column. The product was then flushed from the column using pure ethyl acetate. Thio-HU was then dried as a yellow oil before characterization with ^{1}H NMR, ^{13}C NMR, and high resolution mass

spectrometry. ^{1}H NMR (400 MHz, $CDCl_3$) δ 4.51 (br, 1H), 3.27 (td, J = 6.7, 5.6 Hz, 2H), 2.80 (s, 3H), 2.57 – 2.44 (m, 6H), 1.78 (qi, J = 6.9 Hz, 2H), 1.65 – 1.50 (m, 4H), 1.37 (m, 13H), 1.31 (t, J = 7.8 Hz, 1H). ^{13}C NMR (101 MHz, $CDCl_3$) δ 159.36 (C = O), 55.62 (C), 40.08 (C – N), 33.94 (CH2), 32.16 (S – C), 31.88 (CH3), 30.01 (CH2), 29.96 (CH2), 29.51 (CH2), 29.08 (3CH3), 28.39 (CH2), 28.02 (CH2), 24.64 (CH2). HRMS (ESI) m/z: $[M + H]^+$ calcd for $C_{15}H_{32}N_2OS_2$, 321.1990; found, 321.2041.

3.5.2.16 Synthesis of Hindered Urea-Terminated PBA (PBA-HU)

Thio-HU was added to PBA-Br chain ends via nucleophilic substitution. The bromine-terminated polymer (1 eq.) was dissolved in acetone at 500 mg/mL along with TEA (10 eq.). The solution was then purged with inert gas for 5 minutes before adding thio-HU (2 eq.). The reaction was allowed to proceed for 24 hours before another 2 eq. of thio-HU were added under inert atmosphere. This process was repeated until 5 total additions were made, totaling 10 eq. of thio-HU. The resulting HU-terminated PBA-HU was purified by running the crude solution through a silica plug with 65:35 hexanes:ethyl acetate, where the PBA-HU eluted first, followed by the other reagents. The products were then dried before characterization with ^{1}H NMR and SEC. ^{1}H NMR (400 MHz, $CDCl_3$) δ 4.51 (br, 1H), 4.03 (m, backbone), 3.29 (m, 2H), 2.81 (s, 3H), 2.52 (m, 6H), 2.27 (m, backbone), 1.90 (m, backbone), 1.80 (m, 4H), 1.60 (m, backbone), 1.39 (s, 9H), 1.37 (m, backbone), 0.93 (m, backbone). SEC (THF) M_n = 11,900 g/mol, Đ = 1.04.

3.5.2.17 Functionalization of *c*-CNC-*g*-Polymer in Melt

The *c*-CNC-COOH (30 to 200 mg) were dispersed in 25 mL of deionized water by ultrasonication for 15 min, then solvent exchanged into acetone (see below). Relative to the CNC mass, hindered-urea-terminated polymer of the desired molar ratio was added to the CNC suspension and placed in a sonic bath until completely dissolved. The

solvent was removed under high vacuum overnight to yield a dried powder. Once dry, the mixture was placed in an oil bath at 130°C and 120 mbar vacuum was applied to pull off the released volatile amine. After 2 hours, heat was removed and a mixture of water/acetone in a 1:1 ratio (50 mL) was added to the PEG grafting reactions, or THF for PCL and PBA reactions. The mixture was centrifuged and resuspended in the same solvent 10 times to remove non-attached polymer. The resulting *c*-CNC-*g*-Polymer were suspended in water and freeze-dried to obtain a fluffy powder.

3.5.2.18 Measuring Non-Grafted Polymer Chains

A UV-Vis calibration curve was created for PEG-DO3 in 1:1 water/acetone mixture from 100 mM to 10 nM. The functionalization of *c*-CNC-*g*-PEG was carried out as described before. After the grafting reaction was completed, a mixture of water/acetone in a 1:1 ratio (50 mL) containing 1 eq. of PEG-DO3 (relative to the PEG-HU added to the original reaction) was added to the medium. The mixture was centrifuged and resuspended in the same solvent couple, and the supernatants were analyzed with UV-Vis spectroscopy to track the removal of non-grafted polymer.

3.5.2.19 Solvent Exchange of CNCs

To disperse CNCs in non-aqueous solvents such as acetone, solvent exchange can be done to improve the quality of the suspension. In essence, 100 mg of CNCs are dispersed in 20 mL of DI water in a centrifuge tube using an ultrasonic bath before adding 20 mL of acetone. After mixing, the acetone/water suspension is centrifuged (10,000 g for 10 minutes) and the supernatant is poured off and replace by another 1:1 mixture of acetone:water. The precipitate is resuspended using a sonic bath and vortexer before centrifuging once again. The supernatant is then poured off and replace by pure acetone. Once the precipitate is resuspended, the CNCs form a more stable dispersion in acetone.

3.5.2.20 CNC + PCL and CNC + PBA FTIR Calibration Curves

To measure the polymer content of grafted CNCs, FTIR calibration curves were generated for PCL and PBA. In a small vial, 5-10 mg of *c*-CNC-COOH were mixed with the desired amount of polymer using a 20 mg/mL stock solution in MeOH to target samples with 5, 10, 15, 20, and 25 wt.% polymer. Minimal additional MeOH was added, and a spatula was used to ensure thorough mixing. The vials were immediately placed under high vacuum to remove the methanol and ensure a uniform distribution of polymer within the CNCs. Once dry, the samples were analyzed using FTIR and a calibration curve was developed based the representative carbonyl peak of each polymer (1724 cm^{-1} for PCL, and 1730 cm^{-1} for PBA).

3.5.3 Instrumentation

Atomic Force Microscopy (*AFM*) was done with a Cypher ES Environmental equipped with FS-1500 probes (Asylum Research) to determine the dimensions of CNCs. Crystals were dispersed in water by ultrasonication (10 min, 25% power, 3 s on/off cycle) at a concentration of 0.01% (w/w). A mica surface was mechanically exfoliated, treated with 50 μL poly(L-lysine), gently rinsed with DI water, then 50 μL of the freshly prepared CNC dispersion was drop-cast onto the surface. The dispersions were gently rinsed with DI water after 3 minutes and substrates were air-dried overnight prior to imaging. The images were recorded using tapping mode and the data was analyzed with Gwyddion software (Czech Metrology Institute).

Conductometric titrations of carboxylate and sulfate functional groups on the surface of the CNCs were performed using an Accumet XLbenchtop pH/conductivity meter on aqueous solutions. In brief, 30 mg of the desired CNCs were dispersed in 80 mL of DI water using probe sonication. For *c*-CNC-COOH the solution was acidified to a pH of

2-3 using concentrated HCl, then 0.01 M NaOH was titrated in using a syringe pump. For *c*-CNC-OSO_3, 0.01 M NaOH was directly titrated without acidification. Data was recorded at regular intervals and plotted as Conductivity vs. Volume added to determine the functional group content of the nanoparticles.

Fourier transform infrared (*FTIR*) spectroscopy of solid samples was carried out using a Shimadzu IRTracer-100 Fourier transform infrared spectrometer in the attenuated total reflection (ATR) geometry with a monolithic diamond ATR crystal. The sample temperature was controlled under a vacuum using the PIKE GladiATR accessory. Data was collected in the range of 4000–400 cm^{-1}, averaging over 45 scans, and treated with Shimadzu LabSolutions IR software.

High resolution mass spectrometry (*HRMS*) was performed on an Agilent 6224 ToF-MS using electrospray ionization (ESI).

Nuclear magnetic resonance (*NMR*) was carried out at ambient temperature on a Bruker Avance II+ 400 spectrometer at frequencies 400 MHz for ^{1}H nuclei and 101 MHz for ^{13}C nuclei. Spectra were calibrated to the residual solvent peak of $CDCl_3$ (7.26 ppm ^{1}H NMR, 77.16 ppm for ^{13}C NMR) and processed with MestReNova software. All chemical shifts, δ, are reported in parts per million (ppm) with coupling constant in Hz (multiplicity: s = singlet, d = doublet, dd = double doublet, td = triple doublet, t = triplet, dt = double triplet, tt = triple triplet, ddt = double double triplet, q = quadruplet, dq = double quadruplet, qi = quintuplet, m = multiplet, br = broad signal, ar = aromatic signal).

Size exclusion chromatography (*SEC*) of the polymers was performed on a Shimadzu Prominence High Performance Liquid Chromatography system using an eluent mobile phase of THF at a flow rate of 1 mL/min. Separation was achieved using two PLgel mixed-D columns (Agilent) maintained at ambient temperature with pore sizes suitable for materials with effective molecular weights from ∼200 to 400,000 g/mol. The differential refractive index signal was collected using a Wyatt Optilab

T-rEX differential refractometer (λ = 658 nm), and on-line multi-angle light scattering (MALS) measurement was performed using a Wyatt Dawn Heleos II light scattering detector. Data analysis was carried out using Wyatt Astra VII software. Weight-averaged molecular weights (M_w) were determined by MALS, and number-average molecular weights (M_n) were determined in comparison to narrow dispersity polystyrene calibration standards (from 1,800 to 400,000 g/mol).

Thermogravimetric analysis (*TGA*) was performed using a TA Instruments Discovery thermogravimetric analyzer. Samples ($\sim$5 mg) were loaded in Pt crucibles and heated under a N_2 atmosphere. High resolution dynamic procedure with default settings (sensitivity = 1, ramp = 10 to 700 °C, resolution = 5) were applied. Data was processed in TA Instruments Trios software.

Wide-angle X-ray scattering (*WAXS*) patterns were recorded using a SAXSLAB GANESHA 300XL system with Cu Kα source (λ= 0.154 nm) at a voltage of 40 kV and 40 mA power. Powder samples were tightly packed inside plastic washers and were held in place between two pieces of Kapton tape. The data were collected in the 2-theta angle range of 1-32° for 20 minutes. The crystallinity index was calculated using MATLAB R2018a by modelling the (1,-1,0), (1,1,0), (1,0,2), and (2,0,0) cellulose-Iβ peaks and the residual amorphous component to Gaussian distribution functions as described previously.[50,51]

Probe Ultrasonication was carried out on a Branson SFX 550 instrument equipped with a 13 mm probe. Sonication was conducted at 20% amplitude with 5 seconds on and 5 seconds off per cycle while the sample vial was submerged in ice water to prevent significant heating.

Ultraviolet-Visible Light (*UV-Vis*) *Spectroscopy* was conducted on a Shimadzu UV-3600 Plus UV-Vis-NIR spectrophotometer from 350-800 nm wavelengths. Samples were run at 1 nm resolution in quartz cuvettes.

3.6 Supporting Information

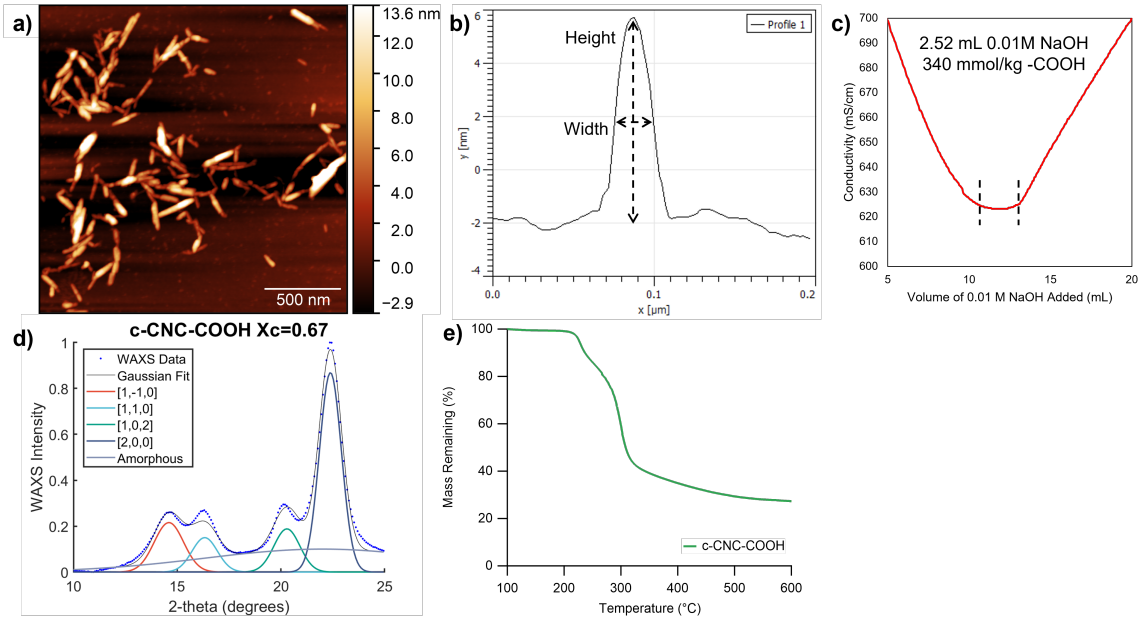

Figure S3.1: a) AFM height image of *c*-CNC-COOH, b) a height profile extracted from the AFM image showing how height and width of the nanoparticles are measured, c) a representative conductivity titration curve of *c*-CNC-COOH showing the weak acid plateau corresponding to -COOH neutralization, d) WAXS of *c*-CNC-COOH showing the crystallinity index, and e) the TGA degradation trace of the *c*-CNC-COOH.

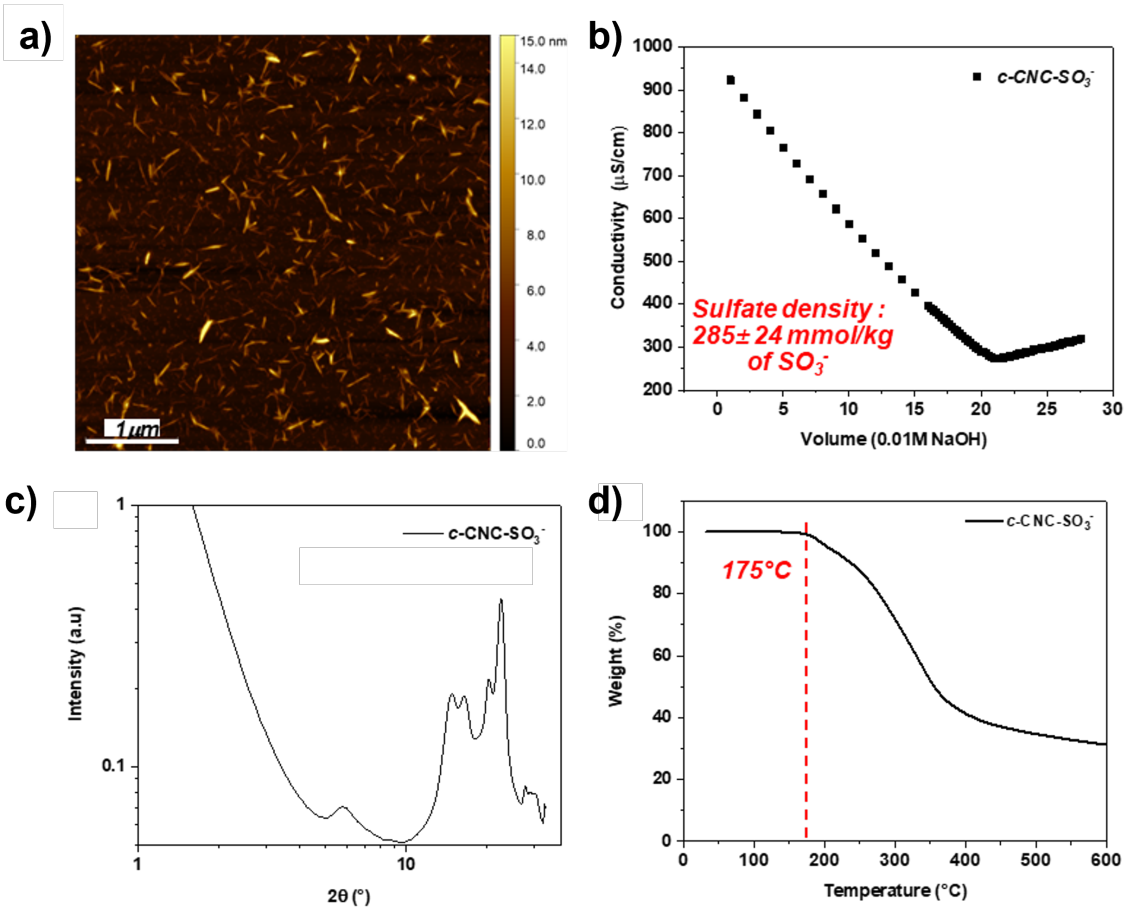

Figure S3.2: a) AFM height image of *c*-CNC-OSO_3, b) a representative conductivity titration curve of *c*-CNC-OSO_3, c) WAXS of *c*-CNC-OSO_3 showing the crystallinity index, and d) the TGA degradation trace of the *c*-CNC-OSO_3.

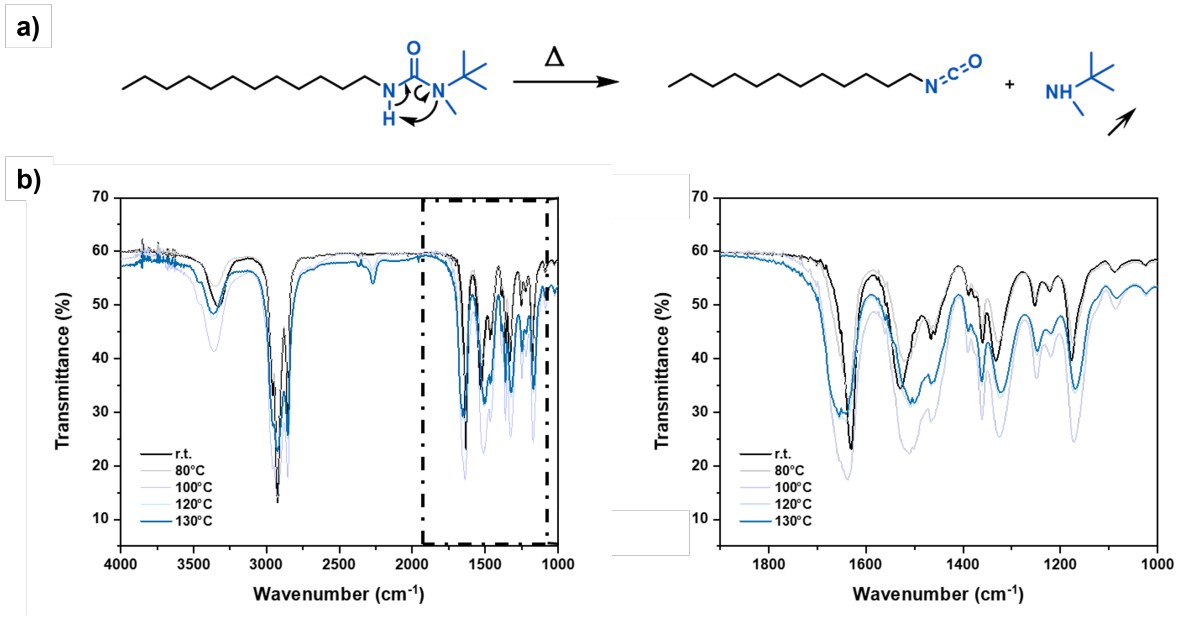

Figure S3.3: a) Scheme of hindered urea (dodecyl-HU) dissociation upon heating and b) FTIR spectra of the dodecyl-HU component at temperatures ranging from 80°C to 130°C, focusing on the signals at 1900-1000 cm^{-1}.

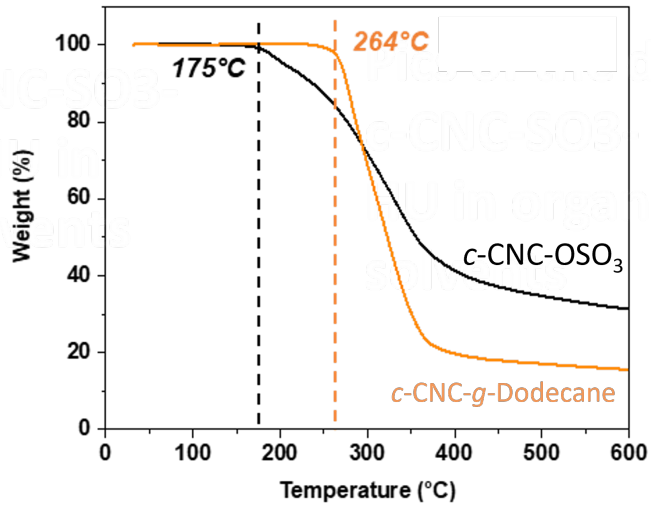

Figure S3.4: TGA of *c*-CNC-OSO_3 and *c*-CNC-*g*-dodecane showing increased thermal stability in the grafted CNCs.

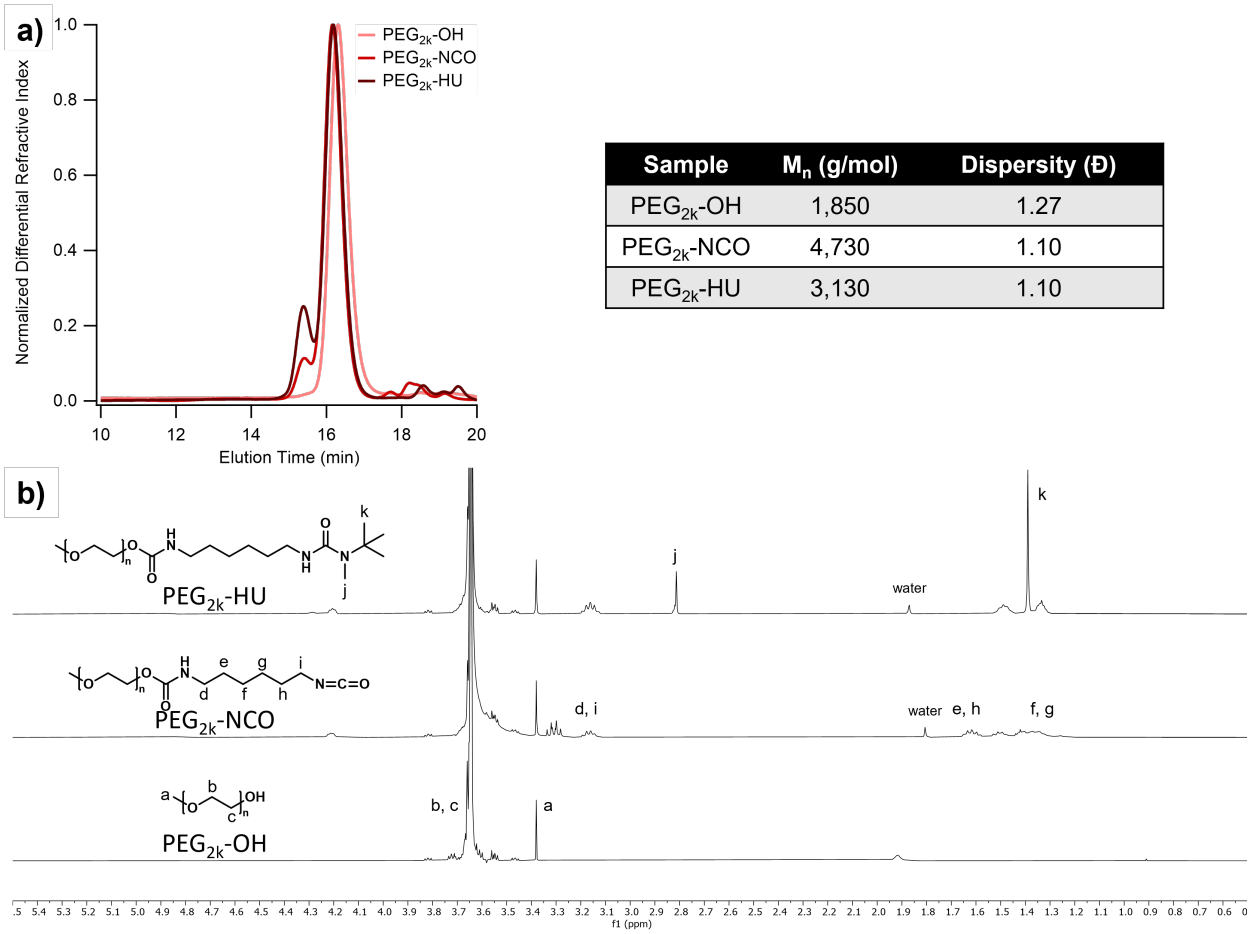

Sample	M_n (g/mol)	Dispersity (Đ)
PEG_{2k}-OH	1,850	1.27
PEG_{2k}-NCO	4,730	1.10
PEG_{2k}-HU	3,130	1.10

Figure S3.5: a) SEC traces and corresponding molecular weight and dispersity for PEG_{2k}-OH, PEG_{2k}-NCO, and PEG_{2k}-HU, and b) ^{1}H NMR spectra of PEG_{2k}-OH, PEG_{2k}-NCO, and PEG_{2k}-HU with key peaks labeled.

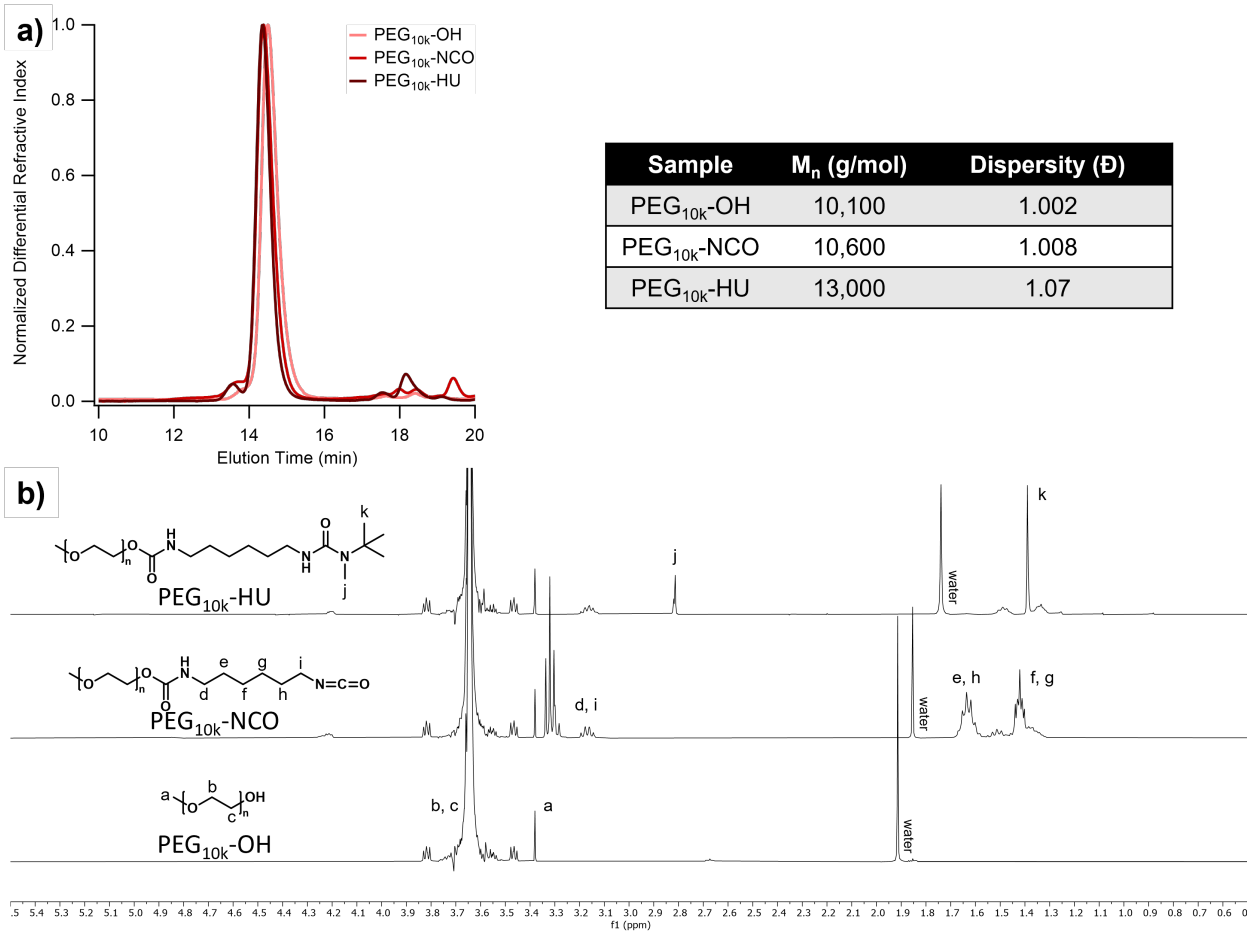

Sample	M_n (g/mol)	Dispersity (Đ)
PEG_{10k}-OH	10,100	1.002
PEG_{10k}-NCO	10,600	1.008
PEG_{10k}-HU	13,000	1.07

Figure S3.6: a) SEC traces and corresponding molecular weight and dispersity for PEG_{10k}-OH, PEG_{10k}-NCO, and PEG_{10k}-HU, and b) ^{1}H NMR spectra of PEG_{10k}-OH, PEG_{10k}-NCO, and PEG_{10k}-HU with key peaks labeled.

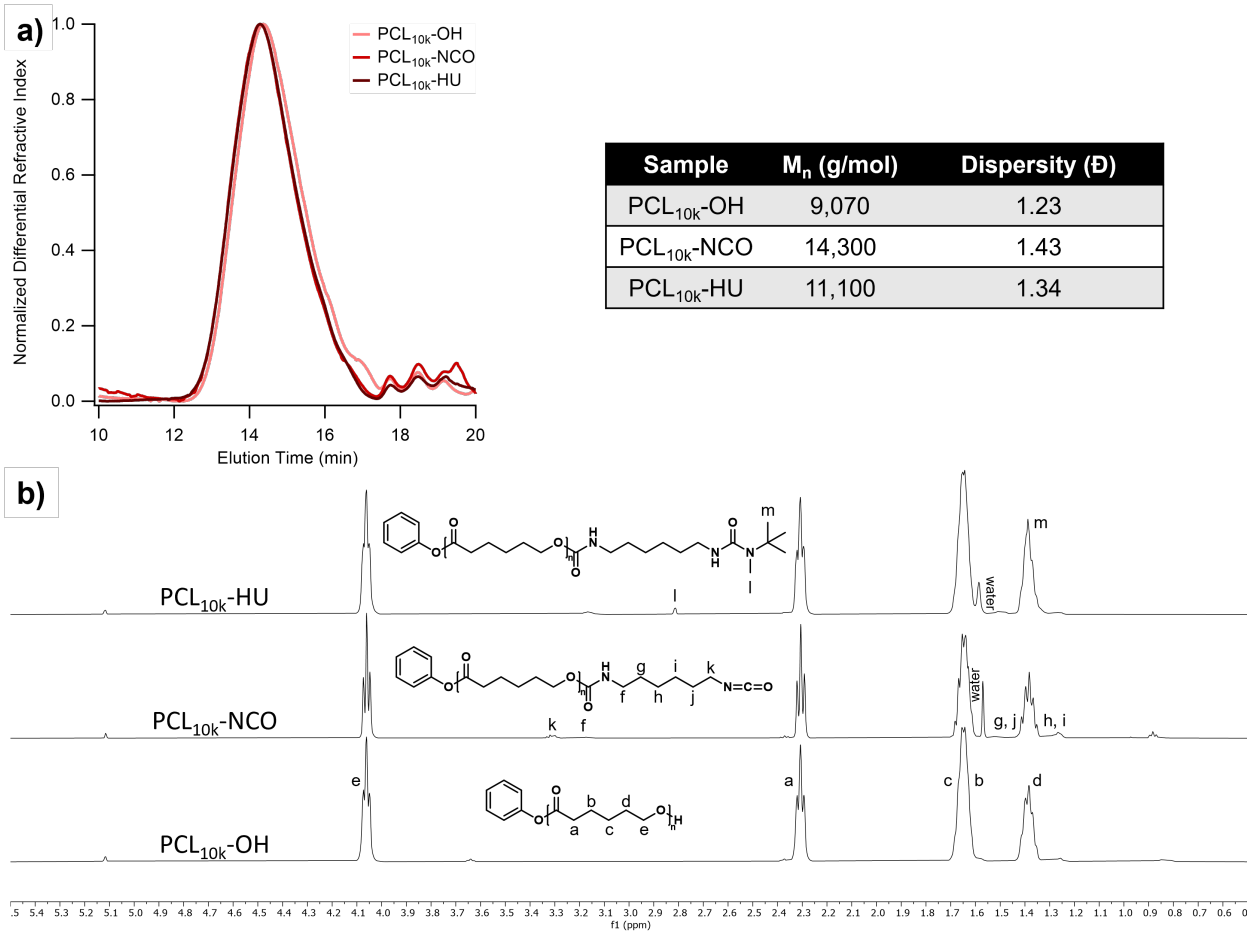

Sample	M_n (g/mol)	Dispersity (Đ)
PCL_{10k}-OH	9,070	1.23
PCL_{10k}-NCO	14,300	1.43
PCL_{10k}-HU	11,100	1.34

Figure S3.7: a) SEC traces and corresponding molecular weight and dispersity for PCL_{10k}-OH, PCL_{10k}-NCO, and PCL_{10k}-HU, and b) ^{1}H NMR spectra of PCL_{10k}-OH, PCL_{10k}-NCO, and PCL_{10k}-HU with key peaks labeled.

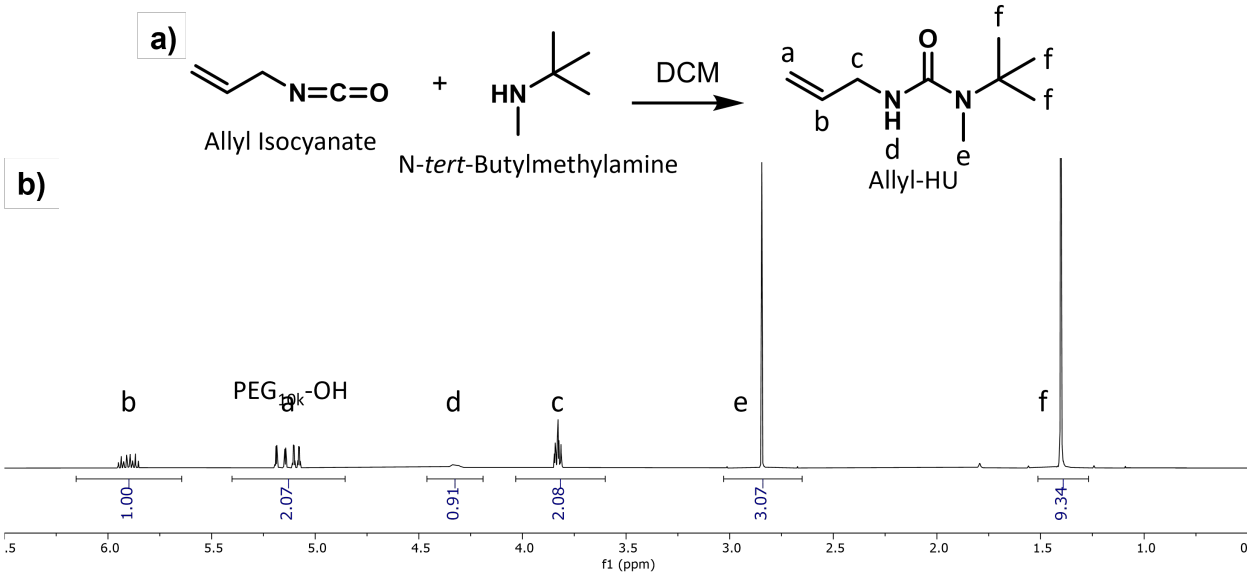

Figure S3.8: a) SEC traces for PBA_{10k}-Br and PBA_{10k}-HU and b) ^{1}H NMR spectra of PBA_{10k}-Br and PBA_{10k}-HU with key peaks labeled.

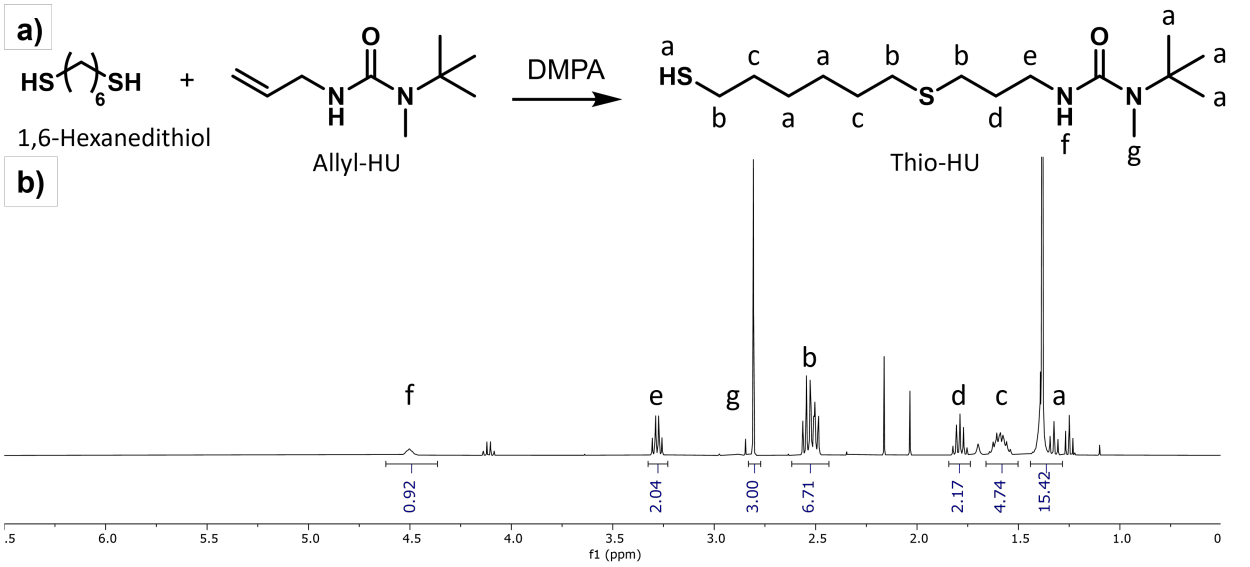

Figure S3.9: a) Schematic for the synthesis of allyl-HU from allyl isocyanate and *N-tert*-butylmethylamine and b) the resulting ^{1}H NMR spectrum.

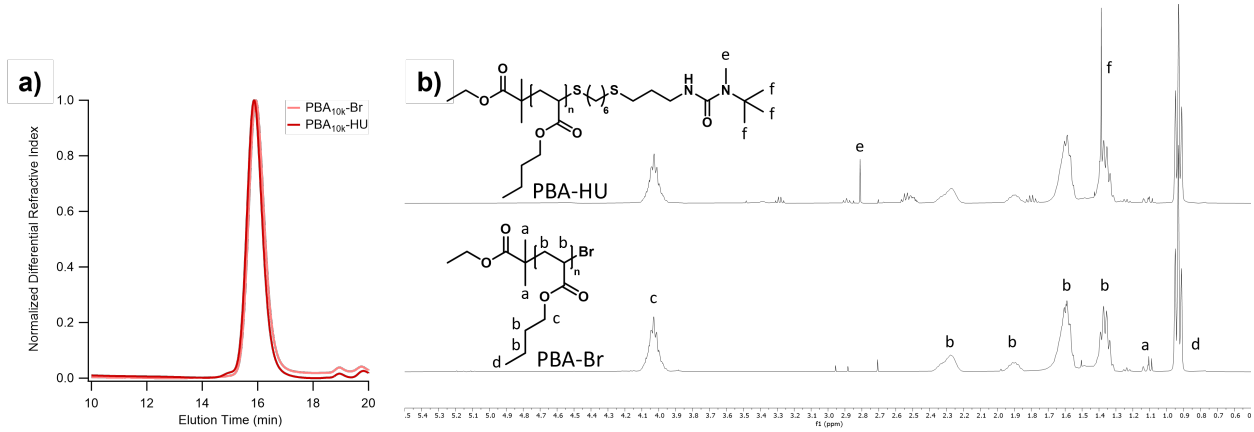

Figure S3.10: a) Schematic for the synthesis of thio-HU from allyl-HU and 1,6-hexanedithiol and b) the resulting ^{1}H NMR spectrum.

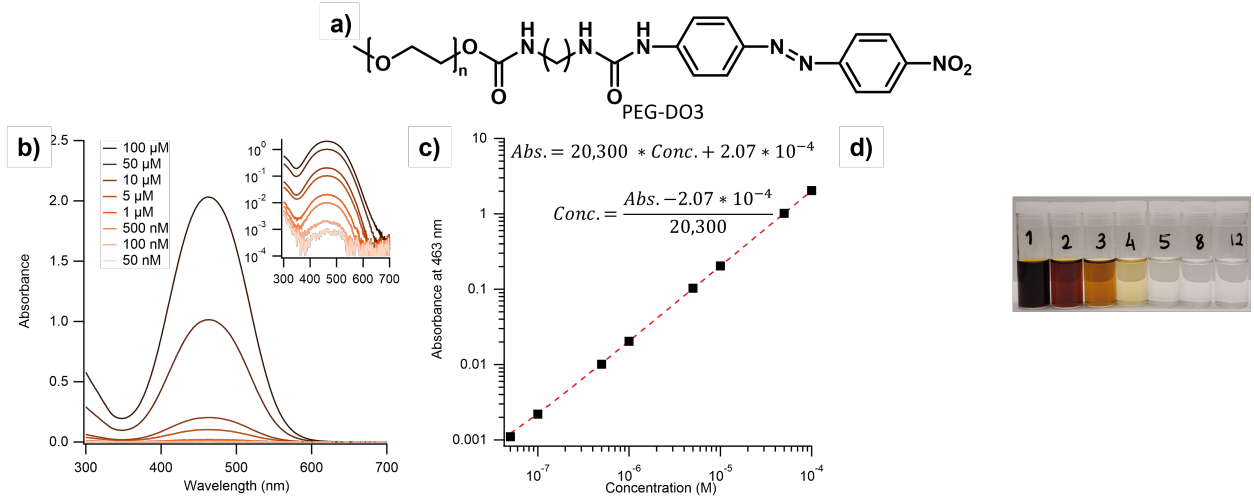

Figure S3.11: a) The chemical structure of PEG-DO3, b) UV-Vis traces of PEG-DO3 in 1:1 acetone:water with concentrations ranging from 50 nM to 100 μM, c) the resulting calibration curve generated from the maximum of the 463 nm absorbance peak, and d) the height of the 463 nm absorbance peak measured from supernatants generated during washing of *c*-CNC-*g*-PEG2k plotted against wash number, showing that all removable polymer is gone at wash 12.

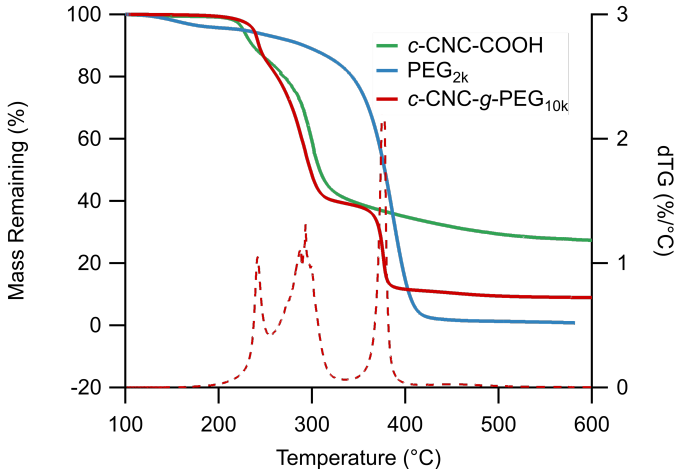

Figure S3.12: TGA traces of *c*-CNC-COOH, PEG_{10k}-Br, and *c*-CNC-*g*-PEG_{10k} along with the dTG curve for *c*-CNC-*g*-PEG_{10k}.

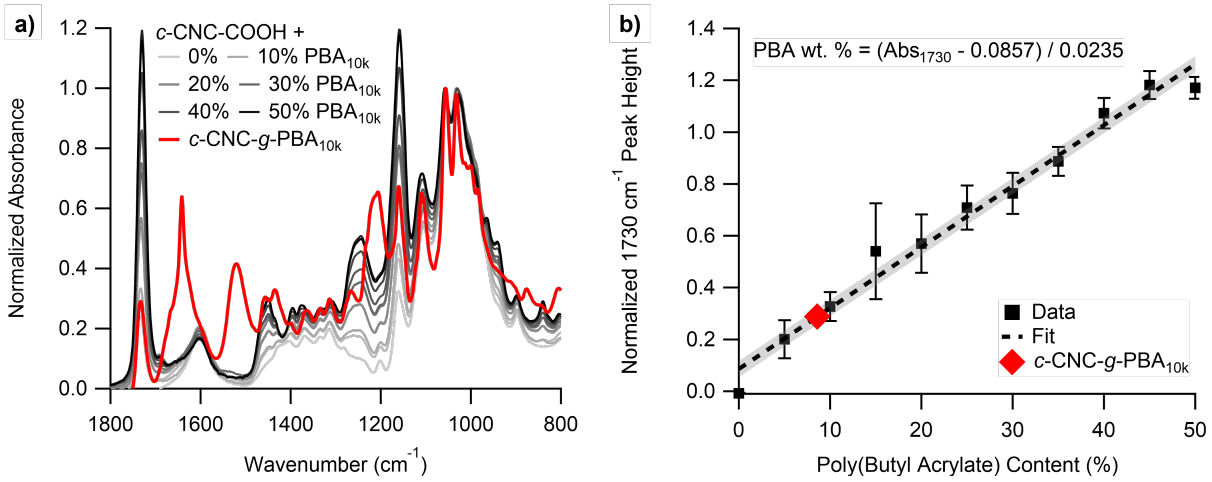

Figure S3.13: a) FTIR spectra for *c*-CNC-COOH mixed with various ratios of PBA_{10k}-Br and b) the resulting calibration curve to measure PBA content on grafted CNCs with the measured *c*-CNC-*g*-PBA_{10k} data placed on the curve.

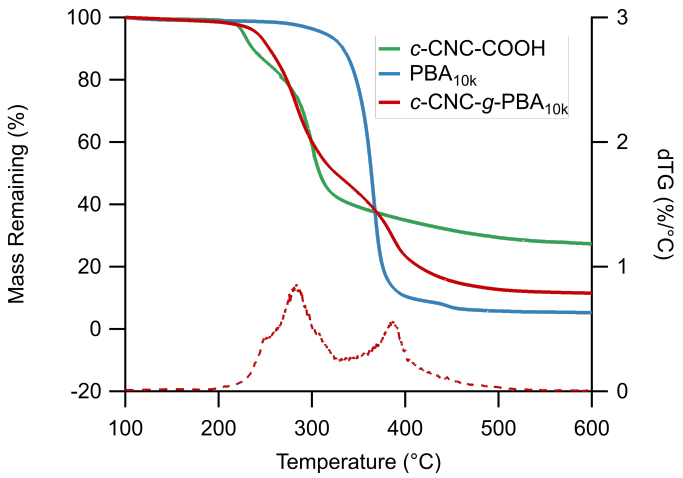

Figure S3.14: TGA traces of *c*-CNC-COOH, PBA_{10k}-Br, and *c*-CNC-*g*-PBA_{10k} along with the dTG curve for *c*-CNC-*g*-PBA_{10k}.

3.7 References

[1] C. Calvino, N. D. Macke, R. Kato, S. J. Rowan, "Development, processing and applications of bio-sourced cellulose nanocrystal composites", *Progress in Polymer Science* **2020**, *103*, 101221.

[2] A. Dufresne, "Processing of polymer nanocomposites reinforced with cellulose nanocrystals: a challenge", *International Polymer Processing* **2012**, *27*, 557–564.

[3] R. J. Moon, A. Martini, J. Nairn, J. Simonsen, J. Youngblood, *Cellulose nanomaterials review: Structure, properties and nanocomposites*, *Vol. 40*, **2011**, pp. 3941–3994.

[4] S. Chanda, D. S. Bajwa, "A review of current physical techniques for dispersion of cellulose nanomaterials in polymer matrices", *REVIEWS ON ADVANCED MATERIALS SCIENCE* **2021**, *60*, 325–341.

[5] Y. Habibi, L. A. Lucia, O. J. Rojas, "Cellulose Nanocrystals : Chemistry , Self-Assembly , and Applications", *Chemical Reviews* **2010**, *d*, 3479–3500.

[6] N. Dhar, D. Au, R. C. Berry, K. C. Tam, "Interactions of nanocrystalline cellulose with an oppositely charged surfactant in aqueous medium", *Colloids and Surfaces A: Physicochemical and Engineering Aspects* **2012**, *415*, 310–319.

[7] H. R. Paul, M. K. Bera, N. Macke, S. J. Rowan, M. V. Tirrell, "Quantitative Determination of Metal Ion Adsorption on Cellulose Nanocrystals Surfaces", *ACS Nano* **2024**, *18*, 1921–1930.

[8] S. Eyley, W. Thielemans, "Surface modification of cellulose nanocrystals", *Nanoscale* **2014**, *6*, 7764–7779.

[9] J. C. Natterodt, A. Petri-Fink, C. Weder, J. O. Zoppe, "Cellulose Nanocrystals: Surface Modification, Applications and Opportunities at Interfaces", *CHIMIA* **2017**, *71*, 376.

[10] Y. Habibi, "Key advances in the chemical modification of nanocelluloses", *Chem. Soc. Rev.* **2014**, *43*, 1519–1542.

[11] S. Wohlhauser, G. Delepierre, M. Labet, G. Morandi, W. Thielemans, C. Weder, J. O. Zoppe, "Grafting Polymers from Cellulose Nanocrystals: Synthesis, Properties, and Applications", *Macromolecules* **2018**, *51*, 6157–6189.

[12] S. A. Kedzior, J. O. Zoppe, R. M. Berry, E. D. Cranston, "Recent advances and an industrial perspective of cellulose nanocrystal functionalization through polymer grafting", *Current Opinion in Solid State & Materials Science* **2019**, *23*, 74–91.

[13] E. Lizundia, E. Meaurio, J. Vilas in *Multifunctional Polymeric Nanocomposites Based on Cellulosic Reinforcements*, Elsevier, **2016**, pp. 61–113.

[14] N. Macke, C. M. Hemmingsen, S. J. Rowan, "The effect of polymer grafting on the mechanical properties of PEG-grafted cellulose nanocrystals in poly(lactic acid)", *Journal of Polymer Science* **2022**, *60*, 3318–3330.

[15] L. Geurds, J. Lauko, A. E. Rowan, N. Amiralian, "Tailored nanocellulose-grafted polymer brush applications", *Journal of Materials Chemistry A* **2021**, *9*, 17173–17188.

[16] S. Minko in *Polymer surfaces and interfaces*, Springer, **2008**, pp. 215–234.

[17] P. V. Kelly, S. Shams Es-haghi, M. E. Lamm, K. Copenhaver, S. Ozcan, D. J. Gardner, W. M. Gramlich, "Polymer-Grafted Cellulose Nanofibrils with Enhanced Interfacial Compatibility for Stronger Poly(lactic acid) Composites", *ACS Applied Polymer Materials* **2023**, *5*, 3661–3676.

[18] S. Wohlhauser, C. Rader, C. Weder, "Facile Method to Determine the Molecular Weight of Polymer Grafts Grown from Cellulose Nanocrystals", *Biomacromolecules* **2022**, *23*, 699–707.

[19] B. Zdyrko, I. Luzinov, "Polymer Brushes by the "Grafting to" Method", *Macromolecular Rapid Communications* **2011**, *32*, 859–869.

[20] R. Kato, J. H. Lettow, S. N. Patel, S. J. Rowan, "Ion-Conducting Thermoresponsive Films Based on Polymer-Grafted Cellulose Nanocrystals", *ACS Applied Materials and Interfaces* **2020**, *12*, 54083–54093.

[21] H. R. Paul, M. V. Tirrell, S. J. Rowan, "One-Component Nanocomposite Membranes from Polymer Grafted Cellulose Nanocrystals", *ACS Applied Nano Materials* **2024**, *7*, 4210–4219.

[22] J. H. Lettow, H. Yang, P. F. Nealey, S. J. Rowan, "Effect of Graft Molecular Weight and Density on the Mechanical Properties of Polystyrene-Grafted Cellulose Nanocrystal Films", *Macromolecules* **2021**, *54*, 10594–10604.

[23] F. Azzam, L. Heux, J.-L. Putaux, B. Jean, "Preparation By Grafting Onto, Characterization, and Properties of Thermally Responsive Polymer-Decorated Cellulose Nanocrystals", *Biomacromolecules* **2010**, *11*, 3652–3659.

[24] E. Kloser, D. G. Gray, "Surface grafting of cellulose nanocrystals with poly(ethylene oxide) in aqueous media", *Langmuir* **2010**, *26*, 13450–13456.

[25] A. Pei, J.-M. Malho, J. Ruokolainen, Q. Zhou, L. A. Berglund, "Strong nanocomposite reinforcement effects in polyurethane elastomer with low volume fraction of cellulose nanocrystals", *Macromolecules* **2011**, *44*, 4422–4427.

[26] D. Viet, S. Beck-Candanedo, D. G. Gray, "Dispersion of cellulose nanocrystals in polar organic solvents", *Cellulose* **2007**, *14*, 109–113.

[27] J. O. Akindoyo, M. D. Beg, S. Ghazali, M. R. Islam, N. Jeyaratnam, A. R. Yuvaraj, "Polyurethane types, synthesis and applications-a review", *RSC Advances* **2016**, *6*, 114453–114482.

[28] H. Abushammala, "On the para/ortho reactivity of isocyanate groups during the carbamation of cellulose nanocrystals using 2,4-toluene diisocyanate", *Polymers* **2019**, *11*, 1–12.

[29] Z. W. Wicks, "Blocked isocyanates", *Progress in Organic Coatings* **1975**, *3*, 73–99.

[30] R. A. Chowdhury, C. M. Clarkson, S. Shrestha, S. M. El Awad Azrak, M. Mavlan, J. P. Youngblood, "High-Performance Waterborne Polyurethane Coating Based on a Blocked Isocyanate with Cellulose Nanocrystals (CNC) as the Polyol", *ACS Applied Polymer Materials* **2020**, *2*, 385–393.

[31] Q. Zhang, S. Wang, B. Rao, X. Chen, L. Ma, C. Cui, Q. Zhong, Z. Li, Y. Cheng, Y. Zhang, "Hindered urea bonds for dynamic polymers: An overview", *Reactive and Functional Polymers* **2021**, *159*, 104807.

[32] H. Ying, Y. Zhang, J. Cheng, "Dynamic urea bond for the design of reversible and self-healing polymers", *Nature Communications* **2014**, *5*.

[33] O. M. Vanderfleet, M. S. Reid, J. Bras, L. Heux, J. Godoy-Vargas, M. K. Panga, E. D. Cranston, "Insight into thermal stability of cellulose nanocrystals from new hydrolysis methods with acid blends", *Cellulose* **2019**, *26*, 507–528.

[34] L. Zhang, S. J. Rowan, "Effect of Sterics and Degree of Cross-Linking on the Mechanical Properties of Dynamic Poly(alkylurea-urethane) Networks", *Macromolecules* **2017**, *50*, 5051–5060.

[35] A. M. Weiss, N. Macke, Y. Zhang, C. Calvino, A. P. Esser-Kahn, S. J. Rowan, "In Vitro and in Vivo Analyses of the Effects of Source, Length, and Charge on the Cytotoxicity and Immunocompatibility of Cellulose Nanocrystals", *ACS Biomaterials Science and Engineering* **2021**, *7*, 1450–1461.

[36] A. Gille, M. Hiersemann, "(-)-Lytophilippine A: Synthesis of a C1-C18 Building Block", *Organic Letters* **2010**, *12*, 5258–5261.

[37] K. Oksman, Y. Aitomäki, A. P. Mathew, G. Siqueira, Q. Zhou, S. Butylina, S. Tanpichai, X. Zhou, S. Hooshmand, "Review of the recent developments in cellulose nanocomposite processing", *Composites Part A: Applied Science and Manufacturing* **2016**, *83*, 2–18.

[38] E. Delebecq, J.-P. Pascault, B. Boutevin, F. Ganachaud, "On the Versatility of Urethane/Urea Bonds: Reversibility, Blocked Isocyanate, and Non-isocyanate Polyurethane", *Chemical Reviews* **2013**, *113*, 80–118.

[39] B. G. Lohmeijer, R. C. Pratt, F. Leibfarth, J. W. Logan, D. A. Long, A. P. Dove, F. Nederberg, J. Choi, C. Wade, R. M. Waymouth, J. L. Hedrick, "Guanidine and amidine organocatalysts for ring-opening polymerization of cyclic esters", *Macromolecules* **2006**, *39*, 8574–8583.

[40] A. Anastasaki, V. Nikolaou, G. Nurumbetov, P. Wilson, K. Kempe, J. F. Quinn, T. P. Davis, M. R. Whittaker, D. M. Haddleton, "Cu (0) -Mediated Living Radical Polymerization : A Versatile Tool for Materials Synthesis", **2016**.

[41] L. Nagy, B. Vadkerti, G. Batta, P. P. Fehér, M. Zsuga, S. Kéki, "Eight out of eight: a detailed kinetic study on the reactivities of the eight hydroxyl groups of sucrose with phenyl isocyanate", *New Journal of Chemistry* **2019**, *43*, 15316–15325.

[42] J. Hu, Z. Chen, Y. He, H. Huang, X. Zhang, "Synthesis and structure investigation of hexamethylene diisocyanate (HDI)-based polyisocyanates", *Research on Chemical Intermediates* **2017**, *43*, 2799–2816.

[43] K. Mohomed, Thermogravimetric Analysis (TGA) Theory and Applications, **2016**.

[44] S. Elazzouzi-Hafraoui, Y. Nishiyama, J.-L. Putaux, L. Heux, F. Dubreuil, C. Rochas, "The Shape and Size Distribution of Crystalline Nanoparticles Prepared by Acid Hydrolysis of Native Cellulose", *Biomacromolecules* **2008**, 57–65.

[45] D. Herrera, J.-C. Zamora, A. Bello, M. Grimau, E. Laredo, A. J. Müller, T. P. Lodge, "Miscibility and Crystallization in Polycarbonate/Poly(ϵ-caprolactone) Blends: Application of the Self-Concentration Model", *Macromolecules* **2005**, *38*, 5109–5117.

[46] L. J. Fetters, D. J. Lohse, D. Richter, T. A. Witten, A. Zirkel, "Connection between Polymer Molecular Weight, Density, Chain Dimensions, and Melt Viscoelastic Properties", *Macromolecules* **1994**, *27*, 4639–4647.

[47] C. Tian, S. Y. Fu, Q. J. Meng, L. A. Lucia, "New insights into the material chemistry of polycaprolactone-grafted cellulose nanofibrils/polyurethane nanocomposites", *Cellulose* **2016**, *23*, 2457–2473.

[48] Q. Huang, J. Huang, P. R. Chang, "Polycaprolactone grafting of cellulose nanocrystals in ionic liquid [BMIM]Cl", *Wuhan University Journal of Natural Sciences* **2014**, *19*, 117–122.

[49] C. Fraschini, G. Chauve, J. Bouchard, "TEMPO-mediated surface oxidation of cellulose nanocrystals (CNCs)", *Cellulose* **2017**, *24*, 2775–2790.

[50] A. D. French, "Idealized powder diffraction patterns for cellulose polymorphs", *Cellulose* **2014**, *21*, 885–896.

[51] S. Park, J. O. Baker, M. E. Himmel, P. A. Parilla, D. K. Johnson, "Cellulose crystallinity index: measurement techniques and their impact on interpreting cellulase performance", *Biotechnology for Biofuels* **2010**, *3*, 1–10.

CHAPTER 4

DEVELOPMENT OF DIBLOCK-GRAFTED CELLULOSE NANOCRYSTALS AND THEIR COMPOSITES WITH POLY(LACTIC ACID)

4.1 Foreword

The work discussed thus far in this thesis has helped to develop an understanding of the surface conditions necessary for effective property enhancement in polymer-grafted cellulose nanocrystal (CNC) composite materials. Additionally, a method has been developed to graft polymer chains on the surface of CNCs in the melt, with relatively high grafting density being achieved with poly(ethylene glycol) (PEG) chains of various sizes. However, the nanoparticles synthesized herein have not enhanced the properties of the resulting composites in any way that would be considered meaningful from a commercial perspective. As the culmination of this work, we designed a polymer-grafted nanoparticle that could be synthesized using the developed melt-grafting method and could theoretically enhance the toughness of resulting composite materials, supported by literature precedent. While ultimately unsuccessful, the pursuit of this idea revealed some interesting details associated with using "grafting-to" techniques on more sterically bulky polymer chains in the melt.

4.2 Summary

Taking inspiration from wormlike micelles, diblock-grafted cellulose nanocrystals (CNCs) have been created in an attempt to toughen poly(lactic acid) (PLA). Copolymers of poly(ethylene glycol)-*b*-poly(butyl acrylate) (PEG-*b*-PBA) were synthesized using copper(0)-mediated living radical polymerization methods at various molecular

weights, then grafted onto *w*-CNC-OSO_3 using thermally-activated hindered urea chemistry. The resulting *w*-CNC-*g*-PBA-*b*-PEG had 5-14 wt.% polymer grafted to the surface, equating to 0.01-0.07 chains/nm^2 on the surface, depending on the molecular weight of the grafted polymer. These nanofillers were then incorporated into PLA at 5 wt.% and mechanically characterized. The composite materials exhibited roughly 90 % higher storage modulus above the glass transition, but 60+ % reduction in elongation at break. None of the generated nanofillers were able to toughen PLA, likely because of the low rubbery polymer content on the grafted nanoparticles. After an analysis of the packing length and Kuhn length of PBA, it is hypothesized that higher surface densities would be difficult to achieve with PBA using current grafting techniques, so alternative routes are suggested.

4.3 Introduction

Poly(lactic acid) (PLA) is often cited as a prime example of how bio-based plastics are unable to compete with traditional, petrochemical-based plastics. From Wikipedia, "superficially, [PLA] is similar to …polystyrene", but "it exhibits inferior impact strength, thermal robustness, and barrier properties …compared to non-biodegradable plastics".[1] Along with these shortcomings, PLA is also extremely brittle, fracturing at less than 10 % strain.[2] This is in contrast to something like polyethylene, which is our most used commodity polymer by volume and can reach strains over 400 % before breaking.[3] Active research is focused on finding new biopolymers with superior properties that could displace the oil-based plastics used around the world everyday.[4]

Despite all of this, PLA continues to be the most in-demand biopolymer on the market, capturing over a quarter of the bioplastics market in 2022.[5] A significant reason for this demand is that infrastructure already exists for mass production as well as end-of-life handling of PLA via industrial composting.[6,7] Because of this existing

investment in PLA as a potential commodity plastic, it continues to be worthwhile to pursue ways to enhance its properties. One such enhancement could be the inclusion of additives to improve thermal, mechanical, and/or barrier properties, as is done in traditional plastic materials.[8] Unfortunately, many modern additives are also sourced from petrochemical feedstocks, which would mean that adding them to a biopolymer matrix would detract from the sustainability of the overall system. For this reason, we seek to develop biomass-based additives that can enhance the mechanical properties of bioplastics broadly, as well as PLA specifically.

Cellulose nanocrystals (CNCs) are a promising class of bio-nanoparticle that has been shown to enhance a range of properties in sustainable composite systems.[9] CNCs are rodlike nanoparticles that can be isolated from a range of bio-sources and have dimensions on the order of 10s of nm in diameter and 100s of nm in length, dependent upon the bio-source.[10] CNCs also have surface alcohol groups that can be modified using a wide variety of chemical approaches, ranging from TEMPO oxidation[11] and electrosorption[12] to surface-initiated polymerization[13] and covalent grafting.[14] This chemical versatility makes CNCs an ideal candidate for a range of applications, including biomaterials,[15,16] water filtration and wicking,[17] ion and electron conduction,[18,19] and mechanical reinforcement.[9] In the realm of mechanical reinforcement, CNCs are generally used to enhance the stiffness of a host matrix at the cost of flexibility. This embrittlement is a significant hinderance to their broad adoption because many applications require elasticity in use. While CNCs have been incorporated into PLA-based composites countless times, this embrittlement is frequently the biggest drawback.

Turning to literature for inspiration, one technique for enhancing the toughness of glassy polymer matrices is the incorporation of wormlike micelles. Wormlike micelles are self-assembled nanostructures that are composed of amphiphilic diblock polymers

where the core phase separates from the surrounding matrix and corona to form a nanodomain within the host matrix. For toughening, the inner core is a rubbery, low glass transition temperature (T_g) polymer that is capable of blunting propagating crack tips, and the corona is a polymer capable of interfacing effectively with the host matrix through entanglements or other interactions. One of the first examples of this was a poly(ethylene oxide)-block-poly(ethylene-alt-propylene) (PEO-PEP) diblock polymer used to toughen epoxy matrices.[20,21] One limitation of these wormlike structures is the need for thermodynamic self-assembly, which requires finely tuned volume fractions of each polymer block during synthesis (~40 vol.% outer block) and sometimes costly and time-intensive thermal annealing during processing.[22] Regardless, Bates and coworkers showed the ability to use poly(ethylene oxide)-*b*-poly(butylene oxide) (PEO-PBO) diblocks to toughen a PLA matrix to over 200 % strain at break and found that the best results were achieved with wormlike micelles on the order of 100s of nm.[23,24]

Coincidentally, CNCs are also "wormlike" in structure and have lengths on the order of 100s of nm; therefore, it seems like an obvious question to ask: can diblock-grafted CNCs be used to toughen a PLA matrix? This work aims to explore that question by synthesizing CNCs grafted with copolymers of poly(ethylene glycol)-*b*-poly(n-butyl acrylate) (PEG-*b*-PBA) (Figure 4.1) and investigating their use as toughening agents for PLA. The grafting reaction is done using thermally-activated hindered urea functional groups that can generate isocyanate groups *in-situ* to react with the CNC surface hydroxyl groups using minimal solvent. The grafting density of the resulting nanoparticles will be examined in depth and the thermomechanical properties of the PLA composites will be analyzed.

Muiruri et al. utilized a comparable system to enhance the toughness of PLA.[25] In their work, CNCs were grafted with diblocks of D-lactide as the outer block and a random copolymer of L-lactide and caprolactone as the rubbery inner block. The

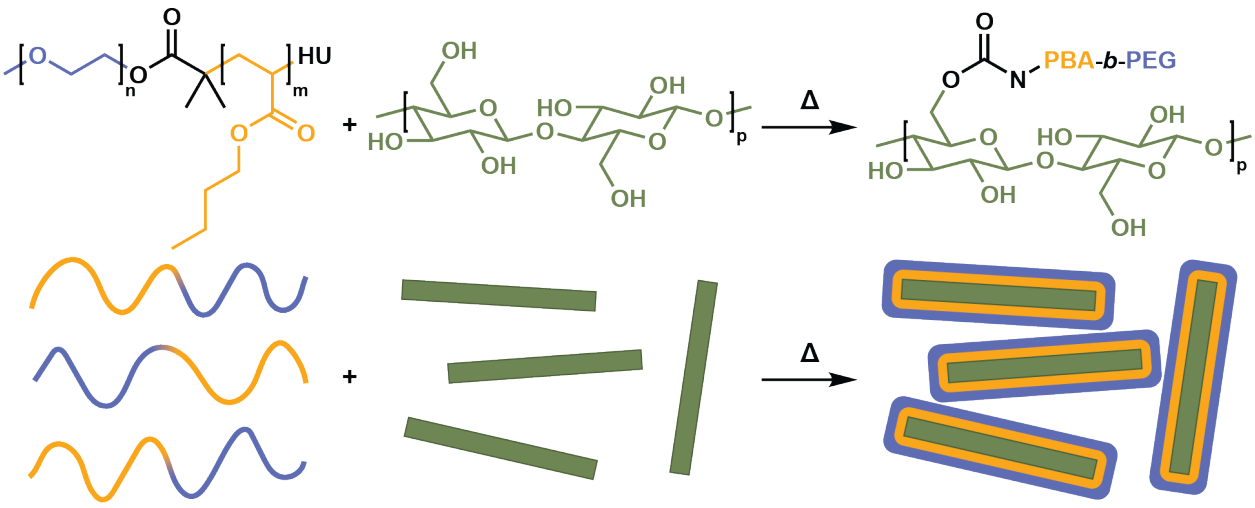

Figure 4.1: Schematic and visualization of PEG-*b*-PBA diblock polymers, cellulose nanocrystals, and diblock-grafted CNCs showing the rubber PBA inner block and outer PEG block for compatibility with PLA.

nanoparticles were incorporated into a matrix of poly(L-lactide) so that the outer block could stereocomplex with the host matrix to effectively transfer stress between the filler and matrix. The resulting composites showed over 150 % strain at break with only 2.5 wt.% filler added.[25] This work was a great proof-of-concept for this idea and acted as inspiration to expand the chemistry used for toughening and understand the physics of the system in more detail.

4.4 Results and Discussion

4.4.1 Characterization of Cellulose Nanocrystals

Sulfate half ester-functionalized cellulose nanocrystals isolated from wood (*w*-CNC-OSO_3) were purchased from the United States Department of Agriculture Forest Products Laboratory via the University of Maine. The dimensions of the CNCs were reported to be 5-20 nm in diameter and 150 nm in length. This was confirmed with AFM height, width, and length measurements of 5.4 ± 1.5, 22.8 ± 3.3, and 167 ± 79 nm,

respectively (Figure S4.1a). The surface sulfur content was reported to be 1.1 wt.%, which equates to 340 mmol of sulfate groups per kg of material or 0.69 sulfate groups per nm^2 of surface based on the CNC dimensions. The crystallinity index was measured via WAXS to be 0.69 for the *w*-CNC-OSO_3 (Figure S4.1b). Finally, the thermal stability of the CNCs was investigated with thermogravimetry (TGA) and the *w*-CNC-OSO_3 had a degradation onset of $T_{d,95}$ = 255 °C (Figure S4.1c). The choice of *w*-CNC-OSO_3 was made because of the primary alcohol groups present on the CNC surface. Unmodified CNC-OH have extensive inter-particle hydrogen bonding and aggregate too much to be useful, and TEMPO-oxidized CNC-COOH have nearly all the primary alcohol groups converted to carboxylates, reducing the reactivity of the CNC surface for isocyanate grafting.

4.4.2 Synthesis and Characterization of Hindered Urea-terminated Diblock Polymers

To prepare diblock polymers of PEG and PBA, a PEG macroinitiator was first synthesized by reacting methoxy-terminated PEG with α-bromoisobutyryl bromide to create monofunctional PEG-Br at 2,000 and 10,000 g/mol (Figure 4.2a).[26] Synthesis was confirmed with NMR (Figure S4.2a and S4.3a), where a peaks at 4.32 and 1.94 ppm appeared, corresponding to the protons adjacent to the ester and isobutyryl bromide groups, respectively. SEC also confirmed functionalization with an increase in the molar mass after addition of the brominated end group (Figure S4.2b and S4.3b).

With the PEG-Br macroinitiator, Cu^0-mediated living radical polymerization was conducted to polymerize butyl acrylate (BA) and create PEG-*b*-PBA-Br diblocks (Figure 4.2b).[27] The kinetics of this reaction were tracked with SEC and NMR for PEG_{2k}-*b*-PBA_{2k}-Br (Figure S4.4), PEG_{10k}-*b*-PBA_{2k}-Br (Figure S4.5), and PEG_{10k}-*b*-PBA_{10k}-Br (Figure S4.6) polymers, with all reactions showing good control throughout the

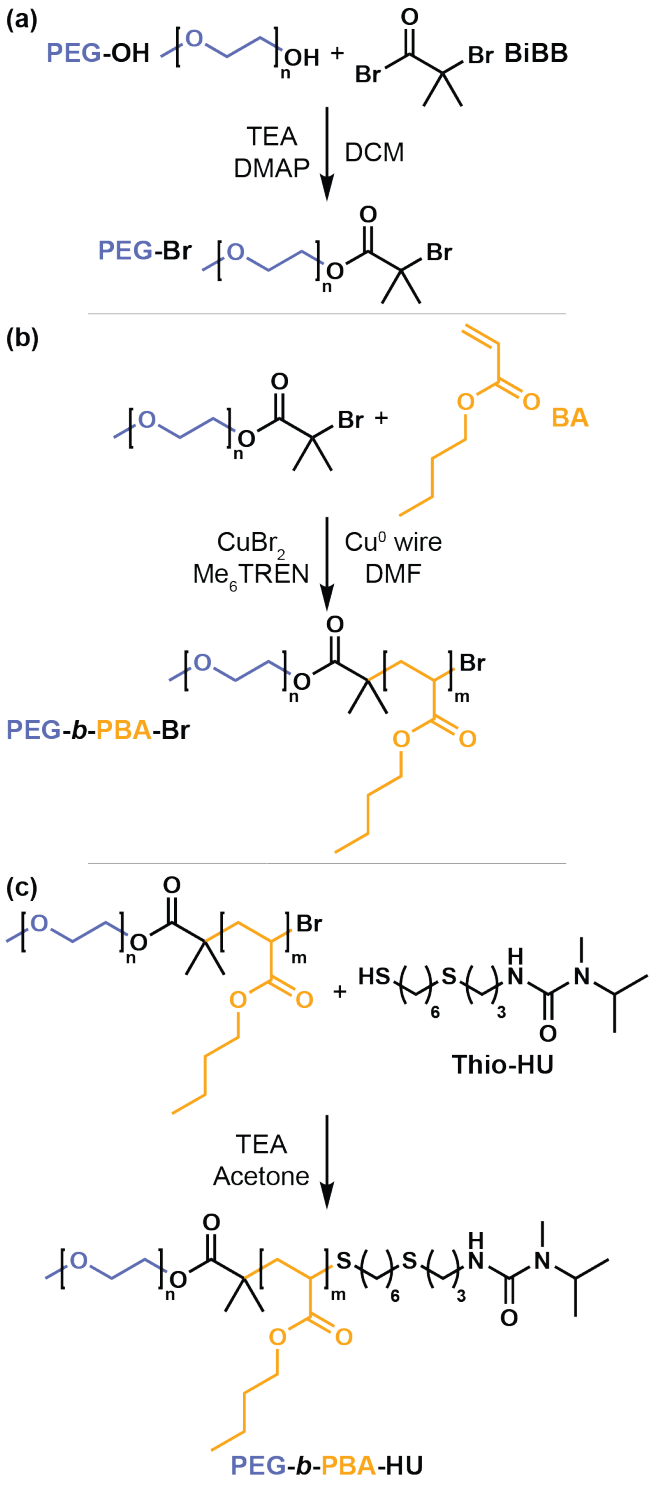

Figure 4.2: (a) Schematic for the preparation of PEG-Br from PEG-OH and BiBB, (b) schematic for the preparation of PEG-*b*-PBA-Br from PEG-Br and butyl acrylate, and (c) schematic for the preparation of PEG-*b*-PBA-HU from PEG-*b*-PBA-Br and thio-HU.

polymerization. After purification, the polymers were characterized with SEC and NMR to verify the products' molecular weights (Table S4.1).

Finally, a hindered urea end group was installed onto the diblocks via nucleophilic substitution (Figure 4.2c). Adapted from prior work,[28] allyl isocyanate was blocked with *N*-isopropylmethylamine before attaching 1,6-hexanedithiol via thio-ene chemistry to obtain a thiol-functionalized hindered urea small molecule. The isopropyl variation, instead of the tert-butyl used previously, was chosen for its higher activation temperature,[29] resulting in greater stability at room temperature and easier handling. The thio-HU molecule was subsequently reacted with the PEG-*b*-PBA-Br diblocks to form PEG-*b*-PBA-HU. After purification, the resulting diblocks were characterized with NMR and SEC (Figure S4.7 and Table S4.1) before being used for CNC grafting.

4.4.3 Synthesis and Characterization of Polymer-grafted CNCs

Grafting onto the surface of *w*-CNC-OSO_3 was conducted in the melt via thermal activation of the hindered urea end groups (Figure 4.3). In brief, *w*-CNC-OSO_3 were directly dispersed in acetone via sonication before dissolving the desired polymer in the dispersion at a ratio of 1 mmol of polymer per 1 g of CNC. After removing the acetone and drying under high vacuum overnight, toluene was added (1 mL per gram of polymer) to promote mixing during the grafting reaction. This addition of toluene is a modification of the literature procedure,[28] but was found necessary for the viscous, higher molecular weight polymers used in this study. In an industrial setting, a superior mixing apparatus should eliminate the need for added solvent. Grafting was then conducted by sealing the reaction under nitrogen and stirring at 140 °C for 8 hours. The resulting *w*-CNC-*g*-PBA-*b*-PEG were washed 5 times with THF to remove any non-attached polymer chains, which has been shown to be an effective cleaning method,[28,30] before freeze drying from water prior to characterization.

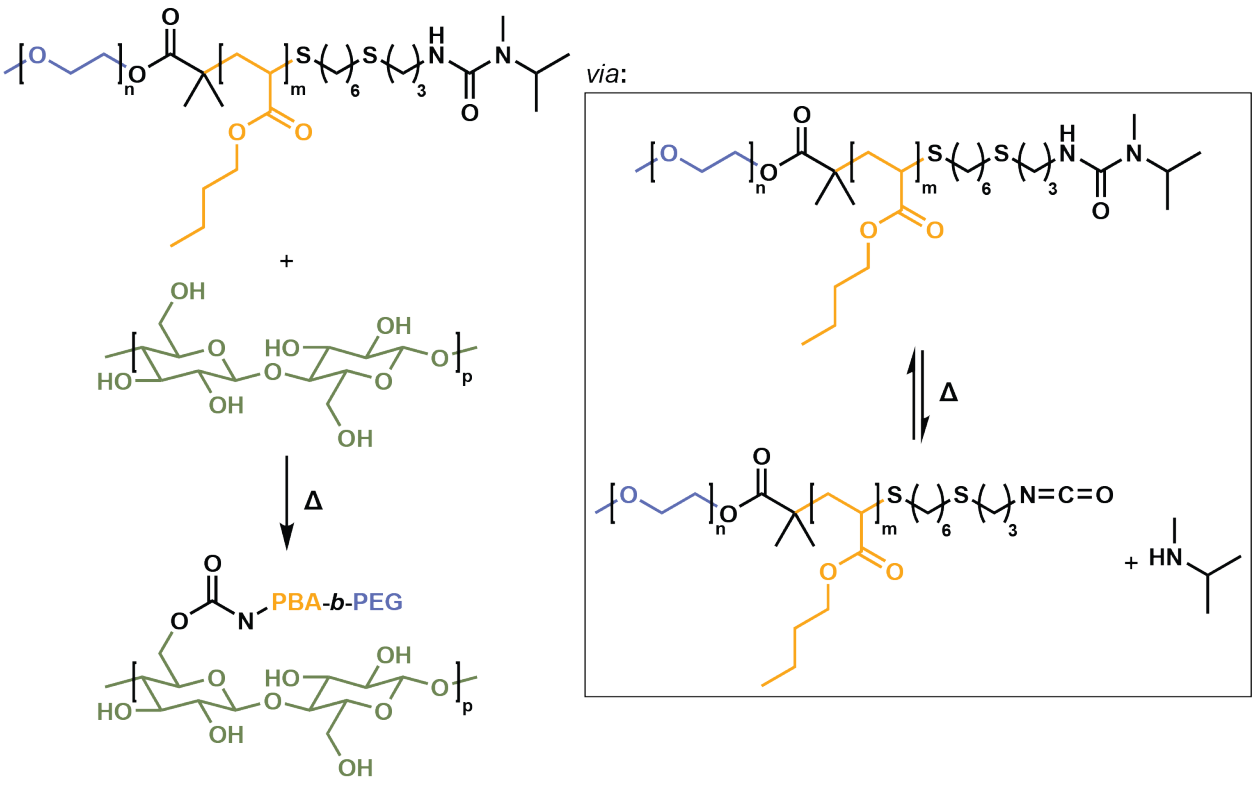

Figure 4.3: Scheme for the grafting of PEG-*b*-PBA-HU onto *w*-CNC-OSO_3 in the melt to create *w*-CNC-*g*-PBA-*b*-PEG.

High resolution dynamic TGA was first used to characterize the grafting density of the synthesized *w*-CNC-*g*-PBA-*b*-PEG. High resolution dynamic TGA is a thermogravimetry technique that reduces the heating rate when mass loss is detected, improving separation between multiple degradation events.[31] When applied to the diblock-grafted CNCs, cellulose degradation occurs between 200-320 °C while polymer degradation occurs between 320-450 °C (Figure 4.4a and 4.4b). By taking the derivative of the TGA trace, the area under the polymer degradation peak can be integrated to estimate the mass fraction of polymer on the grafted CNCs (Table 1). Based on this analysis, the mass fractions and resulting grafting densities of all diblock-grafted CNCs are fairly low (10.3 wt.% polymer or less), so FTIR was used to corroborate the polymer content. By mixing PBA homopolymer with CNCs at varying mass ratios, a calibration curve was created to measure the PBA content of the grafted samples based on the

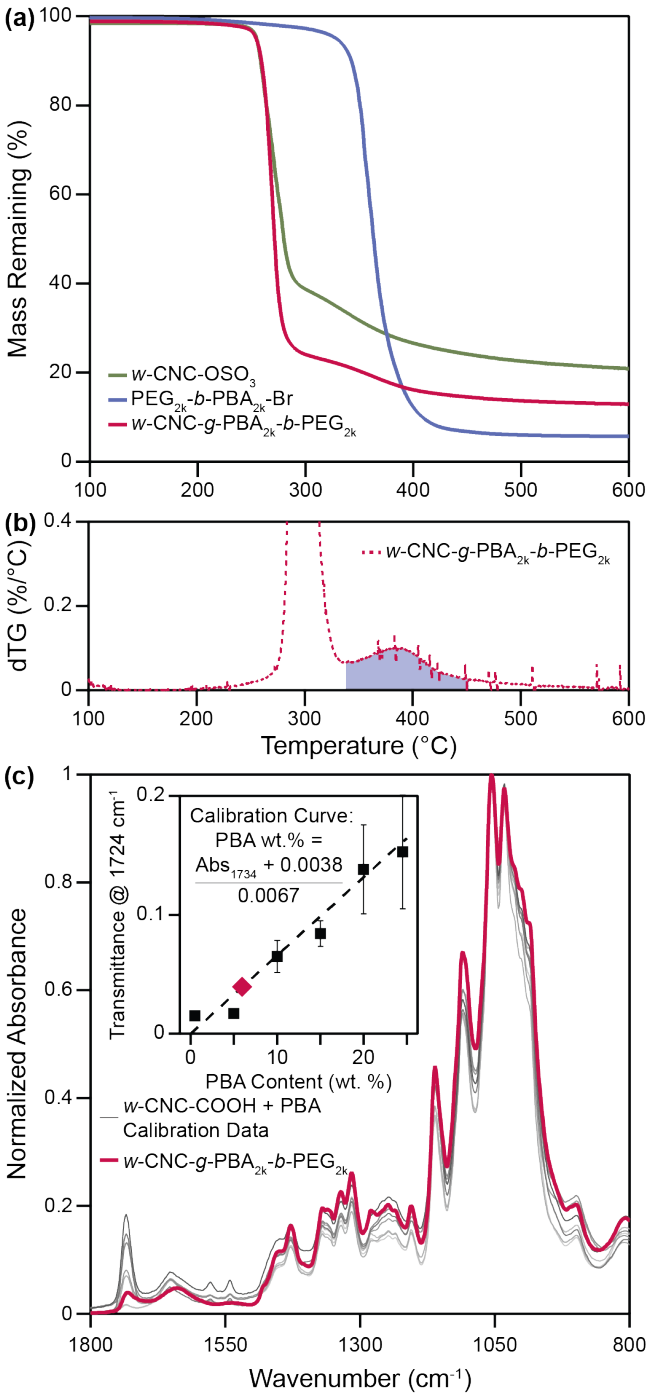

Figure 4.4: (a) TGA curves for *w*-CNC-OSO_3, PEG_{2k}-*b*-PBA_{2k}-HU, and *w*-CNC-*g*-PBA_{2k}-*b*-PEG_{2k}, (b) dTG curve for *w*-CNC-*g*-PBA_{2k}-*b*-PEG_{2k}, highlighting grafted polymer degradation above 300 °C, (c) FTIR data used to generate the calibration curve used to measure the PBA content of grafted samples with the *w*-CNC-*g*-PBA_{2k}-*b*-PEG_{2k} FTIR trace overlayed, and (d) the resulting calibration curve.

absorbance at 1734 cm^{-1}, corresponding to the carbonyl group in the BA monomer unit (Figure 4.4c and 4.4d). The measured PBA content could then be scaled based on the PBA content of the grafted copolymer to calculate a total polymer content. The FTIR results match the TGA results fairly well, with each technique having a difference of less than 7 wt.% for all samples (Table 4.1).

To put these results in context, prior work has shown that a polymer brush on the CNC surface needs to be in the semi-dilute polymer brush regime to be able to entangle with the host polymer matrix and efficiently transfer stress to optimize mechanical properties in composite materials.[30,32] To determine the brush regime of the synthesized nanoparticles, a "phase diagram" was generated based on prior work from Keten and coworkers that modeled the transition between concentrated and semi-dilute brush conformations on CNC surfaces.[33] Based on their work modeling poly(methyl methacrylate)-grafted CNCs, we are able to determine a critical molecular weight where the polymer brush transitions from a concentrated to semi-dilute conformation based on the grafting density on the CNC surface (Figure 4.5). Additionally, a transition from individual polymer "mushrooms" on the CNC surface into a polymer brush can be estimated based on the radius of gyration (R_g) of PBA at various molecular weights. By taking the inverse of the area of a circle defined by R_g, the surface density where polymer chains begin to overlap can be calculated and plotted (Figure 4.5).

Table 4.1: Grafting statistics for all *w*-CNC-*g*-PBA-*b*-PEG materials, measured via FTIR and TGA.

Sample	**FTIR Polymer Content (wt.%)**	**FTIR Grafting Density (chains/nm^2)**	**TGA Polymer Content (wt.%)**	**TGA Grafting Density (chains/nm^2)**
w-CNC-*g*-PBA_{2k}-*b*-PEG_{2k}	11.9	0.07	8.4	0.05
w-CNC-*g*-PBA_{2k}-*b*-PEG_{10k}	13.7	0.03	6.9	0.01
w-CNC-*g*-PBA_{10k}-*b*-PEG_{10k}	5.2	0.01	10.3	0.01

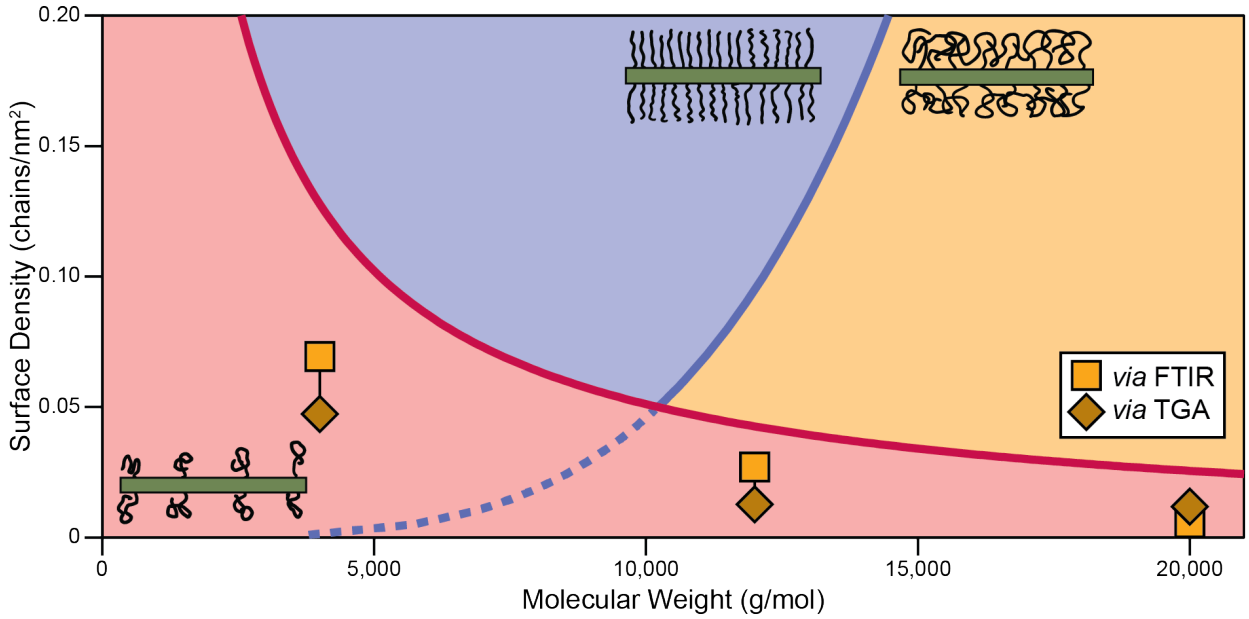

Figure 4.5: Plot of grafted polymer surface density vs. molecular weight, showing the polymer brush conformations for each point. The synthesized *w*-CNC-*g*-PBA-*b*-PEG samples are plotted, all falling within the mushroom regime. The concentrated to semi-dilute brush transition (blue line) is modeled based on poly(methyl methacrylate)[33] and the mushroom to brush transition (red line) is based on the radius of gyration for PBA.

Based on this analysis, all *w*-CNC-*g*-PBA-*b*-PEG samples synthesized fall along or below the mushroom to brush transition (Figure 4.5), implying that it is difficult to fully cover the nanoparticle surface. This relatively low surface density is attributed to the stiff polymeric backbone of PBA as well as the steric bulk of the butyl pendant groups, which will be discussed in more detail later. Additionally, because all samples are within the mushroom regime, it is hypothesized that there is not enough surface coverage to prevent embrittlement from defects at the CNC-PLA interface in composite materials. As seen in prior work, without complete surface coverage, the negative interactions between hydrophilic CNCs and the hydrophobic PLA host matrix result in severe embrittlement in composite materials.[30]

4.4.4 *Preparation and Characterization of PLA Composites*

To test the hypothesis that composite materials would be embrittled by the *w*-CNC-*g*-PBA-*b*-PEG, composites with PLA were made by dispersing the filler directly in chloroform then mixing with PLA dissolved in chloroform to make composites with 5 wt.% filler. This loading was chosen because toughening can be seen with wormlike micelles at less than 1 wt.% additive,[24] so 5 wt.% was expected to be enough to see any toughening without overloading the matrix with CNCs. After drying and melt pressing into uniform films, dogbone samples were cut to test mechanical properties. Dynamic mechanical analysis (DMA) was done on each sample to measure the storage modulus across a range of temperatures as well as the extract the glass transition temperature (T_g) based on the tan(δ) peak (Figure 4.6a and Table 4.2). All filler-reinforced samples showed similar DMA results with the modulus below T_g being dominated by the glassy PLA, showing little difference between all samples. The T_g of all samples is also the same, 60-61 °C, highlighting the fact that the grafted polymer does not plasticize the host matrix. Finally, the modulus above T_g shows the reinforcement that is expected in CNC composite materials, with all samples exhibiting 80-110 % increase in G', relative to neat PLA at 80 °C.

Tensile testing on neat PLA samples showed tensile strength of 48.8 MPa and elongation at break of 9.0 % (Figure 4.6b and Table 4.2). When *w*-CNC-OSO_3 are incorporated into PLA, tensile strength is reduced to 37.6 MPa and elongation at break is significantly reduced to 1.7 %, which is expected from CNC-reinforced PLA. Incorporating the diblock-grafted CNCs into PLA composites also resulted in a reduction in the tensile strength down to roughly 38 MPa for all samples as well as a reduction in elongation at break down to 3.4-3.5 % for all samples. While embrittlement was slightly reduced compared to incorporating bare CNCs (62 % reduction for *w*-CNC-*g*-PBA-*b*-PEG vs 81 % for *w*-CNC-OSO_3), the grafted CNCs do not recover the extensibility of neat PLA,

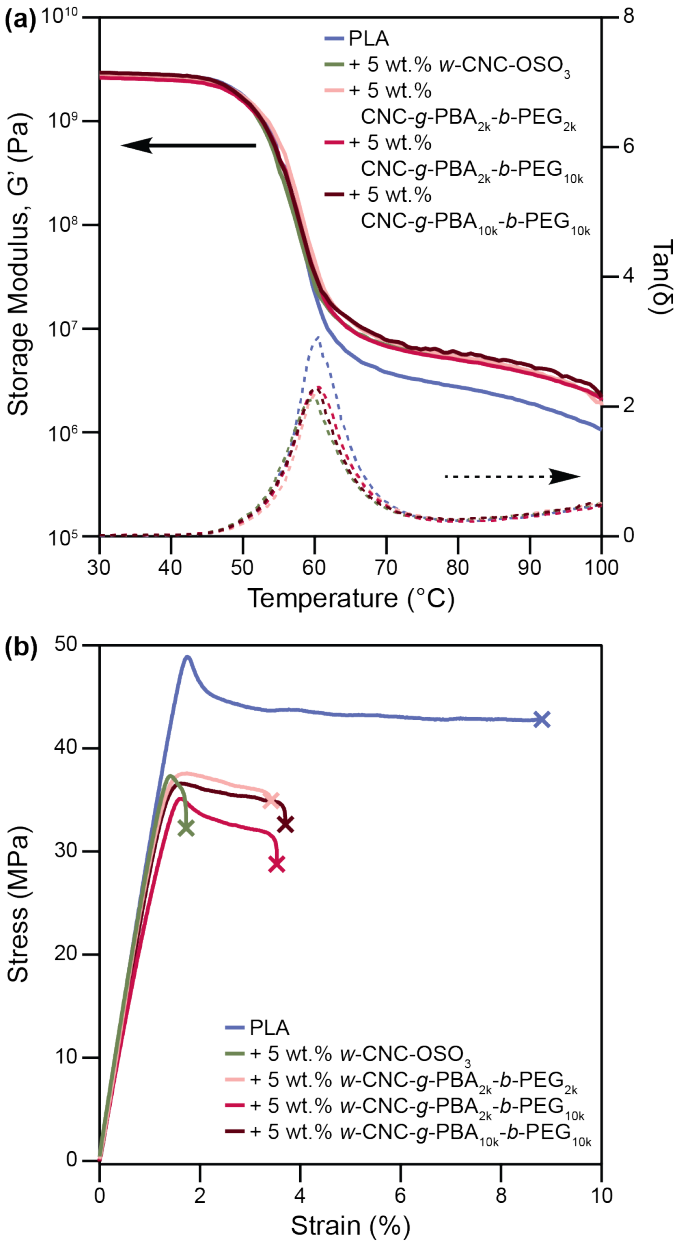

Figure 4.6: (a) DMA storage modulus and tan(δ) curves for neat PLA and composites with 5 wt.% *w*-CNC-OSO_3 and *w*-CNC-*g*-PBA-*b*-PEG and (b) representative tensile curves for the same composites.

nor do they improve it. This result is consistent with prior work showing that utilizing polymer-grafted CNCs where the grafted polymer resides in the mushroom regime results in dramatic embrittlement,[30] confirming the previously stated hypothesis based on the estimated brush conformation. These diblock-grafted *w*-CNC-*g*-PBA-*b*-PEG

Table 4.2: DMA and tensile statistics for neat PLA and composites with 5 wt.% *w*-CNC-OSO_3 and *w*-CNC-*g*-PBA-*b*-PEG (standard deviation presented when possible, n = 5).

Sample	**G′ @ 30 °C (GPa)**	**G′ @ 80 °C (MPa)**	**Peak Tan(δ) (°C)**	**Tensile Strength (MPa)**	**Elongation at Break (%)**
Neat PLA	2.92	2.71	60.5	48.8 $\pm$ 1.2	9.0 $\pm$ 2.4
PLA + 5 wt.% *w*-CNC-OSO_3	2.92	5.13	60.2	36.7 $\pm$ 2.6	1.7 $\pm$ 0.3
PLA + 5 wt.% *w*-CNC-*g*-PBA_{2k}-*b*-PEG_{2k}	2.74	5.37	60.7	38.6 $\pm$ 0.7	3.4 $\pm$ 0.4
PLA + 5 wt.% *w*-CNC-*g*-PBA_{2k}-*b*-PEG_{10k}	2.62	4.95	60.7	37.9 $\pm$ 2.0	3.5 $\pm$ 0.5
PLA + 5 wt.% *w*-CNC-*g*-PBA_{10k}-*b*-PEG_{10k}	2.93	5.68	60.3	37.7 $\pm$ 1.1	3.4 $\pm$ 0.7

additives do not exhibit any "wormlike" characteristics and cannot toughen PLA, likely due to the low polymer content and inability to graft at higher surface densities.

4.4.5 Analysis of Grafting Density and Brush Conformation

Although the proposed system matches the characteristics of wormlike micelles used to toughen epoxies[21] and PLA[23] in literature and matches the style of polymer-grafted CNCs used by Muiruri et al. to toughen PLA,[25] the synthesized *w*-CNC-*g*-PBA-*b*-PEG were unable to toughen PLA, likely because of the low polymer content on the nanoparticles. After many attempts to improve grafting density through different grafting approaches, such as EDC/NHS coupling, DMTMM.BF4 coupling, thiol-ene grafting, and direct nucleophilic substitution onto the CNC surface, no higher grafting density could be achieved. This raises the question of whether there is some limit that is being reached at the CNC surface that is preventing PBA from packing densely enough to achieve the goal of toughening PLA.

Unfortunately, there are very few examples of PBA functionalization using "grafting-

to" methods in the literature, so it is difficult to benchmark the results found herein against prior work. As an adjacent comparison, Sudre et al. reported a thorough investigation of grafting poly(tert-butyl acrylate) (PtBA) onto planar silica surfaces using epoxide chemistry.[34] In this work, they measured a grafting density of 0.42 chains/nm^2 using 6,400 g/mol PtBA chains. This result is significantly higher than was obtained herein, but their use of planar silica likely increases the efficiency of the reaction significantly because of the purity of the substrate, comparing to naturally-sourced cellulose nanocrystals that likely still contain impurities. In the present work, a surface density of roughly 0.07 chains/nm^2 was obtained with the PEG_{2k}-*b*-PBA_{2k}-grafted CNCs, which is approximately 15 % of the optimized literature result.

Since direct comparisons cannot be found, a comparative analysis could potentially elucidate more information. From prior work,[28] hindered urea-based grafting was used to graft both PEG and PBA homopolymer chains onto CNCs. By comparing the results of these two grafting experiments, the differences may reveal why PBA grafting results in low surface densities. Oluz et al. obtained 0.125 chains/nm^2 when grafting PEG_{10k} and 0.031 chains/nm^2 when grafting PBA_{10k} chains. The ratio of these two values shows that for every PEG chain attached to the surface, only 0.248 PBA chains could be attached in the same area. The PEG repeat unit consists of only two carbon atoms and an oxygen atom aligned down the backbone, whereas the PBA repeat unit has five carbon atoms and two oxygen atoms extending off the two carbon backbone as a pendant group. Based on this alone, expecting the same number of PBA chains to fit into the same area as a PEG chain would be ignorant. To quantify this concept, a parameter called the packing length (p) was defined by Lin as the closest approach that a two polymeric backbones could reach in the melt – effectively defining the diameter of the polymer chain.[35] For PEG, the p_{PEG} = 1.94 Å, whereas p_{PBA} = 4.19 Å for PBA, calculated based on literature.[36] This suggests that a PBA chain takes up over twice the diameter of a PEG chain, and since

area scales with the square of diameter, one would expect less than 25 % the number of PBA chains to fit in the same area as a PEG chain, 0.214 chains to be exact. This result reflects the experimental ratio measured by Oluz et al. quite well.

This packing length argument is not necessarily a valid nor rigorous comparison because one would never expect polymer chains to be perfectly packed onto a surface so that the chain diameter is defining their spacing. A more realistic measure of the bulkiness of a polymer coil is the Kuhn length (b), which is defined as the length of chain needed for a segment to reach a random orientation. Simplistically, this can be thought of as the circumference needed for the chain to turn 180°, measuring the stiffness of the chain along the backbone. The Kuhn length for PEG is $b_{\mathrm{PEG}} = 0.76$ nm[37] and for PBA it is $b_{\mathrm{PBA}} = 1.71$ nm.[38] If we use this circumference to measure the area taken up by PEG and PBA chains, the resulting ratio is 0.198 PBA chains per PEG chain, which is once again similar to the experimental ratio of 0.248 obtained by Oluz et al., ignoring any scaling factors based on the grafting surface or polymer molecular weight. While this is by no means an exhaustive analysis of the polymer physics associated with grafting PBA onto the CNC surface, it does provide a potential explanation as to why the surface densities of the diblocks grafted in this work are proportionally lower than PEG chains grafted in prior work.

This raises the question of how can one overcome this practical limit on CNC grafting density with more sterically bulky polymer chains? The most straightforward answer would be to eliminate the bulkiness of the polymer chain. This could mean using an alternative, less sterically bulky polymer that has similar properties, or reducing the molecular weight of the grafted polymer to increase the packing density of the polymer chains. Alternatively, one could switch to a "grafting-from" approach so that individual monomer units can add to the CNC surface before large polymer chains block surrounding surface sites. The problem with these techniques is the inability to

effectively characterize the resulting polymer molecular weight and grafting density. While this is a problem in an academic setting, this could be the most effective technique for commercial functionalization where composite properties matter more than narrow dispersity of the grafted polymer.

4.5 Conclusions

In this work, diblock polymers of PEG and PBA were synthesized at various molecular weights and end-functionalized with hindered urea functional groups. These hindered urea groups were then used to thermally graft the diblocks onto cellulose nanocrystals via *in-situ* regeneration of the isocyanate groups that could then react with surface alcohol groups. The resulting *w*-CNC-*g*-PBA-*b*-PEG were hypothesized to be effective toughening agents for PLA, but the resulting mechanical properties showed no such effect. Composite materials showed an increase in the storage modulus above T_g of 83-110 % depending on the filler, but a reduction in elongation at break of 61-81 % depending on the filler. This embrittlement is likely a result of insufficient surface coverage by the grafted polymer, leaving exposed hydrophilic CNC surface to interact with the hydrophobic PLA host matrix, creating defect points that lead to premature failure. Despite numerous attempts to improve the grafting density, no such feat was accomplished. After further analysis, the PBA chains are likely too bulky to pack onto the CNC surface at a sufficient density to improve the toughness of PLA. The rubbery PBA content will always be too low to counteract the stiffening effects of the rigid CNCs. To alleviate this issue, it is recommended that "grafting-from" approaches should be employed when grafting bulkier monomers onto CNCs.

4.6 Materials, Methods, and Instrumentation

4.6.1 Materials

If not specified otherwise, all compounds and solvents were used as received, without further purification. Cellulose nanocrystals (w-CNC-OSO_3) were purchased from the United States Department of Agriculture Forest Products Lab via the University of Maine. Allyl isocyanate, α-bromoisobutyryl bromide (BiBB), butyl acrylate (BA), chloroform-d ($CDCl_3$), copper (II) bromide ($CuBr_2$), 2,2-dimethoxy-2-phenylacetophenone (DMPA), 4-dimethylaminopyridine (DMAP), hydrochloric acid (HCl), *N*-isopropylmethylamine, methoxy-poly(ethylene glycol) (2,000 g/mol and 10,000 g/mol, PEG_{2k}-OH and PEG_{10k}-OH), sodium chloride (NaCl), triethylamine (TEA), and tris[2-(dimethylamino)ethyl]amine (Me6TREN) were all purchased from Sigma-Aldrich. Basic alumina, neutral alumina, copper (0) wire, and all solvents, acetone, chloroform, dichloromethane (DCM), diethyl ether, N,N-dimethylformamide (DMF), ethyl acetate, hexanes, methanol, tetrahydrofuran (THF), and toluene were purchased from Fisher Scientific. Allyl isocyanate was purchased from Santa Cruz Biotechnology, poly-(L)-lysine was purchased from Ted Pella, 0.2 μm PVDF filter membranes were purchased from Sterlitech, and 1,6,-hexanedithiol was purchased from Oakwood Chemical.

4.6.2 Methods

4.6.2.1 Preparation of PEG-Br Macroinitiator

The procedure for synthesizing the PEG macroinitiator was adapted from prior literature.[26] Sample conditions are given for PEG_{2k}, but the molar ratios and mass concentration was identical for PEG_{10k}. In a vial, PEG_{2k}-OH (2 g, 1.0 mmol) was

dissolved in DCM (200 mg/mL). In the primary reaction flask, DMAP (61 mg, 0.5 mmol) and TEA (697 μL, 5 mmol) were dissolved in a volume of DCM equal to the volume used to dissolve the PEG. To the DMAP and TEA mixture, BiBB (494 μL, 4 mmol) was added dropwise while stirring on ice and under inert atmosphere. Finally, the PEG solution was also added dropwise while stirring on ice under inert atmosphere. The vessel was sealed and the ice was allowed to melt, bringing the reaction up to room temperature while it reacted overnight.

The reaction was purified via liquid/liquid extraction with water followed by concentrating the organic layer and precipitating in ether. After filtration, the resulting powder was redissolved in DCM and extracted with brine again before being run through a plug of neutral alumina. The product was then concentrated and precipitated in ether once more before filtering and drying the afforded white powder. The resulting PEG_{2k}-Br and PEG_{10k}-Br were characterized with ^{1}H NMR and SEC. ^{1}H NMR (400 MHz, $CDCl_3$) δ 4.32 (t, 2H), 3.64 (m, backbone), 3.38 (s, 3H), 1.94 (s, 6H).

4.6.2.2 Polymerization of PBA from PEG-Br Macroinitiator

Diblock polymers were synthesized using single-electron transfer living radical polymerization (SET-LRP) with Cu0 wire, targeting 50 % conversion.[27] For a sample PEG_{2k}-*b*-PBA_{2k}-Br reaction, PEG_{2k}-Br (2 g, 1 mmol) was dissolved in DMF (72.2 mL, 75 vol.% relative to total reactant volume). The BA monomer was run through a plug of basic alumina to remove inhibitor, then the BA (4 g, 31.2 mmol) was added to the flask along with $CuBr_2$ (11.2 mg, 0.05 mmol). The solution was then sparged with inert gas, during which time copper wire (10 cm) was wrapped around a stir bar and immersed in concentrated HCl to clean the copper surface. After 15 minutes of sparging, Me6TREN (32.1 μL, 0.12 mmol) was added, changing the solution from a dark green to seafoam green. The stir bar was then rinsed to remove excess acid before adding it to the reaction

flask to start the polymerization.

To vary molecular weight, the amounts of BA and DMF were changed to maintain 75 vol.% DMF and 50 % monomer conversion. For different sized macroinitiators, all molar ratios remained the same. Aliquots were taken every 15 minutes to track kinetics via ^{1}H NMR and every 30 minutes to track molecular weight via SEC, with most polymerizations taking 90-180 minutes to reach 50 % conversion.

To terminate the reaction, the entire flask was exposed to air and the copper wire-wrapped stir bar was removed from the solution. The reaction was then purified by rotary evaporation of the solvent and monomer at 70 °C. After all monomer was removed, the polymer was redissolved in DCM and run through a plug of neutral alumina to remove any remaining copper while maintaining end group fidelity. The resulting PEG-*b*-PBA-Br were characterized with ^{1}H NMR and SEC. ^{1}H NMR (400 MHz, $CDCl_3$) δ 4.05 (m, $2H_{PBA}$), 3.64 (m, $backbone_{PEG}$), 3.37 (s, $3H_{PEG}$), 2.28 (m, $1H_{PBA}$), 1.91 (m, $1H_{PBA}$), 1.60 (m, $3H_{PBA}$), 1.36 (m, $2H_{PBA}$), 1.14 (s, $3H_{PEG}$), 1.12 (s, $3H_{PEG}$), 0.93 (m, $3H_{PBA}$), (PBA peaks are counted per monomer).

4.6.2.3 Preparation of Thio-isoHU

Thio-isoHU synthesis was adapted from prior literature in a two-step process before being added to the polymer chain end.[28] First, an allyl-hindered urea was synthesized by mixing allyl isocyanate (1 eq.) with *N*-isopropylmethylamine (1.1 eq.) at 1M concentration in DCM. The resulting allyl-isoHU was purified with high vacuum to remove all solvent and remaining reactants, resulting in a colorless oil, before characterizing with ^{1}H NMR, ^{13}C NMR, and HRMS. ^{1}H NMR (400 MHz, $CDCl_3$) δ 5.86 (ddt, J = 17.2, 10.2, 5.6 Hz, 1H), 5.13 (dq, J = 17.2, 1.7 Hz, 1H), 5.05 (dq, J = 10.2, 1.5 Hz, 1H), 4.46 (m, J = 6.8 Hz, 1H), 3.83 (tt, J = 5.6, 1.6 Hz, 2H), 2.67 (s, 3H), 1.06 (d, J = 6.8 6H). ^{13}C NMR (101 MHz, $CDCl_3$) δ 157.75 (C = O), 136.07 (C = C – C), 115.44 (C = C),

45.25 (CH), 43.47 (C = C – C), 26.84 (CH_3), 20.05 ($2CH_3$). HRMS (ESI) m/z: $[M + H]^+$ calcd for $C_8H_{16}N_2O$, 157.1296; found, 157.1353.

A thiol group was added to the allyl-isoHU by dissolving 1 eq. of allyl-isoHU in 15 eq. of 1,6-hexanedithiol along with 0.5 eq. DMPA photoinitiator. Once dissolved, the solution was placed on a low-power UV source (bug zapper) for 30 minutes. The resulting thio-isoHU molecule was purified by loading the crude mixture onto a silica column with 9:1 hexanes:ethyl acetate. This 9:1 mixture pushed the excess dithiol and initiator fragments through, while retaining the product in the column. The product was then flushed from the column using pure ethyl acetate. Thio-isoHU was then dried as a yellow oil before characterization with ^{1}H NMR, ^{13}C NMR, and HRMS. ^{1}H NMR (400 MHz, $CDCl_3$) δ 4.62 (br, 1H), 4.44 (m, J = 6.8 Hz, 1H), 3.31 (td, J = 6.7, 5.6 Hz, 2H), 2.66 (s, 3H), 2.58 – 2.44 (m, 6H), 1.78 (qi, J = 6.9 Hz, 2H), 1.65 – 1.49 (m, 4H), 1.44 – 1.34 (m, 4H), 1.31 (t, J = 7.7, 1H), 1.06 (d, J = 6.8 Hz, 6H). ^{13}C NMR (101 MHz, $CDCl_3$) δ 158.00 (C = O), 45.21 (CH), 40.29 (C – N), 33.91 (CH_2), 32.10 (C – S), 29.93 (CH_2), 29.88 (CH_2), 29.47 (CH_3), 28.36 (CH_2), 27.99 (CH_2), 26.89 (C – SH), 20.11 ($2CH_3$). HRMS (ESI) m/z: $[M + H]^+$ calcd for $C_{14}H_{30}N_2OS_2$, 307.1833; found, 307.1898.

4.6.2.4 Preparation of PEG-PBA-HU

Thio-HU was added to PEG-*b*-PBA-Br chain ends via nucleophilic substitution. The bromine-terminated polymer (1 eq.) was dissolved in acetone at 500 mg/mL along with TEA (10 eq.). The solution was then purged with inert gas for 5 minutes before adding thio-isoHU (2 eq.). The reaction was allowed to proceed for 24 hours before another 2 eq. of thio-isoHU were added under inert atmosphere. This process was repeated until 3 total additions were made, totaling 6 eq. of thio-HU. The resulting HU-terminated PEG-*b*-PBA-HU was purified by running the crude solution through a silica plug with ethyl acetate to flush out unreacted thio-isoHU, then the PEG-*b*-PBA-HU was eluted with

9:1 CHCl3:MeOH. After drying, the resulting PEG-*b*-PBA-HU were characterized with ^{1}H NMR, SEC, and TGA. ^{1}H NMR (400 MHz, $CDCl_3$) δ 4.52 (br, 1H), 4.03 (m, $2H_{PBA}$), 3.64 (m, $backbone_{PEG}$), 3.38 (s, $3H_{PEG}$), 3.29 (m, 2H), 2.81 (s, 3H), 2.52 (m, 6H), 2.28 (m, $1H_{PBA}$), 1.89 (m, $1H_{PBA}$), 1.60 (m, $3H_{PBA}$), 1.39 (m, $2H_{PBA}$ + 6H), 1.14 (s, $3H_{PEG}$), 1.13 (s, $3H_{PEG}$), 0.93 (m, $3H_{PBA}$), (PBA peaks are counted per monomer).

4.6.2.5 Grafting of PEG-*b*-PBA-HU onto *w*-CNC-OSO_3

The *w*-CNC-OSO_3 (500 mg, ca. 0.5 mmol -OH groups) were dispersed in 25 mL of acetone by ultrasonication for 10 min. Relative to the -OH groups present on the CNCs, an equivalent molar quantity of hindered urea-terminated polymer was added to the CNC suspension and placed in a sonic bath until completely dissolved. The solvent was removed via rotary evaporation at 30 °C before being placed under high vacuum overnight to yield a colorless solid. Once dry, toluene was added so that the polymer was dissolved at 500 mg/mL to promote mixing during grafting. The mixture was then placed in an oil bath at 140 °C for 8 hours. When complete, heat was removed and THF (up to 40 mL) was added to wash away any non-grafted polymer and clean the product. The mixture was centrifuged and resuspended in THF 5 times to fully clean the material before being suspended in water and freeze-dried to obtain a fluffy powder. The resulting *w*-CNC-*g*-PBA-*b*-PEG were characterized with AFM, FTIR, and TGA.

4.6.2.6 Characterization of *w*-CNC-*g*-PBA-*b*-PEG via High Resolution Dynamic Thermogravimetry

To measure polymer content on *w*-CNC-*g*-PBA-*b*-PEG, high resolution dynamic TGA was run on each nanoparticle sample. The polymer mass fraction was determined by taking the derivative of remaining mass with respect to temperature, then integrating the area under the dTG curve between 350 – 420 °C. Based on this mass fraction and

the dimensions of the CNCs measured via AFM, a grafting density could be calculated (details explained in prior work[30]).

4.6.2.7 Preparation of *w*-CNC-OSO_3 + PBA Calibration Curve via FTIR

To verify the polymer content of grafted CNCs, an FTIR calibration curve was generated to measure the PBA content in the synthesized nanoparticles. In a small vial, *w*-CNC-OSO_3 (ca. 25 mg) were mixed with the desired amount of PBA homopolymer (synthesis described in prior work[28]) using a 20 mg/mL stock solution in MeOH to target samples with 5 to 50 wt.% polymer in 5 wt.% intervals. Minimal additional MeOH was added, and a spatula was used to ensure thorough mixing. The vials were immediately placed under high vacuum to remove the methanol and ensure a uniform distribution of polymer and CNCs. Once dry, the samples were analyzed using FTIR and a calibration curve was developed based the representative carbonyl peak of PBA at 1730 cm^{-1}.

4.6.2.8 Preparation of PLA Composites

A stock solution of 10 wt.% PLA in chloroform was created by dissolving PLA (20 g) in 180 g of chloroform (180 g). For a 5 wt.% film, *w*-CNC-*g*-PBA-*b*-PEG (75 mg) was added to chloroform (20 mL) and dispersed via probe sonication. PLA stock solution (14.25 g) was then added and the solution was vortexed to mix thoroughly before placing in a sonic bath for 5 minutes. After mixing, the solution was poured into a Teflon petri dish and evaporated overnight at ambient conditions before being transferred to a vacuum oven at 80°C overnight to remove all remaining moisture. The dried film was then melt pressed between two Kapton sheets under 1 ton of pressure at 120°C for 2 minutes to obtain uniform films. If there were bubbles in the resulting film, it was cut up and repressed at the same conditions until no bubbles were seen.

Dogbone samples were cut from the pressed films for tensile testing in accordance

with ASTM D1708. The samples were allowed to equilibrate at ambient conditions for at least two days before testing.[24] The resulting PLA, PLA + *w*-CNC-OSO_3, and PLA + *w*-CNC-*g*-PBA-*b*-PEG composites were characterized with DMA and tensile testing.

4.6.3 Instrumentation

Atomic Force Microscopy (*AFM*) was done with a Cypher ES Environmental equipped with FS-1500 probes (Asylum Research) to determine the dimensions of CNCs. Crystals were dispersed in water by ultrasonication (10 min, 25 % power, 3 s on/off cycle) at a concentration of 0.01 % (w/w). A mica surface was mechanically exfoliated, treated with 50 μL poly(L-lysine), gently rinsed with DI water, then 50 μL of the freshly prepared CNC dispersion was drop-cast onto the surface. The dispersions were gently rinsed with DI water after 3 minutes and substrates were air-dried overnight prior to imaging. The images were recorded using tapping mode and the data was analyzed with Gwyddion software (Czech Metrology Institute).

Dynamic mechanical analysis (*DMA*) was performed on a TA Instruments RSA-G2 DMA on films of each sample ($\sim$ 3 mm × 1 mm × 20 mm). Temperature ramps were run from 25 to 100°C at 3 °C/min at a frequency of 1 Hz.

Fourier transform infrared (*FTIR*) spectroscopy of solid samples was carried out using a Shimadzu IRTracer-100 Fourier transform infrared spectrometer in the attenuated total reflection (ATR) geometry with a monolithic diamond ATR crystal. Data was collected in the range of 4000–400 cm^{-1}, averaging over 45 scans, and analyzed with Shimadzu LabSolutions IR software.

High resolution mass spectrometry (*HRMS*) was performed on an Agilent 6224 ToF-MS using electrospray ionization.

Melt Pressing was done on a Carver AccuStamp Model 3693 melt press at 120 °C at 2 tons of pressure for 3 minutes.

Nuclear magnetic resonance (*NMR*) was carried out at ambient temperature on a Bruker Avance II+ 400 spectrometer at 400 MHz for ^{1}H nuclei and 101 MHz for ^{13}C nuclei. Spectra were calibrated to the residual solvent peak of $CDCl_3$ (7.26 ppm ^{1}H NMR, 77.16 ppm ^{13}C NMR) and processed with MestReNova software. All chemical shifts, δ, are reported in parts per million (ppm) with coupling constant in Hz (multiplicity: s = singlet, d = doublet, td = triple doublet, t = triplet, tt = triple triplet, ddt = double double triplet, dq = double quadruplet, qi = quintuplet, m = multiplet, br = broad signal).

Size exclusion chromatography (*SEC*) of the polymers was performed on a Shimadzu Prominence High Performance Liquid Chromatography system using an eluent mobile phase of THF at a flow rate of 1 mL/min. Separation was achieved using two PLgel mixed-D columns (Agilent) maintained at ambient temperature with pore sizes suitable for materials with effective molecular weights from ∼200 to 400,000 g/mol. The differential refractive index signal was collected using a Wyatt Optilab T-rEX differential refractometer (λ = 658 nm), and on-line multi-angle light scattering (MALS) measurement was performed using a Wyatt Dawn Heleos II light scattering detector. Data analysis was carried out using Wyatt Astra VII software. Weight-averaged molecular weights (M_w) were determined by MALS, and number-average molecular weights (M_n) were determined in comparison to narrow dispersity polystyrene calibration standards (from 1,800 to 400,000 g/mol).

Tensile testing was performed on a Zwick-Roell zwickiLine Z0.5 instrument. Dogbones were tested in accordance with ASTM D1708 (crosshead speed = 1 mm/min) and tracked with a VideoXtens extensometer up to yielding followed by crosshead distance tracking.

Thermogravimetric analysis (*TGA*) was performed using a TA Instruments Discovery thermogravimetric analyzer. Samples (∼5mg) were loaded in Pt crucibles and heated under a N_2 atmosphere. High resolution dynamic procedure with default settings

(sensitivity = 1, ramp = 10 to 700 °C, resolution = 5) were applied. Data was processed in TA Instruments Trios software.

Wide-angle X-ray scattering (*WAXS*) patterns were recorded using a SAXSLAB GANESHA 300XL system with Cu Kα source (λ= 0.154 nm) at a voltage of 40 kV and 40 mA power. Powder samples were tightly packed inside plastic washers and were held in place between two pieces of Kapton tape. The data were collected in the 2-theta angle range of 1-32° for 20 minutes. The crystallinity index was calculated using MATLAB R2018a by modelling the (1,-1,0), (1,1,0), (1,0,2), and (2,0,0) cellulose-1β peaks and the residual amorphous component to Gaussian distribution functions, as described previously.[39,40]

Probe Ultrasonication was carried out on a Branson SFX 550 instrument equipped with a 13 mm probe. Sonication was conducted at 20 % amplitude with 5 seconds on and 5 seconds off per cycle while the sample vial was submerged in ice water to prevent significant heating.

4.7 Supporting Information

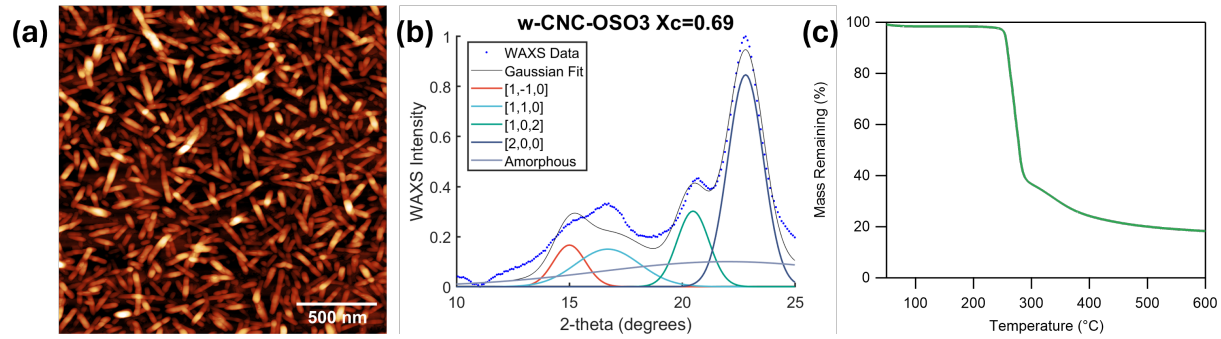

Figure S4.1: (a) AFM height image of *w*-CNC-OSO_3, (b) WAXS spectrum of *w*-CNC-OSO_3 with crystalline peak fitting to measure crystallinity index, and (c) TGA of *w*-CNC-OSO_3 showing a degradation onset of 255 °C.

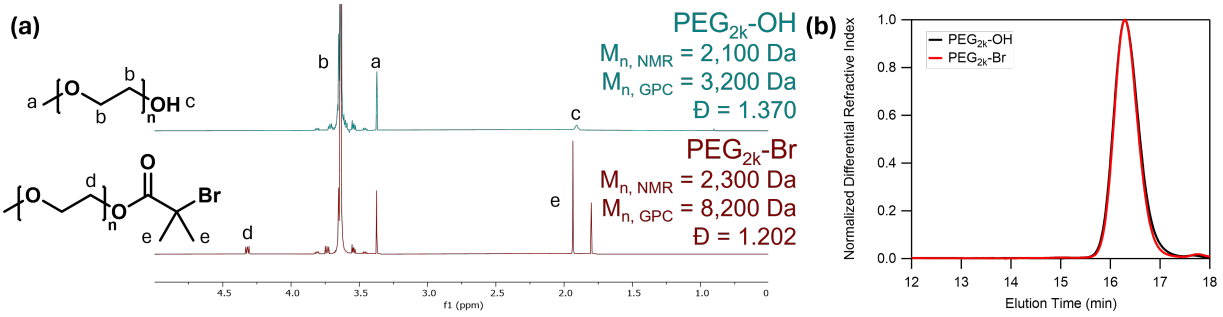

Figure S4.2: (a) ^{1}H NMR spectra for PEG_{2k}-OH and PEG_{2k}-Br with key peaks labeled and (b) SEC traces for PEG_{2k}-OH and PEG_{2k}-Br.

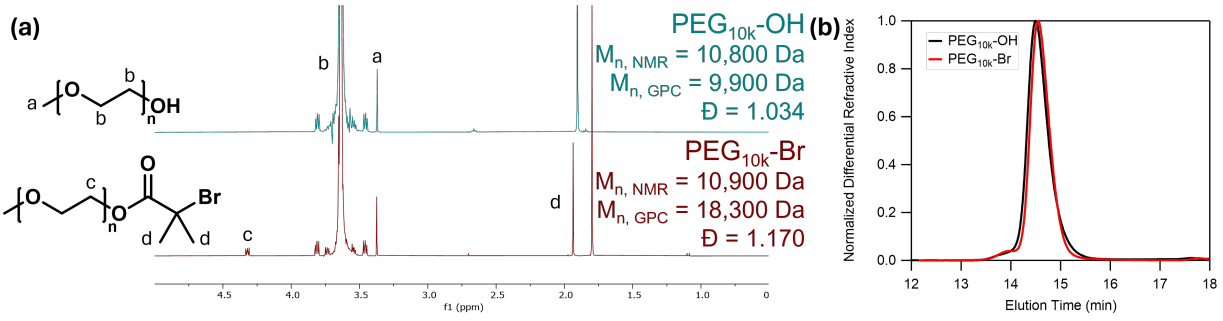

Figure S4.3: (a) ^{1}H NMR spectra for PEG_{10k}-OH and PEG_{10k}-Br with key peaks labeled and (b) SEC traces for PEG_{10k}-OH and PEG_{10k}-Br.

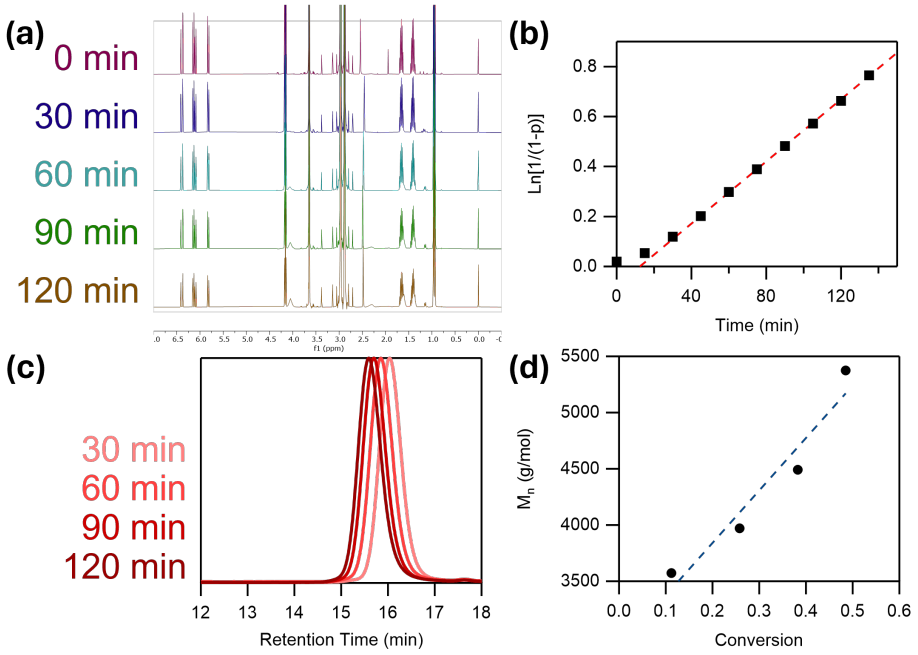

Figure S4.4: (a) ^{1}H NMR spectra for PEG$_{2k}$-*b*-PBA$_{2k}$-Br kinetics, (b) conversion vs. time based on NMR data, (c) SEC traces for PEG$_{2k}$-*b*-PBA$_{2k}$-Br kinetics, and (d) SEC Mn vs. NMR conversion showing consistent molecular weight growth.

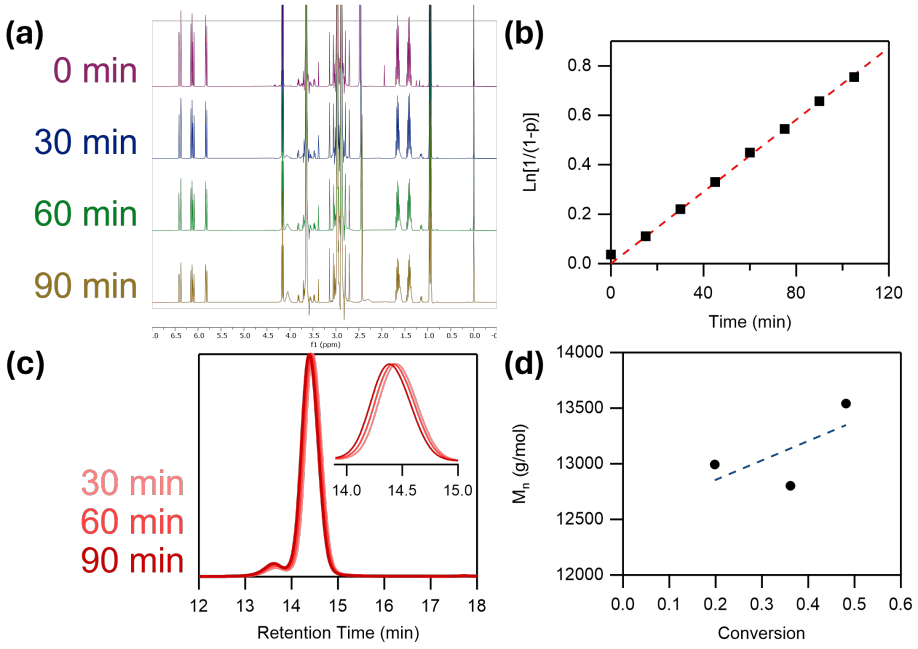

Figure S4.5: (a) ^{1}H NMR spectra for PEG$_{10k}$-*b*-PBA$_{2k}$-Br kinetics, (b) conversion vs. time based on NMR data, (c) SEC traces for PEG$_{10k}$-*b*-PBA$_{2k}$-Br kinetics, and (d) SEC Mn vs. NMR conversion showing consistent molecular weight growth.

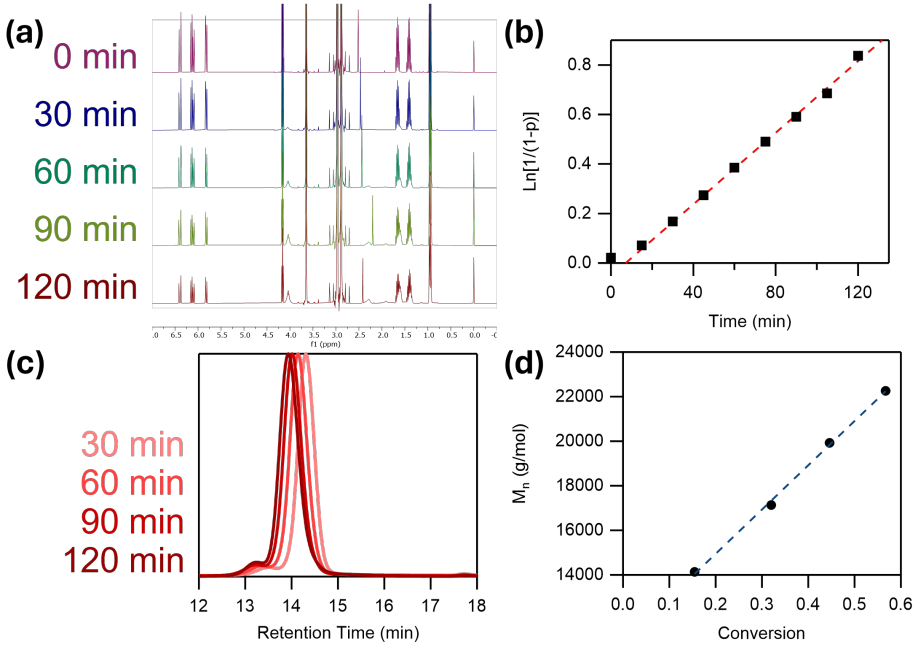

Figure S4.6: (a) ^{1}H NMR spectra for PEG$_{10k}$-*b*-PBA$_{10k}$-Br kinetics, (b) conversion vs. time based on NMR data, (c) SEC traces for PEG$_{10k}$-*b*-PBA$_{10k}$-Br kinetics, and (d) SEC Mn vs. NMR conversion showing consistent molecular weight growth.

Table S4.1: Molecular weight and dispersity statistics for all PEG-*b*-PBA polymers, measured via NMR and SEC.

Sample	**$M_{n,\,NMR}$ (g/mol)**	**$M_{n,\,SEC}$ (g/mol)**	**$Dispersity_{SEC}$ (Đ)**
PEG$_{2k}$-*b*-PBA$_{2k}$-Br	5,100	8,900	1.256
PEG$_{10k}$-*b*-PBA$_{2k}$-Br	13,300	16,200	1.114
PEG$_{10k}$-*b*-PBA$_{10k}$-Br	23,300	22,500	1.171
PEG$_{2k}$-*b*-PBA$_{2k}$-HU	4,700	12,000	1.046
PEG$_{10k}$-*b*-PBA$_{2k}$-HU	11,900	18,100	1.073
PEG$_{10k}$-*b*-PBA$_{10k}$-HU	20,800	23,600	1.050

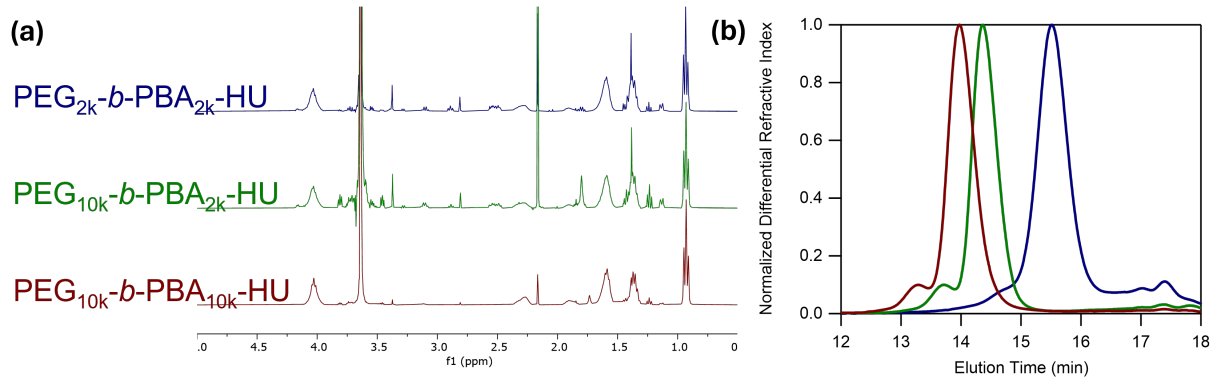

Figure S4.7: (a) ^{1}H NMR spectra for PEG-*b*-PBA-HU at various molecular weights and (b) SEC traces for PEG-*b*-PBA-HU at various molecular weights.

4.8 References

[1] Wikipedia contributors, Bioplastic, **2024**.

[2] S. Farah, D. G. Anderson, R. Langer, "Physical and mechanical properties of PLA, and their functions in widespread applications — A comprehensive review", *Advanced Drug Delivery Reviews* **2016**, *107*, 367–392.

[3] H. Carey, E. F. Schulz, G. J. Dienes, "Mechanical properties of polyethylene", *Industrial & Engineering Chemistry* **1950**, *42*, 842–847.

[4] A. Nandakumar, J.-A. Chuah, K. Sudesh, "Bioplastics: A boon or bane?", *Renewable and Sustainable Energy Reviews* **2021**, *147*, 111237.

[5] M. Garside, Breakdown of global production capacities of bioplastics 2023-2028, by material, **2023**.

[6] E. Castro-Aguirre, F. Iñiguez-Franco, H. Samsudin, X. Fang, R. Auras, "Poly (lactic acid)—Mass production, processing, industrial applications, and end of life", *Advanced Drug Delivery Reviews* **2016**, *107*, 333–366.

[7] G. Gorrasi, R. Pantani, "Effect of PLA grades and morphologies on hydrolytic degradation at composting temperature: Assessment of structural modification and kinetic parameters", *Polymer Degradation and Stability* **2013**, *98*, 1006–1014.

[8] V. Marturano, P. Cerruti, V. Ambrogi, "Polymer additives", *Physical Sciences Reviews* **2017**, *2*, DOI 10.1515/psr-2016-0130.

[9] C. Calvino, N. D. Macke, R. Kato, S. J. Rowan, "Development, processing and applications of bio-sourced cellulose nanocrystal composites", *Progress in Polymer Science* **2020**, *103*, 101221.

[10] Y. Habibi, L. A. Lucia, O. J. Rojas, "Cellulose Nanocrystals : Chemistry , Self-Assembly , and Applications", *Chemical Reviews* **2010**, *d*, 3479–3500.

[11] C. Fraschini, G. Chauve, J. Bouchard, "TEMPO-mediated surface oxidation of cellulose nanocrystals (CNCs)", *Cellulose* **2017**, *24*, 2775–2790.

[12] H. R. Paul, M. K. Bera, N. Macke, S. J. Rowan, M. V. Tirrell, "Quantitative Determination of Metal Ion Adsorption on Cellulose Nanocrystals Surfaces", *ACS Nano* **2024**, *18*, 1921–1930.

[13] S. Wohlhauser, G. Delepierre, M. Labet, G. Morandi, W. Thielemans, C. Weder, J. O. Zoppe, "Grafting Polymers from Cellulose Nanocrystals: Synthesis, Properties, and Applications", *Macromolecules* **2018**, *51*, 6157–6189.

[14] S. J. Eichhorn, A. Dufresne, M. Aranguren, N. E. Marcovich, J. R. Capadona, S. J. Rowan, C. Weder, W. Thielemans, M. Roman, S. Renneckar, W. Gindl, S. Veigel, J. Keckes, H. Yano, K. Abe, M. Nogi, A. N. Nakagaito, A. Mangalam, J. Simonsen, A. S. Benight, A. Bismarck, L. A. Berglund, T. Peijs, *Review: Current international research into cellulose nanofibres and nanocomposites*, *Vol. 45*, **2010**, pp. 1–33.

[15] A. M. Weiss, N. Macke, Y. Zhang, C. Calvino, A. P. Esser-Kahn, S. J. Rowan, "In Vitro and in Vivo Analyses of the Effects of Source, Length, and Charge on the Cytotoxicity and Immunocompatibility of Cellulose Nanocrystals", *ACS Biomaterials Science and Engineering* **2021**, *7*, 1450–1461.

[16] C. Zhang, M. R. Salick, T. M. Cordie, T. Ellingham, Y. Dan, L. S. Turng, "Incorporation of poly(ethylene glycol) grafted cellulose nanocrystals in poly(lactic acid) electrospun nanocomposite fibers as potential scaffolds for bone tissue engineering", *Materials Science and Engineering C* **2015**, *49*, 463–471.

[17] H. R. Paul, M. V. Tirrell, S. J. Rowan, "One-Component Nanocomposite Membranes from Polymer Grafted Cellulose Nanocrystals", *ACS Applied Nano Materials* **2024**, *7*, 4210–4219.

[18] R. Kato, J. H. Lettow, S. N. Patel, S. J. Rowan, "Ion-Conducting Thermoresponsive Films Based on Polymer-Grafted Cellulose Nanocrystals", *ACS Applied Materials and Interfaces* **2020**, *12*, 54083–54093.

[19] J. H. Lettow, R. Y. Kaplan, P. F. Nealey, S. J. Rowan, "Enhanced Ion Conductivity through Hydrated, Polyelectrolyte-Grafted Cellulose Nanocrystal Films", *Macromolecules* **2021**, *54*, 6925–6936.

[20] M. A. Hillmyer, P. M. Lipic, D. A. Hajduk, K. Almdal, F. S. Bates, "Self-Assembly and Polymerization of Epoxy Resin-Amphiphilic Block Copolymer Nanocomposites", *Journal of the American Chemical Society* **1997**, *119*, 2749–2750.

[21] J. Liu, Z. J. Thompson, H. J. Sue, F. S. Bates, M. A. Hillmyer, M. Dettloff, G. Jacob, N. Verghese, H. Pham, "Toughening of epoxies with block copolymer micelles of wormlike morphology", *Macromolecules* **2010**, *43*, 7238–7243.

[22] D. J. Pochan, S. P. Gido, J. Zhou, J. W. Mays, M. Whitmore, A. J. Ryan, "Morphologies of microphase-separated conformationally asymmetric diblock copolymers", *Journal of Polymer Science Part B: Polymer Physics* **1998**, *35*, 2629–2643.

[23] T. Li, J. Zhang, D. K. Schneiderman, L. F. Francis, F. S. Bates, "Toughening Glassy Poly(lactide) with Block Copolymer Micelles", *ACS Macro Letters* **2016**, *5*, 359–364.

[24] C. J. McCutcheon, B. Zhao, K. Jin, F. S. Bates, C. J. Ellison, "Crazing mechanism and physical aging of poly(lactide) toughened with poly(ethylene oxide)-

block-poly(butylene oxide) diblock copolymers", *Macromolecules* **2020**, *53*, 10163–10178.

[25] J. K. Muiruri, S. Liu, W. S. Teo, J. Kong, C. He, "Highly biodegradable and tough polylactic acid–cellulose nanocrystal composite", *ACS Sustainable Chemistry & Engineering* **2017**, *5*, 3929–3937.

[26] X. Sun, H. Zhang, X. Huang, X. Wang, Q. F. Zhou, "Synthesis of poly(ethylene oxide)-block-poly(methyl methacrylate)-block- polystyrene triblock copolymers by two-step atom transfer radical polymerization", *Polymer* **2005**, *46*, 5251–5257.

[27] A. Anastasaki, V. Nikolaou, G. Nurumbetov, P. Wilson, K. Kempe, J. F. Quinn, T. P. Davis, M. R. Whittaker, D. M. Haddleton, "Cu (0) -Mediated Living Radical Polymerization : A Versatile Tool for Materials Synthesis", **2016**.

[28] Z. Oluz, N. Macke, S. Candelaria, A. Ambus, A. Zemborain, C. S. Udemgba, A. M. Weiss, C. Calvino, S. J. Rowan, "Melt-Functionalization of Cellulose Nanocrystals using Dynamic Hindered Ureas", *Journal of Polymer Science* **2024**.

[29] L. Zhang, S. J. Rowan, "Effect of Sterics and Degree of Cross-Linking on the Mechanical Properties of Dynamic Poly(alkylurea-urethane) Networks", *Macromolecules* **2017**, *50*, 5051–5060.

[30] N. Macke, C. M. Hemmingsen, S. J. Rowan, "The effect of polymer grafting on the mechanical properties of PEG-grafted cellulose nanocrystals in poly(lactic acid)", *Journal of Polymer Science* **2022**, *60*, 3318–3330.

[31] K. Mohomed, Thermogravimetric Analysis (TGA) Theory and Applications, **2016**.

[32] A. C. Genix, V. Bocharova, A. Kisliuk, B. Carroll, S. Zhao, J. Oberdisse, A. P. Sokolov, "Enhancing the Mechanical Properties of Glassy Nanocomposites by Tuning Polymer Molecular Weight", *ACS Applied Materials and Interfaces* **2018**, *10*, 33601–33610.

[33] N. K. Hansoge, S. Keten, "Effect of Polymer Chemistry on Chain Conformations in Hairy Nanoparticle Assemblies", *ACS Macro Letters* **2019**, *8*, 1209–1215.

[34] G. Sudre, E. Siband, D. Hourdet, C. Creton, F. Cousin, Y. Tran, "Synthesis and Characterization of Poly(acrylic acid) Brushes: "Grafting-Onto" Route", *Macromolecular Chemistry and Physics* **2012**, *213*, 293–300.

[35] Y. H. Lin, "Number of entanglement strands per cubed tube diameter, a fundamental aspect of topological universality in polymer viscoelasticity", *Macromolecules* **1987**, *20*, 3080–3083.

[36] L. J. Fetters, D. J. Lohse, D. Richter, T. A. Witten, A. Zirkel, "Connection between Polymer Molecular Weight, Density, Chain Dimensions, and Melt Viscoelastic Properties", *Macromolecules* **1994**, *27*, 4639–4647.

[37] H. Lee, R. M. Venable, A. D. MacKerell, R. W. Pastor, "Molecular Dynamics Studies of Polyethylene Oxide and Polyethylene Glycol: Hydrodynamic Radius and Shape Anisotropy", *Biophysical Journal* **2008**, *95*, 1590–1599.

[38] N. M. Ahmad, P. A. Lovell, S. M. Underwood, "Viscoelastic properties of branched polyacrylate melts", *Polymer International* **2001**, *50*, 625–634.

[39] A. D. French, "Idealized powder diffraction patterns for cellulose polymorphs", *Cellulose* **2014**, *21*, 885–896.

[40] S. Park, J. O. Baker, M. E. Himmel, P. A. Parilla, D. K. Johnson, "Cellulose crystallinity index: measurement techniques and their impact on interpreting cellulase performance", *Biotechnology for Biofuels* **2010**, *3*, 1–10.

CHAPTER 5

SUMMARY, PERSPECTIVE, AND OUTLOOK

5.1 Summary

The amount of plastic being used and discarded around the world every day is a problem that does not appear to be subsiding anytime soon. Plastic waste continues to accumulate in terrestrial and aquatic ecosystems, disrupting and harming the flora and fauna all around us. Eliminating these plastic materials from industrial and personal use is all but an impossible task, so we must instead look for alternatives that can offset and replace materials that are sourced from petrochemical feedstocks and do not degrade in reasonable amounts of time. The leading alternative candidates are currently bioplastics such as poly(lactic acid) (PLA), polyhydroxybutyrate (PHB), and polycaprolactone (PCL), among others, but the properties of these materials are subpar. PLA and PHB are too brittle and PCL has low thermal stability. One way to alleviate these issues could be the addition of fillers that enhance the desired properties, but most commercial fillers are either petrochemical- or inorganic-based and do not match the sustainability or degradability profiles of the biopolymers to which they would be added.

Described in Chapter 1[1], cellulose nanocrystals (CNCs) are bio-sourced nanoparticles that could be a promising candidate for this role. CNCs are rodlike nanoparticles that can be isolated from a wide range of bio-sources and incorporated into a variety of polymer matrices. Because of their sourcing, the resulting CNC-based composites are still able to completely biodegrade while also exhibiting enhanced properties, particularly enhanced strength, thermal stability, and barrier properties. One of the key challenges associated with the preparation of CNC-based composites is the dispersion of the nanocrystals within the host matrix. Since CNCs are hydrophilic and most polymer matrices are hydrophobic, the CNCs tend to agglomerate when blended into a

host material. To counter this aggregation, a variety of strategies have been employed, including small molecule surfactant addition, polymeric surfactant addition, electrostatic adsorption of small molecules or polymers, or covalent grafting of small molecules or polymers to enhance the interfacial interations of the CNCs with the hydrophobic host polymer. All of these approaches has had some level of success, but the resulting composites almost always exhibit an increase in the mechanical strength and a reduction in the elongation at break. While this isn't necessarily a negative result, it means that these types of additives would not be useful in PLA, the most common biopolymer, where brittleness is already the biggest limitation. Additionally, nearly all of these strategies rely on the use of water or organic solvents to functionalize the CNC surface, which makes these techniques difficult to translate to a commercial scale. Regardless, CNC-based composites have been made to show their potential for use in packaging, water purification, electronics, and biomedical applications, amongst others.

Chapter 2[2] is focused on the issue of effective interfacial interactions between CNCs and a host matrix. To study the variables that impact stress transfer in CNC composites, poly(ethylene glycol) (PEG)-grafted CNCs were synthesized at multiple grafting densities with multiple molecular weights of PEG chains and incorporated into PLA composites. Using EDC/NHS coupling in water, PEG_{2k} and PEG_{10k} grafting resulted in 0.09 and 0.03 chains/nm^2, respectively. When the grafting reagent was changed to DMTMM.BF_4 in DMF, the same PEG_{2k} and PEG_{10k} grafting resulted in 0.33 and 0.07 chains/nm^2, highlighting the effects of polymer-solvent interactions on polymer grafting. Incorporating these grafted nanoparticles into PLA composites resulted in the expected increase in storage modulus above T_g, up to a 500 % increase with 10 wt.% *MxG*-CNC-*g*-PEG_{550H}, but plasticization was avoided by grafting the polymers to the CNC surface rather than blending all of the components together. Most interestingly, the elongation at break was found to vary based on the grafted polymer molecular weight

and surface density, which determine the polymer brush conformation on the CNC surface. When grafted polymers were in the mushroom regime, dramatic embrittlement was seen, down to 1.6 % strain at break with 10 wt.% *MxG*-CNC-*g*-PEG_{550L}. This occurred because the polymer chains were unable to fully cover the CNC surface, allowing the hydrophilic CNC surface to interact with the hydrophobic PLA matrix, creating defect points that led to premature failure. When surface density or molecular weight were increased so that the polymer chains resided in a concentrated polymer brush on the CNC surface, some amount of the embrittlement was reduced, but the composite materials were still not as extensible as neat PLA because there was not effective stress transfer between the filler and matrix. Only when the grafted polymer had sufficient molecular weight in the semi-dilute brush regime was embrittlement avoided, while still enhancing the mechanical properties above T_g. In this case, the surface-anchored polymers were able to entangle with the PLA, allowing for effective stress transfer and avoiding the embrittling effects caused by the rigid CNCs. These design parameters, sufficiently long polymer chains in the semi-dilute brush regime, will be important tools for designing functional CNC-based additives going forward.

With the ideal polymer grafting parameters determined, Chapter 3[3] developed more sustainable grafting techniques that do not rely on the use of organic solvents or water to bond polymer chains to the CNC surface. The approach was based on hindered urea (HU) chemistry, which consists of an isocyanate group that is blocked by a sterically bulky amine group. This HU group can be thermally activated to kick off the bulky amine and regenerate the isocyanate group *in-situ*, which can subsequently react with alcohol groups on the CNC surface. Synthetic methods were developed to attach HU groups to the end of hydroxy- and bromine-terminated polymer chains and the resulting HU-terminated polymers were grafted to CNCs in the melt. Diagnostic tests were done to compare CNC grafting with HU- and isocyanate-terminated polymer chains,

which showed that improved control over the grafting reaction was afforded by the HU end group. With PEG_{2k} and PEG_{10k}, grafting resulted in 0.58 and 0.13 chains/nm^2, respectively, which was a significant improvement over the solution-based grafting methods used in the prior chapter. Additionally, grafting was done with PCL_{10k}-HU and PBA_{10k}-HU that resulted in 0.07 and 0.03 chains/nm^2, respectively. These reduced grafting densities hint that the steric bulk of the grafted polymer chain plays a significant role in the resulting surface density. Although preparation of the HU-terminated polymer chains required organic solvent, removing solvent from the grafting step while achieving higher surface densities was a significant improvement over prior work and represents a promising method for CNC functionalization with less bulky polymer chains.

Finally, Chapter 4 aimed to combine the concepts learned in Chapters 2 and 3 to design a polymer-grafted CNC nanofiller that would be able to toughen PLA. This work was inspired by the use of wormlike micelles to toughen epoxies and other polymer matrices through the addition of rubbery inclusions capable of blunting propagating cracks within the matrix. By grafting diblock polymers to CNC surfaces where the inner block was a low T_g poly(n-butyl acrylate) (PBA) segment and the outer block was a compatibilizing PEG segment, it was hypothesized that the "wormlike" structure of the CNCs would allow for toughening of PLA without the need for thermodynamic self-assembly of the wormlike structures. PEG-*b*-PBA-HU diblock polymers were synthesized and grafted onto CNCs, but the resulting nanoparticles exhibited extremely low grafting densities, similar to those seen in Chapter 3. This resulted in all surface brushes residing in the mushroom regime, where the CNC surface was only partially covered and conflicting hydrophilic-hydrophobic interactions resulted in severe embrittlement when the nanoparticles were incorporated into PLA composites. This low grafting density was hypothesized to be the effect of increased steric bulk and chain

stiffness in PBA, which was compared to the PEG chains used in Chapters 2 and 3. The packing length of PBA, which is a measure of chain diameter, is 4.19 Å compared to 1.94 Å for PEG; and the Kuhn length, which is a measure of backbone stiffness, is 3.48 nm for PBA and 1.86 nm for PEG. Both of these factors likely impact the ability for subsequent polymer chains to access the CNC surface during the grafting reaction, reducing the expected grafting density of the bulkier polymer chain.

5.2 Perspective and Outlook

During the writing of the review that would eventually become the first chapter of this thesis, there were two clear themes that emerged while reviewing the literature. First, CNC-based composites in the literature were overwhelmingly predictable: the incorporation of CNCs resulted in stiffer and stronger materials, but the flexibility and elongation at break were reduced. This isn't inherently bad, except for the fact that most biopolymers are limited by their flexibility. PLA has an elongation at break of less than 10 %, which is already way too brittle for most commercial applications. Adding CNCs into the network may improve the strength and stiffness, but it exacerbates the core issue with using PLA. For this reason, I wanted to find a nanoparticle that would be able to enhance PLA properties without further reducing its flexibility. Ideally, this would increase the elongation at break and toughness, but the first step was to understand the factors necessary for polymer-grafted CNCs to interface effectively with PLA. This was successfully achieved in Chapter 2 and the brush "phase" diagram was a very cool way to visualize how changes in molecular weight and surface density would impact composite properties.

The second trend that I pulled out of that initial literature review was the lack of sustainable processing methods for CNC-based materials. Almost all techniques for functionalizing CNCs relied on large amounts of water or organic solvent during

synthesis or processing, which was antithetical to the reason for using these sustainable nanoparticles. The hindered urea grafting method developed in Chapter 3 is an extremely versatile technique to graft a wide range of polymer chains onto CNCs without the need for solvent during the grafting step. Although the preparation of the HU-terminated polymers required lots of solvent, I believe that more sophisticated processing methods would reduce this need and, in a commercial setting, the system would be designed so that the CNCs would not need to be purified before being incorporated into the composite materials. Although not written into this thesis, additional work is being done with the Mintz group at Clark Atlanta University to improve melt-mixing procedures to develop CNC-based composites. By combining HU functionalization methods with composite melt-processing techniques, we could almost entirely eliminate solvent during composite production.

The intended culmination of my work was the development of a diblock-grafted CNC that would mimic the toughening properties of wormlike micelles in PLA. Unfortunately, the chosen PEG-*b*-PBA diblocks were too bulky to reach high enough grafting density or polymer content on the CNC surface to have the desired effect. While I do believe that the theory behind this approach is sound, as evidenced by the Muiruri paper,[4] I did not have enough time to pivot into a polymer system that would be more effective. To reach higher surface densities, a less bulky polymer should be used, such as poly(ethyl acrylate) or polyhydroxybutyrate. Additionally, it may be more effective to use grafting-from techniques that are able to fully cover the CNC surface with relatively short polymer chains. Although the dispersity of the resulting polymer brush would likely be higher, full surface coverage with short polymer chains along with a few longer polymers would likely result in better composite properties. The short chains would prevent embrittlement and the longer chains could effectively interface with the host matrix to promote stress transfer. In an academic setting, this is much

harder to characterize because surface initiation and growth behave much different from solution-based polymerization, but from a commercial perspective, the resulting composite properties are all that matter.

Moving forward, I think the diblock-grafted CNC platform is one that has potential to create some very interesting materials. With the template of a functional inner block combined with a compatible outer block, you could introduce a wide range of functionalities into a wide range of materials. This functionality could take the form of rubbery inclusions, transport channels for electrons, ions, or water, biological activity, mechanochromic moieties, or anything else imaginable, and could be incorporated into hydrophilic materials, hydrophobic materials, biological environments, or solution-state systems. If we can continue to enhance surface density with bulkier polymer chains and continue to find more sustainable processing methods for composites, the sky truly is the limit for functional sustainable materials based on cellulose nanocrystals.

5.3 References

[1] C. Calvino, N. D. Macke, R. Kato, S. J. Rowan, "Development, processing and applications of bio-sourced cellulose nanocrystal composites", *Progress in Polymer Science* **2020**, *103*, 101221.

[2] N. Macke, C. M. Hemmingsen, S. J. Rowan, "The effect of polymer grafting on the mechanical properties of PEG-grafted cellulose nanocrystals in poly(lactic acid)", *Journal of Polymer Science* **2022**, *60*, 3318–3330.

[3] Z. Oluz, N. Macke, S. Candelaria, A. Ambus, A. Zemborain, C. S. Udemgba, A. M. Weiss, C. Calvino, S. J. Rowan, "Melt-Functionalization of Cellulose Nanocrystals using Dynamic Hindered Ureas", *Journal of Polymer Science* **2024**.

[4] J. K. Muiruri, S. Liu, W. S. Teo, J. Kong, C. He, "Highly biodegradable and tough polylactic acid–cellulose nanocrystal composite", *ACS Sustainable Chemistry & Engineering* **2017**, *5*, 3929–3937.